Dissertation

submitted to the

Combined Faculties of the Natural Sciences and Mathematics
of the Ruperto-Carola University of Heidelberg, Germany

for the degree of

Doctor of Natural Sciences

Put forward by

Dipl.-Phys. Fabian Rennecke

born in Hamburg, Germany

Oral examination: 20.07.2015

The Chiral Phase Transition of QCD

Referees: Prof. Dr. Jan M. Pawlowski
Prof. Dr. Jürgen Berges

Der Chirale Phasenübergang der QCD

In dieser Arbeit studieren wir verschiedene Aspekte des chiralen Phasenübergangs der Quanten Chromodynamik (QCD). Dieser ist dadurch geprägt, dass sehr verschiedene Freiheitsgrade auf unterschiedlichen Energieskalen relevant sind. Wir widmen uns daher der Frage, wie genau die Hadronen auf niedrigen Energieskalen aus der Dynamik der Quarks und Gluonen bei hohen Energien hervorgehen. Dazu bedienen wir uns der Funktionalen Renormierungsgruppe, welche uns erlaubt, diesen dynamischen Übergang in einem vereinheitlichten Rahmen zu beschreiben. Dadurch sind wir in der Lage, die relevanten Freiheitsgrade zu identifizieren und die zugrundeliegenden Mechanismen des Übergangs von Quarks und Gluonen zu Hadronen in der QCD, einschließlich des Wechselspiels dieser beiden unterschiedlichen Phasen, besser zu verstehen. Das Verhalten der Vektormesonen, welche in experimentellen Studien des Phasenübergangs eine herausragende Rolle spielen, lässt sich dadurch aus der QCD ableiten. Basierend auf diesen Erkenntnissen entwickeln wir ein Niederenergie-Modell zur effektiven Beschreibung des QCD Phasendiagrams bei endlicher Temperatur und Dichte. Unser Fokus liegt dabei auf der quantitativen Präzision unserer Resultate im Sinne von kontrollierten Entwicklungsschemen und dem Effekt von Quark-Meson Streuprozessen auf den chiralen Phasenübergang.

The Chiral Phase Transition of QCD

In this thesis we study various aspects of the chiral phase transition of quantum chromodynamics (QCD). This transition is characterized by very different degrees of freedom at different energy scales. We therefore address the question how hadrons on low energy scales emerge from the underlying quark-gluon dynamics at high energies. To this end, we utilize the functional renormalization group which allows for the description of this dynamical transition within an unified framework. With this method at hand, we are able to identify the relevant degrees of freedom and to deepen our understanding of the underlying mechanisms that drive the transition from quarks and gluons to hadrons in QCD, including the mutual back reaction of these distinct phases. As a result, the properties of vector mesons, which play a prominent role for experimental investigations of the phase transition, can be derived from QCD. These insight are the foundation for the development of a low-energy model that aims at the effective description of the QCD phase diagram at finite temperature and density. There, our focus is on the quantitative precision of our results based on well-controlled expansion schemes and the effect of quark-meson scattering processes on the chiral phase transition.

Contents

1. Introduction **11**
- 1.1. The QCD Phase Diagram . . . 11
- 1.2. Outline of the Thesis . . . 16

2. The Phase Structure of QCD **19**
- 2.1. QCD Basics . . . 19
- 2.2. Finite Temperature and Density . . . 23
- 2.3. QCD Phases . . . 25
- 2.4. Mechanism of Chiral Symmetry Breaking . . . 29

3. The Functional Renormalization Group **33**
- 3.1. The Idea . . . 34
- 3.2. FRG with Scale Dependent Fields . . . 35
- 3.3. Regularization Scheme . . . 40
- 3.4. The Fixed Background Taylor Expansion . . . 41

4. Chiral Symmetry Breaking in QCD **49**
- 4.1. The Effective Action . . . 50
  - 4.1.1. Expansion Scheme . . . 54
- 4.2. Dynamical Hadronization . . . 57
  - 4.2.1. FRG & Dynamical Hadronization . . . 57
  - 4.2.2. Hadronized Flow Equations . . . 64
- 4.3. Gauge Sector . . . 66
- 4.4. Numerical Results . . . 75
  - 4.4.1. Initial Conditions and Fixed Point Behavior . . . 75
  - 4.4.2. Gauge Couplings . . . 76
  - 4.4.3. Unquenched Propagators . . . 77
  - 4.4.4. Masses and Meson Decoupling . . . 79
- 4.5. Conclusions . . . 82

5. The Vacuum Structure of Vector Mesons **85**
- 5.1. The Effective Action . . . 87

5.1.1. Meson Sector . . . 89
5.2. Fluctuations and the Transition from Quarks to Mesons . . . 92
5.2.1. Dynamical Hadronization for Vector Mesons . . . 93
5.2.2. π–a_1 Mixing . . . 94
5.3. Numerical Results . . . 95
5.3.1. Initial Conditions . . . 95
5.3.2. Masses . . . 97
5.3.3. Decoupling of the Mesons . . . 100
5.3.4. Vector Meson Dominance . . . 101
5.4. Conclusions . . . 102

6. From QCD to Low-Energy Effective Models **105**
6.1. Decoupling of the Gauge Sector . . . 105
6.2. Dynamical Hadronization and Low-Energy Effective Models . . . 108

7. The QCD Phase Diagram **111**
7.1. Quark-Meson Model . . . 112
7.1.1. Low Energy Effective Action . . . 113
7.1.2. Higher Order Mesonic Scattering . . . 114
7.2. RG Flows . . . 115
7.2.1. Effective Potential . . . 116
7.2.2. Yukawa Coupling . . . 118
7.2.3. Wave Function Renormalizations . . . 119
7.2.4. Convexity for $\rho < \rho_0$ & Behavior for Large Fields . . . 121
7.3. Numerical Results . . . 123
7.3.1. Initial Conditions . . . 123
7.3.2. The Impact of Higher Order Mesonic Interactions . . . 125
7.3.3. Phase Diagram . . . 126
7.3.4. Background Dependence . . . 130
7.4. Conclusions . . . 132

8. Summary, Conclusions & Outlook **133**

Appendix **136**

A. Field Space **139**

B. Diagrammatic Derivation of Flow Equations **141**

C. Flow Equations **145**
C.1. QCD Flows . . . 145
C.2. Vacuum Polarization of the Gluon . . . 147
C.3. Vector Meson Flows . . . 149
C.4. In-Medium Flows of the Matter Sector . . . 155

D. IR Strength **159**

E. Implications of Convexity on the Quark Mass **161**

Danksagung **165**

Bibliography **167**

CHAPTER 1

Introduction

1.1. The QCD Phase Diagram

The weak, the electromagnetic and the strong force as well as gravity constitute the fundamental interactions of nature. The structure of the sub-atomic realm is determined by the former three forces. Owing to its unprecedented success in the past decades, it is now widely accepted that the quantum theory of these interactions is given by the standard model of particle physics.

In the 1950s numerous particles – the *hadrons* – were discovered. Already their large number suggests that they cannot be fundamental. In the course of this, Gell-Mann and Zweig proposed that hadrons are bound states of *quarks* [1–4]. To fully understand the observed hadron spectrum, a new quantum number associated to the quarks – the *color charge* – was necessary. This was rooted in the fact that some baryons (e.g. the Δ^{++}) would otherwise violate the Pauli principle. In analogy to quantum electrodynamics (QED), the interaction of quarks, i.e. the strong interaction, is therefore described by an $SU(N_c)$ gauge theory. N_c is the number of color charges [5–10]. Consistency with the hadron spectrum requires $N_c = 3$. This theory of the strong interactions is known as *quantum chromodynamics* (QCD). The gauge bosons which mediate these interactions are called *gluons*. Gauge invariance is a fundamental principle in nature and applies to all the fundamental interactions. Since the gauge group of QCD in non-Abelian, the gluons also carry color charge and therefore strongly interact with themselves. As a consequence, the strong interaction is very short ranged, as opposed to gravity and electromagnetic interactions[1].

The theory of strong interactions, formulated in terms of color charged quarks and gluons, was not immediately accepted by the physics community. This hesitation is rooted in one of the most peculiar features of QCD: The absence of color charged objects in nature. Furthermore, there is no *direct* experimental evidence for the existence of colored states to date. This feature of QCD is known as *confinement*. It states that quarks and gluons are always bound into color-neutral objects and is a main characteristic of QCD at low energies. Even though the mechanism of confinement is not fully understood yet, it ultimately arises from the fact that the energy necessary to separate a pair of quarks rises linearly with the distance. The energy

[1] The weak interactions are also short-ranged. Owing to the weakness of the interaction, however, its short range cannot be explained by the non-Abelian nature of the weak force. It is rather due to the large mass of the corresponding gauge bosons, which is generated by the Higgs-mechanism, that the interaction range is short.

from the separation is at some point large enough for a new quark pair to be created from the vacuum, which then pairs with the original quarks and thus prevents the isolation of color charge.

With the discovery of *asymptotic freedom* by Gross, Wilczek and Politzer in 1973 [11, 12], the other peculiar feature of QCD was revealed: The strong interactions become arbitrarily weak at arbitrarily small distances. Thus, at high energies quarks and gluons are basically free particles. This implies that the very nature of the degrees of freedom of QCD must change drastically with the energy scale. While at low energies confinement prevails and quarks and gluons only exist as constituents of color-neutral hadrons, they are free, *deconfined*, particles at high energies. It is therefore natural to expect that a phase transition from the hadronic to the quark-gluon regime occurs.

Indeed, convincing evidence has been collected from both experimental and theoretical efforts that such a confinement-deconfinement phase transition exists in the plane of temperature and density. At low temperature and density the system is in the hadronic phase. The *quark-gluon plasma* (QGP) phase, i.e. the phase populated with individual quarks and gluons, is reached at sufficiently high temperatures and/or densities. Early evidence for such a transition was already found in 1965 by Hagedorn [13]. He pointed out that in a purely statistical model of hadrons, the partition function diverges at a certain temperature. This phenomenon was interpreted as the break-down of the hadronic description of matter, since hadrons "melt" at sufficiently large temperatures. Even though there are much more sophisticated descriptions of QCD in the medium nowadays, the interpretation of these early findings remain true. In numerical ab-initio simulations of QCD on spacetime-lattices at vanishing density, a steep rise in the pressure and the energy density at a certain temperature T_c was found [14–16]. Since both quantities scale with the number of degrees of freedom, this observation signals a phase transition between two regimes which are characterized by very different degrees of freedom. From lattice results it is now well-established that the confinement-deconfinement transition is a crossover with critical temperature $T_c \approx 155\,\mathrm{MeV}$ [17–19]. We want to emphasize that in SI units this temperature is roughly $1.7 \times 10^{12}\,\mathrm{K}$ – about five orders of magnitude hotter than the core of the sun.

This immense temperature indicates that experimental studies of the QCD phase structure require tremendous efforts for the creation of such an extreme environment. This is achieved in ultra-relativistic heavy ion collisions (HIC), i.e. the collision of atomic nuclei in which the center-of-mass energy is much larger that the rest mass of the nucleon. The first experiments of this kind were performed in the 1970s at the Bevelac, Lawrence Berkeley National Laboratory. But it was not until 2005 that large enough energy densities were created to produce a quark gluon plasma. This was achieved at Brookhaven National Laboratory's Relativistic Heavy Ion Collider (RHIC), where HIC research still continues. The other mayor facility that presently performs these experiments is the Large Hadron Collider (LHC) at CERN.

Observables that are easily accessible in theory are often almost impossible to measure. One of the greatest challenges, intersecting both theoretical and experimental efforts, is therefore to identify observables that are sensitive to the different phases of QCD, theoretically well understood and also accessible in experiments. The main reason for this complication is that the quark-gluon plasma state produced experimentally has only a very short lifetime in which it expands and cools rapidly. All informations about the fireball therefore have to be reconstructed from the final states, i.e. the properties of the detected particles. The fact that the phase transitions of QCD are not even well defined, at least for a large part of the phase diagram, additionally complicates these efforts.

Promising signatures of deconfinement are found in heavy quarkonium suppression [20] and hadron yields [21]. Heavy quarkonia such as charmonium probe the heavy quark mass limit of QCD and are therefore sensitive to features of deconfinement [22]. Particle yields are surprisingly well described by the so-called statistical model, which assumes a thermal distribution of a non-interacting hadron resonance gas [21]. Most prominently, temperature and chemical potential of the chemical freeze-out can be extracted from thermal fits of this simple model to particle yields. At small chemical potential, the freeze-out temperature is a good measure for the phase transition temperature [23]. Indeed, the transition temperature extracted from LHC data is in agreement with lattice results at vanishing density [24].

The confining nature of QCD at low energies alone is not sufficient to explain the hadron spectrum. This is rooted in the observation that e.g. the nucleons have a mass of about 1 GeV while their constituents, the lightest quarks flavors *up* and *down*, get masses of about $2-4$ MeV from the Higgs mechanism. This huge discrepancy cannot be explained by binding energy alone, since it can only account for a few MeV. Thus, there must be an additional mechanism for the generation of the nucleon masses, or put differently, the effective mass of the quarks that are bound into hadrons, known as the *constituent quarks*. The masses of the *current quarks*, i.e. the free quarks in the high-energy regime, are generated by the Higgs mechanism at the electroweak scale ~ 246 GeV. As it turns out, the three flavors *up*, *down* and *strange* are much lighter than the other quark flavors *charm*, *bottom* and *top*[2]. Thus, in QCD the light quark sector (u,d,s) is well approximated as massless. In this massless limit, this sector possesses an additional global flavor symmetry known as *chiral symmetry*. It states that left- and right-handed quarks can be rotated independently in flavor-space. The observed hadron spectrum shows a large mass-splitting between mesons that should be degenerate if chiral symmetry would hold. A prominent example is the mass splitting of the chiral partners, the ρ-meson and the a_1-meson, where the mass-difference is about 500 MeV. This cannot be explained by the rather small explicit chiral symmetry breaking due to the finite masses of the light quarks. Hence, chiral symmetry must be broken in the hadronic regime, while it approximately holds in the quark-gluon regime in the light quark sector. In fact, chiral symmetry must be *spontaneously* broken. According to Goldstones theorem, this gives rise to eight very light pseudoscalar mesons[3]. This beautifully explains why there are exactly eight pseudoscalar mesons, the three pions, the four kaons and the eta meson, which are considerably lighter than the rest of the hadrons.

Lattice studies found that the chiral transition is also a crossover and the critical temperature at vanishing density coincides with that of the deconfinement transition within the error [17, 18, 25–30]. The experimental challenge is to identify signatures of chiral symmetry restoration in heavy ion collisions. Promising signals are found in the low-mass spectra dilepton or the transverse momentum spectra of photons [31–33]. The reason is that the precise form of these spectra is sensitive to in-medium modifications of hadrons, in particular the light mesons and most prominently the ρ-meson, to which dileptons couple directly. The ρ, in turn, is likely to show distinct signatures of chiral restoration close to the chiral phase transition, either through characteristic modifications of its mass [34–36] or more generally of its spectral function [37, 38].

We see that the hadronic regime is characterized by both, confinement and the absence of chiral symmetry. The quark-gluon plasma, on the other hand, is characterized by deconfined

[2] We will refer to the six quark flavors as u, d, s, c, b and t for the remainder of this work.

[3] In the case of spontaneous breaking of approximate symmetries, Goldstone bosons are very light rather than exactly massless.

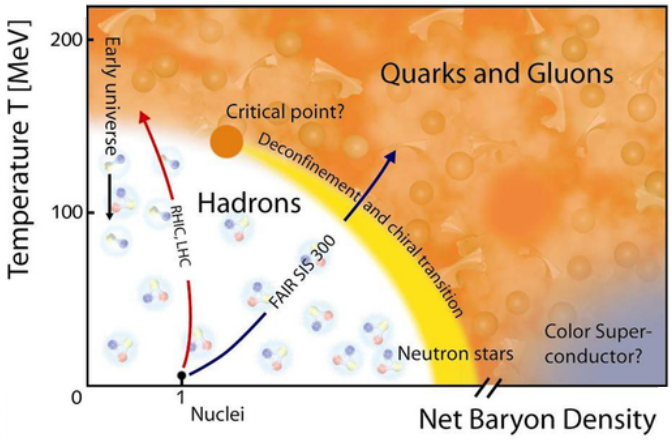

Figure 1.1.: A sketch of the QCD phase diagram [39].

quarks and gluons with approximate chiral symmetry in the light quark sector. The quest for the QCD phase diagram is therefore to a large extent a quest for the understanding of confinement and chiral symmetry breaking. In Fig. 1.1 we show a sketch of the phase diagram in the temperature-density plane. As it was established from lattice simulations, the chiral and deconfinement transitions are crossovers at small densities and approximately coincide with each other. During the evolution of the universe from the big bang, the phase boundary was crossed in this region. Starting from the hot environment created by the big bang, the universe subsequently cooled down and underwent the transition from the quark-gluon plasma to the hadronic phase approximately 10^{-6} seconds after the big bang.

At larger densities, the fluctuations of fermions, i.e. quarks and baryons, are enhanced. This is rooted in the fact that if one compresses a "gas" of fermions, they effectively become lighter. In turn, fermionic fluctuations intensify phase transitions and it is a realistic possibility that at large enough density the crossover transition turn in to a first-order phase transition. Consequently, there is a distinct point in the phase diagram where the crossover and the first-order transition meet, the *critical endpoint* (CEP), and the transition is of second order. Such a point is characterized by enhanced long-range fluctuations which lead to singularities in thermodynamic observables. Thus, owing to its nature, the CEP would show distinct signatures in experiments [40]. However, no conclusive evidence for the existence of such a point has been found yet. From theoretical considerations we only know that there is no CEP for $\mu_B \lesssim \pi T$, where μ_B is the baryon chemical potential[4] [27, 41–47].

At large densities a variety of different phases have been conjectured [48]. The possibility of diquark-condensation (in analogy to the formation of cooper pairs in ordinary superconductivity) can lead to various *color-superconducting* phases [49–57]. Furthermore, the ground state may be characterized by spatially modulated condensates, i.e. inhomogeneous phases [58–61]. In addition, there is the *liquid-gas* transition of nuclear matter at very small temperatures and intermediate densities in the hadronic regime. Since the nucleon mass is about 1 GeV, nucleons can only form at vanishing temperature when the baryon chemical potential is larger than their mass (minus the binding energy). It is a first-order phase transition of the liquid-gas type at very small temperatures, that also ends in a second-order critical point [62].

[4]The density is a monotonously increasing function of the chemical potential. We therefore use both quantities interchangeably.

The main challenges for theoretical studies are rooted in the fact that QCD exhibits vastly different degrees of freedom at different scales and that interactions become very strong at long distances. The latter is a consequence of asymptotic freedom. Since the coupling shrinks towards large energy scales, it increases with decreasing energy scale. Thus, perturbation theory reaches a Landau pole, predicting its own breakdown. For a theoretical description of QCD in the low-energy regime, and in particular its phase structure, the use of *non-perturbative* methods is therefore inevitable.

The only non-perturbative ab-initio method known is lattice gauge theory [63–66], where spacetime is discretized into a lattice. Numerical simulations on the lattice have reliably revealed some of the most important features of the non-perturbative regime of QCD, most notably the order and the transition temperature of the phase transition at vanishing density already mentioned above. Finite density, however, gives rise to the infamous *sign problem*: A real chemical potential leads to a complex spectrum of the Dirac operator and the Monte-Carlo techniques used in lattice gauge theory become inapplicable, since highly oscillating phases spoil random sampling methods. Even though much progress has been made in order to circumvent the sign problem [67,68], there are no reliable results at large densities available to date. Furthermore, including fermions on the lattice is expensive due to their Grassmann-nature and discretization errors as well as finite volume effects are unavoidable, although well under control by now. This is partly due to the use of immense computer power provided by special purpose super computers such as the QCDOC at the Brookhaven National Laboratory.

Continuum alternatives to lattice methods are functional methods, such as *Dyson-Schwinger equations* (DSE) and the *functional renormalization group* (FRG). These methods translate the problem of solving the path integral into solving a system of coupled (functional) differential equations. Both DSE and FRG are exact methods by construction, and in particular non-perturbative. Solving the full theory, however, implies solving a tower of infinitely many coupled differential equations. It is therefore inevitable to truncate the full theory. The inclusion of finite temperature, finite density and chiral fermions, on the other hand, poses no conceptual problem. In this sense, these methods are complementary to lattice gauge theory.

Throughout this work, we will use the functional renormalization group in order to address several of the issues discussed above. It describes the *renormalization group flow* of a given microscopic theory to the macroscopic regime, where long-wavelength excitations and many-body effects dominate. The FRG is a well-suited method to tackle QCD at various energy scales, since it allows for the investigation of physical phenomena involving different degrees of freedom at different energy scales.

A great challenge in this context is to find a consistent unified description of both, the quark-gluon sector and the hadronic sector. This is of great importance since the properties of hadrons ultimately derive from the underlying quark-gluon dynamics of microscopic QCD. Thus, addressing questions concerning the formation of hadrons in the QCD phase transition, the signatures of this transition as well as the structure of the phase diagram requires a thorough understanding of the underlying mechanism of how hadrons emerge from the high-energy QCD sector. An important cornerstone for FRG studies was the realization that bound states have to be described as RG-scale dependent fields in order to consistently connect the bound-state regime with the regime where the constituents are the relevant degrees of freedom [69,70]. This procedure was coined *re-bosonization*. The application of this idea to QCD requires a good understanding of the hadronic and the gauge sector of QCD from functional methods, as well as their mutual feedback.

In this work we will extend these previous works in various directions revolving around the

chiral phase transition of QCD. Based on the good understanding we now have of the pure gauge theory in the Landau gauge from functional methods [71] we will extend the idea of re-bosonization to dynamical two-flavor QCD – which we call *dynamical hadronization* for the application to QCD – and focus on chiral symmetry breaking. We use this to compute the the unquenched ghost, gluon and quark propagators. They play a predominant role in the description of QCD and its phase transitions. As a result of this description, the hadronic sector emerges dynamically from the underlying quark-gluon dynamics and all parameters of the low-energy theory are determined by the RG-flows in the high-energy regime. Furthermore, the mechanism of how mesons decouple when the system enters the quark-gluon regime becomes clear. This also allows us to study the consequences of neglecting gluon fluctuations in effective low-energy descriptions of QCD.

As mentioned above, the ρ meson plays an important role in the experimental exploration of the QCD phase structure. It is therefore necessary to understand its chiral dynamics. By extending the dynamical hadronization technique to the case of vector mesons, we can study the structure of vector mesons, and in particular the ρ, as it emerges from microscopic QCD in the vacuum and, in addition, analyze the behavior of the corresponding low-energy parameters.

The accuracy of our results relies on the quantitative control we have over the gauge and matter sector separately, as well as over their mutual back reaction. An accurate description of the QCD phase diagram requires a detailed understanding of the effects of quark and meson fluctuations. To this end we study the impact of higher-order quark-meson scattering processes on the QCD phase diagram in a well-controlled systematic expansion of the effective action.

1.2. Outline of the Thesis

We start with a more detailed discussion of QCD and its phases with particular emphasis on the chiral symmetry breaking in Chap. 2. After a short recapitulation of the most relevant quantum field-theoretical aspects of QCD and the implementation of finite temperature and density in Sects. 2.1 and 2.2, we discuss aspects of chiral symmetry and confinement in more detail in Sec. 2.3. The mechanism of chiral symmetry breaking from a renormalization group perspective is explained in Sec. 2.4. There, we point out the relevance of effective four-quark interactions and the running of the strong coupling for chiral symmetry breaking.

The relevant aspects of the functional renormalization group are discussed in Chap. 3. The general idea behind the RG is explained in Sec. 3.1. We then derive the flow equation in the presence of scale dependent fields in Sec. 3.2. The resulting equation is a generalized version of the original equation derived by Wetterich and will be the basis for the FRG computations in this thesis. In Sec. 3.3 we explain the optimization criterion that leads to the regularization scheme we use throughout this work. The fixed background Taylor expansion is put forward in Sec. 3.4. It is a particular expansion scheme of the effective action in terms of meson fields that is particularly well-suited for the study of the low-energy sector of QCD in terms of quark-meson models. To demonstrate this, we show its convergence properties in comparison to a more conventional expansion scheme and explicitly check the quality of this expansion by reproducing a highly non-trivial result on the QCD phase diagram from the literature.

Chap. 4 is devoted to chiral symmetry breaking in two-flavor QCD in the vacuum. We motivate our truncation of the effective action in Sec. 4.1 and discuss our expansion scheme in this context. We develop the dynamical hadronization technique in Sec. 4.2.1. As already mentioned above, it is an extension of re-bosonization, specifically tailored for the application to QCD. The corresponding modified flow equations will be derived there. They are a special

case of the more general flow equation derived in Sec. 3.2. The gauge sector of QCD is a key ingredient for dynamical hadronization and we discuss it in detail in Sec. 4.3. We use the ghost and gluon propagators from Yang-Mills theory as an input and self-consistently include the full effect of quark fluctuations to this input in order to capture the dynamics of unquenched QCD. Furthermore, our construction and the involved approximations for the gauge-vertices are discussed and we present flow equations for the quark-gluon, the ghost-gluon and the three-gluon vertex, as well as the vacuum polarization of the gluon. The numerical results are presented in Sec. 4.4. We first specify the initial conditions for the flow equations. Owing to dynamical hadronization and in particular the occurrence of a "bound state fixed point", the only parameters we need to fix are the strong coupling and the current quark mass at a large initial scale in the perturbative quark-gluon regime. Next, we present our solutions of the flow equations of the gauge couplings. Their RG-flow first follows the perturbative running, until non-perturbative effects, specifically the formation of the gluon mass gap, lead to different running of the gauge couplings. The unquenched quark and gluon propagators are also shown there. The screening effect of dynamical quarks is clearly visible in our findings. We then show our result for the meson masses and clarify the details of their decoupling at large energy scales.

The framework developed in Chap. 4 is applied to the QCD with vector mesons, in particular the chiral partners ρ and a_1 in Chap. 5. In this chapter we study the vacuum structure of this mesons in detail, motivated by the discussion above. Our truncation with a detailed discussion of the (vector-) meson sector is discussed in Sec. 5.1. We extend dynamical hadronization to the case of vector mesons and discuss the implications in Sec. 5.2. In Sec. 5.3 we then present the numerical results. We show that the dynamics of the vector mesons is completely determined by the dynamics of the lighter mesons in the hadronic phase. The scaling of the ρ mass as it approaches the scale of chiral symmetry breaking is discussed in detail, as well as our results for the meson masses and their decoupling. Finally, we analyze the validity of the assumption of local flavor symmetry. In the literature, this has been been used in studies related to vector mesons within effective field theories.

Chap. 6 intends to bridge the gap between QCD and low-energy effective models. Within the framework developed in the previous chapters, we can analyze one of the basic assumptions of effective models for the hadronic sector of QCD: The complete decoupling of gluon fluctuations. We do this in Sec. 6.1 on the example of the quark-meson model and show that there is an intermediate range of scales well within the typical range of these effective models, where the effects of the gauge sector still give quantitatively important contributions. In Sec. 6.2 we analyze the relevance of dynamical hadronization for low-energy models and find that it can be neglected.

In Chap. 7 we study the chiral phase diagram of QCD at finite temperature and density in terms of a quark-meson model. Our focus there is on quantitative precision of our description of the low-energy sector of QCD. To this end, we investigate the impact of higher order quark-meson scattering processes on the phase boundary. In Sec. 7.1 we introduce our truncation. Our expansion of the effective action relies on the findings of Sec. 3.4. This is crucial, since the "conventional" expansion scheme leads to severe numerical instabilities. Thus, quantitative precision in terms of a well-controlled expansion of the effective action crucially depends on an appropriate expansion scheme. We discuss some important details of the RG-flows of the parameters of our truncation in Sec. 7.2. The numerical results are presented in Sec. 7.3. After discussing the initial conditions of the flow equations, we show the effect of higher order meson-meson and quark-meson interactions on the chiral order parameter. These interactions play a quantitatively important role for the phase diagram, but also become less relevant with

increasing order in the fields. This implies a rapid convergence of our expansion and allows for the control of quantitative precision in this part of the hadronic sector of QCD. We then show the full phase diagram in the temperature-density plane. We compare different definitions of the crossover. While they show large deviations to one another at small densities, they move towards a unique result at larger densities. There, we find a first-order transition that ends in a critical point. We also point out the individual effects effects that different parts scale-dependent parameters of the truncation have on the phase boundary. Furthermore, we compute the curvature of the phase boundary at vanishing density for various definitions of the crossover and critically compare our findings to lattice results. Finally, we demonstrate the stability of our expansion and extract informations about the field dependence of quark and meson wave function renormalizations from our findings.

We present the conclusion and an outlook of this thesis in Chap. 8. Technical details can be found in the Appendix.

The compilation of this thesis is solely to the author. The results and presentations are largely based on work with my collaborators. Large parts of this thesis are published or available as preprint. The related works are [72–74]:

- *Higher order quark-mesonic scattering processes and the phase structure of QCD*
  with Jan M. Pawlowski
  Physical Review D **90** 076002 (2014)

- *From Quarks and Gluons to Hadrons: Chiral Symmetry Breaking in Dynamical QCD*
  with Jens Braun, Leonard Fister and Jan M. Pawlowski
  e-print available from arXiv:hep-ph/1412.1045 (2014)

- *The Vacuum Structure of Vector Mesons in QCD*
  e-print available from arXiv:hep-ph/1504.03585 (2015)

CHAPTER 2

The Phase Structure of QCD

In this section we give an overview of QCD and its phase structure. We will focus on the aspects relevant for this work.

2.1. QCD Basics

Quantum chromodynamics (QCD) is the theory of strong interactions. It describes the interaction of quarks q and antiquarks $\bar{q}$ as a $SU(N_c)$ gauge theory. The quarks are fermions that transform in the fundamental representation of the gauge group. Their quantum numbers are given by the color $c \in \{1,\dots,N_c\}$, which describes their charge under $SU(N_c)$, and the flavor $f \in \{1,\dots,N_f\}$, which describes the different species u,d,s,c,b,t of quarks. The gauge particles, the mediators of the interactions, are the gluons A_μ. They are spin-1 particles that transform in the adjoint representation of the gauge group. Thus, they carry adjoint color charge $a \in \{1,\dots,N_c^2-1\}$. The number of colors in QCD is $N_c = 3$. In contrast to non-Abelian gauge particles, the gluons carry color charge and are thus self-interacting.

We choose Hermitian $SU(N_c)$ generators t^a, i.e. their anticommutator reads $[t^a,t^b] = if^{abc}t^c$, with the structure constants f^{abc}, and their trace is poitive $\operatorname{tr} t^a t^b = \frac{1}{2}\delta^{ab}$. The quarks transform under local $SU(N_c)$ transformations $\mathscr{U}(x) = e^{i\Theta^a(x)t^a}$ as

$$q(x) \to \mathscr{U}(x)q(x) \quad \bar{q}(x) = \bar{q}(x)\mathscr{U}^\dagger(x)\,. \tag{2.1}$$

In order to ensure gauge symmetry, the partial derivative in the kinetic term of the quarks in the action has to be replaced by the covariant derivative D_μ,

$$D_\mu = \partial_\mu - ig_s A_\mu^a t^a\,. \tag{2.2}$$

Here, we expanded the gauge field in the basis of the generators, $A_\mu = A_\mu^a t^a$. $g_s = \sqrt{4\pi\alpha_s}$ is the strong coupling. The covariant derivative of the quark has to transform under the local transformation in the same way the conventional derivative does under the global transformation, i.e. $D_\mu q(x) \to \mathscr{U}(x)D_\mu q(x)$. This requires the following transformation of the gluons:

$$A_\mu(x) \to A_\mu^{(\Theta)} \equiv \mathscr{U}(x)A_\mu(x)\mathscr{U}^\dagger(x) - \frac{i}{g_s}\left(\partial_\mu \mathscr{U}(x)\right)\mathscr{U}^\dagger(x)\,. \tag{2.3}$$

Locally, this transformation can be written as

$$A_\mu^{(\Theta),a} = A_\mu^a + \frac{1}{g_s}\partial_\mu \Theta^a + f^{abc} A_\mu^b \Theta^c = A_\mu^a + \frac{1}{g_s} D_\mu \Theta^a \,, \tag{2.4}$$

where D_μ is the covariant derivative in the adjoint representation here.

Since the gluons are physical fields, there needs to be a corresponding kinetic term in the action. We therefore need a Lorentz-scalar, gauge invariant object that is at most quadratic in the derivatives. The only CP-invariant object possible is (in Euclidean spacetime)

$$\frac{1}{2}\mathrm{tr}\, F_{\mu\nu} F_{\mu\nu} \,, \tag{2.5}$$

with the field strength tensor

$$F_{\mu\nu} = \frac{i}{g_s}[D_\mu, D_\nu] = \partial_\mu A_\nu - \partial_\nu A_\mu - i g_s [A_\mu, A_\nu] \,. \tag{2.6}$$

Since it is, as the gluons, an element of the Lie algebra, it can be decomposed as $F_{\mu\nu} = F_{\mu\nu}^a t^a$, which yields,

$$F_{\mu\nu}^a = \partial_\mu A_\nu^a - \partial_\nu A_\mu^a + g_s f^{abc} A_\mu^b A_\nu^c \,. \tag{2.7}$$

A cruicial difference between Abelian and non-Abelian gauge theories is now apparent: the term quadratic in the gauge fields in (2.7) is a direct consequence of the non-Abelian nature of the gauge group. As a consequence, the gauge kinetic term (2.5) contains three- and four-gluon self-interactions already at the classical level. In an Abelian gauge theory, these terms are not present and the gauge fields are classically non-interacting.

With all the ingredients at hand now, we can write down the classical action of QCD in Euclidean spacetime[1]:

$$S_{\mathrm{QCD}} = \int_x \left\{ \bar{q}\left(i\gamma_\mu D_\mu + i m_q\right) q + \frac{1}{4} F_{\mu\nu}^a F_{\mu\nu}^a \right\} , \tag{2.8}$$

with the Hermitean gamma matrices obeying $\{\gamma_\mu, \gamma_\nu\} = 2\delta_{\mu\nu}\mathbb{1}$. We use the conventions of [75] throughout this work. For the four-dimensional Euclidean spacetime integration, we use the abbreviation $\int_x = \int d^4x$ and summation over color and flavor degrees of freedom is implied. The second term in (2.8) encodes the pure gauge part and the action containing only this part defines *Yang-Mills* (YM) theory.

The gauge symmetry implies that different gauge fields are physically equivalent. Since the the measure of the path integral a priori contains all possible field configurations, this leads to a redundancy in the description of the quantum theory. The action is unchanged along the infinite number of directions in the space of field configurations corresponding to gauge transformations; all fields which are in the same gauge orbit $[A_\mu^{(\Theta)}]$,

$$[A_\mu^{(\Theta)}] \equiv \left\{ A_\mu^{(\Theta)} = \mathscr{U}(x)\left(A_\mu + \frac{i}{g_s}\partial_\mu\right)\mathscr{U}^\dagger(x) \,\middle|\, \mathscr{U}(x) \in SU(N_c) \right\} , \tag{2.9}$$

are physically the same. In order not to suffer from an (infinite) overcounting in the path integral, we need a measure that picks one representative out of all the gauge equivalent

[1] We use Euclidean signature throughout this work.

configurations in the gauge orbit. For non-Abelian gauge theories this is achieved by the Fadeev-Popov method [76], which imposes a gauge fixing condition

$$\mathsf{F}^a(A^{(\Theta)}) = 0 \tag{2.10}$$

upon the gauge field at each spacetime point. Ideally, the gauge fixing condition is chosen such that it picks exactly one representative of each gauge orbit, where the space of all representatives form a submanifold of the manifold which contains all gauge field configurations. This means that the gauge orbit should intersect each gauge fixing submanifold once. Due to topological obstructions however, this is at best possible locally. This problem is known as the Gribov ambiguity [77] and we note that it is linked to the non-Abelian nature of the gauge symmetry. Let us assume there exists a solution to this problem and thus we have a well-defined gauge-fixed path integral (see e.g. [78]). For this discussion we restrict ourselves to pure Yang-Mills theory,

$$S_{\mathrm{YM}} = \int_x \frac{1}{2}\mathrm{tr}(F_{\mu\nu}F_{\mu\nu}), \tag{2.11}$$

because it is straightforward and without any subtleties to include fermions. Naively one would simply include an delta-distribution $\delta\big(\mathsf{F}^a(A^\alpha)\big)$ in the path integral measure to enforce the gauge fixing condition. But since the determinant transforms non-trivially under gauge transformations, we need an additional factor to compensate this transformation to keep the theory gauge invariant. In analogy to the rule for variable transformation in an ordinary n-dimensional integral, we insert 1 in the path integral in the form

$$1 = \int \mathscr{D}\mathsf{F}^a\, \delta(\mathsf{F}^a) = \int \mathscr{D}\Theta\, \delta\big(\mathsf{F}^a(A^{(\Theta)})\big) \det\left(\frac{\delta \mathsf{F}^a(A^{(\Theta)})}{\delta\Theta}\right), \tag{2.12}$$

with the Faddeev-Popov determinant $\det\big(\delta\mathsf{F}^a(A^{(\Theta)})/\delta\Theta\big)$ and the gauge transformed gauge field $A^{(\Theta)}$. As long as the gauge fixing conditions is linear in Θ, the functional derivative $\delta\mathsf{F}^a(A^{(\Theta)})/\delta\Theta$ is independent of Θ and so is the Faddeev-Popov determinant. In linear covariant gauges,

$$\mathsf{F}^a(A) = \partial_\mu A^a_\mu(x) - \omega^a(x), \tag{2.13}$$

the Faddeev-Popov operator can be expressed in terms of the covariant derivative in the fundamental representation by using (2.4),

$$\frac{\delta \mathsf{F}^a(A^{(\Theta)})}{\delta\Theta^b} = \frac{1}{g_s}\partial_\mu D^{ab}_\mu\,. \tag{2.14}$$

$\omega^a(x)$ is a Gaussian weight which allows us to reformulate the delta distribution in (2.12) as an exponential, $\delta(\mathsf{F}^a) = \exp\left(-\int_x \frac{1}{2\xi}(\partial_\mu A^a_\mu)^2\right)$. ξ is the gauge fixing parameter. It is directly related to the weight ω and can be chosen to be any finite constant. For instance, Landau gauge $\xi = 0$ strictly enforces $\partial_\mu A^a_\mu(x) = 0$.

The Faddeev-Popov determinant can also be re-expressed as an exponential. To this end, one introduces Grassman valued ghost and antighost fields c^a and $\bar{c}^a$ as auxiliary fields and uses the familiar representation of the functional determinant to write (in linear covariant gauge)

$$\det\left(\frac{1}{g_s}\partial_\mu D^{ab}_\mu\right) = \int \mathscr{D}c\mathscr{D}\bar{c}\, e^{-\int_x \bar{c}^a\, \partial_\mu D^{ab}_\mu\, c^b}\,. \tag{2.15}$$

We absorbed the factor $1/g_s$ in the definition of the ghost fields. Note that the ghosts have to be Lorentz-scalars even though they are Grassmann valued, implying that they have a wrong relation between spin and statistics and cannot be physical particles.

The gauge fixing allows us to define QCD as quantum field theory in terms of the generating functional,

$$Z[J,\eta,\bar{\eta},\tau,\bar{\tau}] = \int \mathscr{D}A\mathscr{D}q\mathscr{D}\bar{q}\mathscr{D}c\mathscr{D}\bar{c}\, e^{-S^{(\mathrm{gf})}_{\mathrm{QCD}}+\int_x (JA+\bar{\eta}q+\bar{q}\eta+\bar{\tau}c+\bar{c}\tau)}, \tag{2.16}$$

where $J,\eta,\bar{\eta},\tau,\bar{\tau}$ are the sources of the corresponding fields. The gauge fixed action of QCD $S^{(\mathrm{gf})}_{\mathrm{QCD}}$ contains the classical action, the ghost action and the gauge fixing term,

$$S^{(\mathrm{gf})}_{\mathrm{QCD}} = \int_x \left\{ \bar{q}\left(i\gamma_\mu D_\mu + im_q\right)q + \frac{1}{4}F^a_{\mu\nu}F^a_{\mu\nu} + \bar{c}^a\,\partial_\mu D^{ab}_\mu\, c^b + \frac{1}{2\xi}(\partial_\mu A^a_\mu)^2 \right\}. \tag{2.17}$$

We used that gauge transformations also preserve the path integral measure $\mathscr{D}A = \mathscr{D}A^{(\Theta)}$ since they have Jacobian determinant 1. Hence, the integration $\mathscr{D}\Theta$ in (2.12) is merely a dummy integration in linear covariant gauges and can be factored out into an overall normalization of the path integral.

The manifest gauge symmetry of the action is obviously spoiled by the gauge fixing procedure. However, the gauge fixed action $S^{(\mathrm{gf})}_{\mathrm{QCD}}$ develops a global fermionic symmetry which, in some sense, remembers the gauge invariance of the original theory. This symmetry is known as BRST symmetry [79–81]. Physical observables such as scattering amplitudes have to be gauge independent in accordance with the gauge symmetry of the original theory. Thus, Green's functions, which are manifestly gauge invariant objects and are related to scattering amplitudes, have to satisfy Slavnov-Taylor identities (STI) in order to guarantee gauge invariance [82, 83]. Due to Noether's theorem, there is a conserved charge Q_B associated to BRST invariance. The STI, in turn, are a consequence of this charge conservation. However, conservation of Q_B strictly holds only on the perturbative level and it is yet unclear if it is well-defined non-perturbatively. For instance, the decoupling solution for deep-IR behavior of the ghost and gluon propagators in Landau gauge Yang-Mills theory breaks BRST symmetry [71].

A far-reaching consequence of the non-Abelian nature of QCD is *asymptotic freedom* [11, 12]. For a $SU(N_c)$ gauge theory with N_f quark flavors in the fundamental representation, the one-loop beta-function of the gauge coupling α_s is

$$k\partial_k\alpha_s = \left(2N_f - 11N_c\right)\frac{\alpha_s^2}{6\pi}, \tag{2.18}$$

with the energy scale k. Thus, for a sufficiently small number of quark flavors N_f, the beta function is negative. For QCD with $N_c = 3$ and $N_f = 6$ we have $k\partial_k\alpha_s = -7\alpha_s^2/(2\pi)$. With a reference (or UV-cutoff) scale Λ, the solution to (2.18) is

$$\alpha_s(k) = \frac{\alpha_s(\Lambda)}{1 + b_0\alpha_s(\Lambda)\ln(k/\Lambda)}, \tag{2.19}$$

with $b_0 = -(2N_f - 11N_c)/(6\pi)$. Hence, the larger the energy scale, the smaller the strong coupling. In the limit $k \to \infty$, the strong coupling vanishes and quarks and gluons become free particles. This is called asymptotic freedom. Conversely, α_s gets amplified at large energies

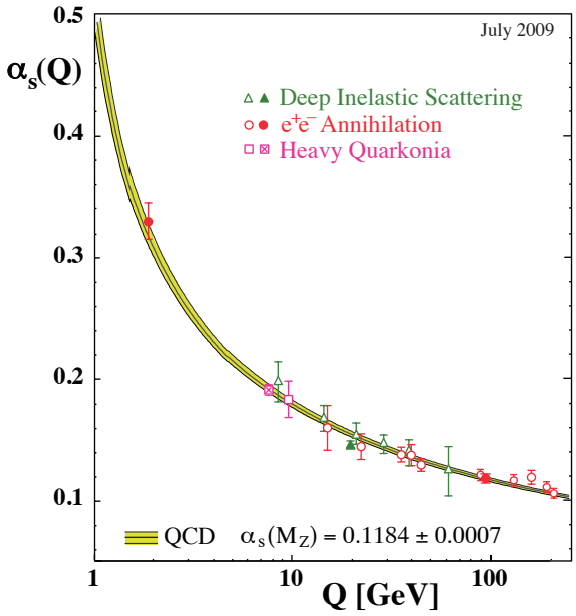

Figure 2.1.: Summary of measurments of α_s as a function of the energy scale Q compared to results from 4-loop perturbation theory [84].

and it becomes apparent that at some point perturbation theory breaks down for QCD at small energy scales. The IR properties of QCD are therefore only accessible with non-perturbative methods. A comparison of experimental and perturbative results of α_s is shown in Fig. 2.1.

Very loosely speaking, one can think of asymptotic freedom as a competition of screening and antiscreening effects of quark and gluon fluctuations: while quark-antiquark pairs created from vacuum fluctuations screen the color charge at large distances (in the same way electron-positron pairs screen the electric charge in QED), gluon fluctuations lead to a net antiscreening, resulting in an effective amplification of the color charge at large distances.

2.2. Finite Temperature and Density

Here we briefly outline how we describe QCD at finite temperature and density in thermal equilibrium. To this end, we exploit the close connection between statistical mechanics and quantum field theory in the imaginary time formalism[2]. By performing a Wick rotation of the time coordinate, i.e. going to imaginary time $t \to -ix_0$, the signature of spacetime changes from Minkowski to Euclidean. This way, the Lagrangian density $\mathscr{L}$ becomes an energy density. The generating functional of a bosonic field φ becomes:

$$Z_M[J] = \int \mathscr{D}\varphi e^{i\int dt d^3x \left[\mathscr{L}_M - J(x)\varphi(x)\right]} \xrightarrow{t\to -ix_0} Z[J] = \int \mathscr{D}\varphi e^{-\int dx_0 d^3x \left[\mathscr{L} - J(x)\varphi(x)\right]}, \tag{2.20}$$

where the index M denotes Minkowski signature. Now, to establish the connection to statistical mechanics, we note that the partition function (in the canonical ensemble) is $Z_C = \mathrm{Tr}\, e^{-\beta\hat{H}}$,

[2] In the real-time formalism, finite temperature is introduced by imposing the Kubo-Martin-Schwinger condition on the Minkowski path integral [85].

with the Hamilton operator $\hat{H}$ and $\beta = 1/T$. The trace basically states that we take the thermodynamical ensemble average. Thus, to define the analogous object in QFT, the generating functional needs to generate ensemble averages. This amounts to the restriction of the (imaginary) temporal integration to a closed path of extend β and corresponding boundary conditions for the fields in x_0 direction. This yields the partition function of QFT at finite temperature T,

$$Z[J] = \int_{\varphi(\beta,\vec{x})=\varphi(0,\vec{x})} \mathscr{D}\varphi e^{-\int_0^\beta dx_0 \int d^3x \left[\mathscr{L}-J(x)\phi(x)\right]}. \tag{2.21}$$

This means that in this Euclidean formulation of QFT at finite temperature, spacetime is compactified on a torus in the imaginary time direction. Note that in the limit $T \to 0$, we recover the original partition function. The corresponding boundary conditions for bosonic and fermionic fields φ and ψ are

$$\varphi(x_0+\beta,\vec{x}) = \varphi(x_0,\vec{x}) \tag{2.22}$$
$$\psi(x_0+\beta,\vec{x}) = -\psi(x_0,\vec{x}), \tag{2.23}$$

i.e. bosons have periodic boundary condition, while fermions are antiperiodic in imaginary time direction.

As usual, compact directions in position space translate into discrete directions in momentum space. In this case, we use the Fourier transformation

$$\varphi(x_0,\vec{x}) = T\sum_{n\in\mathbb{Z}} \int \frac{d^3p}{(2\pi)^3} \varphi(f_n,\vec{p})\, e^{i(f_n x_0 + \vec{p}\vec{x})}, \tag{2.24}$$

where f_n are the discrete frequencies, called *Matsubara modes*. They read explicitly for bosonic and fermionic fields

$$f_n\big|_{\text{boson}} \equiv \omega_n = 2n\pi T \tag{2.25}$$
$$f_n\big|_{\text{fermion}} \equiv \nu_n = (2n+1)\pi T\,. \tag{2.26}$$

Thus, at finite temperature the integral of an arbitrary function g in momentum space has to be replaced by

$$\int \frac{d^4p}{(2\pi)^4}\, g(p_0,\vec{p}) \quad \xrightarrow{T\neq 0} \quad T\sum_{n\in\mathbb{Z}} \int_{\vec{p}} g(f_n,\vec{p}), \tag{2.27}$$

where we abbreviated $\int_{\vec{p}} = \int \frac{d^3p}{(2\pi)^3}$. This allows us to switch to finite temperature with this simple replacements.

The inclusion of finite density is now straightforward if we further exploit the close connection between Euclidean QFT and statistical mechanics. Finite density is included in the grand canonical ensemble by introducing a chemical potential μ[3] together with the conserved particle number operator $\hat{N}$ of the corresponding particle, $Z_{\text{GC}} = \text{Tr}\, e^{-\beta(\hat{H}-\mu\hat{N})}$. Thus, we only have to add the corresponding term to the action in the QFT.

In the case of QCD, we have a finite quark- (or equivalently baryon-) density. Quark number conservation is associated to the global $U(1)$ symmetry of the action and the corresponding conserved charge, i.e. the quark number operator, is $\int_x \bar{q}\gamma_0 q$. The density is a monotonously

[3] μ is the Lagrange multiplier associated to the conserved mean particle number at finite density.

increasing function of the chemical potential. We therefore use the notion of density and chemical potential interchangeably in this work. The microscopic action of euclidean QCD at finite temperature and density therefore reads:

$$S_{\mathrm{QCD}} = \int_0^\beta dx_0 \int_{\vec{x}} \left\{ \bar{q}\left(i\gamma_\mu D_\mu + im_q + i\gamma_0\mu\right)q + \frac{1}{4}F^a_{\mu\nu}F^a_{\mu\nu} \right\}, \tag{2.28}$$

with the corresponding boundary conditions (2.22) for the fields. Note that the additional i in the quark number operator enters through the Wick rotation to Euclidean time.

2.3. QCD Phases

Owing to asymptotic freedom, QCD basically consists of free quarks and gluons at very high energies. At low energies, however, we observe only color neutral objects, i.e. guarks and gluons occur exclusively as constituents of color-neutral composite particles. Thus, the very nature of the QCD vacuum must change drastically in between. It is now widely accepted that strongly interacting matter exhibits a rich phase structure at finite temperature and density. A sketch of the QCD phase diagram is shown in Fig. 1.1.

The two most prominent phases are the hadronic phase with confinement and broken chiral symmetry, and the deconfined quark-gluon plasma (QGP) phase with approximate chiral symmetry. There is now strong evidence that at small and intermediate densities, these phases are separated by a crossover transition. At large densities, the phase structure is still under debate. A popular conjecture is that at large densities and small temperature the transition is of first order. This implies in particular the existence of a critical endpoint of the first-order transition, where it turns into a crossover. At even larger densities, a variety of phases have been conjectured, such as various color superconducting phases or different inhomogeneous phases.

In the following we will discuss some details of chiral symmetry and confinement, as well as their connection.

Chiral Symmetry Breaking. At vanishing quark masses $m_q \to 0$, the so-called *chiral limit*, QCD exhibits a global flavor symmetry called *chiral symmetry*. While this is certainly not true in nature, it is a very good approximation for the light quark sector. In this case, left- and right-handed quarks,

$$q_{L/R} \equiv \left(\frac{1 \mp \gamma_5}{2}\right) q\,, \tag{2.29}$$

only appear strictly separated in the QCD action (2.8). Thus, the theory is symmetric under independent flavor rotations $U(N_f)_L \times U(N_f)_R$ of q_L and q_R. To clarify the structure of this symmetry, we separate it terms of the vector and axial flavor transformations, $U(1)_V \times U(1)_A \times SU(N_f)_V \times SU(N_f)_A$. The vector transformations see no difference between left- and right-handed fields. $U(1)_V$ symmetry implies baryon number conservation and $SU(N_f)_V$ is the isospin symmetry. Isospin is explicitly broken by different quark masses. $U(1)_A$ is broken on the quantum level. This is referred to as axial (or chiral) anomaly [86–89]. Most prominently, it explains the $\eta - \eta'$ mass splitting: since $U(1)_A$ is explicitly broken in the quantum theory, the $SU(3)$ singlet η' is not a Goldstone boson, as opposed to the η which is part of the pseudoscalar octet[4]. The large η' mass can

[4] If $U(1)_A$ would not be broken anomalously, chiral symmetry would be $U(N_f)_A$ and its spontaneous breaking would give nine Goldstone bosons for $N_f = 3$ light quarks up, down and strange.

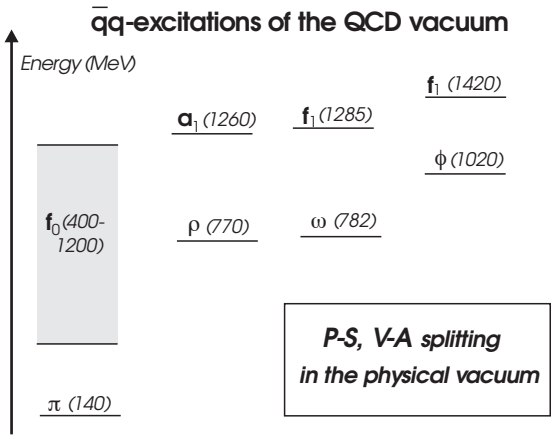

Figure 2.2.: Experimentally observed spectrum of the low-mass mesons. It shows the mass-splitting of scalar and pseudoscalar (P–S), as well as vector and axialvector (V–A) mesons. This figure is taken from [93].

be explained by an instanton induced 't Hooft determinant [90] and is linked (in the large-N_c limit) to the Witten-Veneziano mechanism [91, 92].

The remaining $SU(N_f)_A$ is the chiral symmetry. While it is approximately conserved[5] in the quark-gluon plasma phase, it is spontaneously broken in the hadronic phase at small temperatures and densities, see Fig. 1.1. The spontaneous breakdown of $SU(N_f)$ provides an elegant explanation of the lightest meson masses in the meson spectrum: spontaneous breaking of $SU(3)$ yields eight pseudoscalar[6] Goldstone bosons according to Goldstones theorem [94, 95]. Since chiral symmetry is not exact, these pseudoscalar bosons are rather pseudo-Goldstone bosons with a small mass. They can be identified with the eight lightest particles in the meson spectrum, three pions, four kaons and the eta meson. This explains why these eight pseudoscalar mesons are considerably lighter than the rest of the hadron spectrum. This statement is even stronger in the case of only the lightest two quark flavors, up and down. Spontaneous breaking of $SU(2)_A$ gives rise to three pseudo-Goldstone bosons, the pions, which are by far the lightest hadrons. Within this work, we will concentrate on this two-flavor case.

In addition to the very light pseudoscalar meson octet, chiral symmetry breaking manifests itself in the experimentally observed spectrum of the low-mass mesons via the absence of parity doublets, see Fig. 2.2. If chiral symmetry would hold, we would expect degenerate hadronic isospin doublets of opposite parity. This is clearly not the case, since there is a large mass difference between the mesons in each column of Fig. 2.2, that can not be explained by the small explicit chiral symmetry breaking due to the current quark masses.

Heuristically, on can think of the QCD vacuum at low energies as populated with quark condensates. In this regime, quarks have a strong attractive interaction. Due to their small mass, in particular of the up and down mesons, the energy of creating light quark-antiquark pairs is small. Hence, vacuum fluctuations can create these pairs, which then condense owing to their strong attraction. In a vacuum with zero total and angular

[5] up to small masses in the light quark sector owing to the Higgs mechanism.
[6] The axial vector charge associated to $SU(N_f)_A$ changes sign under parity transormations.

momentum these condensates are given by the *chiral condensate*

$$\langle \bar{q}q \rangle = \langle \bar{q}_L q_R + \bar{q}_R q_L \rangle \,. \tag{2.30}$$

Obviously, this is an order parameter for the chiral phase transition, i.e. $\langle \bar{q}q \rangle \neq 0$ signals chiral symmetry breaking. In terms of a linear sigma model, the chiral condensate (2.30) is proportional to the vacuum expectation value (VEV) of the scalar sigma meson, $\langle \sigma \rangle \propto \langle \bar{q}q \rangle$.

Spontaneous chiral symmetry breaking generates the hadron masses. Put differently, it gives rise to the masses of the constituent quarks, i.e. the effective masses of the valence quarks that are bound into hadrons. In particular for the light quarks (and correspondingly the hadrons they form, e.g. the nucleons), this generates the largest fraction of their mass, see Tab. 2.1. We see that the masses generated through the Higgs mechanism gives only a very small fraction of the total mass of the light quarks in the hadronic regime.

quark flavor	current mass	constituent mass
up	2.3 MeV	336 MeV
down	4.8 MeV	340 MeV
strange	95 MeV	486 MeV
charm	1.28 GeV	1.55 GeV
bottom	4.18 GeV	4.73 GeV
top	173.21 GeV	177 GeV

Table 2.1.: Current and constituent quark masses. The current quark masses are taken from [96]. The exact values of the constituent quark masses are model dependent. We show the values from [97].

Deconfinement. The absence of colored states in the physical spectrum is certainly one of the most characteristic phenomena of the low-energy regime of QCD. This phenomenon is known as confinement. One may define confinement via the statement that asymptotic particle states are always color singlets. However, no rigorous definition of confinement exists, as e.g. the previous statement could equally well be explained by color screening [98]. This is related to the fact that there is still no generally agreed upon explanation for this phenomenon [99].

In the limit of static quarks, i.e. infinitely heavy quarks, deconfinement manifests itself in a linear rising potential $V_{q\bar{q}}(r)$ of static quark and antiquark sources at separation r,

$$\lim_{r\to\infty} V_{q\bar{q}}(r) = \sigma r \,, \tag{2.31}$$

with the string tension σ. This implies a constant force between the quark-antiquark pair and, consequently, an infinite amount of energy to separate them. For finite quark masses, the energy required to create a quark-antiquark pair from the vacuum is finite. In this case, at separation $r \approx 2m_q/\sigma \approx 1\,\text{fm}$ the energy is large enough to create such a pair from the vacuum and the original quark-antiquark pair breaks up into two pairs. This is known as *string breaking*.

Several ideas have emerged that provide promising explanations for different aspects of confinement; for reviews see e.g. [98–103]. In many of these cases, the idea is that the QCD functional integral in the static limit is dominated by a special class of field configurations that causes the expectation value of a large Wilson loop to fall-off exponentially with the area of the loop,

$$\left\langle \mathrm{tr}\left(\mathscr{P} e^{i \oint_c dx_\mu A_\mu} \right) \right\rangle \sim e^{-\sigma F(C)} , \tag{2.32}$$

with the area $F(C)$ of the contour C and path ordering denoted by $\mathscr{P}$. For large loops, this behavior implies a linear static potential. Promising candidates for these configurations are magnetic monopoles [104, 105] and center vortices [106–108].

The infrared-behavior of the gluon and ghost propagators of pure Yang-Mills theory play a crucial role in the confinement scenarios by Kugo-Ojima [109] and Gribov-Zwanziger [77, 78, 110, 111]. The former essentially relies on the existence of a global color charge and the conservation of BRST charge, which are then used to construct the physical Hilbert space in a similar way as the Gupta-Bleuler formalism for Abelian gauge theories. The absence of color-charged particles in the physical state space requires that the gluon propagator is at least finite at vanishing momentum. i.e. develops a mass gap, and the ghost propagator is enhanced, i.e. it diverges faster than the simple p^{-2} pole for $p \to 0$ in Landau gauge.

The confinement scenario by Gribov and Zwanziger relies on the condition that, in Coulomb gauge, the Fadeev-Popov operator (2.14) has only positive eigenvalues. This restricts the allowed gauge field configurations to a so-called Gribov-region, whose boundary, the Gribov-horizon, is characterized by a zero eigenvalue of the Fadeev-Popov operator. Since the configuration space is very large, it is reasonable to assume that the bulk of the configurations is located in the vicinity of the boundary. At large distances, the Coulomb energy of a static quark depends on the inverse of the Fadeev-Popov operator. Thus, a large density of gauge field configurations close to the Gribov-horizon can lead to a confining potential. It can even be shown that confinement in Coulomb gauge is a necessary condition for confinement [112]. This scenario requires the ghost propagator to be IR enhanced, as in the Kugo-Ojima scenario, and the gluon propagator to vanish at zero momentum. Note that a vanishing gluon propagator violates the Osterwalder-Schrader axiom of reflection positivity [113, 114] and therefore implies confinement.

A rather intuitive order parameter for the confinement-deconfinement transition is given by the Polyakov loop [115], which is a temporal Wilson loop with periodic boundary conditions, i.e. at finite temperature T,

$$L(\vec{x}) = \frac{1}{N_c} \mathrm{tr}\, \mathscr{P} e^{ig \int_0^\beta dx_0 A_0(x)} . \tag{2.33}$$

The trace is in the fundamental representation and $\beta = 1/T$. The expectation value of the Polyakov loop is related to the free energy F_q of a static quark [14],

$$\langle L \rangle = e^{-\beta F_q} . \tag{2.34}$$

As discussed above, isolating a single static quark in the confined phase needs an infinite amount of energy. Thus, F_q is infinite and $\langle L \rangle = 0$. In the deconfined phase, on the other hand, the free energy of an isolated quark is finite and hence $\langle L \rangle \neq 0$.

There is also a global symmetry associated to the deconfinement transition in the static limit of QCD, the *center symmetry* [106]. The Euclidean action of $SU(N_c)$ Yang-Mills theory at finite temperature is invariant under topological non-trivial gauge transformations characterized by

$$\mathcal{U}(\vec{x}, x_0 + \beta) = z_n \mathcal{U}(\vec{x}, x_0), \tag{2.35}$$

where z_n is an element of the center[7] $\mathbb{Z}_{N_c}$ of the gauge group. The Polyakov loop, albeit being a gauge invariant object, is not invariant under center transformations; under (2.35) it transforms as $L \to z_n L$. Thus, if center symmetry holds, $\langle L \rangle$ has to vanish and the system is in the confined phase. Deconfinement is characterized by broken center symmetry.

Dynamical quarks explicitly break center symmetry. As discussed above, there is also no area law for the Wilson loop and string breaking prevents the potential $V_{q\bar{q}}(r)$ from developing a linear behavior at large r. Thus, much like in the case of the chiral transition, the deconfinement transition is not a real phase transition, since confinement is only well-defined in the limit of infinitely heavy quarks.

We see that the most prominent phases of QCD are only well-defined in opposite limits of the theory: while chiral symmetry holds only in the limit of massless quarks, confinement is only well-defined for infinitely heavy quarks. Furthermore, at first sight it seems that these phase transitions are driven by completely different sectors of the theory. Matter fluctuations essentially trigger chiral symmetry breaking, while gauge dynamics lead to confinement. It is therefore no surprise that a connection between those very different phases is far from obvious. Above all, both transitions are crossovers in QCD (at least at small density), so e.g. the coincidence of both phase boundaries can not be proven, as there is no strict definition of the transition temperature in the first place. But still, there many reasons to believe that there is indeed a connection between them, at least for some regions in the phase diagram. Heuristically, the fact that the strong quark self-interactions that trigger chiral symmetry breaking are also driven by the gauge sector[8] already hints at a deeper connection between chiral symmetry breaking and confinement.

At small chemical potential lattice simulations show that both phase transitions coincide within the error [17, 18, 25–30]. In the large N_c limit, it was demonstrated that the chiral and deconfinement transition lines split at large chemical potential, resulting in a *quarkyonic* phase, characterized by a pressure $\sim N_c$ [116][9]. It is still confined, but the fate of chiral symmetry is still unclear [48]. A connection between the chiral and deconfinement transition can also be established via the spectrum of the Dirac operator [117, 118]. Furthermore, the results of functional continuum methods suggest that both transition are closely linked, also at large densities [44, 45, 119].

2.4. Mechanism of Chiral Symmetry Breaking

In the previous discussion, we mentioned that chiral symmetry breaking, although seemingly a phenomenon of the matter sector of QCD, is triggered by the strong gauge coupling. Here

[7] The center of a group is given by the set of elements that commute with every element of the group. For $SU(N)$ the center elements are given by $z_n = \exp\left(\frac{2\pi i n}{N}\right) \in \mathbb{Z}_N$ with $n \in \{1, \ldots, N-1\}$.

[8] We elaborate on this point in the next section.

[9] The hadronic phase contains only color-singlets, so the pressure scales as N_c^0. At large temperatures gluons in the adjoint representation deconfine, resulting in a pressure $\sim N_c^2$.

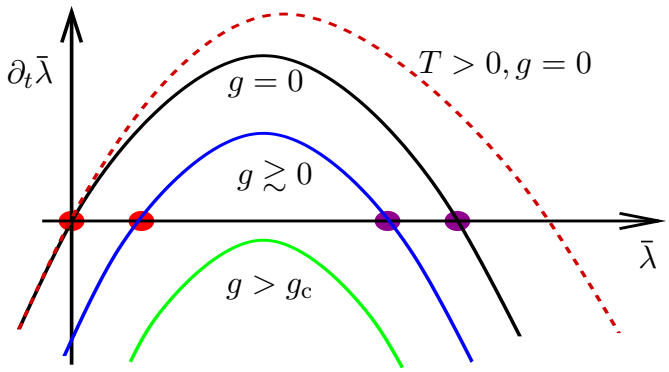

Figure 2.3.: Flow of the four-quark interaction $\bar{\lambda}$ for different values of the strong coupling g (solid lines). The dashed line shows the effect of finite temperature. This figure is taken from [121].

we want to elaborate on this mechanism of spontaneous chiral symmetry breaking in QCD. Our reasoning is based on the importance of effective interactions that are generated from quantum fluctuations in QCD. It was put forward in [69, 70, 120, 121]. Heuristically, the idea is the following: effective four-quark interactions are generated from quark-gluon fluctuations and their strength increases with increasing gauge coupling g. At a critical gauge coupling g_c, the four-quark interaction diverges. This divergence, in turn, signals chiral symmetry breaking since it is directly related to the development of a nontrivial minimum in the free energy of the mesons and therefore the formation of a non-vanishing quark condensate (2.30)[10].

We elaborate on this argument in the following. As already mentioned, effective four-quark interactions $\lambda_k (\bar{q} T q)^2$, where T is some tensor, are generated by quark-gluon fluctuations from first principles, e.g. from 1PI "box" diagrams with two-gluon exchange. The index k represents the scale dependence of the running coupling λ_k. The running of the dimensionless coupling $\bar{\lambda}_k = k^2 \lambda_k$ with the energy scale k is generically given by the following beta function:

$$\beta(\bar{\lambda}_k) \equiv k \partial_k \bar{\lambda}_k = 2\bar{\lambda}_k - A\bar{\lambda}_k^2 - B\bar{\lambda}_k g_k^2 - C g_k^4 + (\text{higher orders}), \tag{2.36}$$

with temperature and density dependent positive coefficients A, B and C. The first term in (2.36) is just the running of the coupling due to its dimensionality. In general, there is also an anomalous dimension of the quarks, but it is small in the chirally symmetric regime and can therefore be neglected for the discussion here. Diagrammatically, (2.36) can be written in terms of 1PI diagrams as

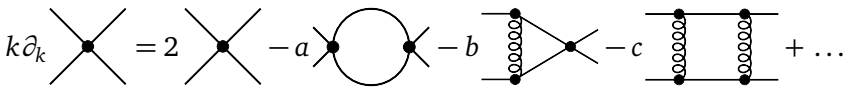

(2.37)

a, b and c are combinatorical prefactors. The box diagram represents the typical contribution, there are of course various different channels. Note that if we use the full propagators and vertices in (2.37), together with appropriate regulator insertions, the diagrams shown above give the full flow equation in terms of the FRG (up to "cross-ladder" diagrams). A schematic plot of $\beta(\bar{\lambda}_k)$ is shown in Fig. 2.3.

[10] In a bosonized formulation, λ_k is proportional to the inverse mass parameter of a Ginzburg-Landau effective potential.

Since the $\beta(\bar{\lambda}_k)$ is quadratic in $\bar{\lambda}_k$ it can exhibit at most two fixed points. At vanishing gauge coupling $g = 0$, i.e. at asymptotically large energies, there is a Gaussian fixed point $\bar{\lambda}_1^\star = 0$ and an interacting fixed point $\bar{\lambda}_1^\star = 2/A$, see the black line in Fig. 2.3. Since $\beta'(\bar{\lambda}_1^\star) > 0$, the Gaussian fixed point is IR-attractive. The interacting fixed point is UV-attractive, since $\beta'(\bar{\lambda}_2^\star) < 0$. Thus, if the system is initially, i.e. at large energy scale Λ, at $0 < \bar{\lambda}_\Lambda < \bar{\lambda}_2^\star$, it will be driven to the Gaussian fixed point, $\bar{\lambda}_k$ remains bounded and chiral symmetry is never broken. Of course, the physically sensible initial value for $\bar{\lambda}_k$ is $\bar{\lambda}_\Lambda = 0$ for $\Lambda \to \infty$. This guarantees that the four-quark coupling is solely generated by quark-gluon dynamics from first principles. Thus, for sufficiently small gauge coupling the system is governed by the Gaussian fixed point, which implies that the quark self-interactions are always RG-irrelevant in this regime, as they should be.

With increasing gauge coupling, both fixed points move closer together and are both interacting, see the blue line in Fig. 2.3. Still, the running of the four-quark interaction is governed by the IR-attractive fixed and chiral symmetry remains intact. When the gauge coupling reaches the critical value $g_c \approx \pi$ (at zero temperature) [70] at sufficiently low scales, both fixed points merge. For $g_k > g_c$ the fixed points vanish and $\beta(\bar{\lambda}_k)$ is always negative, see the green line in Fig. 2.3. This implies that the four-quark coupling is driven to criticality and chiral symmetry will be broken at some small scale k. We see that at large energy scales, where $g_k < g_c$, the running of λ_k is governed by an IR-attractive fixed point. At smaller energy scales, the strong coupling eventually exceeds the critical coupling, the system destabilizes and the four quark coupling diverges. Thus, it is indeed the strong coupling that drives the system towards chiral symmetry breaking.

At finite temperature, quarks acquire a thermal mass which leads to a quark decoupling at $k < T$. As a result, the quark dynamics that drive $\beta(\bar{\lambda}_k)$ to smaller (and eventually negative) values are suppressed and more interaction strength is required to achieve criticality. $\beta(\bar{\lambda}_k)$ gets broader and is shifted to larger positive values, see the dashed red line in Fig. 2.3. This implies that temperature increases the critical coupling. Thus, at temperatures above a critical temperature T_c, the gauge coupling can not become critical and chiral symmetry is preserved.

The requirement $g_k > g_c$ is not sufficient for a realistic picture of chiral symmetry breaking. We know that low energy QCD has a smallest energy scale below which all fluctuations die off. It is given by the mass of the lightest meson in the hadron spectrum, the pion mass $M_\pi \approx 138$ MeV. This scale is dynamically generated from spontaneous chiral symmetry breaking in the first place. Thus, the scale where g_k exceeds g_c must be substantially larger than M_π, since otherwise the system would not have enough "time" to generate realistic hadron masses. It is therefore necessary that g_k exceeds the critical coupling sufficiently early in the RG flow and with enough strength. Put differently, the temperature where g_k only just reaches g_c at some scale can at most be interpreted as an upper bound for the critical temperature [121].

Furthermore, we will demonstrate in Chap. 4 that the gauge couplings, after exceeding the critical coupling at some scale, become subcritical again at lower scales, but chiraly symmetry is nonetheless broken. This implies that it is the area above the critical line that decides on the fate of chiral symmetry. We will elaborate on this in Chap. 4.

CHAPTER 3

The Functional Renormalization Group

As we have seen in Sec. 2.1, the strong coupling rapidly grows towards smaller energy scales and therefore perturbation theory is bound to break down at some point. For a description of the phase structure of QCD and in particular the hadronic regime, non-perturbative methods are indispensable. Inherently non-perturbative first-principle methods are lattice gauge theory, (LGT), Dyson-Schwinger equations (DSE) and the functional renormalization group (FRG). We use the latter method throughout this work and will discuss the details is the next sections. But first, we briefly describe the other two methods mentioned here.

In lattice gauge theory [63–66], spacetime is discretized on a finite lattice. The path integral is then evaluated directly for the remaining finite number of paths using Monte Carlo methods. To date, LGT gives the most reliable results for many aspects of QCD. It provided e.g. the first evidence for the deconfinement transition, established the order of the phase transition as well as its critical temperature at vanishing density and accurately describes the hadron spectrum. Since it relies on statistical sampling methods, it is only applicable in Euclidean spacetime, i.e. non-equilibrium processes are not accessible on the lattice. Furthermore, calculations at finite density are plagued by the infamous sign problem. Lattice calculations are therefore restricted to very small densities, although ways to circumvent this issue are currently subject to very active research. Precise informations about continuum physics require very large/fine lattices. Thus, immense computational effort and power is needed to achieve this. In particular the inclusion of light fermion fields is numerically expensive.

Dyson-Schwinger equations are, as the FRG, a functional continuum method. They are the equations of motion for the Green's functions of the quantum theory. In contrast to LGT, the inclusion of finite density is possible without any restrictions. The full solution of the theory, on the other hand, is impossible and truncation schemes have to be devised. DSE have been used successfully for the description of low-energy QCD, in particular aspects of confinement and the phase structure [71, 101, 102, 122–125].

Alternative ways to address problems concerning the low-energy sector of QCD are effective field theories, such as chiral perturbation theory. The general idea is to describe the physics at a specifically chosen length scale with the appropriate (effective) degrees of freedom at these scales. For instance, chiral perturbation theory describes interactions in terms of pion exchange [126].

3.1. The Idea

The idea of the renormalization group was first introduced by Leo P. Kadanoff in 1966, where he proposed the “block spin” renormalization group [127] in the context of condensed matter physics. The idea and utility of the renormalization group can best be illustrated with systems near a critical point. There, the correlation length ξ is very large and goes to infinity at the critical point. Thus, near the critical point one has fluctuations on all length scales which lead to divergences in the perturbative treatment of the problem. The renormalization group strategy is to divide the full range of fluctuations into subranges of manageable proportions and consider each subrange in sequence. The underlying physical idea is that the many energy or length scales are locally coupled such that fluctuations at a certain scale are primarily affected by fluctuations in the vicinity of this scale. This leads to a cascade effect in the whole system: The short range fluctuations with high energy influence the fluctuations with a little less energy and they influence the fluctuations with lesser energy and so forth. This can be used to effectively reduce the degrees of freedom by successively integrating out fluctuations, starting from small length scales.

We employ the RG idea due to Kenneth Wilson, which is based on the functional formulation of QFT. These ideas are reviewed in [128, 129]. What we said before can be easily transferred, at least in principle, to the path integral. We consider the generating functional in Euclidean space with the fields in momentum space and introduce an UV-cutoff Λ. Starting at Λ with the action that contains the bare parameters of the theory, we integrate out all fields with momenta lying in a small momentum shell $|p| \in [s\Lambda\,, \Lambda]$ with a scale parameter $s < 1$. This integration gives corrections to the original action, which change the original couplings and effectively introduce new couplings. If we rescale the momenta $p' = p/s$ and the fields such that the "new" action gives a propagator of exactly the same form as the initial action, we can view this transformation as a map from the original set of couplings we started with at Λ to a new set of couplings at the scale $s\Lambda$, which contains modified versions of the original couplings as well as new couplings. Repeating this procedure successively will in principle generate all possible interactions of the fields and their derivatives, even higher dimensional interactions which are not perturbatively renormalizable. Since in general every integration step introduces new couplings and modifies the old ones, the couplings are now scale dependent. If we take the scale parameter s to be infinitesimally close to 1, the successive integration of momentum shells from high to low momenta is a continuous transformation and we can interpret the corresponding change of the parameters of the theory as a trajectory or *flow* in the space of all possible Lagrangians, the *theory space*. We note that the fact that degrees of freedom are successively integrated out implies that the renormalization group is not a group, because it has no inverse. Once we integrated out a momentum shell, the detailed information about this scale is lost and effectively stored in the new couplings. This procedure can therefore be thought of as a *coarse-graining*.

The fact that non-renormalizable couplings will be generated by the flow turns out to be in no contradiction to what we know from pertubation theory. Non-renormalizable couplings are *irrelevant* directions in the flow, which means they die away if we further integrate out momentum shells. Those couplings that grow during the flow are called *relevant* and the ones that neither increase nor decrease are called *marginal*. They correspond to super-renormalizable and renormalizable couplings.

3.2. FRG with Scale Dependent Fields

The functional renormalization group is a practical incarnation of Wilson's RG idea. It was introduced in 1992 by Christof Wetterich [130]. The central object is the scale dependent effective action Γ_k. k is the RG scale which tells us down to which scale momentum shells have been integrated out. It can be thought of as an IR-cutoff scale. At large UV-cutoff scales $k = \Lambda$, the scale dependent effective action corresponds to the classical action S, i.e. without any fluctuations taken into account. The full quantum theory including fluctuations on all scales is approached at $k = 0$, where the scale dependent effective action coincides with the full quantum effective action Γ, to wit

$$\Gamma_{k\to\Lambda} \to S\,, \qquad \Gamma_{k\to 0} \to \Gamma\,. \tag{3.1}$$

Thus, by lowering k we resolve the microscopic properties of the system and Γ_k interpolates smoothly between the classical and the full quantum theory. Γ_k is therefore a generalization of the generating functional of one-particle irreducible (1PI) Green's functions. The FRG provides a functional differential equation, the *flow equation* (or Wetterich equation), that captures the Wilsonian shell-by-shell integration and describes the RG flow of Γ_k. It has been applied successfully to a variety of different problems, ranging from ultracold atoms [131], condensed matter physics [132] and gauge theories [133–135], to quantum gravity [136–138]. For reviews related to QCD see [75, 133–135, 139–143].

In QCD, as in many other theories, vastly different degrees of freedom are relevant at different energy scales. For a complete description of QCD, both, quark-gluon degrees of freedom need to be captured at large energy scales and hadrons at low energies. Thus, we need to be able to account for the dynamical transition between these different degrees of freedom. In this sense, one can think of the fields as being RG-scale dependent. In particular composite particles such as the hadrons can be thought of as naturally scale dependent: At large energy scales they are not present. At smaller energy scales, the strong attractive interaction tends to bind quarks and finally confines them into hadrons at small k. Guided by this idea, we will generally assume that all fields are scale dependent[1]. This was put forward in [69, 70, 139, 144]. We will specify the scale dependence of the fields in the following chapters when we apply these ideas to QCD. Here, we will derive the flow equation in the presence of scale dependent fields based on [139].

We work with the generalized quantum field $\tilde{\Phi}_{\mathbf{a}}$, which contains all bosonic and fermionic fields of the theory. The bold index includes both discrete (color, flavor etc.) and continuous (spacetime) indices as well as field-space indices. Summation/integration over repeated indices is implied. Raising and lowering bold indices is done with the non-trivial metric in field-space, $\gamma^{\mathbf{ab}}$, which takes the Grassman nature of fermion fields into account. It is specified in App. A. For gauge fixed QCD, we have for instance $\tilde{\Phi}_{\mathbf{a}} = (\tilde{\phi}, \tilde{q}, \tilde{\bar{q}}, \tilde{A}, \tilde{c}, \tilde{\bar{c}})^T$, where $\tilde{\phi}$ can contain various meson fields of different spin and $\tilde{q}$ in principle includes quarks and nucleons. In addition, we also consider the scale dependent field $\tilde{\Phi}_{k,\mathbf{a}}[\tilde{\Phi}]$ which is a priori an arbitrary functional of the scale-independent fields.

The starting point is the IR-regulated scale dependent Schwinger functional[2]:

$$W_k[J] = \log \int \mathscr{D}\tilde{\Phi} \exp\left\{-S[\tilde{\Phi}] - \Delta S_k[\tilde{\Phi}_k] + J^{\mathbf{a}}\tilde{\Phi}_{k,\mathbf{a}}\right\}, \tag{3.2}$$

[1] This is also useful for the case of scale dependent field reparameterizations.
[2] The Schwinger functional is the generating functional of connected correlators.

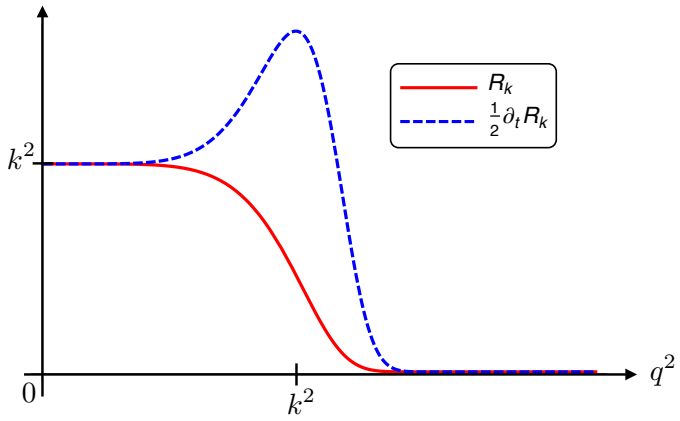

Figure 3.1.: Plot of a typical regulator $R_k(q^2)$ and its scale derivative $\frac{1}{2}\partial_t R_k(q^2)$ at a fixed RG scale k. R_k acts as mass-like IR cutoff as it enters the denominator of the full propagators, see (3.13), and thus cuts-off fluctuations at $q^2 < k^2$. The scale derivative $\partial_t R_k$ ensures the shell-wise integration of fluctuations and guarantees UV regularity of the flow.

with the sources for the scale dependent fields $J_{\mathbf{a}}$, e.g. for QCD, $J_{\mathbf{a}} = (j_\phi, \eta, \bar{\eta}, j_A, \eta_c, \bar{\eta}_c)^T$. The cutoff term ΔS_k has been inserted to regularize the IR regime in a mass-like fashion:

$$\Delta S_k\big[\tilde{\Phi}_k[\tilde{\Phi}]\big] = \frac{1}{2}\tilde{\Phi}_{k,\mathbf{a}} R_k^{\mathbf{ba}} \tilde{\Phi}_{k,\mathbf{b}}\,,. \tag{3.3}$$

For a single scalar field φ in d spacetime dimensions, for instance, this term reads in momentum space

$$\Delta S_k[\varphi] = \frac{1}{2}\int \frac{d^d p}{(2\pi)^d}\varphi(-q)R_k(q)\varphi(q)\,. \tag{3.4}$$

The requirement to recover the classical theory at $k\to\infty$ and the full quantum theory at $k\to 0$, the regulator R_k has to fulfill the following conditions at fixed momentum q^2:

$$R_{k\to\infty} \to \infty\,, \qquad R_{k\to 0} \to 0\,. \tag{3.5}$$

The regulator suppresses momentum modes $q^2 \lesssim k^2$ by adding a mass $\sim k^2$ in this regime. The high momentum modes remain unaffected. This is achieved by demanding

$$R_k(q)\big|_{q^2<k^2} \sim k^2\,, \qquad R_k(q)\big|_{q^2>k^2} = 0\,. \tag{3.6}$$

Thus, at scales $q^2 < k^2$ the fields acquire masses $\sim k^2$, which suppresses their fluctuations and they effectively decouple from the dynamics of the system. By lowering k, we therefore successively integrate out fluctuations. The regulator therefore implements the coarse-graining discussed above. Fig. 3.1 shows a typical regulator as a function of the momentum q^2 at fixed scale k.

With such a mass-like regulator in the theory, special attention has to be payed concerning the symmetries of the theory. In particular condition (3.6) may cause problems in gauge theories, since such a mass term explicitly breaks gauge invariance. But as we have discussed in Sec. 2.1, we need to fix the gauge anyway, so the presence of the regulator is just an additional source

of explicit breaking of gauge invariance. Gauge invariance is then encoded in Slavnov-Taylor identities and one gets modifications of these identities in the presence of the cutoff [145–147].

To arrive at an RG equation, we need to study how the theory changes under variations of the cutoff. We could do this directly with the Schwinger functional, but it is much more convenient to formulate the RG equations in terms of the effective action. To this end, we define the scale dependent effective action Γ_k as the modified Legendre transformation of W_k,

$$\Gamma_k[\Phi_k] + \Delta R_k[\Phi_k] = \sup_J \Big(J^{\mathbf{a}} \Phi_{k,\mathbf{a}} - W_k[J] \Big) . \tag{3.7}$$

The fields without the tilde denote the mean-fields,

$$\Phi = \langle \tilde{\Phi} \rangle . \tag{3.8}$$

In the following, we will always use the sources J at which (3.7) is at the supremum. Note that J is a function of k in this case. (3.7) implies:

$$\frac{\delta(\Gamma_k + \Delta R_k)}{\delta \Phi_{k,\mathbf{a}}} = \gamma^{\mathbf{a}}{}_{\mathbf{b}} J^{\mathbf{b}} . \tag{3.9}$$

Thus, from

$$\frac{\delta(\Gamma_k + \Delta R_k)}{\delta \Phi_{k,\mathbf{a}}} \frac{\delta W_k}{\delta J^{\mathbf{a}}} = \gamma^{\mathbf{a}}{}_{\mathbf{b}} J^{\mathbf{b}} \tilde{\Phi}_{k,\mathbf{a}} \tag{3.10}$$

one can easily derive

$$\frac{\delta^2(\Gamma_k + \Delta R_k)}{\delta \Phi_{k,\mathbf{d}} \delta \Phi_{k,\mathbf{a}}} \frac{\delta^2 W_k}{\delta J^{\mathbf{a}} \delta J^{\mathbf{c}}} = \gamma^{\mathbf{d}}{}_{\mathbf{c}} . \tag{3.11}$$

Since the Schwinger functional generates connected correlators, we define the connected two-point function for the hadronization field:

$$G_{k,\mathbf{ab}} = \frac{\delta^2 W_k}{\delta J^{\mathbf{a}} \delta J^{\mathbf{b}}} = \langle \tilde{\Phi}_{k,\mathbf{b}} \tilde{\Phi}_{k,\mathbf{a}} \rangle_c . \tag{3.12}$$

Now, we can rewrite (3.11) accordingly and find:

$$G_{k,\mathbf{ab}} = (\Gamma_k^{(2)} + R_k)^{-1}_{\mathbf{ac}} \gamma^{\mathbf{c}}{}_{\mathbf{b}} , \tag{3.13}$$

where we defined

$$(\Gamma_k^{(2)} + R_k)^{-1}_{\mathbf{ac}} = \left(\frac{\delta^2(\Gamma_k + \Delta R_k)}{\delta \Phi_{k,\mathbf{a}} \delta \Phi_{k,\mathbf{c}}} \right)^{-1} . \tag{3.14}$$

The scale derivative of the Schwinger functional (3.2) yields:

$$\begin{aligned} \partial_t W_k[J] &= J^{\mathbf{a}} \langle \partial_t \tilde{\Phi}_{k,\mathbf{a}} \rangle - \frac{1}{2} \partial_t R_k^{\mathbf{ba}} \langle \tilde{\Phi}_{k,\mathbf{a}} \tilde{\Phi}_{k,\mathbf{b}} \rangle - R_k^{\mathbf{ba}} \langle \tilde{\Phi}_{k,\mathbf{a}} \partial_t \tilde{\Phi}_{k,\mathbf{b}} \rangle \\ &= J^{\mathbf{a}} \langle \partial_t \tilde{\Phi}_{k,\mathbf{a}} \rangle - \frac{1}{2} \partial_t R_k^{\mathbf{ba}} G_{k,\mathbf{ba}} - \frac{1}{2} \partial_t R_k^{\mathbf{ba}} \Phi_{k,\mathbf{a}} \Phi_{k,\mathbf{b}} - R_k^{\mathbf{ba}} \frac{\delta}{\delta J^{\mathbf{a}}} \langle \partial_t \tilde{\Phi}_{k,\mathbf{b}} \rangle \\ &\quad - R_k^{\mathbf{ba}} \Phi_{k,\mathbf{a}} \langle \partial_t \tilde{\Phi}_{k,\mathbf{a}} \rangle , \end{aligned} \tag{3.15}$$

where we used the definition of the connected two-point function,

$$G_{k,\mathbf{ba}} = \langle \tilde{\Phi}_{k,\mathbf{a}} \tilde{\Phi}_{k,\mathbf{b}} \rangle - \Phi_{k,\mathbf{a}} \Phi_{k,\mathbf{b}} \,, \tag{3.16}$$

and the identity

$$\langle \tilde{\Phi}_{k,\mathbf{a}} \mathscr{O} \rangle = \left(\frac{\delta}{\delta J^{\mathbf{a}}} + \Phi_{k,\mathbf{a}} \right) \langle \mathscr{O} \rangle \,. \tag{3.17}$$

The scale derivative of Γ_k can be extracted from (3.7):

$$\begin{aligned} &\partial_t \big|_\Phi \Gamma_k + \frac{\delta \Gamma_k}{\delta \Phi_{k,\mathbf{a}}} \partial_t \Phi_{k,\mathbf{a}} \\ &\quad = \partial_t J^{\mathbf{a}} \Phi_{k,\mathbf{a}} + J^{\mathbf{a}} \partial_t \Phi_{k,\mathbf{a}} - \partial_t \big|_J W_k - \partial_t J^{\mathbf{a}} \frac{\delta W_k}{\delta J^{\mathbf{a}}} - \frac{1}{2} \partial_t R_k^{\mathbf{ba}} \Phi_{k,\mathbf{a}} \Phi_{k,\mathbf{b}} - R_k^{\mathbf{ba}} \Phi_{k,\mathbf{a}} \partial_t \Phi_{k,\mathbf{b}} \\ &\quad = J^{\mathbf{a}} \partial_t \Phi_{k,\mathbf{a}} - J^{\mathbf{a}} \langle \partial_t \tilde{\Phi}_{k,\mathbf{a}} \rangle + \frac{1}{2} \partial_t R_k^{\mathbf{ba}} G_{k,\mathbf{ba}} + R_k^{\mathbf{ba}} \frac{\delta}{\delta J^{\mathbf{a}}} \langle \partial_t \tilde{\Phi}_{k,\mathbf{b}} \rangle - R_k^{\mathbf{ba}} \Phi_{k,\mathbf{a}} \partial_t \Phi_{k,\mathbf{b}} \\ &\qquad + R_k^{\mathbf{ba}} \Phi_{k,\mathbf{a}} \langle \partial_t \tilde{\Phi}_{k,\mathbf{a}} \rangle \,, \end{aligned} \tag{3.18}$$

where we used $\frac{\delta W_k}{\delta J^{\mathbf{a}}} = \Phi_{k,\mathbf{a}}$ and replaced $\partial_t|_J W_k$ by (3.15).

Until now, we only used that the fields are scale dependent, but made no assumption about the actual form of this dependence. Its precise form can be chosen freely and only depends on the physical situation under consideration. To proceed, we will now make the following assumption about the scale dependence:

$$\langle \partial_t \tilde{\Phi}_{k,\mathbf{a}} \rangle = \dot{\mathbf{A}}_k^{\mathbf{a}} F_{\mathbf{a}}[\Phi_k] \,. \tag{3.19}$$

$\dot{\mathbf{A}}_k$ encodes the scale dependence of the field in terms of running couplings and $F_{\mathbf{a}}[\Phi]$ is an arbitrary functional of the scale-dependent mean-fields Φ_k. Thus, we assume that the flow of the quantum field $\tilde{\Phi}_k$ is given solely in terms of the mean fields Φ_k. This seems like a severe restriction on the scale dependence of the quantum fields. However, we will work exclusively in terms of the effective action in the following and therefore only consider mean fields in the first place. This choice implies in particular:

$$\langle \partial_t \tilde{\Phi}_{k,\mathbf{a}} \rangle = \partial_t \Phi_{k,\mathbf{a}} \,. \tag{3.20}$$

With this, and the use of the identity $\frac{\delta}{\delta J^{\mathbf{a}}} = G_{k,\mathbf{ba}} \frac{\delta}{\delta \Phi_{k,\mathbf{b}}}$, we finally arrive at the modified Wetterich equation for the scale dependent effective action,

$$\partial_t \big|_\Phi \Gamma_k = \frac{1}{2} \partial_t R_k^{\mathbf{ba}} G_{k,\mathbf{ba}} + R_k^{\mathbf{ba}} G_{k,\mathbf{ca}} \frac{\delta \partial_t \Phi_{k,\mathbf{b}}}{\delta \Phi_{k,\mathbf{c}}} - \frac{\delta \Gamma_k}{\delta \Phi_{k,\mathbf{a}}} \partial_t \Phi_{k,\mathbf{a}} \,. \tag{3.21}$$

The first term is the original Wetterich equation for fixed Φ_k, the second terms takes the field dependence of the flow of the fields into account and the third term reflects the scale dependence of the function $\dot{\mathbf{A}}_k$ from (3.19). Thus, for $\partial_t \Phi_k = 0$ we recover the original Wetterich equation. The flow of the effective action is depicted in Fig. 3.2.

Let us give some remarks on the properties of the flow equation:

Truncation. In principle every possible term that respects the symmetries of the theory can be generated during the RG flow. Thus, in order to describe the full theory, we would

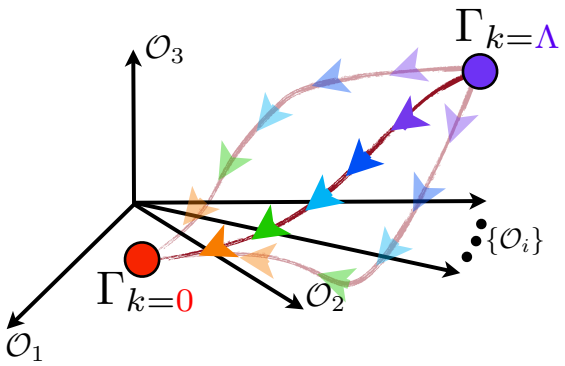

Figure 3.2.: The flow equation (3.21) describes the trajectory of Γ_k from the classical action at $k=\Lambda$ to the full quantum effective action at $k=0$ in theory space, i.e. the infinite dimensional space spanned by all possible couplings/operators of a given theory. Truncating Γ_k amounts to restricting the flow to a (finite dimensional) subspace of the full theory space. The trajectory in theory space therefore depends on the truncation scheme. The same holds for the regularization scheme. Yet, for truncations that capture all the relevant physics of the system, the $k \to 0$ limit should be unique. The picture is taken from [148].

have to include every possible operator in the effective action. This would lead to an infinite tower of coupled functional differential equations, which is certainly impossible to solve. We therefore need a truncation scheme to reduce the number of equations to a manageable size, i.e. we need to restrict ourselves to a subspace of the full theory space. On the other hand, the truncation should describe the theory as good as possible; all relevant dynamics should be incorporated so that neglected terms have only a small effect. Thus, truncations have to be devised based on physical insights. Furthermore, by systematically enlarging a truncation, we can give error estimates and gain insights on relevant and irrelevant effects in a theory.

There are several approaches to non-perturbative approximations, such as the derivative expansion, which is an expansions in the number of derivatives, or the vertex expansion, where one expands Γ_k in n-point functions $\Gamma_k^{(n)}$. Which approximation is suited for a problem depends on the information we want to extract. If we are interested in high momentum modes for example, the derivative expansion would be a bad choice, as it is a small momentum expansion by definition.

One-loop structure. The flow equation is basically the trace over the full field dependent propagator with a regulator insertion. It therefore has a simple graphical representation:

$$\partial_t \Gamma_k = \frac{1}{2}$$

The line with the black dot represents the full propagator and the crossed circle depicts the regulator insertion $\partial_t R_k$. The flow equation is an exact one-loop equation. The price to pay is that propagators and vertices are always those of the full theory, i.e. the dressed propagators and vertices. This one-loop structure is a consequence of the IR cutoff term ΔS_k being quadratic in the fields, see (3.3).

Note however, that the assumption of scale dependent fields essentially implies that $\Phi_k = \Phi_k[\Phi]$, which is in principle an arbitrary non-linear k-dependent map from the fields Φ to Φ_k. Thus, the second term in the modified flow equation (3.21), which accounts for this field dependence, can potentially spoil the one-loop structure of the flow. While this is not a conceptual problem, it may drastically complicate the quest for quantitative precision. To avoid this, we need to restrict the scale dependence of the fields such, that the flow is at most linear in the field itself. This restriction is sufficient since the flow is diagonal in field space. Thus, the second term in (3.21) is only non-zero if the flow of a specific field depends on this field itself. If we restrict this dependence to linear order at most, one can think of the second term in (3.21) as a k-dependent shift of the scale derivative of the regulator in the firs term of (3.21).

Connection to Wilson's RG idea. The full propagator is multiplied by the scale derivative of the regulator $\partial_t R_k$, which is peaked about $q^2 = k^2$, see Fig. 3.1. Furthermore, fluctuations are suppressed for $q^2 \lesssim k^2$ owing to the regulator in (3.12) and the flow is cut-off for $q^2 \gtrsim k^2$ owing to $\partial_t R_k$ in (3.21). This implements Wilson's RG idea of successively integrating out degrees of freedom: in order to to solve the flow equation, we need to integrate it from the UV cutoff scale $k = \Lambda$ down to $k = 0$ and the regulator and its scale derivative ensure that only a thin momentum shell is integrated out at every infinitesimal RG step. Furthermore, no information about the short distance physics is lost as k is lowered, because the flowing action at high momentum scales already contains all operators.

Regularity. IR regularity of the flow is guaranteed by construction. In the final flow equation, this becomes apparent by looking at the full propagator (3.12): R_k enters the denominator and, owing to its property (3.6), suppresses fluctuations for $q^2 < k^2$. The scale derivative $\partial_t R_k$ in (3.21) vanishes for $q^2 \gtrsim k^2$, see Fig. 3.1. Thus, the flow is zero for these momenta and UV regularity is also guaranteed.

3.3. Regularization Scheme

An integral ingredient of the functional renormalization group is the regulator R_k. In principle, every regulator that satisfies the conditions (3.5) and (3.5) is sufficient to formally arrive at the exact flow equation (3.21). If a truncation of the effective action would not be necessary, the regulator choice would not matter either. However, truncations are impossible to avoid for almost every physical system. This in general results in unphysical regulator dependencies. Truncation schemes should therefore be accompanied by criteria for appropriate choices for regulators, e.g. to minimize the regulator dependence of the results or to improve the convergence of the truncation. Furthermore, the (numerical) stability of the flow equations can drastically depend on the regulator choice. Thus, regulators can even be used to improve a truncation and should therefore be regarded as an important part of the truncation scheme.

In [139] general optimization criteria are developed and discussed in great detail and we refer to this work for further details. We will only outline the "stability criterion" put forward in [149, 150], since we will use the resulting regulators throughout this work. This constructive criterion is based on maximal stability and quickest convergence of the flow. A systematic expansion of the truncation involves an expansion in powers of the propagator $G_k(q) = 1/\left(\Gamma_k^{(2)}(q) + R_k(q)\right)$. Hence, minimizing G_k with respect to an appropriate norm relates to the optimization of both, stability and convergence. Stability of the flow is guaranteed as

long as the regularized propagator G_k displays a gap,

$$\min_{q^2\geq 0}\left[\Gamma_k^{(2)}(q)\big|_{\phi=\phi_0}+R_k(q)\right]=Ck^2>0\,. \tag{3.22}$$

A natural choice for ϕ_0 is e.g. the expansion point of an expansion in the powers of fields or the field maximizing an appropriate norm of G_k. Maximizing C is equivalent to minimizing G_k and hence ensuring fastest convergence of a systematic expansion of the truncation. Thus, following these arguments, the optimal regulator is defined by the criterion

$$\max_{R_k}\left(\min_{q^2\geq 0} G_k^{-1}\big|_{\phi=\phi_0}\right). \tag{3.23}$$

A solution to this criterion, which also leads to simple expressions of the flow equations is given by

$$R_k^{(B/F)}(q)=K(q)\,r_{B/F}(q^2/k^2)\,, \tag{3.24}$$

where $K(q)$ reflects the momentum and tensor structure of the kinetic term of the action and the optimized regulator shape functions for bosons and fermions $r_{B/F}$ are given by

$$\begin{aligned} r_B(x)&=\left(\frac{1}{x}-1\right)\Theta(1-x)\\ r_F(x)&=\left(\frac{1}{\sqrt{x}}-1\right)\Theta(1-x)\,, \end{aligned} \tag{3.25}$$

with the Heaviside theta function Θ. These are the optimized regulators for a leading order derivative expansion and we will use them throughout this work. The optimization criterion given above can be generalized, which allows for the construction of optimized regulators for higher orders in the derivative expansion [139].

The coefficient $K(q)$ in (3.24) can be obtained from the two-point functions:

$$K(q)=\Gamma_k^{(2)}(q)-\Gamma_k^{(2)}(0)\,. \tag{3.26}$$

With this choice, the inverse propagator is of the form

$$G_k^{-1}(p)=\left(\Gamma_k^{(2)}(q)-\Gamma_k^{(2)}(0)\right)\left(1+r(q^2/k^2)\right)+\Gamma_k^{(2)}(0)\,. \tag{3.27}$$

Thus, the regulator only acts on the kinetic part of the propagator and leaves the gap $\Gamma_k^{(2)}(0)$ unaffected. This ensures a "clean" coarse-graining in momentum space. Furthermore, this allows us to define RG-invariant scale dependent propagators G_k in the presence of a gap, which leads to particularly simple flow equations. As a consequence, as we will see explicitly later, the flow equations will only depend on the anomalous dimensions of the renormalized fields, but not on their wave function renormalizations themselves.

3.4. The Fixed Background Taylor Expansion

In this section we want to discuss the truncation scheme we primarily employ in this work. We will always restrict ourselves to small momenta and therefore use a low-order derivative expansion. To lowest order, this entails that the effective action contains the kinetic terms of the

fields and the effective potential. This is known as the *local potential approximation* (LPA) and is widely used in the literature owing to its simplicity. Yet, a lot of physical information is stored in the effective potential and therefore the LPA is often sufficient to capture the qualitative features of a theory. A big part of this work is to study QCD beyond LPA.

For illustration purposes in this section, we will consider the two-flavor quark-meson (QM) model. It is an effective model that captures the basic chiral dynamics of low-energy QCD [135, 151]. In the LPA, the QM model for two-flavor QCD at finite temperature and quark chemical potential is

$$\Gamma_k = \int_0^\beta dx_0 \int_{\vec{x}} \left\{ i\,\bar{q}(\gamma_\mu \partial_\mu + \gamma_0 \mu) q + \frac{1}{2}(\partial_\mu \phi)^2 + V_k(\rho) - c\sigma + h\,\bar{q}(\gamma_5 \vec{\tau}\vec{\pi} + i\sigma) q \right\}. \tag{3.28}$$

As already mentioned, the quarks come in two flavors, $q = (u,d)^T$, the mesons are in the $O(4)$ representation $\phi = (\sigma, \vec{\pi})^T$ and $\rho = \phi^2/2$. We use Hermitian gamma matrices, so that $\{\gamma_\mu, \gamma_\nu\} = 2\delta_{\mu\nu}\mathbb{1}$ and $\vec{\tau}$ are the Pauli matrices . The field-independent Yukawa coupling h connects the quark and meson sectors. We added the source term $c\sigma$ to account for finite quark masses. We will elaborate on this truncation in the next chapter. Here, we use it only to make our arguments more explicit.

The only running quantity in (3.28) is the effective potential $V_k(\rho)$. It is an arbitrary function of the $O(4)$-invariant ρ and therefore contains arbitrary powers of meson-meson interactions. The flow of V_k is a partial differential equation which reads with the optimized regulator discussed in Sec. 3.3

$$\begin{aligned} \partial_t V_k(\rho) = \frac{k^5}{12\pi^2} \Bigg\{ & \frac{3}{E_\pi} \coth\left(\frac{E_\pi}{2T}\right) + \frac{1}{E_\sigma} \coth\left(\frac{E_\sigma}{2T}\right) \\ & - \frac{12}{E_q}\left[\tanh\left(\frac{E_q - \mu}{2T}\right) + \tanh\left(\frac{E_q + \mu}{2T}\right)\right]\Bigg\}, \end{aligned} \tag{3.29}$$

where the pion-, sigma- and quark-energies are defined as

$$\begin{aligned} E_\pi &= \sqrt{k^2 + V_k'(\rho)} \\ E_\sigma &= \sqrt{k^2 + V_k'(\rho) + 2\rho V_k''(\rho)} \\ E_q &= \sqrt{k^2 + V_k'(\rho) + 2h\rho}\,. \end{aligned} \tag{3.30}$$

There are now various possibilities to solve (3.29) related to expansion schemes of the effective potential V_k. Most expansion schemes in the literature are either based on a discretization of the effective potential in field-space ("grid method") or a Taylor expansion about the scale dependent minimum $\rho_{0,k}$ of the effective potential ("comoving expansion"). The latter approach is very efficient for low-order truncations with many different interaction channels and has been proven to be very successful e.g. at the description of critical phenomena (see e.g. [152]). The former gives a very detailed global picture of the effective potential and is therefore well suited to study first order phase transitions, see e.g. [151].

While the grid method provides the most accurate global information about the exact form of the effective potential, it is numerically rather involved. Furthermore, going beyond LPA consistently is quite laborious. Within this work, we will therefore resort to a Taylor expansion of the effective potential. Most commonly used in the literature is the expansion about the minimum of the effective potential $\phi_{0,k}$, i.e. the soltution to the quantum equation of motion

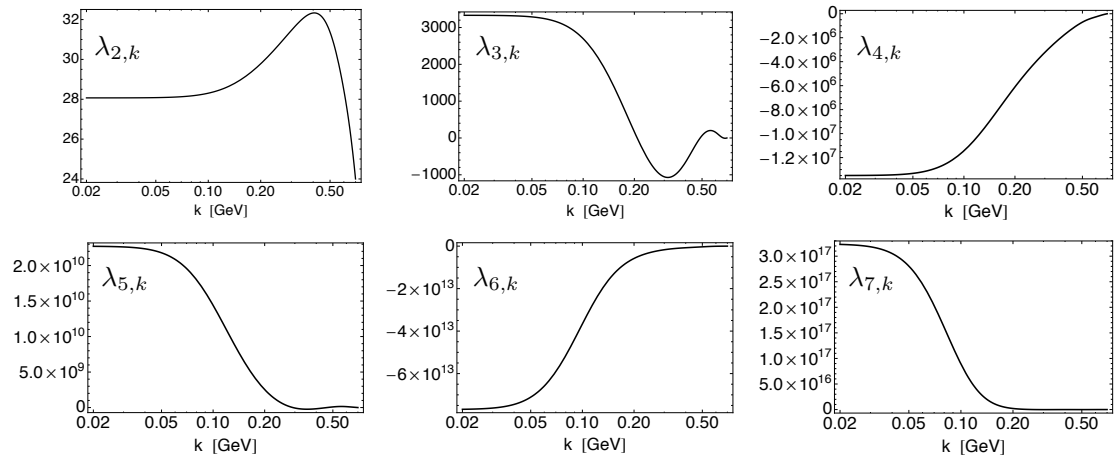

Figure 3.3.: The running of the Taylor coefficients of the effective Potential in the expansion about the running minimum given in (3.32). The couplings $\lambda_{n,k}$ assume increasingly large numerical values with increasing n. This potentially leads to instabilities of the flow equations due to the feedback of $\lambda_{n+1,k}$ to the flow of the mesonic $2n$-point function $\lambda_{n,k}$, see (3.34).

in the presence of the source,

$$\frac{\partial}{\partial\phi}\big(V_k(\rho)-c\sigma\big)\Big|_{\phi_{0,k}}=0\,. \tag{3.31}$$

The $O(4)$-invariant Taylor expansion about the running minimum to order N is given by

$$V_k(\rho)=\sum_{n=1}^{N}\frac{\nu_{n,k}}{n!}(\rho-\rho_{0,k})^n\,. \tag{3.32}$$

$\lambda_{n,k}$ are the scale dependent expansion coefficients that correspond to the running couplings for ϕ^{2n}-interactions. The scale dependence of the expansion point has to be taken into account on the left hand side of (3.29), to wit

$$\dot{V}_k(\rho)=\sum_{n=1}^{N}\frac{\dot{\nu}_{n,k}}{n!}(\rho-\rho_{0,k})^n-\dot{\rho}_{0,k}\sum_{n=2}^{N}\frac{\nu_{n,k}}{(n-1)!}(\rho-\rho_{0,k})^{(n-1)}\,, \tag{3.33}$$

where the dot is a shorthand notation for the RG-time derivative, $\dot{\nu}_{n,k}=\partial_t\nu_{n,k}$. To clarify the structure of this expression, we project on the flow of the mesonic $2n$-point function via

$$\frac{\partial^n\dot{V}_k(\rho)}{\partial\rho^n}\Big|_{\rho_{0,k}}=\dot{\nu}_{n,k}-\dot{\rho}_{0,k}\,\nu_{n+1,k}\,. \tag{3.34}$$

Thus, as a result of the scale dependence of the expansion point, there is always the feedback from the $2(n+1)$-point function $\nu_{n+1,k}$ to the flow of the $2n$-point function $\nu_{n,k}$. Even though the relevance of $\nu_{n,k}$ for the potential itself decreases with increasing n, their numerical value grows rapidly, see Fig. 3.3. This behavior potentially destabilizes the flow equations ant therefore the expansion. Indeed, this expansion shows only very bad convergence properties for QM-like models[3], as is is shown in the left figure of Fig. 3.4.

[3] We note that the situation is different for $O(N)$-models, see e.g. [152, 153]

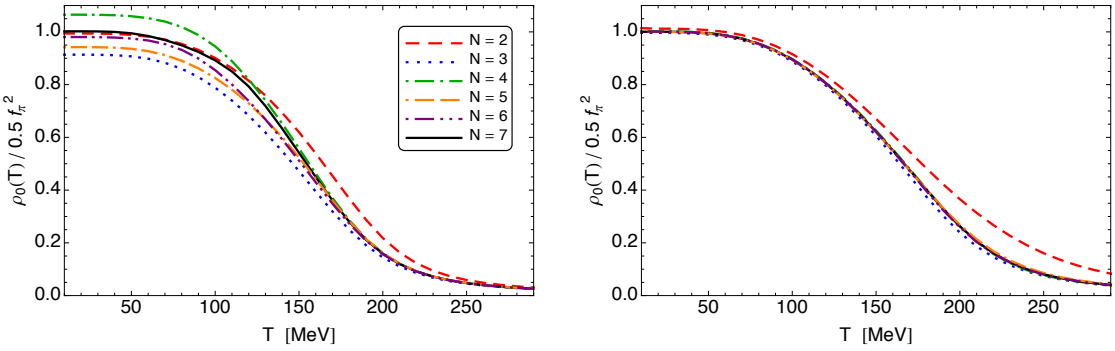

Figure 3.4.: Minimum of the effective potential in the IR, $\rho_0 \equiv \rho_{0,k=0}$ (normalized with the pion decay constant f_π) as a function of the temperature at $\mu=0$ for various expansion orders of the effective potential of the quark-meson model in LPA truncation. The left figure shows the results for the comoving expansion about $\rho_{0,k}$ and the right figure shows the results for the fixed background expansion about $\kappa=\rho_0$. The comoving expansion does not converge for the orders we computed, in particular at small to intermediate temperatures. The fixed background expansion, on the other hand, shows rapid convergence over the full temperature range. There, the expansion is already converged for $N=4$ for all practical purposes. We tuned the initial conditions for both expansions to the same physical values at $N=7$ and used this set of initial conditions for every order.

We see that the expansion (3.32) does is not converge at $N=7$. On the contrary, within the orders we considered here, it seems rather unstable for $T \lesssim 150\,\mathrm{MeV}$. We note that this seems less severe when we tune the initial conditions to the same physical values for every order of expansion. However, a sensible notion of convergence requires that the same results are obtained with the same set of initial conditions. Otherwise we start with a different set of differential equations from the outset. Our claim is that this bad convergence/instability can be ascribed to the linear feedback from the higher order couplings to the flow of the couplings (3.34) as discussed above.

Following our discussion above, in order to avoid the potentially dangerous feedback from higher order couplings in the flow, we need to expand the effective potential about a scale independent point κ with $\partial_t \kappa = 0$, i.e.

$$V_k(\rho) = \sum_{n=1}^{N} \frac{\nu_{n,k}}{n!}(\rho-\kappa)^n\,. \tag{3.35}$$

Note that the expansion point still depends on T and μ, $\kappa=\kappa(T,\mu)$. The minimum $\phi_{0,k}$ of V_k is now obtained from

$$\frac{\partial}{\partial\phi}\left(\sum_{n=1}^{N}\frac{\nu_{n,k}}{n!}(\rho-\kappa)^n - c\sigma\right)\bigg|_{\phi_{0,k}} = 0\,. \tag{3.36}$$

This expansion avoids the problems we faced above and the left hand side of the flow of the effective potential is now

$$\dot{V}_k(\rho) = \sum_{n=1}^{N}\frac{\dot{\nu}_{n,k}}{n!}(\rho-\kappa)^n\,, \tag{3.37}$$

and consequently, the flow of the mesonic $2n$-point function now reads

$$\left.\frac{\partial^n \dot{V}_k(\rho)}{\partial \rho^n}\right|_\kappa = \dot{\nu}_{n,k}\,. \tag{3.38}$$

The remaining question concerns the value of κ. Since all physical quantities are defined at the minimum of the effective potential at $k=0$, i.e. on the solution of the full quantum equations on motion, the most natural choice is $\kappa=\rho_0$, with $\rho_0 \equiv \rho_{0,k=0}$. However, since the effective potential derives from a Legendre transformation[4]. As a consequence, V_k becomes convex for $k\to 0$ and in particular developes a completely flat region between the origin and the minimum. Thus, it may be necessary to shift the expansion point a bit away from the IR minimum, towards larger field values, in order to avoid problems related to the peculiar global form of the effective potential at vanishing k. This puts forward:

$$\kappa(T,\mu) = (1+\epsilon)\,\rho_0(T,\mu)\,, \tag{3.39}$$

where ϵ is a (small) offset parameter. To avoid that the expansion point lies in the flat region of the effective potential, ϵ has to be positive. Furthermore, the physical minimum should be inside the radius of convergence of the expansion r_c to ensure that we capture the physics accurately, thus $0 \leq \epsilon \leq r_c$. In the LPA as in (3.35), there is only a running effective potential and the radius of convergence is solely determined by the quality of its expansion. Beyond LPA, however, one introduces further running couplings and as long as they are not expanded in powers of ρ, the radius of convergence is very limited and thus ϵ should be very small. The reason is that ρ-independent quantities are defined at the expansion point and if this point is too far away from the physical point in the IR, the relevant physics of these quantities may not be captured accurately. In the following chapters, for instance, we will go beyond LPA in various directions and should therefore keep this in mind. We postpone a more elaborate discussion of this important point to Sec. 7.3.4.

In practice, this involves a tuning of the expansion point when tuning the initial conditions of the system, since this usually affects the position of the minimum. The same is true for different temperatures and densities. But this is easily possible algorithmically and certainly worth the effort, given the many advantages this expansion has, as we will discuss in the following.

In the right figure of Fig. 3.4, we show $\rho_0(T)$ for various orders of this fixed background expansion (3.35) for $\kappa=\rho_0$. We clearly see that the convergence properties are far superior compared to the comoving expansion. The order parameter is already converged for $N=4$ over the full temperature range. Note that different observables may show different convergence behavior. However, since ρ_0 is an order parameter for the chiral phase transition, it is of particular relevance in the study of the phase diagram. We also note that already a ϕ^4-expansion is quantitatively precise at small temperatures and densities.

The lack of "linear feedback terms" (3.34) in the fixed background expansion not only stabilizes the system of equations and improves convergence, but it is also numerically much less demanding. The absence of these linear feedback terms in the flow equations and the fact that the physical minimum does not need and additional flow equation, but is rather obtained directly from the solution of the potential (3.36), simplifies the system of flow equations substantially, resulting in faster faster numerical computations.

Another advantage of the fixed background expansion is that it captures the global structure of the effective potential, at least to some extend. This allows us to resolve first-order phase

[4] In the FRG approach, the Legendre transformation is modified due to the presence of the regulator (3.7). However, it turns into the original Legendre transformation at $k\to 0$.

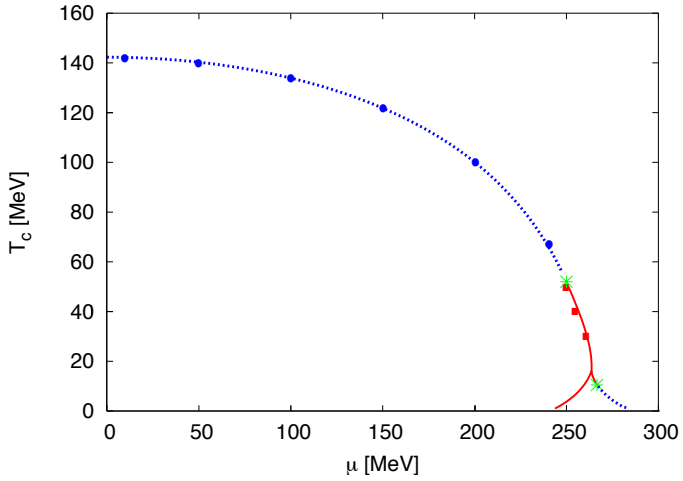

Figure 3.5.: Phase diagram of the quark-meson model in the chiral limit from [151]. The blue dots and red squares show the second and first order transition points we found using the identical model and initial conditions. We see that the comoving expansion to order $N=7$ captures the full phase structure, including the first-order transition and the critical point, down to very small temperatures and very large densities.

transitions. They are characterized by discontinuities in the order parameter. The comoving expansion breaks down at first-order phase transition since the discontinuity is reflected in a divergence of the flow of $\rho_{0,k}$. Thus, first-order transitions are not accessible with the comoving expansion. The fixed background expansion is not subject to this restriction since it does not rely on the flow of the minimum. In terms of the effective potential, a first order transition is signaled by the development of a second, local minimum. At the point where both minima are of the same depth, the phase transition occurs and the vacuum state "jumps" from one minimum to the other. Thus, as long as both minima are within the radius of convergence of the expansion, this transition can be captured reliably. To demonstrate this, we computed the phase diagram of the QM model in the chiral limit, i.e. the truncation (3.28) with $c=0$, with the same initial parameters as in [151]. The authors of this work used the grid method to compute the phase diagram. In Fig. 3.5 we show our results with the comoving expansion in comparison to their grid result.

The fixed background expansion reproduces the full result for the second-order transition, the critical endpoint and and the first part of the first-order transition to an accuracy of about 1 MeV. If we go further along the first-order line, our result starts to deviate from the result of [151] and we are not able to resolve the splitting of the phase diagram. In this region, the distance between the global minimum of the effective potential in the broken phase and the second minimum that emerges and becomes the global minimum in the symmetric phase is fairly large and seems to be larger than our radius of convergence. We note, however, that we expanded the effective potential to order $N_V = 7$ and that higher orders in the expansion may improve this.

As we have mentioned above, the effective potential becomes convex at $k \to 0$, and in particular flat for $\rho < \rho_0$. This implies a non-differentiable point close to the minimum ρ_0. It is certainly impossible to capture this behavior with a simple polynomial expansion such as the Taylor expansion. However, V_k only becomes convex strictly for $k=0$ and if there is a gap in

the theory under consideration, $k=0$ is physically irrelevant. In QCD, for instance, the smallest mass scale is given by the pion mass $M_\pi \approx 138\,\text{MeV}$. For scales $k \approx M_\pi$, the flows of the physical parameters freeze out. The remaining flow for $k < M_\pi$ flattens the potential, but leaves the physical parameters unchanged. Thus, in order to extract the physical informations from the potential, we do not need to resolve convexity as long as the theory has a finite gap.

In conclusion, we demonstrated that the fixed background expansion has superior convergence properties for QM models as compared to the comoving expansion. Furthermore, it allows us to capture the global structure of the effective action with good accuracy without being numerical extensive. However, for more more complicated structures of the effective potential, such as multiple well-separated local minima, the grid method still gives the most reliable results since it truly captures the global structure of the potential without the limitation of a possibly small radius of convergence. It is possible, however, to extend the fixed background expansion to more than one expansion point. Given the good accuracy we already achieved with one expansion point, two expansions points may be sufficient for quantitative precision in most applications. Nonetheless, the statements we made here are far from general and one should carefully check their validity for cases that go beyond the one discussed here. We will present further results concerning the fixed background expansion in a much more refined QM model in Chap. 7.

CHAPTER 4

Chiral Symmetry Breaking in QCD

For an accurate first-principles description of the dynamics of QCD, a reliable inclusion of hadronic states is of great importance. This holds in particular for an approach aiming at the hadron spectrum or the phase structure of QCD at finite density. Here, we develop a theoretical framework for taking into account the fluctuation dynamics of quarks, gluon and hadrons in two-flavor QCD at vanishing temperature and density. This approach is based on previous functional renormalization group studies [154, 155] and a related quantitative study in the quenched limit [156]. The framework presented here allows to dynamically include hadronic states as they emerge from the microscopic quark and gluon degrees of freedom.

We use the FRG approach for QCD, for reviews see [75, 133–135, 139–143, 157], and [71, 101, 102, 122–125] for reviews on related work. In order to describe the transition from quarks and gluons to hadrons, we extend the dynamical hadronization technique (or rebosonization), introduced in Refs. [69, 70, 139, 144]. This technique is applied here to dynamical two-flavor QCD with physical quark masses. We will show how the dominant hadronic low-energy degrees of freedom and their dynamics emerge from the underlying quark-gluon dynamics. The hadronization technique, as further developed in the present work, was also applied in Ref. [156] in a quantitative study of quenched QCD. There, a large number of interaction channels has been taken into account, aiming at full quantitative precision. We will exploit the results from [156] as well as results on the scale-dependent glue sector of Yang-Mills theory from Refs. [71, 158, 159]. This enables us to concentrate on the RG flows of the most relevant couplings from a more phenomenological point of view, paying special attention to unquenching effects.

In summary, the aim of this chapter is threefold: Firstly, we aim at a detailed understanding of the fluctuation physics in the transition regime between the high energy quark-gluon phase to the low energy hadronic phase. Secondly, we want to initiate the quest for the minimal set of composite operators that have to be taken into account for reaching (semi-)quantitative precision, while keeping the study analytic. This deepens the understanding of the fluctuation physics by only taking into account the relevant operators. Moreover, it is also of great interest for low energy effective models. Thirdly, we discuss full unquenching effects in terms of the matter back-coupling to the glue sector that is important for QCD regimes with dominant quark fluctuations such as QCD at high densities or many flavors.

4.1. The Effective Action

Our aim is to describe two-flavor QCD in $d = 4$ Euclidean dimensions at vanishing temperature and density in a vertex expansion. The starting point is the microscopic gauge fixed QCD action (2.17). Thus, we include the quark-gluon, three- and four-gluon vertices as well as the ghost-gluon vertex and the corresponding momentum-dependent propagators. The corresponding part of the effective action therefore reads:

$$\Gamma_k^{(\mathrm{mQCD})} = \int_x \left\{ iZ_{q,k}\,\bar{q}\left(\gamma_\mu D_\mu + m_{q,k}\right)q + \frac{1}{4}F^a_{\mu\nu}F^a_{\mu\nu} + \bar{c}^a\partial_\mu D^{ab}_\mu c^b + \frac{1}{2\xi}(\partial_\mu A^a_\mu)^2 \right\} + \Delta\Gamma_k^{(\mathrm{gauge})}, \tag{4.1}$$

see Sec. 2.1. We included the scale dependent wave function renormalization $Z_{q,k}$ of the quarks to capture some non-trivial momentum dependence of the quark propagator. The covariant derivative D_μ and the field strength $F_{\mu\nu}$ are defined in Sec. 2.1. In order to be able to capture also non-perturbative effects induced by fluctuations, we consider fully momentum dependent ghost and gluon propagators, as well as different gauge couplings. These contributions are stored in $\Delta\Gamma_k^{(\mathrm{gauge})}$. We will explain this in more detail in Sec. 4.3. Here, we only note that due to the presence of a non-classical gluon propagator, we also have a running gluon wave function renormalization $Z_{A,k}$, which has to be included in the definition of the covariant derivative for the sake if RG-invariance, $D_\mu = \partial_\mu - iZ_{A,k}^{1/2}\,g_k A^a_\mu t^a$. Then, the field strength tensor is

$$F^{ab}_{\mu\nu} = \frac{i}{Z_{A,k}^{1/2}\,g_k}[D^a_\mu, D^b_\nu]. \tag{4.2}$$

For more details on the gauge part of our truncation see Sect. 4.3

If we start at large, perturbatively accessible energy scales, say $k = \Lambda \gtrsim 5\,\mathrm{GeV}$, owing to asymptotic freedom, the initial action is related to the classical gauge-fixed action of QCD,

$$\Gamma_\Lambda = \Gamma_\Lambda^{(\mathrm{mQCD})}, \tag{4.3}$$

and $\Delta\Gamma_\Lambda^{(\mathrm{gauge})} = 0$. Thus, the initial parameters for the flow equations are the value of the strong coupling $\alpha_{s,\Lambda}$ and the current quark mass $m_{q,\Lambda}$ at the initial scale Λ. In a consistent formulation of QCD based on first principles, these have to be the only input parameters, since they fix the microscopic theory. Everything else emerges dynamically from there.

As we have already discussed in Sec. 2.4, owing to the increasing strength of the strong interaction $\alpha_{s,k}$, effective four-quark interactions are generated by the flow towards lower scales, see Fig. 2.37. In general, all possible four-quark interactions consistent with the symmetries of the theory are generated,

$$\Gamma_k^{(4\mathrm{q})} = \int_x \sum_i \lambda_{i,k}(\bar{q}T_i q)^2 = \int_x \sum_i \lambda_{i,k}\,\bar{q}^A T_i^{AB} q^B\,\bar{q}^C T_i^{CD} q^D, \tag{4.4}$$

with the tensors T_i. They can carry color-, flavor- and spinor indices, summarized by A, B, C, D. The relevant symmetries for the construction of all possible four-quark interactions are the global flavor symmetries of QCD, gauge symmetry[1] and Lorentz invariance. All possible Lorentz structures of the T_i are found by identifying the basis elements of the Clifford algebra. There are

[1] Gauge symmetry is always guaranteed for the kind of interactions shown in (4.4).

16 elements, given by the 5 tensors $\mathbb{1}_s$, γ_μ, $\sigma_{\mu\nu}$, $\gamma_\mu\gamma_5$ and γ_5. For color and flavor, a complete set of operators is given by the respective identity elements and the generators, $\mathbb{1}_c$, t^a and $\mathbb{1}_f$, $\vec{\tau}$, with the $SU(N_c)$ generators t^a and the Pauli matrices ($SU(2)$ generators) $\vec{\tau}$. Thus, there is a total of 20 bilinears of the form $(\bar{q}T_i q)$ that can be considered in (4.4) in general.

In addition to the restriction that (4.4) has to respect the symmetries of the system, there is an additional restriction related to so-called Fierz transformations. A specific quark-antiquark interaction channel can always be expressed as a linear combination of different interaction channels with two spinor fields interchanged. This can potentially lead to ambiguities in the corresponding bosonized models, since different sets of composite states can be related to one and the same fermionic action (see e.g. [75]). We therefore have to make sure that the set of tensors T_i is *Fierz-closed*, i.e. we only include the maximal set of T_i for which the four-quark interactions are not related by Fierz transformations.

As we have discussed Sec. 2.3, the classical flavor symmetry of two-flavor QCD is given by $U(1)_V \times U(1)_A \times SU(N_f)_V \times SU(N_f)_A$. Owing to the axial anomaly, $U(1)_A$ is broken on the quantum level. Here, we assume $U(1)_A$ to be "maximally broken", i.e. we restrict the flavor symmetry to be $U(1)_V \times SU(N_f)_V \times SU(N_f)_A$ and in particular ignore the possibility of $U(1)_A$-restoration at large temperatures. It is now an easy but tedious exercise to show that there are 6 tensors T_i left that yield Fierz-closed four quark interactions (4.4) and respect the symmetries of QCD, including the flavor symmetry discussed above, see e.g. [75, 160–162].

A complete set of four-quark interactions was considered in [156] for the case of quenched QCD. They found that the scalar-pseudoscalar ($S-P$) channel is by far the most dominant channel among all four-quark interaction channels. Thus dynamical chiral symmetry breaking is almost exclusively driven by this channel and it is therefore sufficient for semi-quantitative purposes to consider only this channel, to wit

$$\Gamma_k^{(4q)} = \int_x \lambda_{S,k}\left[-(\bar{q}\,T^0 q)^2 + (\bar{q}\gamma_5 \vec{T} q)^2\right]. \tag{4.5}$$

$\vec{T}$ are the properly normalized $SU(N_f)$ generators, i.e. $\vec{T} = \vec{\tau}/2$ for $SU(2)$, and $T^0 = \frac{1}{\sqrt{2N_f}}\mathbb{1}_{N_f\times N_f}$. As further simplification, we assume that $\lambda_{S,k}$ only depends on the RG scale, but not on momentum, i.e. we have point-like four-quark interactions.

At low energies close to Λ_{QCD}, the attractive interaction between quarks and antiquarks is strong enough to form mesonic bound states. At this point, a description solely based on quarks and gluons turns out to be inefficient, because the physical degrees of freedom become hadrons. Furthermore, the four-quark interactions diverge at the chiral phase transition as bound state resonances signal the formation of mesons in these quark-antiquark scattering channels. The ($S-P$) channel defined in (4.5) is the one where the pions and their chiral partner, the sigma meson, form. Owing to the bound state resonance, it is in general not possible to enter the hadronic phase within a purely fermionic formulation. We will therefore introduce mesonic degrees of freedom by partially bosonizing the four-quark channel (4.5) via a Hubbard-Stratonivich transformation [163, 164]. It is an exact transformation of the fermionic path integral in terms of (a priori) auxiliary fields ϕ which exploits that the path integral of an action only quadratic in the fields is simply a Gaussian integral,

$$\begin{aligned}\int \mathscr{D}\phi\, e^{-\int_x\left[\frac{1}{2}m^2\phi^2 + h\bar{q}(T\cdot\phi)q\right]} &= \int \mathscr{D}\phi\, e^{-\int_x\left[\frac{1}{2}\left(m\phi+\frac{h}{m}\bar{q}Tq\right)^2 - \frac{h^2}{2m^2}(\bar{q}Tq)^2\right]} \\ &= \mathscr{N} e^{\int_x \frac{h^2}{2m^2}(\bar{q}Tq)^2},\end{aligned} \tag{4.6}$$

where $\mathcal{N}$ is the Gaussian integral, which is a pure number, and can be absorbed into the overall normalization of the path integral. Thus, the four-quark interaction can be rewritten in terms of a mass term of ϕ and a Yukawa term $\sim h$. The remaining path integral is then quadratic in the quark fields. They can be integrated out, yielding the well-known fermionic determinant. By looking at the classical equations of motions for the action given by the action in the first term of (4.6),

$$\phi = \frac{h}{m^2}\bar{q}Tq\,, \tag{4.7}$$

the nature of ϕ as quark-bilinear becomes apparent and we can therefore interpret ϕ as the meson defined by the quantum numbers given by the tensor T in the four-quark channel. In other words, it is the meson that is responsible for the resonance in the scattering channel.

We apply this now the $(S-P)$ channel (4.5) and furthermore also transform the quark mass term in (4.1) into the meson sector in the same way. By further integrating out momentum shells, the initially auxiliary meson fields become dynamical and meson self-interactions are generated by the flow. To account for this, we introduce a scale dependent effective potential V_k to the effective action, which contains arbitrary powers of mesonic self-interactions. To account for higher order quark-meson interactions, we furthermore promote the running Yukawa coupling h_k to be meson field dependent. Partial bosonization then means that we keep both, the mesonic sector and the four-quark sector in our truncation. This is of crucial importance, since a naive description of the high-energy sector of QCD is impossible in terms of mesons, while the hadronic sector is hardly accessible in a purely fermionic language. We will elaborate on this in the next section. There, we will demonstrate how to consistently describe the formation of bound states in QCD via dynamical hadronization. This also will avoid double-/mis-counting problems for formulations in terms of both, quarks and mesons[2].

The remaining question concerning the meson sector is the implementation of chiral symmetry, i.e. the representation of the meson fields and the structure of chiral invariants. In our case, with maximally broken $U(1)_A$, the non-trivial part of chiral symmetry is given by $SU(2)_V \times SU(2)_A$ in our case, i.e. quark-bilinears $\sim\bar{q}Tq$ have to transform in a irreducible representation of this group. A Clebsch-Gordan decomposition decomposition shows that we need an isospin (i.e. $SU(2)$) triplet and a singlet. The triplet then obviously corresponds to the Goldstone bosons of spontaneously broken $SU(2)_A$, i.e. the pions $\vec{\pi}$. The singlet is the scalar sigma meson, σ. Since $SU(2)_V \times SU(2)_A$ is isomorphic to $SO(4)$, the simplest representation of the meson fields can be given in terms of the fundamental representation of this group, i.e. the $O(4)$-vector

$$\phi = \begin{pmatrix} \vec{\pi} \\ \sigma \end{pmatrix}. \tag{4.8}$$

The pion transforms, as mentioned above, as an iso-triplet, i.e. in the subgroup $O(3)$[3]. Note that, following these arguments, the chiral phase transition of two-flavor QCD in the chiral limit lies in the $O(4)$ universality class, as long as $U(1)_A$ is maximally broken [165]. A chiral invariant is then given by

$$\rho = \frac{1}{2}\phi^2 = \frac{1}{2}(\vec{\pi}^2 + \sigma^2)\,, \tag{4.9}$$

[2] A potential double counting problem is apparent here, since the four-quark interaction and the meson sector are related by a Hubbard-Stratonovich transformation. Thus, by naively maintaining both sectors in the effective action, one clearly overestimates the effects of bound states at certain scales.

[3] Note that the isospin group $SU(2)$ is isomorphic to $SO(3)$

and the mesonic effective potential and the field-dependent Yukawa coupling have to be functions of this invariant, $V_k = V_k(\rho)$ and $h_k = h_k(\rho)$. Thus, we can finally write down the bosonized sector of the effective action:

$$\Gamma_k^{(\mathrm{bos})} = \int_x \left\{ h_k(\rho)\left[\bar{q}(i\gamma_5 \vec{T}\vec{\pi} + T^0\sigma)q\right] + \frac{1}{2}Z_{\phi,k}(\partial_\mu\phi)^2 + V_k(\rho) - c\sigma \right\}. \tag{4.10}$$

As for the quarks, we included RG-scale dependent wave function renormalizations $Z_{\phi,k}$ for the mesons. This way, we capture the major part of the momentum dependence of the full meson propagators, as it was demonstrated in [166]. The source term $-c\sigma$ is simply the bosonized version of the current quark mass term $m_{q,\Lambda}\bar{q}q$ and therefore explicitly breaks chiral symmetry. This results in a finite mass of the pions, i.e. they are pseudo-Goldstone bosons in this case. Furthermore, the chiral phase transition is a crossover rather than a second-order phase transition at small densities. The relation between the source c and the current quark mass $m_{q,\Lambda}$ is given by

$$m_{q,\Lambda} = \frac{h_\Lambda}{2v_{1,\Lambda}}\, c\,, \tag{4.11}$$

with the quadratic part of the effective potential $v_{1,\Lambda} = \partial_\rho V(\rho_{0,k})$.

In summary, the scale dependent effective action we use to describe the chiral phase transition is given by

$$\Gamma_k = \Gamma_k^{(\mathrm{mQCD})} + \Gamma_k^{(4\mathrm{q})} + \Gamma_k^{(\mathrm{bos})}, \tag{4.12}$$

with the microscopic QCD/gauge sector $\Gamma_k^{(\mathrm{mQCD})}$ given by (4.1), the four-quark interaction channel $\Gamma_k^{(4\mathrm{q})}$ from (4.5) and the hadronic part of the action $\Gamma_k^{(\mathrm{bos})}$ defined in (4.10).

The effective potential contains all relevant physical informations as its minima determine the vacuum structure of QCD. In particular, a nonzero minimum, which corresponds to a non-vanishing VEV of the sigma meson, $\sigma_{0,k}$, signals chiral symmetry breaking. The minimum is obtained from the quantum equation of motion in the presence of the source,

$$\frac{\partial}{\partial\phi}\big(V_k(\rho) - c\sigma\big)\Big|_{\phi_{0,k}} = 0\,, \tag{4.13}$$

with the meson VEV $\phi_{0,k} = (0, \sigma_{0,k})^T$. The quark and meson mass functions (two-point functions at vanishing momentum) depend on the meson fields in general. The field dependent quark and meson masses are defined via the curvature terms of the effective action,

$$\begin{aligned} m_{q,k}^2 &= \frac{1}{2}h_k^2(\rho)\rho\,, \\ m_{\pi,k}^2 &= V'(\rho)\,, \\ m_{\sigma,k}^2 &= V'(\rho) + 2\rho V''(\rho)\,. \end{aligned} \tag{4.14}$$

The physical masses are defined at the minimum of the effective potential, $\rho_{0,k} = \phi_{0,k}^2/2$. Even though the masses we extract here are the curvature masses, it was shown in [166] on the example of the pion mass in a quark meson model, that the curvature mass of the mesons is almost identical to the pole mass for truncations that include running wave function renormalizations. Thus, as mentioned above, we capture the major part of the momentum dependence of the full meson propagators by including $Z_{\phi,k}$ and the masses are very close to the physical masses.

4.1.1. Expansion Scheme

Here, we will elaborate on the expansion scheme we use for our truncation (4.12). This concerns in particular the effective potential $V_k(\rho)$ and the Yukawa coupling $h_k(\rho)$, which are both arbitrary $O(4)$-invariant functions of the meson fields. We employ the fixed background Taylor expansion discussed in Sec. 3.4, due to its superior convergence properties and numerical convenience. Here, we have to generalize this expansion to the case of running wave function renormalizations.

The scalar potential and the Yukawa coupling are expanded about a scale-independent point κ, $\partial_t \kappa = 0$. Arbitrary powers of meson self-interactions are included to our truncation via the expansion

$$V_k(\rho) = \sum_{n=1}^{N_V} \frac{\nu_{n,k}}{n!} (\rho - \kappa)^n \,. \tag{4.15}$$

The minimal expansion order necessary to capture a crossover or second order phase transition is $N_V = 2$. This would correspond to the well-known *Mexican hat potential*, i.e. a Ginsburg-Landau type ϕ^4-theory. The potential to capture a first-order transition requires $N_V \geq 3$ since a ρ^2 potential can never exhibit more than one local minimum.

Higher order quark-antiquark–multi-meson scattering processes are taken into account by the analogous $O(4)$-symmetric expansion for the ρ-dependent Yukawa coupling,

$$h_k(\rho) = \sum_{n=0}^{N_h} \frac{h_{n,k}}{n!} (\rho - \kappa)^n \,. \tag{4.16}$$

$N_h = 0$ amounts to the standard running Yukawa coupling which couples an quark-antiquark pair to a meson. By increasing N_h the interaction between a quark-antiquark pair and $(2N_h+1)$ mesons can be studied.

By systematically increasing N_V and N_h one can study the impact of higher order mesonic scattering processes e.g. on the chiral phase transition of QCD. We will discuss this in detail in Chap. 7. Here, we will exploit the findings presented later and fix the expansion orders to $N_V = 5$ and $N_h = 3$. As we will demonstrate there, the expansions are converged for these values. Thus, quantitative precision is guaranteed for the meson sector, especially at vanishing temperature and density.

The other running parameters of the truncation are the four-quark interaction $\lambda_{S,k}$, the gauge coupling g_k and the wave function renormalizations of quarks, gluons, ghosts and mesons, $Z_{q,k}$, $Z_{A,k}$, $Z_{c,k}$ and $Z_{\phi,k}$. The running parameters of the gauge sector, i.e. g_k, $Z_{A,k}$ and $Z_{c,k}$ are independent of the meson fields, since meson and gauge sector do not couple directly to one another. However, the remaining matter- sector parameters $\lambda_{S,k}$, $Z_{q,k}$ and $Z_{\phi,k}$ are in general also functions of ρ and should therefore also be expanded in powers of ρ in a consistent expansion in terms of n-point functions. For the wave function renormalizations, this amounts to

$$Z_k(\rho) = \sum_{n=0}^{N_Z} \frac{z_{n,k}}{n!} (\rho - \kappa)^n \,. \tag{4.17}$$

However, we expect a rather mild field dependence of the wave function renormalizations on the meson fields, leading to

$$\partial_\rho Z_k(\rho) \approx 0 \,. \tag{4.18}$$

The quantitative reliability of this hypothesis is tested in Sec. 7.3.4. Equation (4.18) implies, that locally, i.e. for a given expansion point κ, we can use

$$Z_k = Z_k(\kappa) = z_{0,k}\,, \tag{4.19}$$

and we will do so for $Z_{q,k}$ an $Z_{\phi,k}$. Still, for the computation of observables the wave function renormalizations have to be determined at the physical point ρ_0. It is here where the field dependence of the Z_k play a crucial role. Thus, the offset parameter ϵ in condition (3.39) for the expansion point κ has to be as close to zero as numerically possible.

With potentially non-classical dispersion relations, i.e. in the presence of running wave function renormalizations Z_k, physical quantities have to be defined with appropriate rescaling with Z_k in order to ensure RG-invariance. This simply implements the requirement of reparametrization invariance of physical quantities under a rescaling of the fields, $\Phi(x)\to\alpha\Phi(x)$. It is therefore convenient to introduce *renormalized fields*,

$$\bar{\phi} = Z_{\phi,k}^{1/2}\phi \quad \text{and} \quad \bar{\rho} = Z_{\phi,k}\,\rho\,, \tag{4.20}$$

with the locally constant $Z_{\phi,k}$ defined in (4.19). With slight abuse of terminology, we will refer to the non-renormalized fields ρ as the *bare fields*. For the *renormalized* effective Potential $\bar{V}_k$ which is defined via

$$\bar{V}_k(\bar{\rho}) = V_k(\rho)\,, \tag{4.21}$$

this implies

$$\bar{V}_k(\bar{\rho}) = \sum_{n=1}^{N_V} \frac{\bar{v}_{n,k}}{n!}\,(\bar{\rho}-\bar{\kappa})^n\,, \tag{4.22}$$

with the renormalized couplings

$$\bar{v}_{n,k} = \frac{v_{n,k}}{Z_{\phi,k}^n}\,. \tag{4.23}$$

Note that the expansion of the effective potential starts with linear order in the chiral invariant ρ. A zero-order term would amount to a shift in the global vacuum energy, i.e. a scale- and field-independent volume-term in the effective action Γ_k, which can simply be normalized away.

In analogy to (4.20), the renormalized expansion point is defined as

$$\bar{\kappa} = Z_{\phi,k}\,\kappa\,. \tag{4.24}$$

This implies that in terms of renormalized fields in the presence of running wave function renormalizations, the renormalized expansion point $\bar{\kappa}$ has the scale dependence induced by the running of $Z_{\phi,k}$,

$$\partial_t\bar{\kappa} = -\eta_{\phi,k}\,\bar{\kappa}\,. \tag{4.25}$$

Note that the analogous flow equation applies to the renormalized field $\bar{\rho}$. Here, we used that the anomalous dimension η_k is defined as

$$\eta_k = -\frac{\partial_t Z_k}{Z_k}\,. \tag{4.26}$$

We discussed in Sec. 3.4 that the advantage of the fixed background expansion is that the flow of the $2n$-point function $\nu_{n,k}$ has no additional feedback from the $2(n+1)$-point function $\nu_{n+1,k}$, see (3.34). Owing to the field-reparametrization invariance of the theory, the flow of the renormalized $2n$-point function $\bar{\nu}_{n,k}$ still possesses this desirable property. This can most easily be seen if we look at the flow of (4.22),

$$\begin{aligned}\partial_t \bar{V}(\bar{\rho}) &= \sum_{n=1}^{N_V} \frac{\partial_t \bar{\nu}_{n,k}}{n!} (\bar{\rho}-\bar{\kappa})^n + \partial_t(\bar{\rho}-\bar{\kappa}) \sum_{n=1}^{N_V} \frac{\bar{\nu}_{n,k}}{(n-1)!} (\bar{\rho}-\bar{\kappa})^{n-1} \\ &= \sum_{n=1}^{N_V} \frac{\left(\partial_t - n\eta_{\phi,k}\right)\bar{\nu}_{n,k}}{n!} (\bar{\rho}-\bar{\kappa})^n \,,\end{aligned} \tag{4.27}$$

where we exploited (4.26). This implies for the flow of the renormalized $2n$-point function:

$$\partial_{\bar{\rho}}^n \dot{\bar{V}}_k(\bar{\rho})\big|_{\bar{\rho}=\bar{\kappa}} = -n\eta_{\phi,k}\bar{\nu}_{n,k} + \partial_t \bar{\nu}_{n,k} \,. \tag{4.28}$$

Thus, the anomalous dimension induces a new term proportional to $\bar{\nu}_{n,k}$ to the left hand side of the flow equation, but a linear feedback term $\sim \bar{\nu}_{n+1,k}$ is still absent for the fixed background expansion. It is important to emphasized that the bare expansion point κ has to be scale independent here $\partial_t \kappa$, not the renormalized expansion point $\bar{\kappa}$. If we were to fix $\bar{\kappa}$, we would introduce an additional term $-\eta_{\phi,k}\bar{\kappa}\,\bar{\nu}_{n+1,k}$ to (4.28), which would obviously spoil the stability of our expansion according to our discussion in Sec. 3.4.

The choice of the expansion point is unique if we require no linear feedback from higher order couplings and correct IR physics (up to the small offset parameter ϵ). Suppose we have some general renormalized expansion point $\bar{\xi}_k$. The left hand side of the flow of the $2n$-point function is then

$$\partial_{\bar{\rho}}^n \dot{\bar{V}}_k(\bar{\rho})\big|_{\bar{\rho}=\bar{\xi}_k} = \left(\partial_t - n\eta_{\phi,k}\right)\bar{\nu}_{n,k} - \bar{\nu}_{n+1,k}\left(\partial_t + \eta_{\phi,k}\right)\bar{\xi}_k \,. \tag{4.29}$$

Demanding that the $\bar{\nu}_{n+1,k}$-term vanishes implies that $\partial_t \bar{\xi}_k = -\eta_{\phi,k}\,\bar{\xi}_k$ and therefore $\bar{\xi}_k = \bar{\kappa}$.

The arguments given above apply just as well to field dependent renormalized Yukawa coupling $\bar{h}_k$, which is defined as

$$\bar{h}_k(\bar{\rho}) = \frac{h_k(\rho)}{Z_{q,k} Z_{\phi,k}^{1/2}} = \sum_{n=0}^{N_h} \frac{\bar{h}_{n,k}}{n!} (\bar{\rho}-\bar{\kappa})^n \,. \tag{4.30}$$

The renormalized expansion coefficients $\bar{h}_{n,k}$, i.e. the physical quark-antiquark–$(2n+1)$-meson couplings, are defined as

$$\bar{h}_{n,k} = \frac{h_{n,k}}{Z_{q,k} Z_{\phi,k}^{(2n+1)/2}} \,. \tag{4.31}$$

The physical masses are defined from the renormalized potential and Yukawa coupling at the physical minimum $\bar{\phi}_0 \sim \bar{\phi}_{0,k=0}$, which can directly be obtained from the renormalized analogue of (4.13),

$$\partial_{\bar{\phi}}\left(\bar{V}_k(\rho) - \bar{c}\bar{\sigma}\right)\Big|_{\bar{\phi}_{0,k}} = 0 \,. \tag{4.32}$$

with the renormalized symmetry breaking source,

$$\bar{c}\bar{\sigma} = c\sigma \quad \text{with} \quad \bar{c} = \frac{c}{Z_{\phi,k}^{1/2}}\,. \tag{4.33}$$

With this, the physical (renormalized) quark and meson masses are

$$\begin{aligned} M_{q,k}^2 &= \frac{m_{q,k}}{Z_{q,k}} = \frac{1}{2}\,\bar{h}_k^2(\bar{\rho}_{0,k})\bar{\rho}_{0,k}\,, \\ M_{\pi,k}^2 &= \frac{m_{\pi,k}}{Z_{\phi,k}^{1/2}} = \bar{V}'(\bar{\rho}_{0,k})\,, \\ M_{\sigma,k}^2 &= \frac{m_{\sigma,k}}{Z_{\phi,k}^{1/2}} = \bar{V}'(\bar{\rho}_{0,k}) + 2\bar{\rho}_{0,k}\bar{V}''(\bar{\rho}_{0,k})\,. \end{aligned} \tag{4.34}$$

Note that in the presence of the explicit symmetry breaking $c>0$, the first derivative of the effective potential at the physical point, $\bar{V}'(\bar{\rho}_{0,k})$, i.e. the physical pion mass, is always non-zero.

4.2. Dynamical Hadronization

Quantum fluctuations are included into the truncation (4.12) by means of the functional renormalization group as discussed in Chap. 3. For QCD related reviews and corresponding low-energy models, we refer the reader to Refs. [75, 133–135, 139–143, 167]. A consistent description of the dynamical transition from quark-gluon degrees of freedom to hadronic degrees of freedom is achieved by the dynamical hadronization technique. Loosely speaking, it is a way of storing four-quark interaction channels, which are resonant at the chiral phase transition, in mesonic degrees of freedom and therefore allows for a unified description of the different degrees of freedom governing the dynamics at different momentum scales. It is based on the formulation of the FRG with scale dependent fields we discussed in Sec. 3.2.

4.2.1. FRG & Dynamical Hadronization

In the case of QCD, the multi-field is $\Phi = (A, q, \bar{q}, c, \bar{c}, \phi)$ and we denote the VEV as $\Phi_{0,k} = (0,0,0,0,0,\phi_{0,k})$. First, let us assume that all fields are k-independent. Then, the flow equation is given by the first term of (3.21). The regulator in field space is given by

$$R_k = \begin{pmatrix} R_k^A & 0 & 0 & 0 & 0 & 0 \\ 0 & 0 & R_k^q & 0 & 0 & 0 \\ 0 & -R_k^q & 0 & 0 & 0 & 0 \\ 0 & 0 & 0 & 0 & R_k^c & 0 \\ 0 & 0 & 0 & -R_k^c & 0 & 0 \\ 0 & 0 & 0 & 0 & 0 & R_k^\phi \end{pmatrix}. \tag{4.35}$$

We choose the same regulator of π and σ fields in order to avoid introducing an additional explicit chiral symmetry breaking by our regularization scheme. With this, the flow equation decomposes into individual parts of the different fields and reads

$$\begin{aligned} \partial_t \Gamma_k[\Phi] = \frac{1}{2}\mathrm{Tr}\big(G_{AA,k}[\Phi]\cdot\partial_t R_k^A\big) - \mathrm{Tr}\big(G_{c\bar{c},k}[\Phi]\cdot\partial_t R_k^c\big) \\ - \mathrm{Tr}\big(G_{q\bar{q},k}[\Phi]\cdot\partial_t R_k^q\big) + \frac{1}{2}\mathrm{Tr}\big(G_{\phi\phi,k}[\Phi]\cdot\partial_t R_k^\phi\big)\,. \end{aligned} \tag{4.36}$$

We have explicitly written down the traces which sum over discrete and continuous indices of the fields, including momenta and species of fields. The first line on the right hand side of (4.36) is the flow in the pure glue sector, the second line creates the matter fluctuations. Diagrammatically, the QCD flow can be written as

$$\partial_t \Gamma_k = \frac{1}{2}$$ 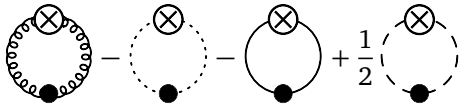 (4.37)

with the loops corresponding to the gluon, ghost, quark and meson contributions.

$G_k[\Phi]$ denote the scale and field-dependent full propagators of the respective fields and are defined in (3.13). For the quarks, for instance, we have

$$G_{q\bar{q},k}[\Phi] = \left(\frac{\delta^2 \Gamma_k[\Phi]}{\delta q(-p) \delta \bar{q}(p)} + R_k^q \right)^{-1} . \tag{4.38}$$

Note that we absorbed the minus sign for fermion fields from the field-space metric γ in (3.13) into the overall minus for the fermionic contributions to the flow equation (4.36). At $k=0$ and the fields set to their vacuum expectation value, $G_{k=0}[\Phi_0]$ is the full propagator.

We use the optimized cutoffs discussed Sec. 3.3, which explicitly read for our truncation

$$\begin{aligned} R_k^A(p^2) &= Z_{A,k}\, p^2 r_B(p^2/k^2)\, \Pi^{\perp} , \\ R_k^c(p^2) &= Z_{c,k}\, p^2 r_B(p^2/k^2) , \\ R_k^q(p^2) &= Z_{q,k}\, \gamma_\mu p_\mu r_F(p^2/k^2) , \\ R_k^\phi(p^2) &= Z_{\phi,k}\, p^2 r_B(p^2/k^2) , \end{aligned} \tag{4.39}$$

with the transversal projection operator

$$\Pi^{\perp}_{\mu\nu} = \delta_{\mu\nu} - \frac{p_\mu p_\nu}{p^2} . \tag{4.40}$$

These regulators have the advantage that the loop-momentum integration can be performed analytically for vanishing external momenta and, consequently, all beta functions can be given in analytical form.

If we insert the truncation (4.12) and the regulators (4.39) into the flow equation (4.36), we can extract the set of coupled ordinary differential equations for the running couplings in the truncation. We will present the results for the flow equations of the matter sector for scale-independent fields in the following. Modifications of these equations due to dynamical hadronization will be given in the next section. The flow equations of the gauge couplings will be discussed in Sec. 4.3. For a general discussion on the derivation of flow equations, we refer to App. B.

Flow of the Effective Potential. The flow equation of the effective potential including the symmetry breaking source, $V_k(\rho) - c\sigma$, is obtained by evaluating (4.36) for constant meson fields, $\phi(x) \to \phi$ and vanishing gluon, quark and ghost fields. In this case, the effective action reduces to $\Gamma_k = \Omega^{-1}(V_k(\rho) - c\sigma)$, where Ω is the space-time volume. The flow of the effective potential $\bar{V}_k(\bar{\rho}) = V_k(\rho)$ is then given by:

$$\begin{aligned} \partial_t \big|_\rho \bar{V}_k(\bar{\rho}) = 2k^4 v(d) \Big\{ \Big[(N_f^2 - 1) l_0^B(\bar{m}^2_{\pi,k}; \eta_{\phi,k}) + l_0^B(\bar{m}^2_{\sigma,k}; \eta_{\phi,k}) \Big] \\ - 4 N_f N_c l_1^F(\bar{m}^2_{q,k}; \eta_{q,k}) \Big\} , \end{aligned} \tag{4.41}$$

where $v(d) = (2^{d+1}\pi^{d/2}\Gamma(d/2))^{-1}$. The scale derivative $\partial_t\big|_\rho$ is for fixed renormalized fields, i.e. $\partial_t\big|_\rho \bar{\rho} = 0$. The threshold functions l_0^B and l_1^F are defined in App. C.1 and the dimensionless renormalized masses are defined in (4.63). The flows of the couplings $\bar{\nu}_{n,k}$ in (4.22) can be derived from the above equation via:

$$\partial_{\bar{\rho}}^n \, \partial_t|_\rho \bar{V}_k(\bar{\rho})\Big|_{\bar{\rho}=\bar{\kappa}_k} = (\partial_t - n\eta_{\phi,k})\,\bar{\nu}_{n,k}\,, \tag{4.42}$$

See the discussion in Sec. 4.1.1 and in particular (4.28). Rescaling the expansion point and the symmetry breaking source in order to formulate RG invariant flows introduces a canonical running for these parameters:

$$\begin{aligned} \partial_t \bar{\kappa}_k &= -\eta_\phi \bar{\kappa}_k\,, \\ \partial_t \bar{c} &= \frac{1}{2}\eta_\phi \bar{c}\,. \end{aligned} \tag{4.43}$$

The renormalized minimum of the effective potential $\bar{\rho}_{0,k} = \bar{\sigma}_{0,k}^2/2$, which determines the pion decay constant at vanishing IR-cutoff, $\bar{\sigma}_{0,k=0} = f_\pi$, and serves as an order parameter for the chiral phase transition, is obtained from:

$$\partial_{\bar{\rho}}\left[\bar{V}_k(\bar{\rho}) - \bar{c}_k\bar{\sigma}\right]\Big|_{\bar{\rho}_{0,k}} = 0\,. \tag{4.44}$$

All physical observables such as f_π and the masses are defined at vanishing cutoff-scale $k = 0$ and at the minimum of the effective potential $\bar{\rho} = \bar{\rho}_{0,k=0}$.

Since the the explicit symmetry breaking term $-c\sigma$ is linear in the field, but the flow equation contains at least two functional field-derivatives of the effective action, c never enters the flow equations. It merely tilts the effective potential, resulting in a small finite minimum in the symmetric phase. Thus, the effect of explicit symmetry breaking is included after the system of flow equations is solved via (4.44) and can be viewed a a simple shift of the physical minimum of the theory in the chiral limit.

Flow of the Field Dependent Yukawa Coupling. We define the field-dependent Yukawa coupling via the relation $m_{q,k}(\rho) = \sigma h_k(\rho)/2$ at vanishing external momentum and constant meson fields, leading to the following projection:

$$\partial_t h_k(\rho) = -\frac{1}{\sigma}\frac{i}{4N_c N_f}\lim_{p\to 0}\mathrm{Tr}\left(\frac{\delta^2\partial_t\Gamma_k}{\delta q(-p)\delta\bar{q}(p)}\right)\Big|_{\rho(x)=\rho}\,. \tag{4.45}$$

Thus, our projection is based on the quark two-point function. It is directly related to the more customary projection where an additional derivative with respect to the pion fields is applied. One finds

$$-\frac{i}{\sigma}\mathrm{Tr}\left(\partial_t\Gamma_k^{(q\bar{q})}\right) = \mathrm{Tr}\left(\gamma_5\vec{\tau}\,\partial_{\vec{\pi}}\partial_t\Gamma_k^{(q\bar{q})}\right)\Big|_{\vec{\pi}=0}\,. \tag{4.46}$$

Note that a projection using an additional derivative with respect to the sigma field would contaminate the flow with additional contributions from the derivative of the Yukawa coupling.

The resulting flow is given by:

$$\begin{aligned}\partial_t|_{\bar\rho}\bar h(\bar\rho) = &\left(\eta_{q,k}+\frac{1}{2}\eta_{\phi,k}\right)\bar h_k(\bar\rho)\\ &-v(d)\bar h_k(\bar\rho)^3\Big[(N_f^2-1)\,L_{1,1}^{(FB)}(\bar m_{q,k}^2,\bar m_{\pi,k}^2;\eta_{q,k},\eta_{\phi,k})\\ &-L_{1,1}^{(FB)}(\bar m_{q,k}^2,\bar m_{\sigma,k}^2;\eta_{q,k},\eta_{\phi,k})\Big]\\ &+8v(d)\bar h_k(\bar\rho)\bar h_k'(\bar\rho)\bar\rho\left[\bar h_k(\bar\rho)+2\bar\rho\bar h_k'(\bar\rho)\right]L_{1,1}^{(FB)}(\bar m_{q,k}^2,\bar m_{\sigma,k}^2;\eta_{q,k},\eta_{\phi,k})\\ &-2v(d)k^2\Big[\left(3\bar h_k'(\bar\rho)+2\bar\rho\bar h_k''(\bar\rho)\right)l_1^B(\bar m_{\sigma,k}^2;\eta_{\phi,k})+3\bar h_k'(\bar\rho)l_1^B(\bar m_{\pi,k}^2;\eta_{\phi,k})\Big]\\ &-8(3+\xi)\,C_2(N_c)\,v(d)\,g_{\bar qAq,k}^2\,\bar h_k(\bar\rho)L_{1,1}^{(FB)}(\bar m_{q,k}^2,0;\eta_{q,k},\eta_{A,k}),\end{aligned} \tag{4.47}$$

ξ is the gauge fixing parameter, which we set to zero since we use Landau gauge in this work. The threshold function $L_{1,1}^{(FB)}$ is defined App. C.1. The flows of the renormalized couplings $\bar h_{n,k}$ in (4.30) are:

$$\partial_{\bar\rho}^n\,\partial_t|_\rho\bar h(\bar\rho)\Big|_{\bar\rho=\bar\kappa_k} = (\partial_t - n\eta_{\phi,k})\bar h_{n,k}\,, \tag{4.48}$$

in analogy to the flow of the expansion parameters of the effective potential (4.42).

Flow of the Four-Quark Interaction. For the flow of the four-quark coupling we choose the projection in [75]. This yields

$$\begin{aligned}\partial_t\bar\lambda_{S,k} = &-g_{\bar qAq,k}^4\left(\frac{2N_c^2-3}{N_c}\right)v(d)L_{1,2}^{(FB)}(\bar m_{q,k}^2;\eta_{q,k},\eta_{A,k})\\ &+\bar h_k(\bar\kappa)^4\left(\frac{2}{N_c}+1\right)v(d)L_{1,1,1}^{(FB)}(\bar m_{q,k}^2,\bar m_{\pi,k}^2,\bar m_{\sigma,k}^2;\eta_{q,k},\eta_{\phi,k}).\end{aligned} \tag{4.49}$$

In Eq. (4.49), we anticipate full dynamical hadronization for the four fermi interaction. This leads to a vanishing four-quark coupling $\bar\lambda_{S,k}=0$ on the right-hand side: the self-coupling diagram proportional to $\bar\lambda_{S,k}^2$ is dropped. Furthermore, we neglect contributions from higher order quark-meson vertices related to field-derivatives of $\bar h_k(\bar\rho)$, since they are subleading. The field dependence of this coupling is also ignored, i.e. we evaluate the flow at the expansion point $\bar\kappa$.

Quark and Meson Anomalous Dimensions. The anomalous dimensions are related to the flow of the wave-function renormalizations, $\eta=-\partial_t Z/Z$. The Z's encode the non-trivial momentum dependence of the propagators. Here, as already discussed above, we approximate the full momentum, scale and field dependence of the anomalous dimensions by only scale-dependent ones in the leading order expansion in the fields following the discussion in Sec. 4.1.1:

$$Z_{\phi,k}(p^2,\rho)=Z_{\phi,k}(\kappa)\quad\text{and}\quad Z_{q,k}(p^2,\rho)=Z_{q,k}(\kappa). \tag{4.50}$$

For the meson anomalous dimension, we therefore use the following projection:

$$\eta_{\phi,k} = -\frac{1}{2Z_{\phi,k}}\lim_{p\to0}\frac{\partial^2}{\partial|p|^2}\mathrm{Tr}\left(\frac{\delta^2\partial_t\Gamma_k}{\delta\pi_i(-p)\delta\pi_i(p)}\right)\Big|_{\rho=\kappa}, \tag{4.51}$$

where the choice of $i = 1, 2, 3$ does not matter, owing to the $O(3)$ symmetry of the pions. This yields

$$\begin{aligned}\eta_{\phi,k} = {} & 8\, v(d) k^{-2} \bar{\kappa}_k \bar{V}_k''(\bar{\kappa}_k)^2 \mathscr{M}_{2,2}(\bar{m}^2_{\pi,k}, \bar{m}^2_{\sigma,k}) \\ & + 2N_c N_f\, v(d) \bar{h}_k(\bar{\kappa}_k)^2 \left[\mathscr{M}_4(\bar{m}^2_{q,k}; \eta_{q,k}) + \frac{1}{2} k^{-2} \bar{\kappa}_k \bar{h}_k(\bar{\kappa}_k)^2 \mathscr{M}_2(\bar{m}^2_{q,k}; \eta_{q,k}) \right].\end{aligned} \tag{4.52}$$

Note that it is crucial that the functional derivatives in (4.51) are with respect to the pions, since sigma-derivatives would contaminate the flow with contributions proportional to higher orders in the derivative expansion, which we do not take into account here.

For the anomalous dimension of quarks, we use the projection

$$\eta_{q,k} = -\frac{1}{8 N_f N_c Z_{q,k}} \lim_{p\to 0} \frac{\partial^2}{\partial |p|^2} \mathrm{Tr} \left(\gamma_\mu p_\mu \frac{\delta^2 \partial_t \Gamma_k}{\delta q(-p) \delta \bar{q}(p)} \right) \Bigg|_{\rho=\kappa}, \tag{4.53}$$

which yields:

$$\begin{aligned}\eta_q = {} & 2\, v(d)\, C_2(N_c) g^2_{\bar{q}Aq} \left[(3-\xi) \mathscr{M}_{1,2}(\bar{m}^2_{q,k}, 0; \eta_{A,k}) \right. \\ & \left. - 3(1-\xi) \tilde{\mathscr{M}}_{1,1}(\bar{m}^2_{q,k}, 0; \eta_{q,k}, \eta_{A,k}) \right] \\ & + \frac{1}{2} v(d) \left[\left(\bar{h}_k(\bar{\kappa}_k) + 2\bar{\kappa}_k \bar{h}_k'(\bar{\kappa}_k) \right)^2 \mathscr{M}_{1,2}(\bar{m}^2_{q,k}, \bar{m}^2_{\sigma,k}; \eta_{\phi,k}) \right. \\ & \left. + (N_f^2 - 1) \bar{h}_k(\bar{\kappa}_k)^2 \mathscr{M}_{1,2}(\bar{m}^2_{q,k}, \bar{m}^2_{\pi,k}; \eta_{\phi,k}) \right].\end{aligned} \tag{4.54}$$

The corresponding threshold functions can be found in App. C.1.

We have shown in Sec. 3.4 and also show in Sec. 7.3.2 that already a ϕ^4 expansion of the effective potential, corresponding to $N_V = 2$ in (4.22) gives quantitatively precise results for small temperatures and densities. On the other hand, a leading order expansion of the Yukawa coupling, i.e. $N_h = 0$, is not sufficient since the expansion is not yet converged, see Sec. 7.3.2. Here, we choose $N_h = 3$ in (4.30) to ensure that we take the effect of the full field-dependent Yukawa coupling into account. Note that we have to choose $N_V \geq N_h$ for numerical stability and therefore choose $N_V = 5$.

In the infrared regime of QCD, the dynamical degrees of freedom are hadrons, while quarks and gluons are confined inside them. This entails that a formulation in terms of local composite fields with hadronic quantum numbers is more efficient in this regime. Note that these composite fields are directly related to hadronic observables at their poles.

Let us illustrate this at the relevant example of the scalar-pseudoscalar mesonic multiplet at a given cutoff scale k. At a fixed large cutoff scale, where the mesonic potential $V_k(\rho)$ is assumed to be Gaußian, we can resort to the conventional Hubbard-Stratonovich bosonization as explained in Sec. 4.1: the local part of the scalar–pseudo-scalar channel of the four-quark interaction with coupling $\lambda_{S,k}$, see (4.5), can be rewritten as a quark-meson term, see (4.6) and (4.10), on the equations of motion for ϕ, that is ϕ_{EoM}. This leads to

$$\lambda_{S,k} = \frac{h_k^2}{2\nu_{1,k}}, \qquad \phi_{j,\mathrm{EoM}} = \frac{h_k}{\nu_{1,k}} \bar{q} \tau_j q, \tag{4.55}$$

where ν_1 is the curvature mass of the mesonic field and $\tau = (\gamma_5 \vec{T}, iT^0)$, $j \in \{1,2,3,4\}$. Note that (4.55) is only valid for $Z_\phi \equiv 0$ and a Gaußian potential $V_k(\rho) = \nu_1 \rho$. Moreover, miscounting of degrees of freedom may occur from an inconsistent distribution of the original

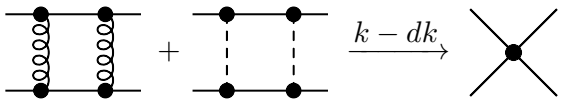

Figure 4.1.: Re-generation of four-quark interactions from the RG-flow.

four-fermi interaction strength to the Yukawa coupling and the four-fermi coupling. The dynamical hadronization technique used in the present work, and explained below, resolves these potential problems.

One advantage of the bosonized formulation concerns the direct access to spontaneous chiral symmetry breaking via the order parameter potential $V_k(\rho)$: spontaneous symmetry breaking is signaled by $v_1 = 0$ at the symmetry breaking scale k_χ, which relates to a resonant four-quark interaction. It also facilitates the access to the symmetry-broken infrared regime.

Before we discuss dynamical hadronization, we briefly recap the conventional bosonization procedure. So let us assume that we have performed the above complete bosonization at some momentum scale $k \gg k_\chi$. There, the above conditions for the bosonization in (4.55) are valid. Hence, we can remove the four-fermi term completely in favor of the mesonic Yukawa sector. However, four-quark interactions are dynamically re-generated from the RG flow via quark-gluon and quark-meson interactions, see Fig. 4.1.

Indeed, these dynamically generated contributions dominate due to the increase of the strong coupling $\alpha_{s,k}$ for a large momentum regime, leading to a quasi-fixed point running of the Yukawa coupling, see Refs. [69, 70] and also our discussions below. Thus, even though $\lambda_{S,k}$ was exactly replaced by $m_{\phi,k}$ and h_k at a scale $k \gg k_\chi$, there is still a non-vanishing RG-flow of $\lambda_{S,k}$ at lower scales which was eliminated by the complete bosonization, but cannot be neglected, especially in the quark-gluon regime at high energies. Note, however, that we have explicitly checked that this is only a minor quantitative effect as long as one considers low-energy effective models, i.e. if the scale one performs a full bosonization is close to k_χ, see Sec. 6.2.

In summary, it is not possible to capture the full dynamics of the system in the quark-gluon phase with the conventional Hubbard-Stratonovich bosonization. As a consequence, within conventional bosonization, the scale where composite fields take over the dynamics from fundamental quarks and gluons is not an emergent scale generated by the dynamics of QCD, but is fixed by hand by the scale where the Hubbard-Stratonovich transformation is performed.

In the present approach we employ dynamical hadronization. It is a formal tool that allows for a unified description of dynamically changing degrees of freedom and consequently is not plagued by the shortcomings of conventional bosonization discussed above. It has been introduced in [69] and was further developed in [70, 139, 144]. The construction works for general potentials $V_k(\rho)$ (more precisely general $\Gamma_k[\Phi]$), and implements the idea of bosonizing multi-fermion interactions at every scale k rather than just at the initial scale. Consequently, the resulting fields of this bosonization procedure, i.e. the mesons, become scale-dependent and can be viewed as hybrid fields: while they act as conventional mesons at low energies, they encode pure quark dynamics at large energy scales.

We already derived the flow equation for general scale dependent fields in Sec. 3.2. Dynamical hadronization is a special case of this more general formulation, where only the meson fields are k-dependent, while all the other fields are not. Thus, we get a special case of (3.21) with

$\Phi_k = (A, c, \bar{c}, q, \bar{q}, \phi_k)$. For the flow of the composite meson fields ϕ_k, we choose

$$\partial_t \phi_k = \dot{A}_k \bar{q} \tau q + \dot{B}_k \phi_k \,. \tag{4.56}$$

For now, the coefficients $\dot{A}_k$ and $\dot{B}_k$ remain unspecified. Specifying them will fix the hadronization procedure as discussed below. Note that the first term in (4.56) reflects the bound state nature of the mesons.

Thus, while the gluon, ghost and quark contributions to the flow (4.36) remain unchanged, the mesonic part now reads according to (3.21)

$$\partial_t\big|_\phi \Gamma_k[\Phi_k] = \frac{1}{2}\mathrm{Tr}\Big[G_{\phi\phi,k}[\Phi]\cdot\big(\partial_t R_k^\phi + 2R_k^\phi \dot{B}_k\big)\Big] - \mathrm{Tr}\left[\frac{\delta\Gamma_k[\Phi]}{\delta\phi_i}\big(\dot{A}_k\bar{q}\tau_i q + \dot{B}_k\phi_i\big)\right]. \tag{4.57}$$

The first term on the right hand side of (4.57) corresponds to the mesonic part of the flow equation (4.36) with a shift in the scale derivative of the regulator owing to the part of $\partial_t\phi_k$ which is proportional to ϕ_k itself. Note that, following our discussion in Sec. 3.2, this term will not spoil the one-loop structure of the flow equation, since we have chosen $\partial_t\phi_k$ such that it is only linear in ϕ_k itself, (4.56). The second term stems from the scale derivative of ϕ_k.

The scale derivative of the meson regulator defined in (C.1) can be written as

$$\partial_t R_k^\phi(p^2) = \big(\partial_t\big|_Z - \eta_{\phi,k}\big) R_k^\phi(p^2), \tag{4.58}$$

with the anomalous dimension of the scale-dependent mesons,

$$\eta_{\phi,k} = -\frac{\partial_t Z_{\phi,k}}{Z_{\phi,k}}, \tag{4.59}$$

and the RG-time derivative for fixed Z_k, $\partial_t\big|_Z$. This choice of the regulator functions implies that the flow equations of RG-invariant quantities only contain the anomalous dimension which stems from the scale derivative of the regulator whereas the wave function renormalizations drop out completely. With this, we can rewrite (5.26) into:

$$\begin{aligned}\partial_t\big|_\phi \Gamma_k[\Phi_k] = {}& \frac{1}{2}\mathrm{Tr}\Big[G_{\phi\phi,k}[\Phi]\cdot\big(\partial_t\big|_Z - (\eta_{\phi,k} - 2\dot{B}_k)\big)R_k^\phi\Big] \\ & - \mathrm{Tr}\left[\frac{\delta\Gamma_k[\Phi]}{\delta\phi_i}\big(\dot{A}_k\bar{q}\tau_i q + \dot{B}_k\phi_i\big)\right].\end{aligned} \tag{4.60}$$

It is now obvious that the first line of the modified flow equation above gives the original flow equations without scale-dependent fields, but with a shifted meson anomalous dimension:

$$\eta_{\phi,k} \to \eta_{\phi,k} - 2\dot{B}_k \,. \tag{4.61}$$

The coefficient, $\dot{B}_k$, in (4.56) is at our disposal, and we may use it to improve our truncation.

The second line of (4.60) induces additional contributions in particular to the flows of the four-quark and the Yukawa couplings, owing to the particular ansatz we made for $\partial_t\phi_k$. This allows us to specify the hadronization procedure: we choose the coefficient $\dot{A}_k$ such that the flow of the four-quark interaction $\lambda_{S,k}$ vanishes within our truncation, $\partial_t\lambda_{S,k} = 0$. This way, all informations about the multi-quark correlations are stored in the flow of the Yukawa coupling. Thus, h_k encodes the multi-quark correlations in the quark-gluon phase and the meson–constituent-quark correlations in the hadronic phase, including a dynamical transition between these different regimes.

4.2.2. Hadronized Flow Equations

Here, we specify the hadronization procedure and give the resulting modified flow equations of the scale-dependent parameters of the truncation (4.12). These modifications are given by explicitly evaluating the second line of (4.60). Note that the explicit form of the modified flow equations depends on the details of our projection procedures, see also App. C.1.

In the following, we rescale all fields with their respective wave-function renormalization, $\bar{\Phi} = Z_{\Phi,k}^{1/2}\Phi$ and introduce the RG-invariant parameters $\bar{v}_{n,k}$ as in (4.23), $\bar{h}_{n,k}$ as in (4.31), $\bar{c}$ as in (4.33) and

$$\bar{\lambda}_{S,k} = \frac{\lambda_{S,k}}{Z_{q,k}^2}\,. \tag{4.62}$$

Our conventions for the gauge sector imply that the gauge coupling is already RG-invariant, $\bar{g}_k = g_k$, see (4.1). The RG-invariant dimensionless masses are defined accordingly as

$$\begin{aligned} \bar{m}_{q,k} &= k^{-1} M_{q,k} = \frac{m_{q,k}}{k\, Z_{q,k}}\,, \\ \bar{m}_{\pi/\sigma,k} &= k^{-1} M_{\pi/\sigma,k} = \frac{m_{\pi/\sigma,k}}{k\, Z_{\phi,k}^{1/2}}\,. \end{aligned} \tag{4.63}$$

Note that we rescale mesonic parameters with the wave-function renormalization $Z_{\phi,k}$ of the scale-dependent mesons ϕ_k. The constant source c has a canonical running after rescaling, given only by the running of $Z_{\phi,k}$. Consequently, we also rescale the hadronization functions:

$$\dot{\bar{A}}_k = Z_{\phi,k}^{1/2} Z_{q,k}^{-1} \dot{A}_k\,, \qquad \dot{\bar{B}}_k = \dot{B}_k\,. \tag{4.64}$$

With this, we proceed now to the modified flow equations of these RG-invariant quantities.

For the flow of the four-quark interaction $\bar{\lambda}_{S,k}$ we find:

$$\partial_t\big|_\phi \bar{\lambda}_{S,k} = 2\eta_{q,k}\bar{\lambda}_{S,k} + \partial_t \bar{\lambda}_{S,k}\big|_{\eta_{\phi,k}\to\eta_{\phi,k}-2\dot{\bar{B}}_k} + \left(\bar{h}_k(\bar{\rho}) + 2\bar{\rho}\bar{h}_k'(\bar{\rho})\frac{4N_f N_c - 1}{2N_f N_c + 1}\right)\dot{\bar{A}}_k\,. \tag{4.65}$$

Here, $\partial_t \bar{\lambda}_{q,k}$ denotes the flow without dynamical hadronization which is given by (4.49). As already discussed above, this contribution is subject to a shift in the meson anomalous dimension, indicated by $\eta_{\phi,k} \to \eta_{\phi,k} - 2\dot{\bar{B}}_k$.

Following the discussion in the previous section, we choose $\dot{\bar{A}}_k$ such that the flow of $\bar{\lambda}_{S,k}$ vanishes. This is achieved by the following choice:

$$\dot{\bar{A}}_k = -\left(\bar{h}_k(\bar{\rho}) + 2\bar{\rho}\bar{h}_k'(\bar{\rho})\frac{4N_f N_c - 1}{2N_f N_c + 1}\right)^{-1} \partial_t \bar{\lambda}_{S,k}\big|_{\eta_{\phi,k}\to\eta_{\phi,k}-2\dot{\bar{B}}_k}\,. \tag{4.66}$$

Together with the initial condition $\bar{\lambda}_{S,\Lambda} = 0$, this yields

$$\partial_t\big|_\phi \bar{\lambda}_{S,k} = 0. \tag{4.67}$$

The flow of the Yukawa coupling assumes the following form:

$$\begin{aligned} \partial_t\big|_\phi \bar{h}_k = &\left(\eta_{q,k} + \frac{1}{2}\eta_{\phi,k}\right)\bar{h}_k + \partial_t \bar{h}_k\big|_{\eta_{\phi,k}\to\eta_{\phi,k}-2\dot{\bar{B}}_k} \\ &- \left(p^2 + \bar{V}_k'(\bar{\rho})\right)\dot{\bar{A}}_k - \left(\bar{h}_k + 2\bar{\rho}\bar{h}_k'\right)\dot{\bar{B}}_k\,, \end{aligned} \tag{4.68}$$

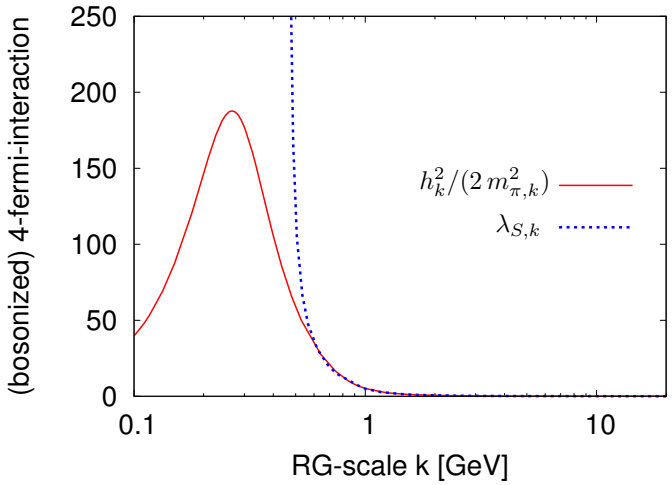

Figure 4.2.: Flow of the $(S-P)$-channel four-quark interaction from a purely quark-gluonic theory in comparison to the ratio $h_k^2/(2m_{\pi,k})$ from the dynamically hadronized theory. We see that $h_k^2/(2m_{\pi,k})$ mimics $\lambda_{S,k}$ at large scales down to the chiral transition scale k_χ, where $\lambda_{S,k}$ becomes resonant. Thus, owing to dynamical hadronization and in particular (4.68), the four-quark dynamics are essentially encoded in h_k for $k \gtrsim k_\chi$. For scales smaller than k_χ, $h_k^2/(2m_{\pi,k})$ follows a typical mesonic flow, while $\lambda_{S,k}$ can not access this regime. This Figure is taken from [156]. Note that the results are obtained with finite pion masses. Thus, the scale of the minimum of the pion mass does not necessarily coincide with the transition scale.

where $\bar{h}_k = \bar{h}_k(\bar{\rho})$ is implied and $\partial_t \bar{h}_k$ is given by (4.47). From Eq. (4.66), it is now clear that the flow of the quark interaction and, therefore, all information about the multi-quark correlations within our truncation, is incorporated into the flow of the hadronized Yukawa coupling.

At large energy scales, meson are not present and therefore their interactions are irrelevant. The mesonic part of the effective action can therefore be thought of as purely Gaußian. Thus, the Hubbard-Stratonovich relation (4.55) between the four-quark interaction, the Yukawa coupling and the curvature mass holds with dynamical hadronization over a large range of scales. This is shown in Fig. 4.2. There, $\lambda_{S,k}$ from a purely quark-gluonic theory, i.e. $\Gamma_k^{(\mathrm{qg})} = \Gamma_k^{(\mathrm{mQCD})} + \Gamma_k^{(4\mathrm{q})}$, is compared to the ratio $h_k^2/(2m_{\pi,k})$ from the dynamically hadronized theory (4.12).

It is left to specify the hadronization function $\dot{\bar{B}}_k$, which also enters (4.68). It can be used to improve the current approximation by absorbing a part of the momentum-dependence of the mesonic wave-function renormalization and the Yukawa coupling. This will be discussed elsewhere. Here, we use

$$\dot{\bar{B}}_k \equiv 0\,. \tag{4.69}$$

Let us comment on the precise form of the flow of the hadronization field ϕ_k given in (4.56). Owing to relation (4.55) for the conventional Hubbard-Stratonovich bosonization, the strength of the four quark interaction can be arbitrarily distributed between the Yukawa coupling h_k and the mass of the pion $m_{\pi,k}$. Thus, if no further conditions on h_k and $m_{\pi,k}$ are applied, an unambiguous definition of the meson masses from the quark-gluon dynamics is impossible, since only the ratio $\sim h_k^2/m_{\pi,k}^2$ is fixed from $\lambda_{S,k}$, which, in turn, derives from quark-gluon

fluctuations at large energies. Dynamical hadronization is based on the requirement of a vanishing four-quark interaction at all scales (5.27), $\partial_t \lambda_{s,k}=0$. Without any assumptions on the flow of ϕ_k, the last term of (3.21) gives rise to the condition

$$\begin{aligned}\frac{\delta\Gamma_k}{\delta\phi_{i,k}}\partial_t\phi_{i,k} &= \left[Z_{\phi,k}p^2\phi_{i,k}+\phi_{i,k}V_k'(\rho_k)+\phi_{i,k}h_k'(\rho_k)\bar{q}(\boldsymbol{\tau}\cdot\boldsymbol{\phi}_k)q+h_k(\rho_k)\bar{q}\tau_i q\right]\partial_t\phi_{i,k}\\ &\stackrel{!}{=} C_k(\bar{q}\tau_i q)^2\,,\end{aligned} \tag{4.70}$$

in order to fulfill the hadronization requirement, because otherwise the four quark interaction (4.5) could not be canceled for every k. C_k is an k-dependent coefficient whose precise form is irrelevant for the argument. It is now immediately clear that $\partial_t\phi_k \propto \bar{q}\tau_i q$ is the simplest choice. As we have shown above, this choice leads to (4.68), which implies that *all* information about the four-quark interaction is stored in the Yukawa coupling. Thus, our specific choice for the hadronization procedure provides the additional condition we need to remove the ambiguity related to the distribution of the strength of the four-quark interaction between the Yukawa coupling and the meson masses. Furthermore, we will explicitly demonstrate in Sects. 4.4.4 and 5.3.3 the the running of the meson masses in the quark-gluon regime is exclusively driven by the meson anomalous dimensions. This implies that the meson masses can unambiguously be defined from quark-gluon dynamics.

We see that our hadronization procedure enforces a vanishing four-quark interaction. The effect of four-quark correlations is then stored in the Yukawa coupling, which now serves a dual purpose: while it captures the current-quark self-interactions in the quark-gluon phase, it describes the meson–constituent-quark interactions in the hadronic phase. This is exactly what we need to describe the dynamical transition from quarks and gluons to mesonic degrees of freedom.

4.3. Gauge Sector

In this section, we discuss the gauge sector of the truncation given in (4.1). Most importantly, this permits to distinguish the quark-gluon coupling from pure gluodynamics. This directly signals the transition from the perturbative quark-gluon regime at large momenta, where all couplings scale canonically, to the hadronic regime where non-perturbative effects are dominant.

The couplings induced from three-point functions play a dominant role in the description of interactions. Hence, we solve the flow equations for all three-point functions in QCD, the quark-gluon, three-gluon and ghost-gluon vertices. In addition, the effects from the four-gluon vertex are important [71,158,159]. Thus, we employ an ansatz which has proven to be accurate in previous studies [158,159]. For the computation presented here, we take the gluon and ghost propagators from pure gauge theory as input [71,159] and augment them by unquenching effects. In the perturbative domain this procedure is accurate, as the error is order $\alpha_{s,k}^2$. At scales below the confinement transition the gluon is gapped and therefore decouples from the dynamics.

Perturbation theory gives a direct relation between the number of gluon legs m attached to the vertex $\Gamma^{(n)}$ and the order in the strong coupling, $\Gamma^{(n)} \sim (4\pi\alpha_{s,k})^{m/2}$. Nevertheless, the RG running is different, although purely induced by the external legs attached. Their wave function renormalizations cancel exactly those from the propagators, see (4.74) below. As a result of this truncation, the flow equations for the couplings depend on the anomalous dimensions only, as discussed above and also shown below.

In this analysis we restrict ourselves to classical tensor structures of the gauge action $S[\Phi]$. Omitting color and Lorentz indices for clarity, we parametrize the quark-gluon, three- and four-gluon and the ghost-gluon vertices as

$$\begin{aligned}
\Gamma_k^{(\bar{q}Aq)} &= Z_{A,k}^{\frac{1}{2}} Z_{q,k}\, g_{\bar{q}Aq,k}\, S^{(3)}_{\bar{q}Aq}\,, \\
\Gamma_k^{(A^3)} &= Z_{A,k}^{\frac{3}{2}}\, g_{A^3,k}\, S^{(3)}_{A^3}\,, \\
\Gamma_k^{(A^4)} &= Z_{A,k}^{2}\, g^2_{A^4,k}\, S^{(4)}_{A^4}\,, \\
\Gamma_k^{(\bar{c}Ac)} &= Z_{A,k}^{\frac{1}{2}} Z_{c,k}\, g_{\bar{c}Ac,k}\, S^{(3)}_{\bar{c}Ac}\,.
\end{aligned} \tag{4.71}$$

The classical tensor structures $S^{(n)}_{\Phi_1\dots\Phi_n}$ are obtained from (4.1) by

$$S^{(n)}_{\Phi_1\dots\Phi_n} = \left.\frac{\delta^n \Gamma_\Lambda}{\delta\Phi_1\dots\delta\Phi_n}\right|_{g_k=1}\,. \tag{4.72}$$

Here, we use as input the gluon/ghost two-point functions $\Gamma^{(2),\mathrm{YM}}_{A/c,k}(p)$ computed in [159,168],

$$\begin{aligned}
\Gamma^{(2),\mathrm{YM}}_{A,k}(p) &= Z^{\mathrm{YM}}_{A,k}(p^2)\, p^2\, \Pi^{\perp}\,, \\
\Gamma^{(2),\mathrm{YM}}_{c,k}(p) &= Z^{\mathrm{YM}}_{c,k}(p^2)\, p^2\,.
\end{aligned} \tag{4.73}$$

In order to make full use of this non-trivial input, we expand the flow equation for the gluon propagator in QCD about that in Yang-Mills theory as explained below. This way, we obtain the gluon dressing function of QCD, $Z_{A,k}$, i.e. including the effects of dynamical quarks, based on the Yang-Mills dressing function $Z^{\mathrm{YM}}_{A,k}$. The freedom in defining the cutoff function R^A_k, is used to simplify the analysis. This is done by choosing the same prefactor $Z_{A,k}$ for the gluon regulator as for the vertex parametrizations in (4.71). Note that the gluon propagator enters in loop integrals with momenta $p^2 \lesssim k^2$. If we estimate the full gluon propagator with the simple expression (omitting the tensor structure for clarity)

$$G_{A,k}(p) = \frac{1}{Z_{A,k}(p^2)p^2 + R^A_k} \approx \frac{1}{Z_{A,k}\, p^2 + R^A_k} = \frac{1}{Z_{A,k}}\,\frac{1}{p^2\,(1 + r_B(p^2/k^2))}\,, \tag{4.74}$$

i.e. we consider the RG-scale and momentum dependent gluon wave function renormalization $Z_{A,k}(p)$ to be only scale dependent, the system of flow equations under consideration is tremendously simplified. The error of such a simple estimate relates to

$$p^3\left(\frac{1}{Z_{A,k}(p^2)p^2 + R^A_k} - \frac{1}{Z_{A,k}p^2 + R^A_k}\right)^n = p^{3+2n}\left(\frac{Z_{A,k} - Z_{A,k}(p^2)}{\left(Z_{A,k}(p^2)p^2 + R^A_k\right)\left(Z_{A,k}p^2 + R^A_k\right)}\right)^n\,, \tag{4.75}$$

where the factor p^3 stems from the momentum integration $\sim dp\, p^3$. The expression in (4.75) occurs with powers $n \geq 1$ in the difference of the full flow equations and the approximated flows with (4.74), and is evaluated for momenta $p^2 \lesssim k^2$. For small momenta it tends towards zero while its value for maximal momenta $p^2 \approx k^2$ is proportional to the difference $Z_{A,k} - Z_{A,k}(k^2)$. Consequently, we choose

$$Z_{A,k} = Z_{A,k}(k^2)\,. \tag{4.76}$$

We have checked that the difference between full flows and approximated flows is less than 5% for all k.

Within approximations (4.71) and (4.74), the gluon propagator enters flow equations only via the anomalous dimension $\eta_{A,k}$ with

$$\eta_{A,k} = -\frac{\partial_t Z_{A,k}}{Z_{A,k}}\,. \tag{4.77}$$

Note that, as a consequence of (4.76), $\eta_{A,k}$ has two contributions from the full dressing function $Z_{A,k}(p^2)$,

$$\partial_t Z_{A,k} = \partial_t Z_{A,k}(p^2)\big|_{p^2=k^2} + 2k^2 \frac{\partial Z_{A,k}(p^2)}{\partial p^2}\bigg|_{p^2=k^2}\,. \tag{4.78}$$

The first term stems from the genuine k-dependence of the dressing function, while the second term results from its momentum dependence. As it is the case for any flow of a coupling in a gapped theory (away from potential fixed points), the first term of (4.78) vanishes in the limit $k\to 0$,

$$\lim_{k\to 0} \partial_t Z_{A,k}(p^2)\big|_{p^2=k^2} = 0\,. \tag{4.79}$$

The second term of (4.78) carries the information about the momentum dependence of the dressing function and in particular of the (bare) mass gap $m_{\rm gap}$ at small momenta. The gluon propagator exhibits a gap at small momentum scales and hence the dressing function of the full quantum theory, $Z_{A,k=0}(p^2)$, is of the form

$$\lim_{p^2\to 0} Z_{A,k=0}(p^2) \propto \frac{m_{\rm gap}^2}{p^2}\,. \tag{4.80}$$

This implies for the second term in (4.78)

$$\lim_{k\to 0} 2k^2 \partial_{p^2} \ln\big(Z_{A,k}(p^2)\big)\Big|_{p^2=k^2} = -2\,. \tag{4.81}$$

Thus, the second term of (4.78), which is a result of our specific definition of the purely RG-scale dependent gluon wave function renormalization (4.76), is responsible for a non-vanishing gluon anomalous dimension $\eta_{A,k}$ as defined in (4.77) for $k\to 0$.

We note that this difference between the pure k-dependence and the momentum dependence of the gluon dressing function is a highly non-trivial observation, since it implies that RG-scale dependence alone does not suffice to capture the non-perturbative physics of YM/QCD in the gauge sector, even on a qualitative level. It is indispensable to resolve the full momentum dependence of the gluon (and ghost) propagators in order to capture the confining properties of the theory, because the information about the mass gap is only stored in the momentum dependence, not in the k dependence. This is in contrast to the chiral properties of the matter sector of QCD, where approximations based on solely k-dependent parameters capture all the relevant physics at least qualitatively.

It is crucial that $Z_{A,k}$ does not appear explicitly in the flow equations, and hence flows do only depend on $\eta_{A,k}$, the vertex couplings g, masses and further couplings. Note that this is only partially due to the approximation in (4.74). It mainly relates to the parameterization

(4.71) of the vertices which stores most of the non-trivial information in the associated vertex couplings

$$\alpha_i = \frac{g_i^2}{4\pi}, \quad \text{with} \quad i = \bar{c}Ac\,, A^3\,, A^4\,, \bar{q}Aq\,. \tag{4.82}$$

This freedom to choose the parametrization of the vertices directly relates to the reparametrization invariance of the theory and hence to RG invariance. The above discussion in particular applies to the anomalous dimension itself: first, we note that the glue part $\eta_{\text{glue},k}$ of the anomalous dimension $\eta_{A,k}$ only depends on the vertex couplings:

$$\eta_{\text{glue},k} = \eta_{\text{glue},k}(\alpha_{\bar{c}Ac}\,, \alpha_{A^3}\,, \alpha_{A^4})\,. \tag{4.83}$$

In the semi-perturbative regime these couplings agree due to the (RG-)modified Slavnov–Taylor identities [139, 146, 169, 170], which themselves do not restrict the couplings in the non-perturbative transition regime, see Ref. [156]. In turn, in the non-perturbative regime the couplings differ already due to their different scalings with the gluonic dressing $Z_{A,k}$. For small cutoff scales $k \to 0$, following our discussion above, this dressing diverges proportional to the QCD mass gap,

$$\lim_{k\to 0} Z_{A,k} \propto \bar{m}_{\text{gap}}^2 = \frac{m_{\text{gap}}^2}{k^2}\,. \tag{4.84}$$

This is a slight abuse of notation since $\bar{m}_{\text{gap}}^2$ in (4.84) is not renormalized as the other dimensionless mass ratios $\bar{m}^2$. Here it simply relates to the wave-function renormalization $Z_{A,k}$ defined in (4.76). Hence, it is not RG-invariant and should not be confused with the physical mass gap of QCD. It is related with the latter upon an appropriate renormalization.

As a consequence, while we expect $\alpha_{\bar{c}Ac} \approx \alpha_{\bar{q}Aq}$ down to small scales, the purely gluonic couplings α_{A^3/A^4} should be suppressed to compensate the higher powers of diverging $Z_{A,k}$ present in the vertex dressing in (4.71). This also entails that we may parameterize the right hand side of (4.84) with powers of $1/\alpha_i$. For $i = \bar{c}Ac$, $\bar{q}Aq$, for example, we expect $1/\alpha_i$. In accordance with this observation, we parameterise the difference of the various vertex couplings in η_{glue} with the gap parameter $\bar{m}_{\text{gap}}$ defined in (4.84) and conclude for the gluon anomalous dimension of QCD

$$\eta_{A,k} = \eta_{\text{glue},k}(\alpha_s, \bar{m}_{\text{gap}}) + \Delta\eta_{A,k}(\alpha_{\bar{q}Aq}, \bar{m}_q)\,, \tag{4.85}$$

where α_s stands for either $\alpha_{\bar{c}Ac}$ or α_{A^3}. We shall check that our results do not depend on this choice which justifies the identification of the couplings in (4.85). Note that this does not entail that the couplings agree but that they differ only in the regime where the glue fluctuations decouple. Moreover, in the present approximation α_{A^4} is not computed separately but identified with α_{A^3}. $\Delta\eta_{A,k}$ is the vacuum polarization of the gluon due to virtual quark-antiquark pairs created from the vacuum. Thus, $\Delta\eta_{A,k}$ contains the direct contribution of quark fluctuations to the gluon dressing. Note that quark fluctuations also enter indirectly, since they influence the gauge couplings of QCD as well.

We note that a simple reduction of (4.85) is given by

$$\eta_{A,k} = \eta_{A,k}^{\text{YM}} + \Delta\eta_{A,k}(\alpha_{\bar{q}Aq}, \bar{m}_q)\,. \tag{4.86}$$

This amounts to a gluon propagator, where the vacuum polarization is simply added to the Yang-Mills propagator. This approximation has been used in an earlier work, [140, 154, 155],

and subsequently in related Dyson-Schwinger works, see e.g. [45, 171–173]. We will refine this approximation based on the discussion above (in particular (4.85)) and explain the details in the following.

The quark contribution to the gluon anomalous dimension, $\Delta\eta_{A,k}$, is computed from

$$\Delta\eta_{A,k} = \frac{Z_{A,k}^{-1}}{3(N_c^2-1)} \left(\frac{\partial^2}{\partial p^2} \Pi^{\perp}(p) \cdot \right. \left. \right) \Big|_{p=0} \tag{4.87}$$

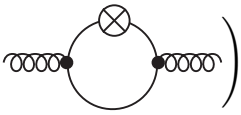

Here, p is the modulus of the external momentum and $\Pi^{\perp}$ is the transversal projection operator defined in (4.40). Note that the dots represent the full vertices and the lines stand for the full propagators. The crossed circle represents the regulator insertion. For $N_f = 2$ and $N_c = 3$ we find

$$\Delta\eta_{A,k} = \frac{1}{24\pi^2}\, g_{\bar{q}Aq,k}^2 (1+\bar{m}_{q,k}^2)^{-4} \left[4 - \eta_{q,k} + 4\bar{m}_{q,k}^2 + (\eta_{q,k}-1)\,\bar{m}_{q,k}^4 \right] \tag{4.88}$$

The derivation of this equation is shown in App. C.2. The approximation (4.87) works well as long as the quark contribution has only a mild momentum dependence. This is the case due to the gapping of the quarks via spontaneous chiral symmetry breaking, and has been checked explicitly. Note that in the perturbative limit, $\eta_{q,k}, \bar{m}_{q,k} \to 0$, (4.88) reduces to the well-known result of one-loop perturbation theory, $\Delta\eta_{A,k} = g_{\bar{q}Aq,k}^2/(6\pi^2)$.

This leaves us with the task of determining $\eta_{\mathrm{glue},k}(\alpha_s, m_{\mathrm{gap}}^2)$ of (4.85), the pure glue contribution to $\eta_{A,k}$. The loop expression for η_{glue} only consists of Yang-Mills diagrams. As, according to our discussion above, it depends solely on the value of the coupling α_s, we arrive at

$$\eta_{\mathrm{glue}}(\alpha_s, \bar{m}_{\mathrm{gap}}^{\mathrm{QCD}}) = \eta_A^{\mathrm{YM}}(\alpha_s, \bar{m}_{\mathrm{gap}}^{\mathrm{QCD}}), \tag{4.89}$$

i.e. the pure gauge part of the qluon anomalous dimension of QCD is identical to the gluon anomalous dimension of pure Yang-Mills theory with the YM couplings replaced by the QCD couplings. η_A^{YM} can be determined in Yang-Mills theory or in quenched QCD as a function of α_s and $\bar{m}_{\mathrm{gap}}$.

For using (4.89), of course, a trackable form of η_A^{YM} as well as $\bar{m}_{\mathrm{gap}}^{\mathrm{QCD}}$ is required. To this end, we first note that $\alpha_{s,k}$ is a multi-valued function in both Yang-Mills theory/quenched QCD and QCD, see Fig. 4.3. This is obvious, since $\alpha_{s,k}$ is a non-monotonous function of k. The two branches meet at $k = k_{\mathrm{peak}}$, the peak of the strong coupling, with

$$\partial_t \alpha_{s,k}\big|_{k=k_{\mathrm{peak}}} = 0\,. \tag{4.90}$$

We have an UV branch $\eta^+(\alpha_s, \bar{m}_{\mathrm{gap}})$ for $k > k_{\mathrm{peak}}$ and an IR branch $\eta^-(\alpha_s, \bar{m}_{\mathrm{gap}})$ for $k < k_{\mathrm{peak}}$. In the left plot in Fig. 4.3 we show η_A^{YM} as a function of the coupling. Interestingly, $\eta^+(\alpha_{s,k})$ is well-described by a quadratic fit in α_s up to couplings close to $\alpha_{s,k_{\mathrm{peak}}}$. In turn, $\eta^-(\alpha_{s,k})$ is well-described as a function of the cutoff scale as indicated by (4.84). In the deep IR, the gluon dressing function is basically given by the bare gap, $Z_{A,k\to 0} \propto m_{\mathrm{gap}}^2/k^2$ and hence

$$\lim_{k\to 0} \eta_{A,k} = 2\,, \tag{4.91}$$

see also the discussion above and in particular (4.81). This is seen in Fig. 4.3. We also see in this figure that the whole IR branch η^- is almost constant. This implies that the mass gap which

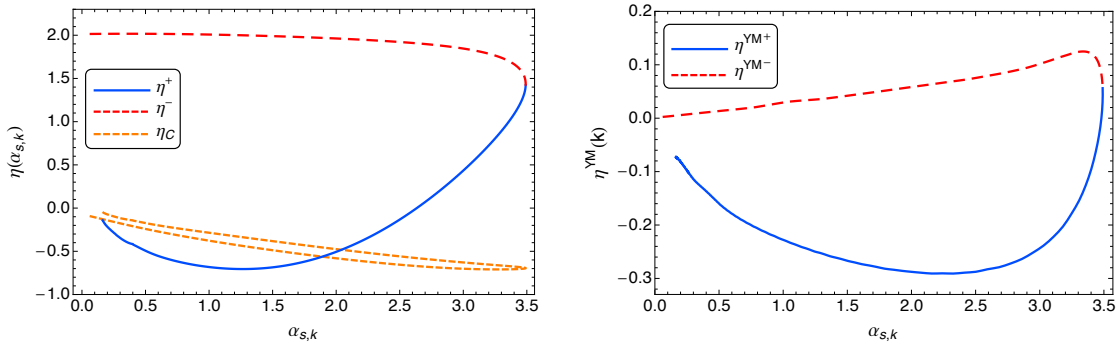

Figure 4.3.: UV and IR branches of the Yang-Mills contribution to the gluon anomalous dimension as a function of the strong coupling. The left figure shows $\eta^{\mathrm{YM}}_{A,k}$, defined in (4.77), as well as $\eta^{\mathrm{YM}}_{c,k}$. η^+ is the UV branch and η^- the IR branch of $\eta^{\mathrm{YM}}_{A,k}$. The right figure shows the UV and IR branches $\eta^{\mathrm{YM}+}$ and $\eta^{\mathrm{YM}-}$ of $\tilde{\eta}^{\mathrm{YM}}_{A,k}(k)$, which is defined in (4.95). Note that the different values of η^- and $\eta^{\mathrm{YM}-}$ at vanishing $\alpha_{s,k}$ are a consequence of the specific definitions $\eta^{\mathrm{YM}}_{A,k}$ and $\eta^{\mathrm{YM}}_{A,k}(k)$, see in particular (4.80) and (4.81).

suppresses $\alpha_{s,k}$ develops very quickly around $k \approx k_{\mathrm{peak}}$ and is then almost constant for the rest of the flow for $k \lesssim k_{\mathrm{peak}}$. Following these arguments, we can derive a simple parametrization for the IR-branch as a function of the RG-scale,

$$\eta^-(k) = 2 - c^- k^2, \quad \text{with} \quad c^- = \frac{2 - \eta^{\mathrm{YM}}_A(\alpha_{\mathrm{peak}})}{k^2_{\mathrm{peak}}}, \tag{4.92}$$

where the mass gap $\bar{m}^2_{\mathrm{gap}}$ relates to $\eta^{\mathrm{YM}}_A(\alpha_{\mathrm{peak}})$. Note that the quality of these simple fits entails that the transition from the semi-perturbative regime to the non-perturbative IR regime happens very rapidly and asymptotic fits in both areas work very well. In summary we arrive at the final representation of η^{YM}_A with

$$\eta^{\mathrm{YM}}_{A,k} = \eta^+(\alpha_{s,k})\theta(\alpha_{s,k} - \alpha_{s,\mathrm{peak}}) + \eta^-(k)\theta(\alpha_{s,\mathrm{peak}} - \alpha_{s,k}). \tag{4.93}$$

Inserting (4.93) on the right hand side of (4.89) gives us a closed equation for $\eta_{A,k}$ in (4.85). Its integration also provides us with the QCD mass gap.

The same analysis as for η_A can be applied to the ghost anomalous dimension η_c of dynamical QCD, leading to a similar representation with the only difference that $\eta_{c,k=0} = 0$. It turns out that an even simpler global linear fit gives quantitatively reliable results for matter correlations,

$$\eta_{c,k}(\alpha_{s,k}) = \frac{\alpha_{s,k}}{\alpha} \eta^{\mathrm{YM}}_{c,k}(\alpha), \tag{4.94}$$

where $\alpha_{s,k} = \alpha_{\bar{c}Ac,k}$, see Fig. 4.3. This modification is used in the equation for the ghost-gluon vertex. Note that this overestimates ghost-gluon correlations in the deep infrared, but there the glue-sector has decoupled from the matter sector. Hence this is of no relevance for the physics of chiral symmetry breaking discussed in the present work.

We are now in a position to finally determine the momentum dependent ghost and gluon propagators at vanishing cutoff scale in dynamical QCD. Again, we could use the $\alpha, \bar{m}_{\mathrm{gap}}$

representation for extracting the full dressing function $Z_{A,k}(p)$ on the basis of the results. To that end, the momentum-dependent flows as functions of $\alpha, \bar{m}_{\rm gap}$ are required,

$$\tilde{\eta}^{\rm YM}_{A,k}(p) = -\frac{\partial_t Z^{\rm YM}_{A,k}(p)}{Z^{\rm YM}_{A,k}(p)}\,, \qquad \partial_t \Delta\Gamma^{(2)}_{A,k}(p)\,, \tag{4.95}$$

where $\Delta\Gamma^{(2)}_{A,k}(p)$ stands for the momentum-dependent flow of the vacuum polarization. The first term in (4.95) again is well approximated in terms of a low order polynomial in α_s. This is expected because is relates directly to the standard anomalous dimension of the gluon. In the right plot of Fig. 4.3 it is shown for momentum $p = k$ as a function of $\alpha_{s,k}$. The definition of $\tilde{\eta}^{\rm YM}_{A,k}(p)$ implies that only the first term in (4.78) contributes here. Thus, for vanishing k (4.80) holds and hence $\lim_{k\to 0} \tilde{\eta}^{\rm YM}_{A,k}(k) = 0$ as observed in the right plot of Fig. 4.3.

An already very good estimate for the dressing function is

$$Z_{A,k=0}(p) \simeq Z_{A,k=p}(p) = Z_{A,k=p}\,, \tag{4.96}$$

as the flow of the propagators decay rapidly for momenta larger than the cutoff scale, $p \gtrsim k$. Moreover, the momentum derivative of the dressing is only large in the UV-IR transition regime. In Fig. 4.4, the inverse dressing $1/Z_{A,0}(p)$ and its approximation $1/Z_{A,p}$ are shown. Clearly, there are only minor deviations in the UV-IR transition regime. The same argument holds true to an even better degree for the quark contribution, and we have checked the smoothness of the flow $\Delta\Gamma_{A,k}(p)$. This leads to a very simple, but quantitative estimate for the full dressing function with

$$Z^{\rm glue}_{A/c,k=0}(p) \simeq \frac{Z^{\rm YM}_{A/c,k=0}(k_\alpha)}{Z^{\rm YM}_{A/c,k_\alpha}}\, Z^{\rm glue}_{A/c,k=p}\,, \tag{4.97}$$

with

$$Z^{\rm glue}_{A/c,k} = \exp\left\{-\int_\Lambda^p \frac{dk}{k}\eta^{\rm glue}_{A/c,k}\right\}\,, \tag{4.98}$$

where $Z_{A/c,\Lambda} = 1$, and $k_\alpha = k(\alpha_{s,k})$ is the YM-cutoff value that belongs to a given coupling α_s.

In summary we conclude that, based on Fig. 4.4, an already quantitative approximation to the fully unquenched propagator is achieved if putting the ratio in (4.97) to unity. This leads to

$$Z_{A/c}(p) \simeq \exp\left\{-\int_\Lambda^p \frac{dk}{k}\eta_{A/c,k}\right\}\,, \tag{4.99}$$

with $\eta_{A/c,k}$ defined in (4.85) and (4.94). In the non-perturbative regime, diagrams involving an internal gluon are suppressed with the generated gluon mass. Hence, albeit the approximation by itself may get less quantitative in the infrared, the error propagation in the computation is small.

In summary this leaves us with relatively simple analytic flow equations for the fully back-coupled unquenching effects of glue and ghost propagators. A full error analysis of the analytic approximations here is advisable and should be done in the future, since it is very important for the reliable application of the present procedure to finite temperature and density.

In the following, we will outline the definition and derivation of the gluonic vertices we use. First of all, we only take into account the classical tensor structure of the vertices. Moreover,

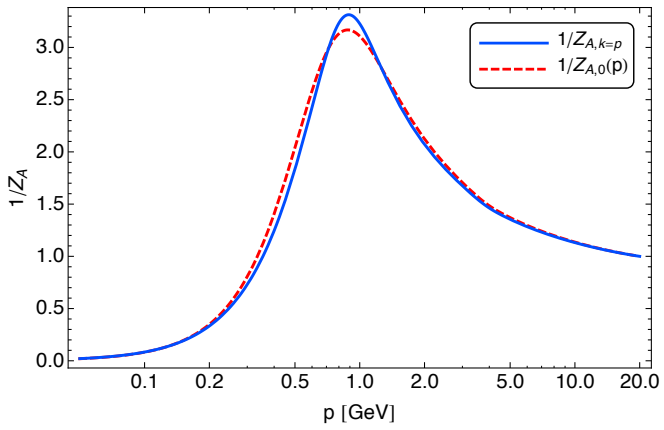

Figure 4.4.: Comparison of the momentum dependent gluon dressing function $Z_{A,0}(p)$ and $Z_{A,k=p}$.

throughout this work, we define the running coupling at vanishing external momentum. Together with our choice for the regulators, this has the advantage that the flow equations are analytical equations. In particular, loop-momentum integrations can be performed analytically. This approximation is semi-qunatitative as long as the dressing of the classical tensor structures do not show a significant momentum dependence, and the other tensor structures are suppressed.

This approximation is motivated by results on purely gluonic vertices, see Refs. [148, 158, 174–180], which show non-trivial momentum-dependencies only in momentum regions where the gluon sector already starts to decouple from the system. In turn, the tensor structures and momentum dependences of the quark-gluon vertex are important, see the DSE studies [181–183] and the fully quantitative FRG study [156] in the quenched limit. To take this effectively into account, we introduce an infrared-strength function for the strong couplings, which is discussed below and in App. D.

To extract the flow of the quark-gluon coupling $g_{\bar{q}Aq}$, we use the following projection procedure,

$$\partial_t g_{\bar{q}Aq} = \frac{1}{8N_f(N_c^2-1)} \lim_{p\to 0} \mathrm{Tr}\left(\gamma_\mu t^a \frac{\partial_t \Gamma_k}{\delta q \delta A_\mu^a \delta \bar{q}}\right)\bigg|_{\Phi=\Phi_0}, \tag{4.100}$$

which leads to the equation

$$\begin{aligned}\partial_t g_{\bar{q}Aq,k} = \frac{1}{2}\left(\eta_{A,k} + 2\eta_{q,k}\right) - v(d)\, g_{\bar{q}Aq,k}\, \bar{h}_k^2 \Big\{ & \mathcal{N}_{2,1}^{(m)}(\bar{m}_{q,k}^2, \bar{m}_{\sigma,k}^2; \eta_{q,k}, \eta_{\phi,k}) \\ & + (N_f^2-1)\, \mathcal{N}_{2,1}^{(m)}(\bar{m}_{q,k}^2, \bar{m}_{\pi,k}^2; \eta_{q,k}, \eta_{\phi,k})\Big\} \\ & + g_{\bar{q}Aq,k}^3 \frac{12v(d)}{N_c}\, \mathcal{N}_{2,1}^{(g)}(\bar{m}_{q,k}^2; \eta_{q,k}, \eta_{A,k}) \\ & + g_{\bar{q}Aq,k}^2\, g_{A^3,k}\, 3v(d) N_c\, \mathcal{N}_{1,2}^{(g)}(\bar{m}_{q,k}^2; \eta_{q,k}, \eta_{A,k})\,.\end{aligned} \tag{4.101}$$

The threshold functions appearing on the right-hand side can be found in App. C.1. For the quark-gluon vertex, no ghost diagrams are present. Furthermore, the mesonic contributions

dominate in the infrared. These contributions have the same sign as the gluonic ones and therefore lead to an effective infrared enhancement of the quark-gluon vertex.

The three-gluon vertex $g_{A^3,k}$ is defined via

$$\partial_t g_{A^3,k} = \frac{i}{12N_c(N_c^2-1)} \lim_{p\to 0} \frac{\partial^2}{\partial p^2} \mathrm{Tr}\left(\delta_{\mu\nu} p_\sigma f^{abc} \frac{\partial_t \Gamma_k}{\delta A(p)^a_\mu \delta A(-p)^b_\nu \delta A^c_\sigma(0)} \right)\Bigg|_{\Phi=\Phi_0} . \tag{4.102}$$

Note that in the limit of vanishing external momentum the flow is independent of the kinematic configuration in the projection procedure. Thus, we find for the flow equation for $N_c=3$ and $N_f=2$:

$$\begin{aligned} \partial_t g_{A^3,k} = \frac{3}{2}\eta_{A,k}\, g_{A^3,k} - \frac{1}{6\pi^2}\, g^3_{\bar{q}Aq,k}\left(1-\frac{\eta_{q,k}}{4}\right)\frac{(1+2\bar{m}^2_{q,k})}{(1+2\bar{m}^2_{q,k})^4} \\ + \frac{3}{64\pi^2}\, g^3_{A^3,k}\,(11-2\eta_A) + \frac{1}{64\pi^2}\, g^3_{\bar{c}Ac,k}\left(1-\frac{\eta_{C,k}}{8}\right), \end{aligned} \tag{4.103}$$

The second term in the first line of (4.103) corresponds to the quark-triangle diagram and the two terms in the second line are the gluon- and ghost-triangle diagrams, respectively. Note that the $g^3_{A^3,k}$-term also includes the contribution from the diagram containing the four-gluon vertex, which we approximate as explained below.

Within our approximation, the ghost-gluon vertex $g_{\bar{c}Ac,k}$ has only canonical running since the diagrams that contribute to the flow of $g_{\bar{c}Ac,k}$ are proportional to the external momentum. Thus, at vanishing external momentum they vanish and we are left with:

$$\partial_t g_{\bar{c}Ac,k} = \left(\frac{1}{2}\eta_{A,k} + \eta_{C,k}\right) g_{\bar{c}Ac,k}. \tag{4.104}$$

Lastly, we comment on our approximation for the four-gluon vertex $g_{A^4,k}$. For the sake of simplicity, we restrict here to a semi-perturbative ansatz for this vertex, which ensures that $g_{A^4,k}$ has the correct perturbative running. To this end, we set

$$g^2_{A^4,k} = g^2_{A^3,k}\,. \tag{4.105}$$

This approximation is valid for $k \gtrsim 1.5$ GeV. For smaller scales, non-perturbative effects potentially lead to a different running.

As discussed above, in the present study we focus on the RG flows of the most relevant couplings from a phenomenological point of view. In particular, we concentrate on the effects of fluctuations on the relevant and marginal parameters of the classical gauge action in (5.3). Consequently, non-classical interactions which are potentially relevant are not taken into account here. Furthermore, we only consider vertices at vanishing external momenta, although momentum dependencies may play an important quantitative role. As an example, this becomes apparent in the flow of the ghost-gluon vertex (4.104): while the diagrams driving the flow of $g_{\bar{c}Ac,k}$ vanish within our approximation, they give finite contributions at non-vanishing momenta. This was studied in more detail in the case of quenched QCD [156]. Indeed, it turned out that both, momentum dependencies and the inclusion of non-classical vertices, lead to large quantitative effects. It was shown there that within an extended truncation the approach put forward in the present work leads to excellent quantitative agreement with lattice QCD studies.

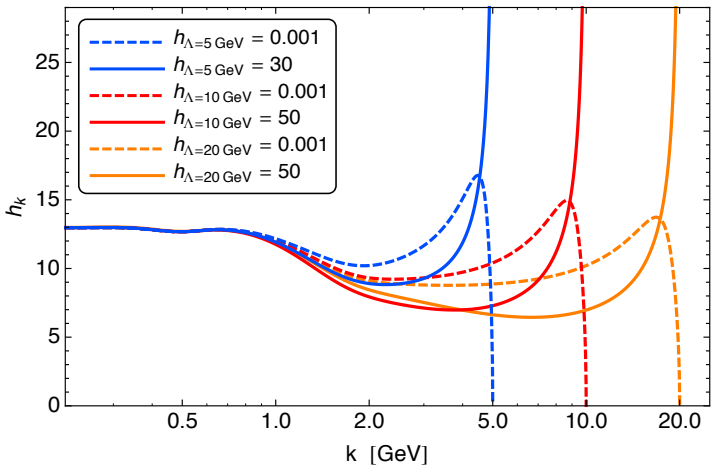

Figure 4.5.: Yukawa coupling as a function of the RG scale for various initial scales Λ and initial conditions h_Λ. Due to the presence of a partial IR-attractive fixed point in the regime of small gauge coupling, the different trajectories in the UV regime are attracted to a unique solution.

We take the findings in [156] as a guideline for a phenomenological modification of the gauge couplings. Effectively, this provides additional infrared strength to the gauge couplings in the non-perturbative regime with $k \lesssim 2$ GeV. This additional strength is adjusted with the current quark mass at vanishing momentum. This is reminiscent to similar procedures within Dyson-Schwinger studies, see e.g. [102, 122], the details are given in App. D. Here, we choose $a = 0.29$ for the IR-strength parameter. This implies that we enhance the strength of the gauge couplings by about 29% in the non-perturbative regime.

4.4. Numerical Results

4.4.1. Initial Conditions and Fixed Point Behavior

The starting point of the present analysis is the microscopic action of QCD. We therefore initiate the RG flow at large scales, deep in the perturbative regime. The initial values for the strong couplings are fixed by the value of α_s obtained from 1-loop perturbation theory. Since the different strong couplings we use here (see Eq. (4.82)) need to be identical in the perturbative regime, they consequently have the same initial value α_s. It is shown in Fig. 4.6 that indeed the different strong couplings agree to a high degree of accuracy with the 1-loop running of the strong coupling for scales $k > 3\,\mathrm{GeV}$. This is a very important benchmark for the consistency of the approximations we use. Note that the value of α_s implicitly determines the absolute physical scale. Here we choose $\alpha_{s,\Lambda} = 0.163$, which relates to $\Lambda \approx 20\,\mathrm{GeV}$. A quantitative determination requires the determination of the RG-condition in relation to standard ones such as the $\overline{\mathrm{MS}}$-scheme as well as the extraction of $\alpha_{s,k=0}(p = \Lambda)$, using Λ as the renormalization point. This goes beyond the scope of the present work and we shall restrict ourselves to observables that are ratios of scales, our absolute scales are determined in terms of $\Lambda = 20$ GeV. The other microscopic parameter of QCD, the current quark mass, is in our case fixed by fixing the symmetry breaking parameter c. We choose $\bar{c}_\Lambda = 3.6\,\mathrm{GeV}^3$ which yields a infrared pion mass of $M_{\pi,0} = 137\,\mathrm{MeV}$.

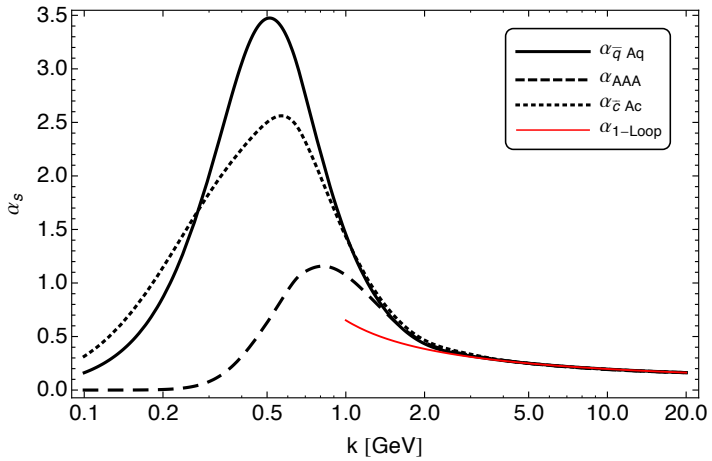

Figure 4.6.: The running of the different strong couplings in comparison to the 1-loop running.

The initial conditions of the mesonic parameters can be chosen arbitrarily. In the regime of weak gauge coupling, the flows of these couplings are governed by an infrared-attractive fixed point [70]. This fixed point is exactly the IR-attractive fixed point discussed in Sec. 2.4. Thus, as long as the initial scale is large enough, we find unique solutions for the meson parameters at low energies. This is demonstrated for the Yukawa coupling in Fig. 4.5, where we see that, with initial values that differ by many orders of magnitude, we always get the same solution in the IR. Loosely speaking, the memory of the initial conditions is lost in the RG flow towards the IR regime due to the presence to a pseudo fixed-point on intermediate scales. This is given as long as the initial meson masses are chosen larger than the UV-cutoff scale, $M_{\phi,\Lambda} \gtrsim \Lambda$. That way, the mesons do not contribute to the dynamics of the system at high energies. We therefore choose $M^2_{\pi,\Lambda} = M^2_{\sigma,\Lambda} = 10^4\Lambda^2$, but we confirmed that our results do not depend on this choice as long as the initial meson masses are larger than the UV-cutoff. Furthermore, to ensure that our initial conditions correspond to QCD, the ratio $h^2_{S,\Lambda}/(2m^2_{\pi,\Lambda})$ has to be much smaller than $\Lambda^{-2}\alpha_s^2$. It corresponds to the four-quark coupling $\lambda_{S,\Lambda}$ at the initial scale. A large initial value of the four-quark coupling would describe a gauged Nambu–Jona-Lasinio model with strong coupling, rather than QCD.

4.4.2. Gauge Couplings

The results for the different running gauge couplings $\alpha_{\bar{q}Aq}$, $\alpha_{\bar{c}Ac}$ and α_{A^3} discussed in Sec. 4.3 are shown in Fig. 4.6. While they all agree with each other and follow the perturbative running at scales $k \gtrsim 3$ GeV, non-perturbative effects induce different runnings at lower scales. The former statement is a highly non-trivial consistency check of the approximation we make here.

The different strength of the gauge couplings in the non-perturbative regime is a direct consequence of the mass gap that develops in the gluon dressing function $Z_{A,k}$. Owing to our construction for the vertices and the gluon propagator, (4.71) and (4.74), all non-trivial informations about the gauge sector are encoded in the gauge couplings. In particular, they are dressed with with powers of $Z^{1/2}_{A,k}$ that correspond the number of external gluon legs attached to them. Hence, the more external gluonic legs the coupling has, the more its strength is suppressed by the emerging gluon mass gap. This explains why the three-gluon vertex α_{A^3} is

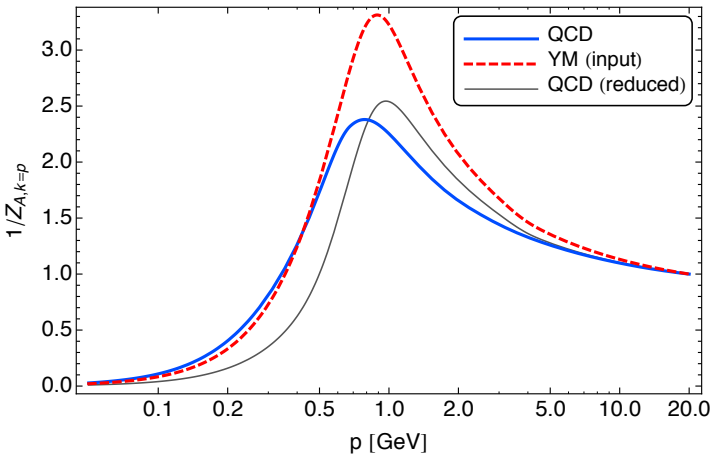

Figure 4.7.: Comparison between the quenched and the unquenched running gluon propagators $1/Z_A^{\mathrm{YM}}(p^2)$ and $1/Z_A(p^2)$ as defined in (4.99). We also show the curve for QCD (reduced) where the gluon propagator is a direct sum of Yang-Mills propagator and vacuum polarization, see Eq. (4.86).

much weaker in the non-perturbative regime than $\alpha_{\bar{q}Aq}$ and $\alpha_{\bar{c}Ac}$: it is suppressed by $Z_{A,k}^{3/2}$, while the quark-gluon and ghost gluon couplings are only suppressed by $Z_{A,k}^{1/2}$. The gluon dressing function as we defined it here diverges for $k \to 0$ and thus, all gauge couplings become zero in this limit.

Note that the fact that $\alpha_{\bar{c}Ac}$ is weaker than $\alpha_{\bar{q}Aq}$ can be attributed to the neglected momentum dependencies in this sector. Since all diagrams that drive the flow of the ghost-gluon vertex are proportional to the external momentum, they vanish for our approximation and $\alpha_{\bar{c}Ac}$ only runs canonically, see (4.104). If these momentum-dependencies were taken into account, the ghost-gluon vertex would even be stronger than the quark-gluon vertex, at least in the quenched case [156].

4.4.3. Unquenched Propagators

Following the discussions above, we are in the position to study the unquenching effects due to the full back-coupling of the matter dynamics to the glue sector. In an earlier work, [140, 155], $\eta_{\mathrm{glue},k} = \eta_{A,k}^{\mathrm{YM}}$ was directly identified at the same cutoff scale k, see Eq. (4.86). This means that the vacuum polarization is simply added to the Yang-Mills propagator without feedback. We will refer to this as partial unquenching in the following. It is well-adapted for taking into account even relatively large matter contributions to the gluonic flow qualitatively: the main effect of the matter back-coupling is the modification of scales, most importantly Λ_{QCD}, which is already captured well in (one-loop) perturbation theory, if the initial scale is not chosen too large. This approximation has also been subsequently used in related Dyson-Schwinger works, see e.g. [45, 171–173], extending the analysis also to finite density. Here, we improve these approximations by taking the back-reaction of matter fluctuations on the pure gauge sector into account. Furthermore, the gluon vacuum polarization was based on a one-loop improved approximation in previous FRG studies. Here, we compute the full vacuum polarization self-consistently.

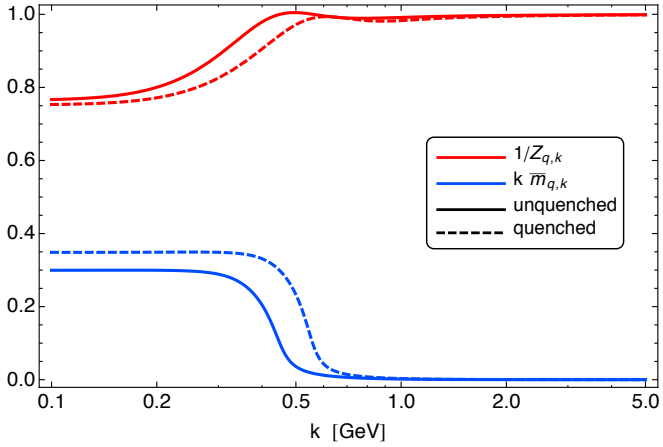

Figure 4.8.: Dressing function (red) and mass (blue) of the quark as function of the RG scale at vanishing momentum. We compare our present model (solid) to the quenched model (dashed) with the parameters fixed to match those of [156].

In Fig. 4.7 we show the quenched and unquenched gluon propagators. The quenched gluon propagator (dotted red line), which is a FRG input from [159, 168], is compared to the fully unquenched propagator (solid blue line). We clearly see that the screening effects of dynamical quarks decrease the strength of the gluon propagator. We also explicitly checked that the smaller the quark mass, the weaker the gluon propagator. Furthermore, the peak position of the unquenched propagator is smaller than that of the YM propagator. This indicates a smaller gluon mass gap in the presence of dynamical quarks. Note that this observation provides further evidence for a deep connection between confinement and chiral symmetry breaking: The magnitude of screening of color charge from quark-antiquark pairs is determined by the quark mass, which is generated by chiral symmetry breaking. This has direct influence to the gluon mass gap which in turn signals confinement. The strength of chiral symmetry breaking therefore directly influences the confinement transition. In a preliminary qualitative study, we have checked that no chiral symmetry breaking, i.e. (almost) massless quarks, implies no gluon mass gap and therefore no confinement. A thorough analysis of these findings are postponed to future work.

Fig. 4.7 also shows the partially unquenched propagator (4.86) (thin black line, denoted by "QCD (reduced)"). The results show considerable deviations from the fully unquenched computation. Most strikingly, the peak position of the partially unquenched result is almost identical (if not larger) that that of the YM result. This counterintuitive finding emphasizes the importance of the back-reaction of matter fluctuations for a physically sensible description of the gluon propagator. This is seemingly surprising as it is well-tested that partial unquenching works well even at finite temperature, see e.g. [45, 140, 155, 171–173]. However, we first notice that the importance of quark fluctuations is decreased at finite temperature due to the Matsubara gapping of the quarks relative to the gluons. This improves the reliability of the partial unquenching results at finite temperature. Moreover, in these works the infrared strength is phenomenologically adjusted with the constituent quark mass in the vacuum. This effectively accounts for the difference between unquenching and partial unquenching.

On the other hand, this also entails that the full unquenching potentially is relevant in

situations where the vacuum balance between pure glue fluctuations and quark fluctuations is changed due to an enhancement of the quark fluctuations. Prominent cases are QCD with a large number of flavors, and in particular QCD at finite density.

We also compare the quenched and unquenched quark propagators in see Fig. 4.8. We took the parameters of [156] to compute the quenched case in the present work. As for the gluon propagator, Fig. 4.7, we see large unquenching effects. The dashed lines show the quenched results and the solid lines the unquenched. Unquenching results in smaller quark masses (blue lines) and larger wave function renormalizations $Z_{q,k}$, and therefore enhanced quark fluctuations, as expected. Furthermore, we see that the generation of constituent quark masses takes place at smaller scales in the unquenched case. This can again be traced back to screening effects: The effects of gauge fluctuations are suppressed in the presence of dynamical quark which results in weaker gauge couplings. Since the strength of the gauge couplings triggers chiral symmetry breaking according to our discussion in Sec. 2.4, criticality of the four-quark interactions is reached later in the flow for weaker gauge couplings. Hence, chiral symmetry breaking takes place at smaller scales in the presence of dynamical quarks.

4.4.4. Masses and Meson Decoupling

The present approach allows an easy access to the relative importance of quantum fluctuations of the respective fields: we find that for the renormalized, dimensionless mass being larger than one,

$$\bar{m}_\Phi^2 \geq 1\,, \tag{4.106}$$

all threshold functions that depend on the propagator of the respective field mode are suppressed with powers of $1/\bar{m}_\Phi^2$. This entails that the dynamics of the system is not sensitive to fluctuations of this field. In turn, for $\bar{m}_\Phi^2 \leq 1$ the field mode is dynamical. Note that, of course, $\bar{m}_\Phi^2 = 1$ is not a strict boundary for the relevance of the dynamics.

In Fig. 4.9 we show the physical (remormalized) masses M_Φ for the matter fields as defined in (4.34). In the shaded area the condition (4.106) applies, and the respective matter fields do not contribute to the dynamics. This already leads to the important observation that the resonant mesonic fluctuations are only important for the dynamics in a small momentum regime with momenta $p^2 \lesssim 800$ MeV, see also Fig. 4.10. While the σ- and quark-modes decouple rather quickly at about 300 - 400 MeV, the $\vec{\pi}$ as a pseudo-Goldstone mode decouples at its mass scale of about 140 MeV.

In turn, in the ultraviolet regime, the mesonic modes decouple very rapidly, see Fig. 4.10 for the size of the effective propagator (C.28) measured in units of the cutoff. They directly measure the relevance of the fluctuations of the corresponding fields for the flow equations. At about 800 MeV this ratio is already 0.1 and above this scale the mesonic modes are not important, and QCD quickly is well-described by quark-gluon dynamics without resonant interactions. This observation is complementary to the fact that the initial condition of the Yukawa coupling does not play a role for the physics at vanishing coupling, see Fig. 4.5. For all initial cutoff scales $\Lambda \gtrsim 5$ GeV, its initial value is washed out rapidly, leading to a universal infrared regime with the prediction of $\bar{h}$ at $k = 0$.

The overall magnitude of π and σ masses is fixed by spontaneous chiral symmetry breaking. Since the pions are the (pseudo) Goldstone bosons of two-flavor QCD, chiral symmetry breaking is characterized by (small) vanishing $M_{\pi,k}$ for $k \lesssim k_\chi$, or equivalently by the resonance in the $(S-P)$-channel four-quark interaction $\lambda_{S,k}$. Thus, the small finite pion mass is an immediate

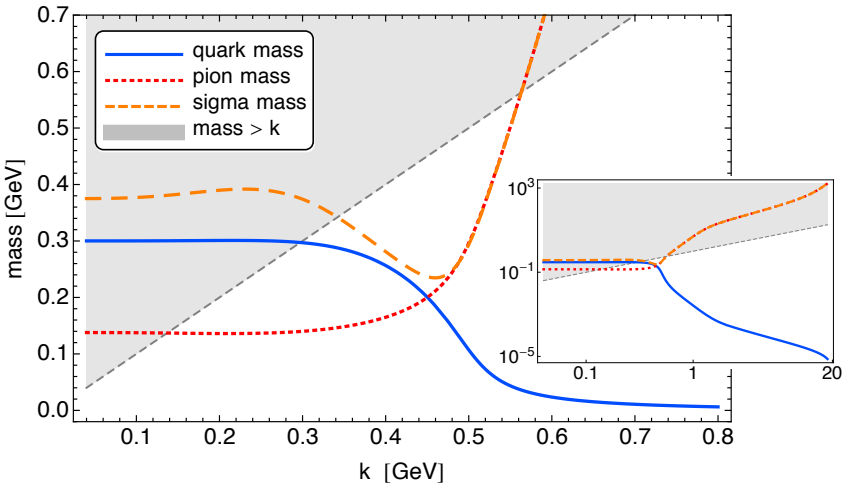

Figure 4.9.: The renormalized quark, pion and sigma masses as a function of the RG scale. The inset figure shows the masses for a larger range of scales. The shaded gray area indicates which fields contribute dynamically: masses within the gray area exceed the cutoff scale and the corresponding fields are therefore decoupled from the dynamics. On the other hand, fields with masses within the white area are dynamical.

result of chiral symmetry breaking together with small finite current quark masses. Since the σ is the chiral partner of the π, their masses can only lose their degeneracy at $k \approx k_\chi$. $M_{\sigma,k}$ is therefore small at $k \approx k_\chi$ and achieves is finite value from the meson VEV via the splitting-term $2\bar{\rho}_{0,k}\bar{V}_k''(\bar{\rho}_{0,k})$, see (4.34). Note that this only applies to the $(S-P)$-channel, as it contains the Goldstones. For other mesons, the magnitude of the masses is fixed from the running of the corresponding four-quark interaction. We will come back to this point when we consider vector mesons in the next chapter.

We add that the Yukawa coupling relates to the ratio between constituent quark mass and the vacuum expectation value of the field $\bar{\sigma}$,

$$\bar{h} = \frac{M_q}{\bar{\sigma}_0}\,. \tag{4.107}$$

Note that it cannot be tuned and is a prediction of the theory. On the other hand, in low-energy model studies, the (renormalized) quantities M_q and $\bar{\sigma}_0$ corresponding to physical observables are related to model parameters, and have to be tuned such that M_q and $\bar{\sigma}_0$ assume their physical values.

Mesons are not present in the quark-gluon plasma. In a formulation of the dynamics of QCD on a very wide range of scales in terms of one scale dependent effective action, as in the present case, however, hadronic parameters are necessarily a part of the action also at very large scales. As we have demonstrated here, the meson masses are much larger than the cutoff scale in the quark-gluon regime and therefore they are completely decoupled in this phase. We want to emphasize that this physically desirable picture is achieved with dynamical hadronization. The decoupling of the mesons is triggered by a rapid fall-off of the meson wave function renormalization $Z_{\phi,k}$ at the pseudocritical scale. Its running is shown in the left plot of Fig. 4.11. While $Z_{\phi,k}$ stays almost constant in the hadronic regime, it rapidly falls-off at about 400 MeV and drops more than seven orders of magnitude towards the UV. The fastest drop-off

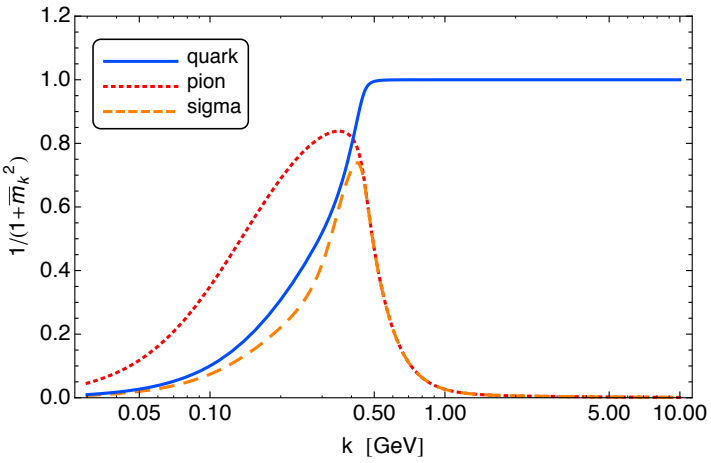

Figure 4.10.: Dimensionless RG-invariant propagators ("effective propagators") as functions of the RG scale. They are a measure for the effective strength of the fluctuations of the fields, see (C.28).

is in the vicinity of the pseudocritical scale $k_\chi \approx 400$ MeV. The reason is that quark fluctuations decrease the meson wave function renormalization in the quark-gluon regime. Its flow (4.52) is proportional to the squared Yukawa coupling, $\partial_t Z_{\phi,k} \propto -\bar{h}_k^2 Z_{\phi,k}$, at scales $k \gtrsim k_\chi$, resulting in large negative beta functions, see Fig. 4.5. Since the wave function renormalizations are the coefficients of the kinetic terms in the effective action, their vanishing implies that the mesons become auxiliary fields and are therefore not part of the physical spectrum at large energy scales.

This is reflected in the behavior of the bare masses, i.e. the masses without rescaling with the wave function renormalizations, $m_\phi^2 = Z_{\phi,k} M_{\phi,k}^2$, shown in the right plot of Fig. 4.11. The bare masses would not decouple in the quark-gluon regime: while they do not differ from the renormalized masses in the hadronic regime where the wave function renormalizations are almost constant and of order one, they are constant in the quark-gluon regime. Thus, at large scales the bare meson masses are always much smaller than the the cutoff scale. Without the rapid fall-off of the meson wave function renormalizations, the mesons show no decoupling, resulting in an unphysical high-energy phase. Note that the constant bare masses imply in particular that the running of the physical masses is exclusively driven by the anomalous dimensions of the corresponding mesons at large energy scales. This has important consequences also for low energy models in the local potential approximation, since for scales larger than about 800 MeV, the effect of running wave-function renormalizations can not be neglected.

Since the wave function renormalizations only enter the set of flow equations through the corresponding anomalous dimensions, the flow equations for the wave function renormalizations do not need to be integrated for the solution of the system and all results are independent of the initial values Z_Λ. For illustration purposes, we have chosen the initial conditions such that $Z_{S/V,0} = 1$.

Finally, we discuss further consequences of our findings for low energy effective models. To that end we note that the gluon modes decouple at momenta below 500 − 700 MeV. This is seen from the plot of the gluon dressing functions, Fig. 4.7, as well as that of the gluonic couplings

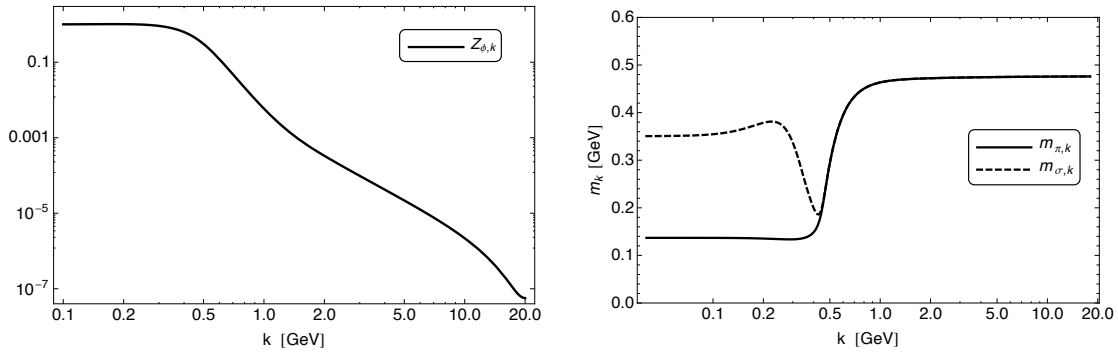

Figure 4.11.: The left figure shows the wave-function renormalization of the mesons. The bare masses of the mesons, $m_{\pi/\sigma,k} = \sqrt{\Gamma^{(2)}_{\sigma/\pi}(0)} = Z^{1/2}_{\phi,k}\bar{m}_{\pi/\sigma,k}$, are shown on the right.

in Fig. 4.6. This overlaps with the scale regime where the mesonic degrees of freedom start to dominate the dynamics.

Consequently, low energy effective models aiming at quantitative precision that do not take into account any glue fluctuations should be initiated at a UV-scale of about 500 MeV. In this regime, however, the quark-meson sector of QCD carries already some fluctuation information in non-trivial mesonic and quark-meson couplings. In other words, the standard initial effective Lagrangian of these models has to be amended by additional couplings. These couplings, however, can be computed from QCD flows. We will come back to this discussion in Chap. 6.

It has been shown in [166] that in these low energy effective models thermal fluctuations affect the physics at surprisingly large scales, for thermodynamical consequences, see Ref. [184]. This is even more so for density fluctuations that lack the exponential suppression present for thermal fluctuations. Thus, we conclude that the low UV cutoff scale for quantitatively reliable low energy effective models enforces the computation of temperature- and density-dependent initial conditions. Indeed the same argument holds true for other external parameters such as the magnetic field.

4.5. Conclusions

In this chapter, we have set up a non-perturbative FRG approach to QCD, concentrating on the effects of a full unquenching of the glue sector. We provided a detailed study of the fluctuation physics in the transition regime from the quark-gluon phase to the hadronic phase. This includes a discussion of the relative importance of the fluctuations of quark, meson and glue fluctuations. A detailed discussion is found in the previous section. Here we simply summarize the main results.

Firstly, we have shown that the full back-coupling of the matter fluctuations in the glue sector plays a quantitative role in the vacuum. In the present two-flavor case, it accounts for about 10-15% of fluctuation strength in the strongly correlated regime at about 1 GeV. This hints strongly at the importance of these effects in particular at finite density, where the importance of quark fluctuations is further increased and the effect is amplified.

Secondly, the still qualitative nature of the present approximation necessitates the adjustment of the infrared coupling strength, fixed with the constituent quark mass. However, owing to

the inclusion of dynamical hadronization which re-enforces the four-fermion running, this phenomenological tuning is much reduced. In future work we plan to utilize the findings of the quantitative study [156] in quenched QCD for improving our current approximation towards quantitative precision, while still keeping its relative simplicity.

Finally, we have also discussed how low energy effective models emerge dynamically within the present set-up due to the decoupling of the glue sector: the present results and their extensions can be used to systematically improve the reliability of low energy effective models by simply computing the effective Lagrangian of these models at their physical UV cutoff scale of about 500 - 700 MeV. Moreover, the temperature- and density-dependence of the model parameters at this UV scale can be computed within the present set up.

Future work aims at a fully quantitative unquenched study by also utilizing the results of [156], as well as studying the dynamics at finite temperature and density.

CHAPTER 5

The Vacuum Structure of Vector Mesons

As we already discussed above, a crucial question concerning the QCD phase diagram is how to detect the formation of the quark-gluon plasma in heavy-ion collisions at ultrarelativistic energies. Vector mesons play a very important role in this context because they provide promising evidence for both deconfinement and chiral symmetry restoration. While the suppression of heavy quarkonium could be a signature of deconfinement [20], in-medium modifications of light vector mesons may signal chiral symmetry restoration [186]. The latter manifest themselves in low-mass dilepton data from heavy-ion collisions [31–33]. Dileptons escape the fireball essentially without interaction and couple directly to light vector mesons such as the ρ. Thus, dilepton spectra show prominent vector meson peaks which allow for the investigation of in-medium modifications of these mesons [93], see Fig. 5.1.

A connection between the modifications of vector mesons and chiral symmetry restoration in a hot and/or dense medium can be established e.g. by considering the scaling of the ρ mass with temperature [34–36] or the melting of the ρ resonance [37,38]. This connection is based on the fact that chiral symmetry restoration implies the degeneration of chiral partners such as ρ and a_1. A thorough understanding of the dynamics of these mesons in QCD is therefore essential for a complete picture of the QCD phase structure.

Here, we present first results on the properties of the chiral partners ρ and a_1 as they emerge from quark-gluon fluctuations at high energies. To this end, we study dynamical QCD as it was put forward in the previous chapter. This way, the properties of the hadrons are determined by the underlying dynamics of microscopic QCD and we can conveniently describe the transition from quarks and gluons to hadrons non-perturbatively without suffering from a fine-tuning of model parameters.

Again, we concentrate on two-flavor QCD at vanishing temperature and density in Euclidean spacetime and develop a scale dependent effective action that captures the relevant dynamics in both, the quark-gluon phase and the hadron phase, on a qualitative level. Furthermore, we extend the dynamical hadronization technique to include vector mesons. The present analysis will serve as an starting point for qualitative and quantitative in-medium studies of vector mesons. It has been demonstrated in [156] for QCD in the quenched limit, that quantitative precision is indeed feasible with the FRG approach to QCD.

Even though we work in the vacuum, the RG-scale dependence of parameters such as the

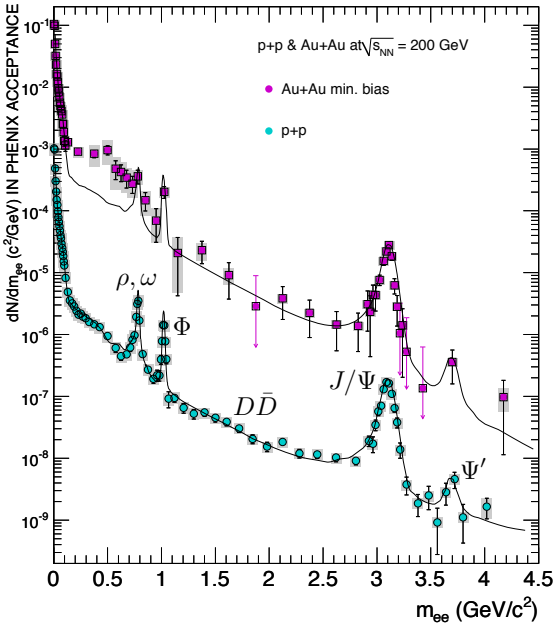

Figure 5.1.: Dilepton spectra as function of the invariant mass from the Phenix experiment. The lower line shows the result for lead-lead collisions and the upper line shows the result from gold-gold collisions. The peaks are associated to the decay of the mesons indicated in the plot. Since a quark-gluon plasma can only be created in the latter case, the modification of the spectrum at low masses and in particular the ρ-peak in Au–Au collisions as compared to p–p collisions indicates strong in-medium modifications of the ρ meson. The plot is taken from [185].

masses reflects their finite temperature behavior. In particular, there is a critical scale k_χ which separates the phases with broken and restored chiral symmetry. This allows us to study the behavior of hadronic parameters as they approach the scale of chiral symmetry restoration and clarify how mesons decouple from the physical spectrum at high energies. The scaling of the low-energy parameters is uniquely fixed from microscopic QCD. The reason is that the running of the hadronic parameters is governed by an infrared-attractive fixed point as long as the gauge coupling is small. This guarantees that the memory of the initial conditions of the RG flows of these parameters, initiated at large, perturbatively accessible energy scales, is lost and the hadronic phase is uniquely determined within our truncation.

By exploiting this fact, we can analyze the validity of *vector meson dominance* (VMD) [187]. The idea of VMD is to promote the $SU(2)_L \times SU(2)_R$ flavor symmetry to a gauge symmetry. This way, ρ and a_1 naturally appear as gauge bosons [188]. The main advantage is that VMD significantly reduces the number of different interactions involving vector mesons. The obvious conceptual shortcoming is that chiral symmetry is only a global symmetry in QCD. Furthermore, even though VMD has lead to accurate predictions in some cases at low energies [189], it gives e.g. the wrong phenomenology of ρ and a_1 mesons [190]. We therefore keep chiral symmetry global and compare our results to the corresponding VMD predictions.

This chapter is organized as follows: We motivate our ansatz for the quantum effective action used in this work in Sec. 5.1. In Sec. 5.2 we first introduce the FRG and dynamical hadronization in the presence of vector mesons and continue with a discussion of the implications of $\pi - a_1$

mixing within our approach. Our results are presented in Sec. 5.3. After discussing the initial conditions of the RG flows of our model, we present our results on the meson and quark masses with particular emphasis on the scaling of the ρ mass towards the chiral symmetry breaking scale. Then, we show in more detail how the mesons disappear from the physical spectrum at large scales. Lastly, we discuss the validity of VMD.

5.1. The Effective Action

The scale dependent effective action we use here is based on the one put forward in Sec. 4.1. In particular the truncation of the gauge sector is the same. In addition, we aim at describing the vacuum properties of the chiral partner vector mesons ρ and a_1 since they play a prominent role for the phenomenology of chiral symmetry breaking/restoration.

As we already discussed earlier, the tensor structure of the four-quark interaction channels is directly related to the quantum numbers of the corresponding mesons that are formed in the respective scattering channel. Therefore, we need to include at least those interaction channels, that carry the quantum numbers of the mesons we are interested in. In the present case, these are the Lorentz–scalar-pseudoscalar iso–scalar-vecor and the Lorentz–vector-axialvector iso–vector-vector channels $\lambda_{S,k}$ and $\lambda_{V,k}$. On the mesonic side, these channels correspond to the σ and the π, and the ρ and the a_1 respectively. As before, we construct the action such that it obeys the global flavor symmetry $U(1)_V \times SU(2)_V \times SU(2)_A$. Thus we include the $(S-P)$-channel four-quark interaction with coupling $\lambda_{S,k}$ as in (4.5)[1]. The relevant vector channel that respects these symmetries is the vector-axialvector $(V+A)$-channel with the coupling $\lambda_{V,k}$, and in total we have for the four-quark interaction part of the action

$$\Gamma_k^{(4q)} = \int_x \left\{ \frac{\lambda_{S,k}}{2} \left[(\bar{q}q)^2 - (\bar{q}\gamma_5 \vec{\tau} q)^2 \right] - \frac{\lambda_{V,k}}{2} \left[(\bar{q}\gamma_\mu \vec{\tau} q)^2 + (\bar{q}\gamma_\mu \gamma_5 \vec{\tau} q)^2 \right] \right\} . \tag{5.1}$$

The scalar-pseudoscalar channel is the dominant channel among all possible quark-antiquark scattering channels in vacuum. This has been explicitly checked by considering a complete basis of four-quark interactions [156]. This implies in particular, that the pions and the sigma mesons dominate the dynamics in the hadronic phase. In this work we demonstrate explicitly on the example of vector mesons, that there is an emergent scale hierarchy where only the lightest mesons, i.e. pions and sigma, can contribute to the dynamics of the system at low energies. Thus, the properties of the heavier meson states in Euclidean space are completely fixed by quark-gluon dynamics at large energies and pion-sigma dynamics at low energy scales.

To properly take into account the dynamics in the hadronic phase, we model this sector by an effective meson potential which in principle includes arbitrary orders of mesonic self-interactions. Furthermore, we consider momentum dependent propagators of the quarks and mesons, based on a small-momentum expansion, by including scale dependent wave function renormalizations Z_k. To account for non-vanishing current quark masses, a source term $-c\sigma$ in the meson sector explicitly breaks chiral symmetry. It is directly related to finite current quark masses. As a consequence, pions are massive rather than Goldstone bosons and the chiral transition is a crossover.

To connect the the quark sector with the meson sector, we include scalar channel and vector channel Yukawa couplings $h_{S,k}$ and $h_{V,k}$. They are related to the four-quark interactions (5.1)

[1] Note that we use a slightly different notation here. The only difference is a relative factor of two between the $(S-P)$ channel here and in the previous chapter.

via a Hubbard-Stratonovich transformation as long as the meson potential is Gaußian. Thus, $h_{V,k}$ can be obtained from $\lambda_{V,k}$ analogously to $h_{S,k}$ from $\lambda_{S,k}$, as discussed in the previous chapter. To wit,

$$\Gamma_k^{(\text{Yukawa})} = \int_x \left\{ h_{S,k} \left[\bar{q}(\gamma_5 \vec{\tau}\vec{\pi} + i\sigma) q \right] + h_{V,k} \left[\bar{q}(\gamma_\mu \vec{\tau}\,\vec{\rho}^{\,\mu} + \gamma_\mu\gamma_5 \vec{\tau}\,\vec{a}_1^{\,\mu}) q \right] \right\}. \tag{5.2}$$

In order to consistently account for the dynamical change of degrees of freedom from the quark-gluon phase to the hadronic phase, we use dynamical hadronization as it was put forward in in the previous chapter. We will elaborate on this in the next section. As we will demonstrate there, it is inevitable to use this formulation here, since the the elimination of the π–a_1 mixing results in manifestly scale dependent a_1 fields.

In summary, we use the following scale dependent effective action:

$$\begin{aligned}
\Gamma_k = \int_x \Big\{ & Z_{q,k}\, \bar{q} \left(i\gamma_\mu D_\mu \right) q + \frac{1}{4} F^a_{\mu\nu} F^a_{\mu\nu} + \bar{c}^a \partial_\mu D^{ab}_\mu c^b + \frac{1}{2\xi} (\partial_\mu A^a_\mu)^2 + \Delta\mathscr{L}_{\text{glue}} \\
& + \frac{\lambda_{S,k}}{2} \left[(\bar{q}q)^2 - (\bar{q}\gamma_5 \vec{\tau} q)^2 \right] - \frac{\lambda_{V,k}}{2} \left[(\bar{q}\gamma_\mu \vec{\tau} q)^2 + (\bar{q}\gamma_\mu\gamma_5 \vec{\tau} q)^2 \right] \\
& + h_{S,k} \left[\bar{q}(\gamma_5 \vec{\tau}\vec{\pi} + i\sigma) q \right] + h_{V,k} \left[\bar{q}(\gamma_\mu \vec{\tau}\,\vec{\rho}^{\,\mu} + \gamma_\mu\gamma_5 \vec{\tau}\,\vec{a}_1^{\,\mu}) q \right] \\
& + \frac{1}{2} Z_{S,k} (\partial_\mu \phi)^2 + \frac{1}{8} Z_{V,k}\, \mathrm{tr} \left(\partial_\mu V_\nu - \partial_\nu V_\mu \right)^2 + U_k(\phi, V_\mu) \Big\},
\end{aligned} \tag{5.3}$$

The first line of (5.3) contains the microscopic gauge fixed action of QCD. As mentioned above, we introduced a running quark wave function renormalization $Z_{q,k}$ to capture some non-trivial momentum dependence of the quark propagator. $\Delta\mathscr{L}_{\text{glue}}$ stands for the fluctuation-induced part of the full momentum dependence of ghost and gluon propagators as well as non-trivial ghost-gluon, three-gluon and four-gluon vertex corrections. Since the gauge sector here is identical to the one considered in the previous chapter, we refer to the discussion there, in particular Sec. 4.3.

The four-quark interaction channels and the corresponding Yukawa interactions are in the second and third line of (5.3). The Yukawa sector arises from the bosonization of the quark sector. With dynamical hadronization as explained in the next section, these interactions will basically carry the quark self-interactions in the quark-gluon regime (see also (C.36) and (C.38)). For now, we are primarily interested in the qualitative features of the system and therefore do not take the general field dependence of the Yukawa couplings into account, as in the previous chapter, i.e. $\partial_\Phi h_{S/V,k} = 0$.

The fourth line of (5.3) contains the meson sector of our truncation. ϕ are the scalar fields and V_μ are the vector fields. U_k contains the meson interactions and is discussed in the next section, see in particular (5.20). With the running wave function renormalizations $Z_{S,k}$ and $Z_{V,k}$ for the scalar and vector mesons respectively, we capture the major part of the momentum dependence of the full meson propagators [166]. Furthermore, as we explicitly demonstrate in Sec. 5.3.3 and also have shown for the scalar mesons in Sec. 4.4.4, the wave function renormalizations play a crucial role for the decoupling of the mesons at high energies. They are therefore indispensable for the identification of the physical meson masses. In the next section, we will elaborate on the meson sector of our truncation.

We note that even though the action contains massive vector bosons, it is not necessary to use the Stueckelberg formalism to ensure renormalizability [191]. UV regularity is always

guaranteed for the functional renormalization group, as long as the scale derivative of the regulator decays fast enough for momenta much larger than the cutoff scale.

5.1.1. Meson Sector

Here, we will construct the meson sector of our truncation. Our construction principle is based on VMD: we first promote the global flavor symmetry $SU(2)_L \times SU(2)_R$ to a gauge symmetry in a linear sigma model which contains only scalar mesons [188]. The vector mesons then naturally arise as the corresponding gauge bosons. We then relax the requirement of local chiral symmetry and include terms that only respect the global symmetry.

Let us start with a linear sigma model invariant under global $SU(2)_L \times SU(2)_R$ with the scalar mesons $\phi = (\vec{\pi}, \sigma)^T$ in the fundamental representation of $O(4)$ as before,

$$\mathscr{L}_{\text{LSM}} = \frac{1}{2}(\partial_\mu \phi)^2 + V(\phi^2)\,. \tag{5.4}$$

To proceed, we need to find an appropriate representation of $O(4)$. The Lie-algebra of $O(4)$ is $\mathfrak{so}(4)$ with dimension $\frac{1}{2}(n-1)n = 6$, i.e. we need 6 antisymmetric (4×4)-matrices. It is physically sensible to choose the first three of these generators by conventional isospin rotations in the π-subspace, i.e. a block of $SU(2)$ in the adjoint representation:

$$(T_i)_{jk} = \begin{pmatrix} -i\epsilon_{ijk} & \vec{0} \\ \vec{0}^T & 0 \end{pmatrix}, \tag{5.5}$$

with the totally antisymmetric Levi-Civita tensor ϵ_{ijk}. The remaining three generators are those antisymmetric matrices that mix the $\pi-\sigma$ components,

$$(T_i^5) = \begin{pmatrix} 0_{3\times3} & -i\vec{e}_i \\ i\vec{e}_i^T & 0 \end{pmatrix}, \tag{5.6}$$

with $i,j,k \in \{1,2,3\}$ and $\vec{e}_i^T = (\delta_{1i}, \delta_{2i}, \delta_{3i})$. It can be easily verified that they obey the following commutation relations:

$$\begin{aligned} [T_i, T_j] &= i\epsilon_{ijk} T_k\,, \\ [T_i^5, T_j^5] &= i\epsilon_{ijk} T_k\,, \\ [T_i, T_j^5] &= i\epsilon_{ijk} T_k^5\,, \end{aligned} \tag{5.7}$$

and their traces are given by

$$\operatorname{tr} T_i T_j = 2\delta_{ij}\,, \quad \operatorname{tr} T_i^5 T_j^5 = 2\delta_{ij}\,, \quad \operatorname{tr} T_i T_j^5 = 0\,. \tag{5.8}$$

To clarify the physical meaning of $\vec{T}$ and $\vec{T}^5$, we look at

$$\begin{aligned} T_i^+ &= \frac{1}{2}\left(T_i + T_i^5\right), \\ T_i^- &= \frac{1}{2}\left(T_i - T_i^5\right). \end{aligned} \tag{5.9}$$

They form two copies of $SU(2)$ representation since they individually obey the well-known commutation relations,

$$[T_i^+, T_j^+] = i\epsilon_{ijk} T_k^+\,, \quad [T_i^-, T_j^-] = i\epsilon_{ijk} T_k^-\,, \quad [T_i^+, T_j^-] = 0\,, \tag{5.10}$$

and hence $\{\vec{T}^+, \vec{T}^-\}$ form a representation of $SU(2)_L \times SU(2)_R$. The vector and axialvector currents $\vec{j}_\mu = (\bar{q}\gamma_\mu \vec{\tau} q)$ and $\vec{j}_{\mu 5} = (\bar{q}\gamma_\mu\gamma_5 \vec{\tau} q)$ of (two-flavor) QCD associated to chiral symmetry are then constructed from $\vec{T}^+ + \vec{T}^- = \vec{T}$ and $\vec{T}^+ - \vec{T}^- = \vec{T}^5$. We conclude that $\vec{T}$ is associated to $\vec{j}_\mu$ and $\vec{T}^5$ to $\vec{j}_{\mu 5}$. We therefore introduce the vector field V_μ in suggestive notation,

$$V_\mu = \vec{\rho}^{\,\mu}\vec{T} + \vec{a}_1^{\,\mu}\vec{T}^5 \,. \tag{5.11}$$

$\vec{\rho}^{\,\mu}$ and $\vec{a}_1^{\,\mu}$ are identified with the corresponding physical particles since they carry the correct quantum numbers. From this definition, it is obvious that V_μ is in the adjoint representation of $O(4)$.

Under these $O(4)$ transformations the scalar field ϕ transforms as

$$\varphi \to \mathcal{U}\varphi \,, \quad \text{with} \quad \mathcal{U} = e^{i\vec{\alpha}\vec{T} + i\vec{\beta}\vec{T}^5} \,. \tag{5.12}$$

We now promote this to a gauge transformation, i.e. $\mathcal{U} = \mathcal{U}(x)$ with $\vec{\alpha} = \vec{\alpha}(x)$ and $\vec{\beta} = \vec{\beta}(x)$. For the Lagrangian $\mathcal{L}_{\text{LSM}}$ (5.4) to be symmetric under this local transformation, we need to replace the conventional partial derivative ∂_μ in the kinetic terms of (5.4) by a covariant derivative D_μ that transforms as ϕ,

$$D_\mu\phi \to \mathcal{U}(x) D_\mu \phi \,. \tag{5.13}$$

The potential term of (5.4) is obviously invariant under $\mathcal{U}(x)$, without any modifications. If we make the canonical Ansatz

$$D_\mu = \partial_\mu - igV_\mu \,, \tag{5.14}$$

with the "chiral gauge coupling" g, the condition (5.13) requires the vector field to transform as

$$V_\mu \to \mathcal{U}(x) V_\mu \mathcal{U}^\dagger(x) + \frac{i}{g}\mathcal{U}(x)\partial_\mu \mathcal{U}^\dagger(x) \,. \tag{5.15}$$

As for any gauge theory, we can add a field-strength term to the action. The gauge invariant linear sigma model (gLSM) then reads:

$$\mathcal{L}_{\text{gLSM}} = \frac{1}{2}(D_\mu\phi)^2 + V(\phi^2) + \frac{1}{8}\operatorname{tr} V_{\mu\nu}V_{\mu\nu} \,, \tag{5.16}$$

with the field strength

$$V_{\mu\nu} = \frac{i}{g}[D_\mu, D_\nu] = \partial_\mu V_\nu - \partial_\nu V_\mu - ig[V_\mu, V_\nu] \,. \tag{5.17}$$

Note that since the gauge symmetry is non-Abelian, the field strength term also contains three- and four–vector-meson self-interactions.

We proceed by decomposing (5.16) to identify the individual contributions. The kinetic term yields:

$$\frac{1}{2}(D_\mu\phi)^2 = \frac{1}{2}(\partial_\mu\phi)^2 - ig\partial_\mu\phi \cdot V_\mu\phi - \frac{g^2}{2}(V_\mu\phi)\cdot(V_\mu\phi) \,, \tag{5.18}$$

i.e. in addition the the standard kinetic term of the scalar mesons, we get an explicitly momentum dependent scalar-scalar-vector interaction and a two-scalar–two-vector interaction. The field strength terms yields

$$\frac{1}{8}\operatorname{tr} V_{\mu\nu}V_{\mu\nu} = \frac{1}{8}\operatorname{tr}\left(\partial_\mu V_\nu - \partial_\nu V_\mu\right)^2 - \frac{ig}{2}\operatorname{tr}\partial_\mu V_\nu [V_\mu, V_\nu] - \frac{g^2}{8}\operatorname{tr}[V_\mu, V_\nu]^2 \,. \tag{5.19}$$

Thus, we get a kinetic term of the vector mesons and three- and four-vector interactions from the field strength.

We now relax the requirement of local chiral symmetry. To this end, we introduce additional terms that explicitly break symmetry and assume different scalar-vector and vector-vector couplings instead of one gauge coupling g. A mass term for the vector mesons, $m_V^2 \operatorname{tr} V_\mu V_\mu/4$, explicitly breaks gauge invariance but is certainly physically very relevant and will therefore be included. We introduce another marginal term that explicitly breaks gauge symmetry, $g_{3,k}\phi^2 \operatorname{tr} V_\mu V_\mu/4$.

For the final meson part of the scale dependent effective action Γ_k, we promote all the couplings to be RG-scale dependent. Furthermore, we introduce running scalar and vector meson anomalous dimension $Z_{S,k}$ and $Z_{V,k}$ to the respective kinetic terms in order to capture the major part of the momentum dependence of the full meson propagators as in the previous chapter. These terms are explicitly shown in (5.3). As usual, the effective action contains all terms that respect the symmetries of the system. As a first step and for the sake of simplicity, we restrict ourselves to relevant and marginal operators. This is sufficient to capture the qualitative features of the system. Hence, we will only keep the vector-vector and scalar-vector meson interactions introduced above and expand the scalar meson effective potential $V(\phi^2)$ in (5.16) only up to order ϕ^4.

In summary, the final meson interactions that are stored in $U_k(\varphi, V_\mu)$ in (5.3) are

$$\begin{aligned} U_k(\phi, V_\mu) = {} & \frac{1}{2} m_{S,k}^2 \left(\phi^2 - \phi_0^2\right) + \frac{1}{8} \nu_k \left(\phi^2 - \phi_0^2\right)^2 - c\sigma \\ & - i g_{1,k} V_\mu \phi \cdot \partial_\mu \phi - \frac{1}{2} g_{2,k} \left(V_\mu \phi\right)^2 + \frac{1}{4} g_{3,k} \phi^2 \operatorname{tr} V_\mu V_\mu \\ & + \frac{1}{4} m_{V,k}^2 \operatorname{tr} V_\mu V_\mu - \frac{i}{2} g_{4,k} \operatorname{tr} \partial_\mu V_\nu [V_\mu, V_\nu] - \frac{1}{4} g_{5,k} \operatorname{tr} V_\mu V_\nu [V_\mu, V_\nu] . \end{aligned} \tag{5.20}$$

Irrelevant operators are potentially non-negligible if one is interested in quantitative precision, see in particular Chap. 7. We postpone such a study to future work. Note that U_k is not an effective potential, since it also contains the terms $g_{1,k}$ and $g_{4,k}$ with explicit derivatives of the meson fields. Note that we did not choose the fixed background expansion here, but resorted to the comoving expansion about the running minimum of the effective potential $\phi_{0,k}$. We are using this method since the expansion in terms of n-point functions here is nor as systematic as the one in the previous case. Our construction principle here is rather phenomenologically motivated. For a more systematic expansion, one should formulate the meson sector in terms of a single chiral invariant instead of relying on an invariant construction in terms of fields in different representation of $O(4)$. This is of course possible without any restrictions, but beyond the scope of the present study.

With the explicit definitions of the scalar and vector mesons, the scalar-vector interactions in (5.20) can be rewritten in terms of the physical fields as

$$\begin{aligned} -i g_{1,k} V_\mu \phi \cdot \partial_\mu \phi &= g_{1,k} \left[(\vec{\rho}^{\,\mu} \times \vec{\pi}) \cdot \partial_\mu \vec{\pi} - \sigma \vec{a}_1^{\,\mu} \cdot \partial_\mu \vec{\pi} + \vec{a}_1^{\,\mu} \cdot \vec{\pi} \partial_\mu \sigma \right], \\ -\frac{g_{2,k}}{2} \left(V_\mu \phi\right)^2 &= \frac{g_{2,k}}{2} \left[(\vec{\rho}^{\,\mu} \times \vec{\pi} - \sigma \vec{a}_1^{\,\mu})^2 + (\vec{a}_1^{\,\mu} \cdot \vec{\pi})^2 \right], \\ \frac{g_{3,k}}{4} \phi^2 \operatorname{tr} V_\mu V_\mu &= \frac{g_{3,k}}{2} \left(\vec{\pi}^{\,2} + \sigma^2\right) \left((\vec{\rho}^{\,\mu})^2 + (\vec{a}_1^{\,\mu})^2 \right) , \end{aligned} \tag{5.21}$$

and the vector-vector meson interactions in (5.20) as

$$
\begin{aligned}
-\frac{i}{2} g_{4,k} \operatorname{tr} \partial_\mu V_\nu [V_\mu, V_\nu] &= g_{4,k} \left[\partial_\mu \vec{\rho}^{\,\nu} \cdot \left(\vec{\rho}^{\,\mu} \times \vec{\rho}^{\,\nu} + \vec{a}_1^{\,\mu} \times \vec{a}_1^{\,\nu} \right) + \partial_\mu \vec{a}_1^{\,\nu} \cdot \left(\vec{\rho}^{\,\mu} \times \vec{a}_1^{\,\nu} - \vec{a}_1^{\,\mu} \times \vec{\rho}^{\,\nu} \right) \right], \\
-\frac{1}{4} g_{5,k} \operatorname{tr} V_\mu V_\nu [V_\mu, V_\nu] &= \frac{g_{5,k}}{4} \left[\left(\vec{\rho}^{\,\mu} \times \vec{\rho}^{\,\nu} + \vec{a}_1^{\,\mu} \times \vec{a}_1^{\,\nu} \right)^2 + \left(\vec{\rho}^{\,\mu} \times \vec{a}_1^{\,\nu} - \vec{a}_1^{\,\mu} \times \vec{\rho}^{\,\nu} \right)^2 \right].
\end{aligned} \tag{5.22}
$$

Following our discussion above and as it is now evident from (5.20), we do not assume VMD and hence have a priori different scalar-vector and vector vector meson couplings instead of a unique gauge coupling. The gauge principle would lead to to the following relations between the different couplings of our truncation:

$$
g_{1,k}^2 = g_{2,k} = g_{4,k}^2 = g_{5,k} \quad \text{and} \quad g_{3,k} = 0. \tag{5.23}
$$

By inspection of the renormalization group flow of these couplings, we will show that VMD would lead to an oversimplification of the dynamics of the system. Nonetheless, VMD turns out to be a good approximation at low energies, see Sec 5.3.4.

We emphasize that the advantage of VMD is obvious for effective model studies: VMD restricts the vector meson interactions to be described by a single coupling. This tremendously simplifies the necessary fine tuning of model parameters in these approaches. Owing to the fixed point behavior of the RG-flows with dynamical hadronization, we can easily include many different interactions in the meson sector. Their physical values are uniquely fixed by the QCD dynamics and hence, no fine-tuning of parameters, no matter how large the parameter space is, is required.

In the present setup, the masses of the quarks and the mesons are given by

$$
\begin{aligned}
m_{q,k}^2 &= h_{s,k}^2 \sigma_{0,k}^2 , \\
m_{\pi,k}^2 &= m_{S,k}^2 , \\
m_{\sigma,k}^2 &= m_{S,k}^2 + \lambda_{4,k} \sigma_{0,k}^2 , \\
m_{\rho,k}^2 &= m_{V,k}^2 + g_{3,k} \sigma_{0,k}^2 , \\
m_{a_1,k}^2 &= m_{V,k}^2 + (g_{2,k} + g_{3,k}) \sigma_{0,k}^2 .
\end{aligned} \tag{5.24}
$$

We see that the π and the σ meson as well as the ρ and a_1 meson have degenerate masses in the chirally symmetric phase which is characterized by $\sigma_{0,k} = 0$. When chiral symmetry is broken, this degeneracy is lifted. The mass-splitting of the scalar mesons is then determined by the quartic scalar meson coupling $\lambda_{4,k}$. The mass-splitting of the vector mesons is determined by the strength of the interaction $g_{2,k}$. Note that, owing to the symmetry breaking source $c > 0$, we are not in the chiral limit. Thus, the chiral order parameter $\sigma_{0,k}$ is always nonzero.

Even though the masses we extract here are the curvature masses, it was shown in [166] on the example of the pion mass in a quark meson model, that the curvature mass of the mesons is almost identical to the pole mass for truncations that include running wave function renormalizations. Thus, as mentioned above, we capture the major part of the momentum dependence of the full meson propagators by including $Z_{S,k}$ and $Z_{V,k}$ and the masses are very close to the physical masses.

5.2. Fluctuations and the Transition from Quarks to Mesons

We are interested in the dynamical transition from UV to IR degrees of freedom. To achieve this, we include quantum fluctuations by means of the functional renormalization group.

Furthermore, in order to consistently describe the dynamical change of degrees of freedom, we use dynamical hadronization as it was put forward in Sec. 4.2. This allows for a unified description of the interplay between different degrees of freedom at different scales in terms of a single effective action.

5.2.1. Dynamical Hadronization for Vector Mesons

Here, we will generalize the dynamical hadronizetion technique to the case of vector mesons. Again, the starting point is the modified flow equation (3.21) with RG-scale dependent meson fields. It reads with $\Phi = (A, q, \bar{q}, c, \bar{c}, \pi, \sigma, \rho, a_1)$ in a shorthand notation:

$$\partial_t\big|_\varphi \Gamma_k[\Phi] = \frac{1}{2}\mathrm{Tr}\left[\left(\Gamma_k^{(2)}[\Phi] + R_k^\Phi\right)^{-1} \cdot \partial_t R_k^\Phi\right] - \frac{\delta\Gamma_k}{\delta\varphi_i} \cdot \partial_t \varphi_i \,, \tag{5.25}$$

where $\varphi = (\pi, \sigma, \rho, a_1)$ summarizes the meson fields. $\Gamma_k^{(2)}[\Phi]$ denotes the second functional derivative of the effective action with respect to all combinations of the fields. R_k^Φ is the regulator function for the field Φ. It is diagonal in field space. Note that in order not to break chiral symmetry explicitly by our regularization scheme, we introduced the same regulators for the scalar mesons and the vector mesons respectively. For details we refer to App. C.3. By inserting the truncation (5.3) into the flow equation (5.25), one gets a closed set of fully coupled RG-flow equations for the scale-dependent parameters of the truncation.

$\frac{\delta\Gamma_k}{\delta\varphi_i} \cdot \partial_t \varphi_i$ stands for the modifications of the flow equation due to dynamical hadronization. In addition to the scalar mesons π and σ, we also apply dynamical hadronization to the vector mesons ρ and a_1 here. Hence, all mesons fields are scale dependent here. The gauge sector as well as the quarks are not affected by the hadronization. The scale dependence of the mesons is given by their flow $\partial_t \varphi_i$, which reads for the individual mesons

$$\begin{aligned}
\partial_t \vec{\pi} &= \dot{A}_k \bar{q}\gamma_5 \vec{\tau} q \,, \\
\partial_t \sigma &= \dot{A}_k \bar{q} i q \,, \\
\partial_t \vec{\rho}^{\,\mu} &= \dot{B}_k \bar{q}\gamma_\mu \vec{\tau} q \,, \\
\partial_t \vec{a}_1^{\,\mu} &= \dot{B}_k \bar{q}\gamma_\mu\gamma_5 \vec{\tau} q - \dot{C}_k \partial_\mu \vec{\pi} \,.
\end{aligned} \tag{5.26}$$

Note that the structure of the mesons as quark-antiquark bilinears becomes apparent in this formulation. $\dot{A}_k$ and $\dot{B}_k$ are the hadronization functions. Their precise form is determined by our hadronization procedure. In analogy to the discussion in Sec. 4.2, we fix them such that the fermionic self-interactions that drive chiral symmetry breaking and reflect the meson content of our theory are stored in the meson sector at every scale k. Thus, the the four-quark interactions are completely absorbed into the meson sector, enforcing

$$\partial_t\big|_\varphi \lambda_{S,k} = 0 \quad \text{and} \quad \partial_t\big|_\varphi \lambda_{V,k} = 0 \,. \tag{5.27}$$

Note that this formulation eliminates all double- and/or mis-counting problems, which potentially occur in models including both quark and hadron degrees of freedom. (5.27) yields the following hadronization functions:

$$\begin{aligned}
\dot{A}_k &= -\frac{1}{2h_{S,k}} \partial_t \lambda_{S,k} \\
\dot{B}_k &= -\frac{1}{2h_{V,k}} \partial_t \lambda_{V,k} \,,
\end{aligned} \tag{5.28}$$

where $\partial_t \lambda_{S/V,k}$ are the flows with with fixed hadronization fields. These hadronization functions give rise to modified running couplings of (5.3). In analogy to the previous case, the precise choice of the scale dependence of the mesons in terms of quark-bilinears (5.26) implies that the running of the four quark interactions $\lambda_{S/V,k}$ is completely sored in the corresponding Yukawa couplings $h_{S/V,k}$. The flow equations are discussed in App. C.3.

In addition to the quark-bilinear term with the quantum numbers of the corresponding meson in (5.26), the flow of the a_1-meson has an additional contribution proportional to $\partial_\mu \vec{\pi}$. This term arises because the so-called $\pi - a_1$ mixing leads to an additional scale dependence of the a_1 meson, which has to be taken into account and fixes $\dot{C}_k$. We will elaborate on this point in the next section.

5.2.2. $\pi - a_1$ Mixing

Spontaneous chiral symmetry breaking leads to a non-vanishing vacuum expectation value σ_0 of the σ meson and the resulting mixing term

$$\Gamma_{\pi a_1} = -\int_x g_{1,k}\, \sigma_0\, \vec{a}_1^{\,\mu} \cdot \partial_\mu \vec{\pi}\,, \tag{5.29}$$

implies an off-diagonal two-point function $\Gamma_k^{(2)}$. This is referred to as $\pi - a_1$ mixing. There are two ways to cope with this problem. One can either take these additional off-diagonal contributions into account or one diagonalizes the two-point function in order to eliminate this mixing by an appropriate field redefinition. We note that the first option may give rise to problems concerning regularity: since our regulators are diagonal in field space, off-diagonal two-point function can potentially lead to non-regular expressions. However, this should be investigated in more detail. Here, we will eliminate this mixing by a redefinition of the a_1 field,

$$\vec{a}_1^{\,\mu} \longrightarrow \vec{a}_1^{\,\mu} + \frac{g_{1,k}\sigma}{m_{V,k}^2 + (g_{2,k} + g_{3,k})\sigma^2}\, \partial_\mu \vec{\pi}\,. \tag{5.30}$$

This redefinition of the a_1 field renders it explicitly RG-scale dependent, $\partial_t \vec{a}_1^{\,\mu} \neq 0$. Before we discuss the implications of this scale dependence, we turn toward the resulting modifications of the effective action (5.3).

If we plug (5.30) into the truncation (5.3), the part of the action leading to the mixing term (5.29) is canceled and various new terms appear. Since the replacement (5.30) introduces terms $\sim \partial_\mu \vec{\pi}$, the interactions of our original ansatz (5.3) receive modifications with explicit momentum dependence. Within this work, we define all running coupling at vanishing external momentum, see App. C.3. Thus, for interactions that are not explicitly momentum dependent in our original action, these modifications simply drop out of the beta functions. Only the meson anomalous dimension $Z_{S,k}$ and the scalar-scalar vector interaction $g_{1,k}$ receive non-vanishing modifications. The new term $\sim (\partial_\mu \vec{\pi})^2$ yields for the pion wave function renormalization

$$Z_{\pi,k} = Z_{S,k} - \frac{g_{1,k}^2 \sigma_{0,k}^2}{m_{a_1}^2}\,. \tag{5.31}$$

While the wave function renormalizations do not enter RG-invariant beta functions, their anomalous dimensions $\eta_k = -(\partial_t Z_k)/Z_k$ do. Thus, (5.31) yields a modified pion anomalous dimension.

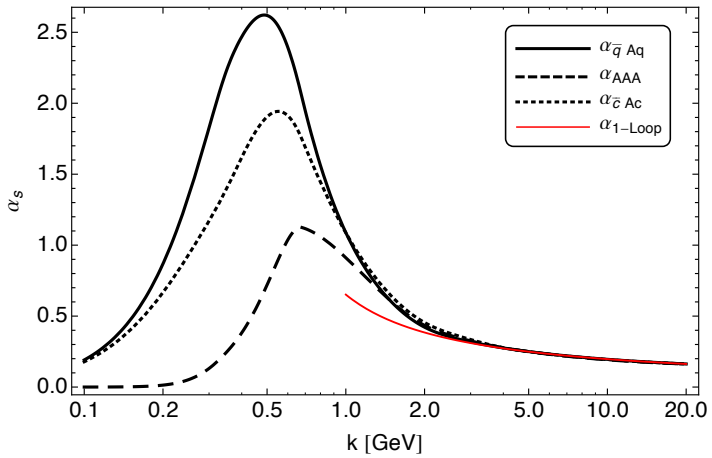

Figure 5.2.: The running of the different strong couplings in comparison to the 1-loop running.

The other relevant modification affects the $\rho\pi\pi$ vertex, which now reads

$$\Gamma^{(3)}_{\rho\pi\pi} = g_{1,k}\left(1 - \frac{g_{2,k}\sigma^2_{0,k}}{m^2_{a_1,k}}\right). \tag{5.32}$$

Since we define the coupling $g_{1,k}$ via this vertex, this has to be taken into account in the corresponding beta function, see App. C.3.

The elimination of the $\pi - a_1$ mixing entails a shift of the a_1 field which includes running couplings. As a consequence, the a_1 field becomes RG-scale dependent itself. As we have discussed in the previous section, we use the dynamical hadronization technique which implies that all meson fields are scale dependent. The scale dependence of a_1 induced by (5.30) is additional to the one induced by dynamical hadronization. The total scale dependence of a_1 is now given by the RG flow

$$\partial_t \vec{a}_1^{\,\mu} = \dot{B}_k \bar{q}\gamma_\mu\gamma_5\vec{\tau}q - \dot{C}_k\partial_\mu\vec{\pi}\,. \tag{5.33}$$

The first term stems from dynamical hadronization and reflects the quark-bilinear nature of the a_1 meson. The hadronization function $\dot{B}_k$ is given in Eq. (5.28). The second term is a result of the diagonalization of the meson two-point function and according to (5.30) $\dot{C}_k$ is given by

$$\dot{C}_k = \partial_t\left(\frac{g_{1,k}\,\sigma}{m_V^2 + (g_{2,k}+g_{3,k})\sigma^2}\right)\Bigg|_{\sigma=\sigma_{0,k}}. \tag{5.34}$$

In summary, chiral symmetry breaking leads to an off-diagonal meson two-point function. Diagonalization leads to modifications of the pion anomalous dimension and the $\rho\pi\pi$ interaction and introduces an additional scale dependence to the a_1 meson.

5.3. Numerical Results

5.3.1. Initial Conditions

We initiate the RG flow of the effective action (5.3) at the initial scale $\Lambda = 20\,\mathrm{GeV}$ and therefore deep in the perturbatively accessible quark-gluon regime. Hadronic degrees of freedom will

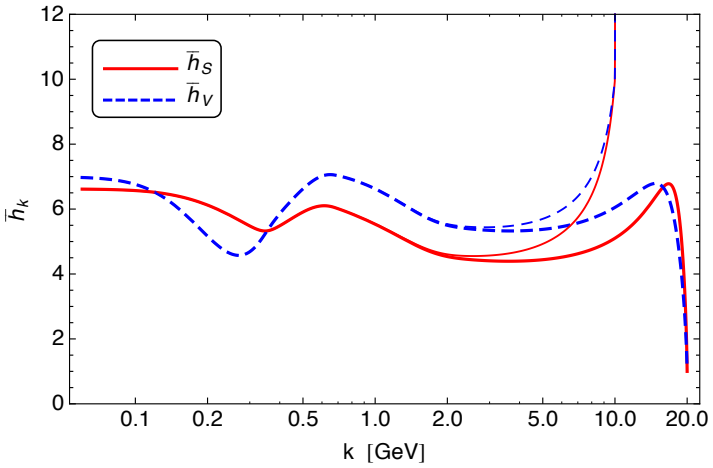

Figure 5.3.: The RG-flows of the scalar and vector yukawa couplings $\bar{h}_{S,k}$, $\bar{h}_{V,k}$. The thick and thin lines correspond to different initial values of the couplings at different initial scales.

become relevant at much lower, non-perturbative scales. Owing to the dynamical hadronization procedure, the RG flows of our model are completely fixed by specifying the free parameters of the microscopic gauge fixed action of QCD, i.e. the strong coupling and the current quark mass. Even though we choose a priori different flow equations for the strong couplings $\alpha_{\bar{q}Aq}$, α_{A^3}, $\alpha_{\bar{c}Ac}$, the gauge principle enforces them to be identical in the perturbative regime. The initial value of the strong couplings implicitly sets the scale, and we choose $\alpha_{i,\Lambda}=0.163$ for $i=\bar{q}Aq, A^3, \bar{c}Ac$, which corresponds to $\Lambda \approx 20\,\text{GeV}$.

Fig. 5.2 shows our result for the gauge couplings. Note that vector mesons lead to additional contributions to the flow of the quark-gluon vertex $\alpha_{\bar{q}Aq}$ through triangle diagrams with internal meson lines. But as we will show in the following, the vector mesons are always decoupled from the flow due to their large mass. Thus, there are no contribution from vector meson fluctuations. The only difference between the gauge couplings shown in Fig. 4.6 and Fig. 5.2 stems from the fact that in the former case, we used the fixed background expansion about $\bar{\kappa}$, while here we use the comoving expansion about the running minimum $\bar{\phi}_{0,k}$.

As in the previous case, we also added an IR-strength to the gauge couplings in order to compensate the effects of neglected tensor structures and momentum dependencies. Owing to the different expansion scheme, we need a little less IR strength as in the previous chapter, to wit $a = 0.17$, see App. D.

The current quark mass m_q^{UV} is related to the explicit symmetry breaking parameter c in (5.20) via

$$m_q^{\text{UV}} = \frac{h_{S,\Lambda}}{m_{S,\Lambda}^2}\, c. \tag{5.35}$$

We choose for the renormalized parameter $\bar{c}_\Lambda = 3.9\,\text{GeV}^3$, which yields an pion mass in the IR of $M_{\pi,0} = 137.5\,\text{MeV}$.

We note that the physical parameters are rescaled with appropriate powers on the wave function renormalizations to ensure RG invariance, see App. C.3 and in particular (C.22). The

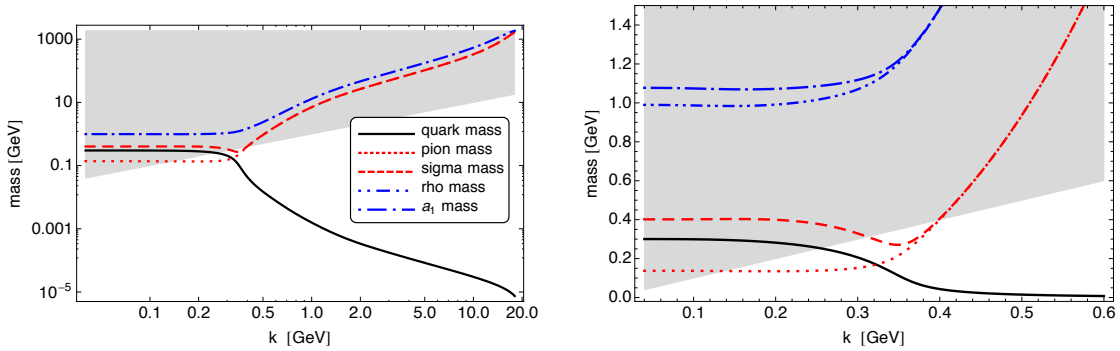

Figure 5.4.: Renormalized masses (5.36) as a function of the RG-scale. Masses in the shaded area are larger than the cutoff scale and therefore decoupled from the dynamics.

physical (or renormalized) quark and meson masses are defined as

$$M_{q,k} = \frac{m_{q,k}}{Z_{q,k}}, \quad \text{and} \quad M_{\varphi,k} = \frac{m_{\varphi,k}}{Z_{\varphi,k}^{1/2}}. \tag{5.36}$$

With slight abuse of terminology, we refer to m_k as bare mass. They are given in (5.24).

As already discussed in the previous chapter, the initial conditions of the mesonic parameters can be chosen arbitrarily. This is due to the fact that, as long as the initial scale is large enough, we find unique solutions for the meson parameters at low energies owing to the existence of the IR-attractive fixed point in the high-energy regime. We only have to make sure that initial meson masses are chosen larger than the UV-cutoff scale, $M_{S/V,\Lambda} \gtrsim \Lambda$. Furthermore, to ensure that our initial conditions correspond to QCD, the ratio $h^2_{S/V,\Lambda}/m^2_{\pi/\rho,\Lambda}$ has to be much smaller than $\Lambda^{-2}\alpha_s^2$.

The independence of the IR-physics on the initial values of the meson sector is demonstrated in Fig. 5.3 and Fig. 5.9. There, we have chosen initial values at different initial scales (10 and 20 GeV) that differ by many orders of magnitude and one nicely sees that the initially different trajectories are attracted towards a unique solution in the hadronic regime.

5.3.2. Masses

In Fig. 5.4 we show our results for the quark and meson masses. The left figure shows the masses over the full range of scales we consider here, while the right figure shows the region for $k < 600\,\text{MeV}$. For scales $k \gtrsim 400\,\text{MeV}$ all mesons are decoupled from the flow. At these scales the dynamics are driven completely by current quarks and gluons. At about 400 MeV, the degeneracy of the π and σ masses as well as the ρ and a_1 masses is lifted due to chiral symmetry breaking. π, σ and the constituent quarks are the dynamical degrees of freedom in this region. The vector mesons are always decoupled. Thus, the vacuum structure of the vector mesons is determined by quark and gluon fluctuations at large scales and the fluctuations of the lightest mesons, the π and σ, at lower scales.

This is also shown in Fig. 5.5, where the effective propagators also reflect this scale hierarchy. They are defined in App. C.3 and in particular (C.28) and are a measure for the strength of the fluctuations of the fields. Vanishing of the effective propagator of a field implies that this

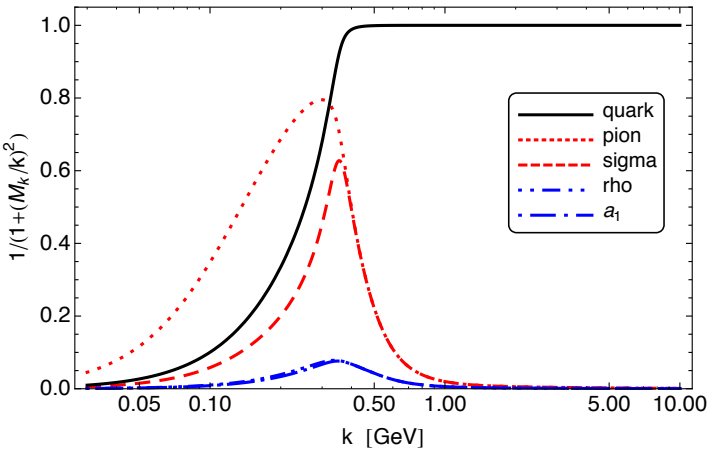

Figure 5.5.: Effective propagators (C.28) of the matter fields as a function of the RG scale. They are a measure for the effective strength of the fluctuations of the fields.

field does not contribute to the dynamics of the system. Thus, we see that at large energy scales the quarks are the only dynamical matter fields. There is only a relatively small window, $100\,\text{MeV} < k < 500\,\text{MeV}$, where the scalar mesons are dynamical and one nicely sees that the sigma mesons decouples earlier that the lighter pions. Vector meson fluctuations are always negligible.

Indeed, an explicit calculation of a complete set of four-quark interactions in Euclidean spacetime shows that the scalar-pseudoscalar channel is the dominant channel [156]. This implies that the only relevant meson degrees of freedom in vacuum are π and σ. We note that this picture will change in Minkowski space, since different channels will become relevant as soon as the momentum is close to the corresponding mass pole.

The behavior of the masses as function of the RG scale k reflects their scaling with temperature T. In particular, the running of the masses at vanishing temperature is qualitatively very similar to the temperature dependence at $k = 0$. As we have discussed above, the behavior of the vector mesons masses, in particular the ρ mass, in the vicinity of the chiral phase transition is potentially relevant for the observation of chiral symmetry restoration in experiments. This is motivated by the strong modifications that the light vector meson peaks receive in the quark-gluon plasma, see Fig. 5.1. The most prominent conjecture is the Brown-Rho scaling [34], which states that the ρ mass decreases towards the phase transition in a similar manner as the σ mass or the pion decay constant f_π.

In Fig. 5.4 we see that the ρ mass is almost constant in the hadronic phase and only grows slowly close to the pseudocritical scale. If we take a closer look at the $M_{\rho,k}$, we see that, starting from $k=0$, it first decreases slightly with increasing k, before it increases starting from $k \gtrsim M_\pi$. This is shown in Fig. 5.6 and we note that $M_{a_1,k}$ shows the same behavior. At scales $k \lesssim M_\pi$ the only dynamical contributions stem from small pion fluctuations, while all other contributions are completely decoupled. This can be seen in Fig. 5.5. There, we also see that at scales $k \gtrsim M_\pi$ constituent quark fluctuations play an important role. Since bosonic and fermionic fluctuations drive the mesonic parameters in opposite directions, the change of the scaling of the ρ mass can be explained qualitatively by this change of the relative importance of bosonic and fermionic fluctuation above and below $k \approx M_\pi$.

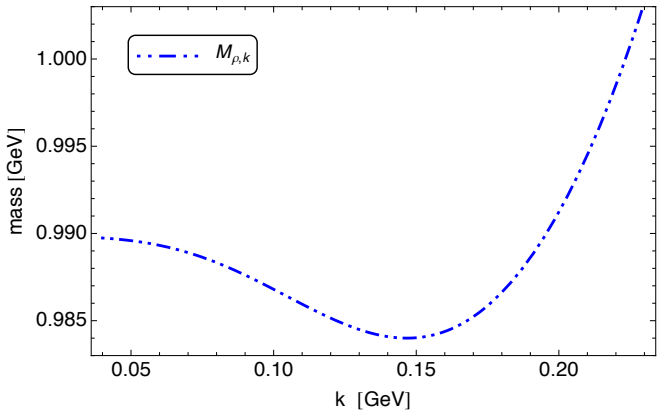

Figure 5.6.: The renormalized mass of the ρ meson, $M_{\rho,k}$, as a function of the RG-scale. We see that it first decreases with increasing k, before it starts increasing for $k \gtrsim M_\pi$.

For the ρ mass, this behavior was also found in [36], where a gauged linear sigma model was studied at finite temperature. But there the a_1 mass first grows and than decreases towards the chiral transition, i.e. it shows the opposite behavior of our findings, where $M_{a_1,k}$ scales just as $M_{\rho,k}$.

In summary, we observe a very weak Brown-Rho behavior at small scales and a more pronounced anti-Brown-Rho behavior close to the chiral transition. This in line with the in-medium behavior of the ρ mass observed within effective field theory studies, which reproduce the data on vector meson spectral functions and dilepton spectra very well [93]. For a sensible comparison, however, we also need to compute the in-medium modifications of the masses within our QCD-based approach.

Our predicted masses for the vector mesons show a quite large discrepancy from the observed masses. We find for the renormalized ρ mass $M_{\rho,0} = 990\,\text{MeV}$, which is about 29% larger than the observed mass of 770 MeV [96]. For the a_1 mass we find $M_{a_1} = 1077\,\text{MeV}$, which is about 15% smaller than the observed mass of 1260 MeV. The value of the ρ mass is fixed mainly by the fluctuations in the quark-gluon sector. This can be seen from the definition of the masses, (5.24), the observation that $\bar{m}_{V,k}$ runs only very little in the hadronic regime and that $\bar{g}_{3,k}$ is very small (see Fig. 5.9). Thus, the strength of the four-quark interaction $\lambda_{V,k}$, which is determined by the strong coupling, essentially fixes the ρ mass. Furthermore, according to (5.24), the mass-splitting of ρ and a_1 and therefore the mass of a_1 is determined by the flow of the hadronic sector at low energies. We already discussed in Sec. 4.4.4 that the situation is different for π and σ: the mass of the pion is fixed by its nature as a (pseudo) Goldstone boson and the strength of explicit symmetry breaking in terms of a finite current quark mass. In any case, the mass-splitting of chiral partners in the phase with broken chiral symmetry is sensitive to the quality of our truncation in the hadronic sector. Thus, the small mass of a_1 is a signal for a shortcoming of our truncation there and may be related to momentum dependencies that were taken into account insufficiently. The large value for the ρ mass can also be attributed to the insufficient inclusion of momentum dependence, but in the quark-gluon sector and in particular in the four-fermi interaction $\lambda_{V,k}$. We evaluate this interaction at vanishing external momentum, see App. C.3, and it is possible that we underestimate its strength this way. A larger $\lambda_{V,k}$ leads to smaller vector meson masses. Since the present work is the first study in this direction, aimed at capturing the qualitative features, we defer a thorough quantitative

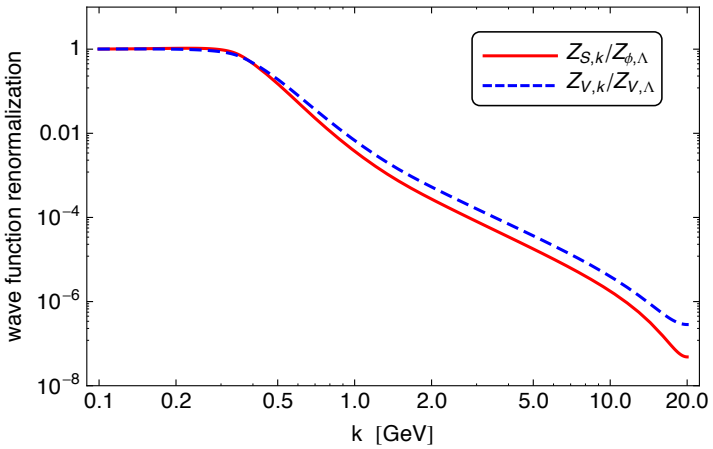

Figure 5.7.: Scalar and vector wave function renormalization as function of the RG scale. We normalized them to be 1 at the IR scale $k = 30\,\text{MeV}$.

analysis to future work.

5.3.3. Decoupling of the Mesons

As in Sec. 4.4.4, we again demonstrate here that the mesons are completely decoupled in the quark-gluon phase as a result of the consistent treatment of bound states via dynamical hadronization. We also see that the decoupling of the mesons is triggered by a rapid fall-off of the meson wave function renormalizations $Z_{S/V,k}$ at the pseudocritical scale. The mechanism is the same for scalar and vector mesons. We show the running of $Z_{S,k}$ and $Z_{V,k}$ in Fig. 5.7. While they stay almost constant in the hadronic regime, they rapidly fall-off at the chiral transition scale. The scalar meson wave function renormalization $Z_{S,k}$ drops about eight orders of magnitude and that of the vector mesons, $Z_{V,k}$, about seven orders of magnitude towards the UV. The fastest drop-off is in the vicinity of the pseudocritical scale $k_\chi \approx 400$ MeV. The reason is that quark fluctuations decrease the meson wave function renormalizations in the quark-gluon regime. Their flows are proportional to the corresponding squared Yukawa couplings, $\partial_t Z_{S/V,k} \propto -\bar{h}^2_{S/V,k} Z_{S/V,k}$, at scales $k \gtrsim k_\chi$, resulting in large negative beta functions, see Fig. 5.3. Vanishing wave function renormalizations imply that the corresponding particles become auxiliary fields and are therefore no longer part of the physical spectrum at large energy scales.

Again, this is reflected in the behavior of the bare masses, $m^2_\varphi = Z_{\varphi,k} M^2_{\varphi,k}$, shown in Fig. 5.8. They are constant in the quark-gluon regime, implying that without the rapid fall-off of the meson wave function renormalizations, the mesons show no decoupling and hence an unphysical high-energy phase. The running of the physical masses is therefore exclusively driven by the anomalous dimensions of the corresponding mesons at large energy scales. This is crucial for the unambiguous definition of the mesons masses, as discussed in Sec. 4.2.2.

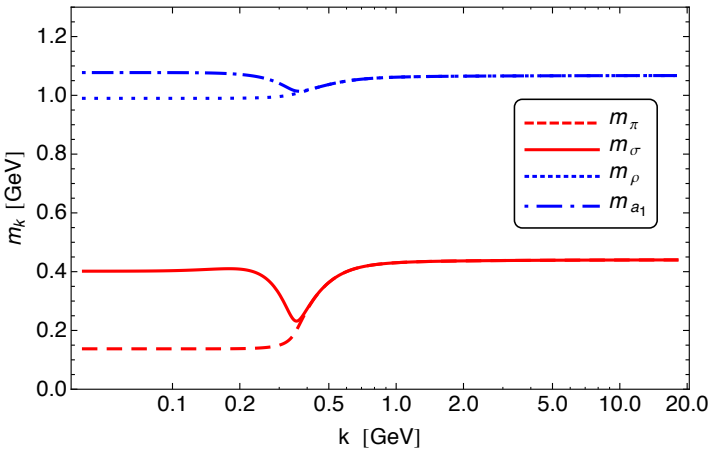

Figure 5.8.: Bare masses of the mesons, $m_\varphi^2 = Z_{\varphi,k} M_{\varphi,k}^2$, see (5.24) and (5.36). Note that we normalized the wave function renormalizations to be 1 in the IR at $k = 20\,\text{MeV}$ here.

5.3.4. Vector Meson Dominance

The principle of vector meson dominance entails that the $SU(N_f)_A \times SU(N_f)_V$ flavor symmetry is treated as a gauge symmetry. In this case, the vector and axial-vector mesons appear as gauge bosons of the scalar and pseudoscalar mesons. This simplifies the effective action in the hadronic sector, since the gauge principle significantly restricts the number of possible different interactions and there is only one running coupling for interactions involving vector mesons. Here, we do not apply VMD. As a consequence, we have a priori different running couplings $g_{1-5,k}$, while VMD implies

$$g_{1,k} = g_{4,k} = \sqrt{g_{2,k}} = \sqrt{g_{5,k}} \quad \text{and} \quad g_{3,k} = 0\,. \tag{5.37}$$

As we have discussed above, the advantage of our approach is that the hadronic parameters are uniquely determined by the dynamics in the quark-gluon phase, i.e. microscopic QCD. Thus, even though we have a large parameter space in the meson sector, model parameter tuning is not necessary. This allows us to study the validity of VMD in an unbiased way by comparing our results to (5.37). In Fig. 5.9 we show our results for the running of $\bar{g}_{1-5,k}$.

Or results show that, while VMD does not hold exactly, it is a good approximation. In particular the couplings $\bar{g}_{2,k}$, $\bar{g}_{4,k}$ and $\bar{g}_{5,k}$ are very close together. Only $\bar{g}_{1,k}$ is considerably larger than the other couplings. If we define the error one would make by assuming VMD by the standard deviation of these couplings in the IR, we find it to be about 16% of the mean average of these couplings. $g_{3,k}$, which is explicitly forbidden for local chiral symmetry, is well approximated by VMD. It is very close to $g_{3,k} = 0$ at the pseudocritical scale and assumes only a small finite value at lower scales. The flow of $g_{3,k}$ is proportional to the chiral order parameter $\sigma_{0,k}$. Thus, with large positive anomalous dimensions, the renormalized coupling $\bar{g}_{3,k}$ is driven to values very close to zero at large energy scales.

The construction of our effective action is based on a small momentum expansion (derivative expansion) and we define all running coupling at vanishing external momentum, see App. C.3. The momentum scale of our results is therefore given by k. Thus, our findings in the hadronic regime correspond to small momentum scales $k \leq 400\,\text{MeV}$. A comparison of effective field

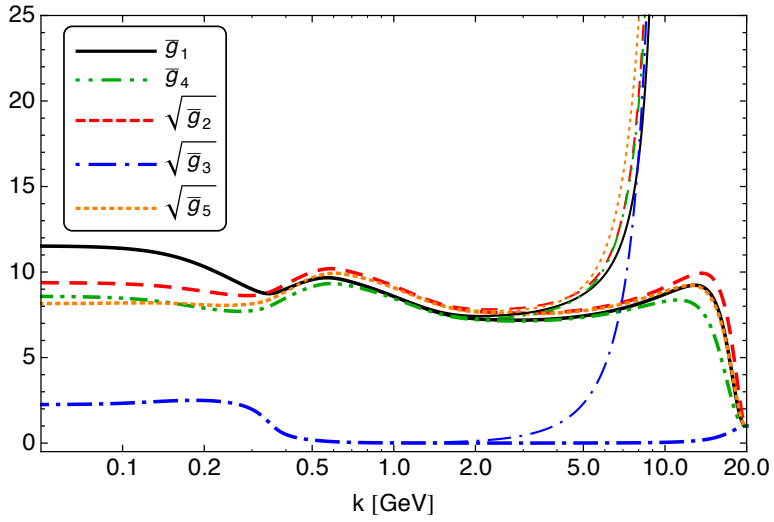

Figure 5.9.: The RG-flow of the vector-vector and vector-scalar meson couplings $\bar{g}_{1-5,k}$. The thick and thin lines correspond to different initial values of the couplings at different initial scales. Vector meson dominance would imply (5.37).

theory predictions assuming VMD with experimental results for the electromagnetic form factor of the pion show that they agree within 10-20% accuracy at momentum transfer $q^2 \lesssim 1\,\mathrm{GeV}^2$ [189]. Thus, our results for the validity of VMD are in very good agreement with phenomenological findings.

We note again that the thick and thin lines in Fig. 5.9 correspond to very different initial conditions for the flow of the couplings. The flows in the hadronic phase as well as the final value of the couplings in the IR are prediction of our analysis without any model parameter fixing.

5.4. Conclusions

A thorough understanding of the dynamics of vector mesons in QCD is essential for our understanding of the phase structure of strongly interacting matter. Since these low-energy degrees of freedom ultimately derive from microscopic QCD, the dynamical connection between the high- and low-energy sector of QCD needs to be captured. To this end, we have presented at functional renormalization group study of vector mesons in QCD. Our focus was on how the dynamics of the lightest meson chiral partners, π, σ and ρ, a_1, emerge from the dynamics of quarks and gluons. We have developed a scale dependent effective action that captures the dynamical transition from the quark-gluon regime to the hadronic regime, including vector mesons, in a qualitative manner. The key ingredient is the dynamical hadronization technique, which allows for a consistent description of the transition from high-energy to low-energy degrees of freedom. This entails in particular that the properties of the hadronic regime are fixed by the quark-gluon fluctuations at high energies. Thus, no fine-tuning of model parameters is necessary and e.g. the meson masses and the running of the mesonic parameters can be viewed as predictions from first-principle QCD.

We have demonstrated explicitly that, within this Euclidean formulation, there is an intriguing

scale hierarchy emerging, where the hadronic contributions to the dynamics of the heavier mesons are determined solely by the fluctuations of π and σ.

The masses of ρ and a_1 are almost constant and only slightly grow towards the pseudocritical scale. Since the behavior of the masses as a function of the RG-scale reflects their finite temperature behavior, this gives a hint for the in-medium scaling of these masses. Our predictions are in agreement with the findings of phenomenologically motivated effective models.

We have emphasized the important role that the meson wave function renormalizations play for the decoupling of the meson degrees of freedom at high energies. They fall-off many orders of magnitude in the vicinity of the pseudocritical scale. This triggers a rapid growth of the renormalized meson masses and the mesons become auxiliary fields in the quark-gluon phase.

Since the properties of the mesonic parameters in our model are fixed by the QCD flow, we have been able to make an unbiased analysis of the validity of vector-meson dominance. Our results show that while VMD does not hold exactly, it is a good approximation within an accuracy of about 16% at small momentum scales. This is in agreement with phenomenological findings.

In this study we focused on qualitative features and given the lack of quantitative precision, in particular for the mass-splitting of the mesons in the chirally broken phase, there is a lot of room for improvement and refinement. In particular the extension of our truncation in the hadronic sector and a thorough analysis of momentum dependencies are important next steps.

This work serves as a starting point for the study of the in-medium modifications of the vector mesons and their spectral functions within functional renormalization group methods for QCD.

CHAPTER 6

From QCD to Low-Energy Effective Models

In this chapter we want to take a closer look on the relation between QCD and low-energy effective models. It is fair to say that to date no self-consistent study of QCD at finite temperature and density has been done, even though much progress has been made in this directions with various methods. Effective models are therefore a valuable tool to gain insights on the physical effects relevant for the QCD phase diagram. Their construction is based on restricting the theory to a certain range of scales and only taking into account the relevant degrees of freedom there. Limitations of these models are thus given by the fact that they are only valid on a limited range of scales and that potentially relevant dynamical contributions are neglected. However, we demonstrated in the previous chapters how the low-energy sector of QCD emerges from fluctuations of the microscopic degrees of freedom. It is then only natural to ask at which point the hadronic sector can be viewed as self-sufficient, i.e. at which scale all relevant gluon fluctuations are effectively stored in the hadronic sector.

The framework presented in the previous chapters allows us to gain insight into the range of validity of quark-meson type models. We used these models to describe the hadronic sector. In contrast to effective models, however, the dynamics of the low-energy degrees of freedom were determined by the QCD flow. The general strategy to test the range of applicability of QM-models here is to determine at which scales the gauge sector can be neglected. This can either be seen from a complete decoupling of the gauge sector or the possibility to effectively store some of the effects of gluon fluctuations into the hadronic sector by IR-parameter fine-tuning. We will investigate the first possibility in the following. For a meaningful analysis of the second point, we would have to compare physically relevant parameters that are not fixed by a parameter tuning in the effective model, such as the critical temperature. Since we only studied dynamical QCD in the vacuum, we postpone this to future work when we extend the analysis presented in the previous chapters to finite temperature.

6.1. Decoupling of the Gauge Sector

To find the scale where gauge dynamics decouple, we directly look at the different contributions to the flow of the dynamically hadronized renormalized Yukawa coupling $\partial_t \bar{h}_k(\bar{\kappa})$ given in (4.47) and (4.68). This is shown in Fig. 6.1. The solid blue line shows the full flow. To obtain

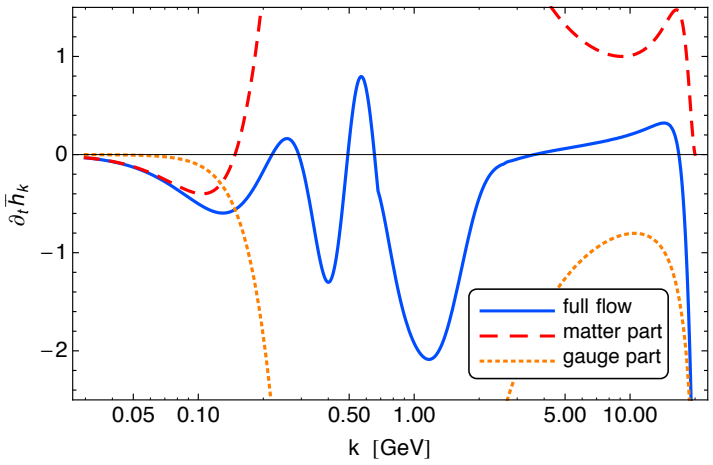

Figure 6.1.: The full flow of the Yukawa coupling $\bar{h}_k(\bar{\kappa})$ in comparison to the pure matter and pure gauge contributions to the flow. In this direct analysis it turns out, that the effect of gauge fluctuations can only be neglected for scales $k \lesssim 120\,\mathrm{MeV}$.

the pure matter contributions to this flow, we ignored all gluon diagrams contributing to (4.47). Note that this has to be done for the anomalous dimensions as well, since we consider the flow of the renormalized Yukawa coupling. In practice, this can most easily be achieved by setting the gauge couplings to zero in the full flow of $\bar{h}_k$. The dotted orange line shows the gauge contribution to $\partial_t \bar{h}_k(\bar{\kappa})$, which is then given by the difference of the full and the pure matter flows.

We see that the gauge part is, as expected, quantitatively of major importance over the largest part of the scales considered here. This is also true for most of the hadronic sector. It is only for scales $k \lesssim 120\,\mathrm{MeV}$, that the gauge part becomes less important than the matter part. Thus, in order to reproduce the full flow accurately only in terms of matter fluctuations, one has to go to very low scales, much lower than the pseudocritical scale k_χ. At first glance, this disqualifies QM-type models that neglect gauge fluctuations as reliable description of low-energy QCD, since according to this analysis, their range of validity is much to low for a description of the phase structure.

However, a different approach, which is more in the spirit of an embedding of low-energy models in full QCD, is to study at which initial scale Λ of the effective model, the initial values provided by full QCD yield the same results in the effective theory as in the full theory. The idea behind this is that an effective model that is truly embedded in QCD should accurately reproduce the results of full QCD within its range of validity. In particular, if the effective model gets its initial values from full QCD at an initial scale within its range of validity, than it should give the same results for physical observables in the IR as QCD. To this end, we use the results of our QCD analysis in Chap. 4 for the effective potential $\bar{V}_k(\bar{\rho})$, the Yukawa coupling $\bar{h}_k(\bar{\rho})$ and the explicit symmetry breaking source $\bar{c}$ and take them as initial conditions for the QM-model given by the scale dependent effective action

$$\Gamma_k^{(\mathrm{QM})} = \int_x \left\{ i Z_{q,k}\, \bar{q}\,(\gamma_\mu \partial_\mu)\, q + h_k(\rho)\, \bar{q}\,(\tau\phi)\, q + \frac{1}{2} Z_{\phi,k} (\partial_\mu \phi)^2 + V(\rho) - c\sigma \right\}. \tag{6.1}$$

Thus, at the initial scale Λ of this effective model, we identify the model parameters with the

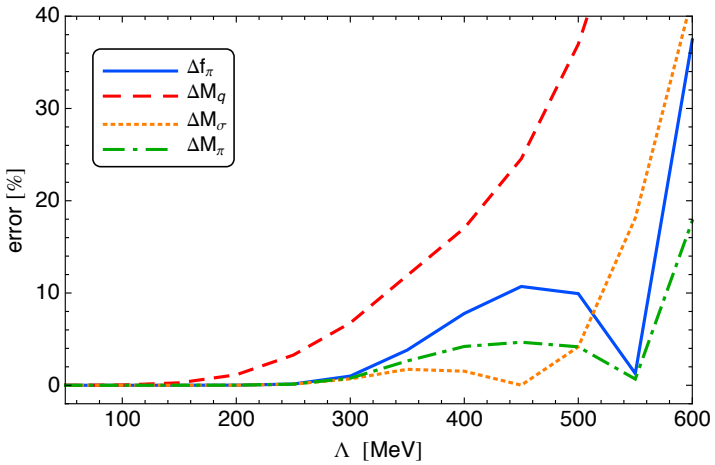

Figure 6.2.: The ratios (6.3) of physical observables in the IR. They measure the relative error one makes by neglecting gluon fluctuations in the low-energy sector described solely in terms of an effective QM-model (6.1) which is initiated at different scales Λ. The initial values are provided by the the solution of the system including gauge dynamics from Chap. 4.

QCD parameters,

$$\begin{aligned}\bar{V}_\Lambda^{(\mathrm{QM})}(\bar{\rho}) &= \bar{V}_\Lambda^{(\mathrm{QCD})}(\bar{\rho})\\ \bar{h}_\Lambda^{(\mathrm{QM})}(\bar{\rho}) &= \bar{h}_\Lambda^{(\mathrm{QCD})}(\bar{\rho})\\ \bar{c}_\Lambda^{(\mathrm{QM})}(\bar{\rho}) &= \bar{c}_\Lambda^{(\mathrm{QCD})}(\bar{\rho})\end{aligned} \tag{6.2}$$

and solve the flow equations for (6.1). We then compare the results for the physical IR-parameters of the model to the QCD results. The results are shown in Fig. 6.2. We compare the pion decay constant f_π, the quark mass M_q and the meson masses M_σ and M_π at the IR scale $k=30\,\mathrm{MeV}$ for various initial scales Λ, at which we give over the QCD parameters to the QM model. We show the ratios

$$\Delta O = \left| 1 - \frac{O_{\mathrm{IR}}^{(\mathrm{QM})}}{O_{\mathrm{IR}}^{(\mathrm{QCD})}} \right| , \tag{6.3}$$

with $O \in \{f_\pi, M_q, M_\sigma, M_\pi\}$. This effectively measures the error we make by neglecting the gauge part.

We see that at initial scale $\Lambda \approx 600\,\mathrm{MeV}$ the error is larger than 10% for every observable. For the quark mass, it is even larger that 80%. The error we make for mesonic observable is less than 10% for $\Lambda \lesssim 550\,\mathrm{MeV}$. Since the quark mass, unlike the mesonic parameters, has a direct contribution from the gauge sector, it is much more sensitive to gluon fluctuations. Hence, neglecting these effects has a more severe effect on M_q than on the other observables. Only for initial scales $\Lambda \lesssim 320\,\mathrm{MeV}$ is the error in the quark mass less than 10%.

We note that for initial scales $\Lambda \lesssim 120\,\mathrm{MeV}$, the scale where gluon contributions to the flow of the Yukawa coupling can be neglected as discussed above, all errors here are below 0.1%. Thus, even though the impact of gauge fluctuations seems quantitatively important down to very low scales, the scale where they can be neglected without introducing a large error in physical observables is considerably higher.

Here, we found that the error of neglecting quark fluctuations is less than 10% in all observables considered here for initial scales $\Lambda \lesssim 320\,\mathrm{MeV}$ and for only the mesonic observables for $\Lambda \lesssim 550\,\mathrm{MeV}$. The latter is in a realistic range for physically sensible initial scales of QM-models. For the study of the phase structure, the initial scale should as a minimal requirement exceed the chiral transition scale $\Lambda > k_\chi$. Furthermore, it should also exceed the scale of the relevant thermal fluctuations of the system. The range of validity of the particular QM model studied here is dangerously low nonetheless. However, the typical procedure in low energy models is to fix the IR-physics by a fine-tuning of the initial parameters. This has the effect that some of the neglected fluctuations from the gauge sector are effectively taken into account and shifts the range of applicability of low-energy modes to larger cutoff scales. Our results show that a thorough analysis of this important issue should be done in the near future. It is important to quantify the range of validity of effective models in order to corroborate the reliability of such models.

Note that these findings do not render studies of QM-like models futile, since they certainly provide valuable informations about the relevant parameters in the hadronic sector of QCD.

6.2. Dynamical Hadronization and Low-Energy Effective Models

In low energy models of QCD, such as (Polyakov-loop enhanced) Nambu–Jona-Lasinio models or quark-meson models, gluons are considered to be integrated out and one is left with effective four-quark interactions, either explicitly or in a bosonized formulation. The latter is particularly convenient as the phase with spontaneous broken chiral symmetry is easily accessible. There, the formulation of the effective theory is usually based on the conventional Hubbard-Stratonovich bosonization rather than dynamical hadronization. Following our arguments given in Sect. 4.2.1, the question arises whether dynamical hadronization leads to quantitative and/or qualitative corrections in the context of low energy effective model.

Since the matter part of our truncation (5.3) is that of a quark-meson model, we will consider here the special case of the quark-meson model defined by switching off all gluon contributions in (5.3), i.e. we again consider the action (6.1). To see the effect of dynamical hadronization, we look at the ratios of IR observables obtained with and without dynamical hadronization. To this end, we choose $\Lambda_{\mathrm{LE}} = 1$ GeV as a typical UV-cutoff scale and use the same set of initial conditions in both cases. For results see Tab. 6.1.

$f_\pi/\tilde{f}_\pi$	$M_q/\tilde{M}_q$	$M_\pi/\tilde{M}_\pi$	$M_\sigma/\tilde{M}_\sigma$
0.995	0.997	1.003	0.990

Table 6.1.: Effect of dynamical hadronization on a quark-meson model: The quantities with/without a tilde are the results obtain from a solution of the flow equations of the quark-meson model with/without dynamical hadronization techniques.

We see that the effect of dynamical hadronization on physical observables of a low-energy quark-meson model (without gluons) is negligible, since it only gives corrections of less than 1%. This does not change if we vary the UV-cutoff within the range of typical values for this type of models, i.e $\Lambda_{\mathrm{LE}} \in [0.5, 1.5]$ GeV. Furthermore, it implies in particular that the mis-counting problem discussed in Sect. 4.2.1 is less severe in low energy models.

This observation can be understood by looking at the flow of the four-quark interaction $\lambda_{S,k}$,

see Eq. (4.49). In case of the quark-meson model, only the meson box diagrams $\sim \bar{h}_k^4$ contribute to the flow, see also Fig. 4.1, while the gluon box diagrams are neglected. In the chirally symmetric regime, the mesons are decoupled and the corresponding contributions to the flow are therefore suppressed. Furthermore, in the hadronic phase, the quarks acquire a large constituent mass and, in addition, the pions become light. Therefore, the contribution from dynamical hadronization to the flow of the Yukawa coupling (4.68), $\sim \bar{m}_{\pi,k}^2 \partial_t \bar{\lambda}_{S,k}$, is suppressed by these two effects in broken phase. Thus, following our present results, in particular Fig. 4.9, the only regime where dynamical hadronization can play a role in a low-energy model is in the vicinity of chiral symmetry breaking scale. However, since this region is small compared to range of scales considered even in low-energy models, only very small corrections related to the re-generation of four-quark interactions are accumulated from the RG flow.

Note, however, that we checked this statement only in vacuum and it might not be true in medium, especially at large chemical potential where quark fluctuations are enhanced. This can potentially lead to larger, non-negligible corrections from dynamical hadronization. We also emphasize that we used the same initial conditions for our comparison of the RG flow of the quark-meson model with and without dynamical hadronization techniques. However, usually the parameters of low-energy models are fixed in the vacuum, independent of the model truncation. Once the parameters are fixed, these models are then used to compute, e.g., the phase diagram of QCD at finite temperature and chemical potential. In this case, it may still very well be that the use of dynamical hadronization techniques yield significant corrections.

CHAPTER 7

The QCD Phase Diagram

The understanding of the formation and the properties of hadronic matter requires that of the phase structure of Quantum Chromodynamics (QCD). For fixed density the QCD vacuum changes drastically with decreasing temperature from a deconfined quark-gluon plasma phase with effective chiral symmetry to a hadronic phase with confined quarks and broken chiral symmetry.

The main challenge for theoretical studies of the QCD phase diagram lies in its non-perturbative nature, and the – related – dynamical change of relevant degrees of freedom. However, in the past decade rapid progress has been made in the first principle description of QCD at finite temperature and density, both with continuum methods, see e.g. [45, 140, 154, 155, 171, 172, 184], and on the lattice, see e.g. [67, 192–194]. Within the continuum approach it has been worked-out in detail how low energy effective models are systematically embedded in first principle QCD, see [44, 73, 74, 140, 155, 184, 195–197]. In the previous chapters we demonstrated in detail how the hadronic sector emerges from the underlying quark-gluon dynamics. It is a particular strength of such an approach that the necessary quantitative control over the matter and glue sector can be achieved separately, followed by a systematic combination of both sectors including their mutual back-reaction. We already demonstrated in the previous chapters that there is an intermediate range of scales, $300\,\mathrm{MeV} \lesssim k \lesssim 800\,\mathrm{MeV}$, where fluctuations from both, the hadronic and the quark-gluon sector have to be taken into account. This puts an even bigger emphasis on the systematic improvement of the corresponding low energy effective models of QCD. It not only furthers our understanding of the mechanisms underlying the physics phenomena responsible for the phase structure of QCD but also is necessary for quantitatively describing the phase structure within a first principle continuum approach.

For small chemical potential the lightest hadronic states, the pions and the sigma-meson, drive the chiral dynamics in the vicinity of the phase boundary. We demonstrated this explicitly in Chap. 5. Thus, in order to achieve quantitative control over the matter sector of QCD, and in particular the phase stucture, one has to accurately take into account the effects of mesonic fluctuations. The importance of such a procedure has been already observed in the context of higher order mesonic self-scatterings. These have been taken into account within low energy effective models in terms of full mesonic effective potential, for reviews see e.g. [75, 135, 142, 143]. We have shown in Sec. 3.4 that the fixed background Taylor expansion

is a well-suited method to study such effects, owing to its superior convergence properties for QM models. For a fully self-consistent expansion it is important to realize that quark–anti-quark multi-meson interactions have to be taken into account as well. Indeed, these terms contribute directly to the computation of the effective potential in the functional renormalization group approach.

Hence, we systematically also include higher order quark–anti-quark multi-meson interactions within the quark-meson model, and study their effect on the chiral phase structure of two-flavor QCD. In the QM model this amounts to a meson-field–dependent Yukawa coupling. The quantum, thermal, and density fluctuations are then taken into account by means of the FRG. This also allows us to consider the momentum-dependence of the propagators in terms of scale-dependent wave function renormalizations. Such effects are particularly relevant in the presence of massless excitations such as the pions close to a second order phase transition. The higher quark-meson interactions are included in a – convergent – Taylor expansion in the order of the mesonic fields. In total this leads to a significant extension of the local potential approximation of the quark meson model which has been used extensively to study the chiral phase transition of QCD, see e.g. [135, 142, 151].

We present results on the chiral phase boundary in the T-μ plane, including the critical endpoint and the curvature of the phase boundary. We also compare different definitions of the phase boundary. This is particularly important in the region of the phase diagram where the system undergoes a crossover transition and the exact location of the phase boundary is not uniquely defined. We find that the inclusion of the higher order couplings lead to quantitatively significant changes in the phase structure. An intriguing observation is the rapid convergence of our results if the orders of meson-meson and quark-meson couplings are increased.

Our present findings are fully in the spirit of the systematic embedding of the low energy effective models in first principle QCD. They constitute significants steps towards quantitative precision in terms of convergence of a self-consistent truncation for the matter sector of QCD.

This chapter is organized as follows: In Sec.7.1 we briefly introduce the quark-meson model in the context of full QCD, including the higher order quark-meson scattering processes in terms of an effective meson potential, a field-dependent Yukawa coupling and quark and meson wave function renormalizations. Sec. 7.2 summarizes the renormalization group approach and provides some details about the resulting flow equations of our model. Our results are presented in Sec. 7.3, where we demonstrate the convergence of our expansion scheme and discuss the chiral phase structure at finite temperature and quark chemical potential including the critical endpoint and the curvature at vanishing chemical potential.

7.1. Quark-Meson Model

In the present work we concentrate on two-flavor QCD by employing a quark-meson model as a low energy effective model for QCD. We now have a good understanding of how such low-energy effective models are embedded in first principle QCD within functional methods. The key concept behind this embedding in full QCD the the consistent treatment of the dynamical change of the relevant degrees of freedom. Starting from the high temperature/large cut-off scale quark-gluon phase, the system is dynamically driven towards the low temperature/small cut-off scale hadronic phase, where chiral symmetry breaking is triggered by the increasing gauge coupling. This transition from a description in terms of quarks and gluons to a hadronic description is achieved by dynamical hadronization. Furthermore, while the hadronic degrees of freedom get dynamical at the hadronization scale $\Lambda \approx 800\,\mathrm{MeV}$, the contributions from quark

and gluon degrees of freedom start to become less relevant. This is most simply seen in the Landau gauge, where the gluon propagator is infrared gapped, the gapping being directly related to the QCD mass gap, see e.g. [71, 124] and also our results in Sec. 4.4.3. Hence, the gluons can be integrated out first, leading to an effective theory with quarks and hadrons in a gluonic background potential, such as Polyakov-loop enhanced low-energy models. This setting entails that first-principle QCD flows can be employed to provide initial parameters and further glue input, such as background potentials, for model calculations, thereby systematically removing ambiguities in these approaches. In particular, no double counting of degrees of freedom is present in quark-meson models in this context, since the initial parameters of the low-energy theory are fixed by the first-principle QCD flows. This picture has successfully been applied to first-principle QCD [140, 155] as well as to low energy effective models [44, 196, 197], where quantitative agreement of QCD thermodynamics with lattice QCD is achieved [184]. However, we emphasize that our results of the precious chapter indicate that gauge fluctuations are quantitatively relevant down to scales $k \approx 320\,\text{MeV}$, especially for quantities related to the constituent quarks, as they have direct contributions from gluon fluctuations due to the strong coupling. One should therefore analyze this in more detail in the future.

Here, our focus is on the chiral dynamics of QCD at energy scales $k \leq 700\,\text{MeV}$ and we therefore neglect the gluonic background. In addition, dynamical hadronization is also not taken into account. We have demonstrated in Sec. 6.2 that the error we make by not using dynamical hadronization is well below 1%, at least in the vacuum.

7.1.1. Low Energy Effective Action

For an effective description of the low energy matter sector of QCD at not too high densities, a model based solely on quarks and the lightest meson is a good approximation. The ultraviolet cut-off scale Λ of such a description, as already mentioned above, relates to the scale where the pure glue sector of QCD starts to decouple and the fluctuations of the lightest mesons and constituent quarks dominate the dynamics. Here we consider $N_f = 2$ degenerate quark flavors with pseudo-scalar pions $\vec{\pi}$ and the scalar sigma meson as the dominant mesonic degrees of freedom for not too large chemical potential at $\Lambda \approx 1$ GeV. At this scale the low energy effective action Γ_Λ is approximated by that of the quark-meson model as in Sec. 4.1. Following the discussion there, the corresponding scale-dependent effective action reads, now at finite temperature and density (see Sec. 2.2),

$$\begin{aligned}\Gamma_k = \int_x \Big\{ & iZ_{q,k}(\rho)\bar{q}(\gamma_\mu\partial_\mu + \gamma_0\mu)q + h_k(\rho)\,\bar{q}(\gamma_5\vec{\tau}\vec{\pi} + i\sigma)q \\ & + \frac{1}{2}Z_{\phi,k}(\rho)(\partial_\mu\phi)^2 + V_k(\rho) - c\sigma\Big\}\,,\end{aligned} \tag{7.1}$$

with the meson fields in the $O(4)$ representation, $\phi = (\vec{\pi}, \sigma)$, and

$$\rho = \frac{1}{2}\phi^2 = \frac{1}{2}(\vec{\pi}^2 + \sigma^2)\,. \tag{7.2}$$

In (7.1) we used the abbreviation $\int_x = \int_0^{1/T} dx_0 \int d^3x$. The quark fields q are two flavor Dirac-spinors and μ is the quark chemical potential. For $N_f = 2$ the chiral symmetry $SU(N_f)_L \times SU(N_f)_R$ is isomorphic to $SO(4)$, hence the $O(4)$-symmetry of the scalar effective potential $V_k(\rho)$. Quarks and mesons are coupled via a meson field-dependent Yukawa coupling $h_k(\rho)$. $\vec{\tau}$ are the Pauli matrices.

This model captures spontaneous chiral symmetry breaking $SU(N_f)_L \otimes SU(N_f)_R \to SU(N_f)_V$. The expectation value of the sigma meson serves as order parameter for the chiral phase transition and the three pions are Goldstone bosons of the spontaneous breaking of the axial $SU(2)_A$. In the presence of explicit symmetry breaking, introduced by the linear breaking term $-c\sigma$, the pions are not massless but rather pseudo-Goldstone bosons with finite mass and the chiral second order transition turns into a crossover.

The inverse quark and meson propagators are dressed with wave function renormalizations $Z_{q,k}(\rho)$ and $Z_{\phi,k}(\rho)$. Note that at finite temperature there are in general two different wave function renormalizations quarks and mesons, one perpendicular, $Z = Z^{\perp}$, and one parallel to the heat bath, $Z^{\parallel}$. Here we only compute the perpendicular one and identify $Z^{\parallel} = Z^{\perp}$. Moreover, we expect a weak dependence of the Z's on the meson field ρ and hence we drop all terms proportional to $\partial_\rho Z(\rho)$. This approximation is discussed in section 7.2.3. The explicit breaking of $O(4)$-symmetry in the meson-sector of our model through the linear term $-c\sigma$ is related to a finite current quark mass m_q^c via the relation

$$m_q^c = \frac{h_\Lambda}{\nu_{1,\Lambda}} c \,, \tag{7.3}$$

where $\nu_{1,\Lambda}$ is the squared meson mass in the UV.

7.1.2. Higher Order Mesonic Scattering

The present approximation includes field-dependent wave function renormalizations $Z_k(\rho)$ for quarks and mesons, a full effective potential $V_k(\rho)$, and a field-dependent Yukawa-coupling $h_k(\rho)$. We implement higher order mesonic scattering processes via a systematic expansion in n-point functions $\Gamma^{(n)}$ of the effective action (7.1). This is discussed in detail in Sect. 3.4 and 4.1.1. Here, we just summarize the results there and discuss the implications of finite temperature and density. The latter implies in particular, that all parameters considered here are T and μ dependent, in addition to their RG-scale dependence.

We first discuss the wave function renormalizations. The ρ-dependence of the mesonic wave function renormalization contains momentum-dependent meson self-interactions while that of the quarks contains momentum-dependent scattering of a quark–anti-quark pair with mesons. Note that both processes vanish at vanishing momenta. The wave function renormalizations can be expanded about a temperature and chemical potential dependent expansion point $\kappa(T,\mu)$, to wit

$$Z_k(\rho) = \sum_{n=0}^{N_Z} \frac{Z_{n,k}}{n!} (\rho - \kappa(T,\mu))^n \,. \tag{7.4}$$

However, we expect a rather mild dependence of the wave function renormalization on the meson field, leading to

$$\partial_\rho Z_k(\rho) \approx 0 \,. \tag{7.5}$$

The quantitative reliability of this hypothesis is tested in Sec. 7.3.4, see in particular Fig. 7.11. Eq. (7.5) implies that locally (about a given expansion point κ) we can use

$$Z_k = Z_{0,k} \,. \tag{7.6}$$

Still, for the computation of observables the wave function renormalization has to be determined at the expectation value ρ_0 of the mesonic field which does not necessarily agree with the expansion point κ. It is here where the field dependence of the Z's play a role.

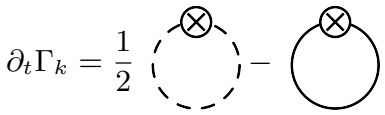

Figure 7.1.: Diagrammatic representation of the flow equation for the matter sector of QCD. The dashed line represents the full meson propagator, the solid line the full quark propagator and the crossed circle depicts the regulator insertion.

Meson self-interactions are contained in the renormalized effective potential $\bar{V}_k(\bar{\rho})$. As for the wave function renormalizations we expand the effective potential in powers of ρ about the renormalized expansion point $\bar{\kappa}_k(T,\mu)$, to wit

$$\bar{V}_k(\bar{\rho}) = \sum_{n=1}^{N_V} \frac{\bar{\nu}_{n,k}}{n!}\left(\bar{\rho}-\bar{\kappa}\right)^n . \tag{7.7}$$

In (7.7) we have dropped all T,μ-dependence for the sake of brevity. Eq. (7.7) captures a chiral crossover and a second order transition for $N_V \geq 2$. A first order transition requires at least $N_V \geq 3$. The effect of higher order mesonic self-interactions on the matter sector of QCD can be systematically studied by increasing the order of the expansion N_V.

Quark–multi-meson interactions are taken into account in (7.1) by the coupling of two quarks and a meson with a ρ-dependent Yukawa coupling $h_k(\rho)$. Analogous to the effective potential, we also expand the Yukawa coupling in a $O(4)$-symmetric manner in powers of $(\bar{\rho}-\bar{\kappa})$,

$$\bar{h}_k(\bar{\rho}) = \sum_{n=0}^{N_h} \frac{\bar{h}_{n,k}}{n!}\left(\bar{\rho}-\bar{\kappa}\right)^n . \tag{7.8}$$

$N_h = 0$ amounts to the standard Yukawa interaction which couples a quark–anti-quark pair and a meson. By increasing N_h the interaction between a quark–anti-quark pair and $(2N_h+1)$ mesons can be taken into account.

The convergence of these expansions implies that the higher order couplings get increasingly irrelevant with increasing order of the meson field, see section 7.3.2.

7.2. RG Flows

We include quantum, thermal and density fluctuations with the FRG. The evolution of Γ_k is governed by the Wetterich equation [130]. For the quark-meson model it reads,

$$\partial_t \Gamma_k[\phi,q,\bar{q}] = \frac{1}{2}\mathrm{Tr}\left[\left(\Gamma_k^{(2)}[\phi,q,\bar{q}]+R_k\right)^{-1}_{\phi\phi}\partial_t R_k^{\phi}\right] - \mathrm{Tr}\left[\left(\Gamma_k^{(2)}[\phi,q,\bar{q}]+R_k\right)^{-1}_{q\bar{q}}\partial_t R_k^{q}\right]. \tag{7.9}$$

The traces sum over the corresponding discrete and continuous indices including momenta and species of fields. $\Gamma_k^{(2)}[\phi,q,\bar{q}]$ is the matrix of second functional derivatives of Γ_k with respect to the fields. The indices $\phi\phi$ and $q\bar{q}$ indicate the components in field space. In this notation the regulator R_k is also a matrix in field space, where R_k^{ϕ} and R_k^{q} are the entries corresponding to the meson and quark regulators respectively. The flow equation has a simple diagrammatic representation, see Fig. 7.1.

The specific regulators used in the present work are three-dimensional optimized regulators and are specified in (C.55). This is a suitable choice for finite temperature, since Lorentz

symmetry is broken explicitly anyway in a heat bath. As we have discussed in Sec. 2.2, the momentum integration in imaginary time direction is replaced by a sum over Matsubara frequencies. As it turns out, this sum is always finite and thus regularization is not necessary for the thermal direction.

On the one hand such an approximation to the full QCD-flow is only satisfactory in the low energy regime of QCD at scales $k \lesssim 1$ GeV and k should be chosen as small as possible. On the other hand the initial cut-off scale Λ has to be far bigger than any other physical scale under investigation, i.e. T, μ and the physical masses. In the present work we shall adopt $\Lambda = 700\,\text{MeV}$. Note that Λ receives a physical meaning in this context since it is directly related to the scale where hadrons form.

It is left to project the flow equation (7.9) for the effective action on the scale- and field-dependent parameters of the effective action defined in (7.1):

7.2.1. Effective Potential

The flow equation of the effective potential $V_k(\rho) - c\sigma$ is obtained by evaluating (7.9) for constant meson fields, $\phi(x) \to \phi$, and vanishing quark fields. For these field configurations the effective action reduces to $\Gamma_k = \text{Vol}_4^{-1}\left(\bar{V}_k(\bar{\rho}) - \bar{c}_k\bar{\sigma}\right)$, see (7.1). Note that the explicit symmetry breaking term is linear in the meson field, and hence is nothing but a source term. The right hand side of the flow equation (7.9) only involves second derivatives w.r.t. the fields. Thus, the explicit symmetry breaking term does not appear on the right hand side of the flow equation, which only depends on symmetric terms. Moreover the flow equation (7.9) is derived with cut-off–independent source terms, which implies $\partial_t c = 0$. For the renormalized source, this leads to

$$\partial_t \bar{c}_k = \frac{1}{2}\eta_{\phi,k}\,\bar{c}_k\,, \tag{7.10}$$

with the (perpendicular) meson anomalous dimension

$$\eta_{\phi,k} = -\frac{\partial_t Z_{\phi,k}}{Z_{\phi,k}}\,. \tag{7.11}$$

This has the remarkable consequence, that in terms of fluctuations the theory is effectively evaluated in the chiral limit. Hence, this also applies to the effective potential V_k. The explicit $O(4)$ symmetry breaking introduced via the linear term $c\,\sigma$ simply entails that the vacuum expectation value of the fields is shifted relative to that in the chiral limit. In other words, the physical observables that can be derived from V_k and its derivatives are evaluated away from the minimum of V_k. Note also in this context that we could choose any k-dependence for c, only the value at $k = 0$ is fixed by the physical quark masses. The flow for $\bar{V}_k(\bar{\rho}) = V_k(\rho)$ reads

$$\begin{aligned}\partial_t|_\rho\,\bar{V}_k(\bar{\rho}) = \frac{k^4}{4\pi^2}\Big\{&\Big[(N_f^2-1)\,l_0^{(B,4)}(\bar{m}^2_{\pi,k},\eta_{\phi,k};T) + l_0^{(B,4)}(\bar{m}^2_{\sigma,k},\eta_{\phi,k};T)\Big]\\ &- 4N_cN_f\,l_0^{(F,4)}(\bar{m}^2_{q,k},\eta_{q,k};T,\mu)\Big\}\,,\end{aligned} \tag{7.12}$$

with the (perpendicular) quark anomalous dimension,

$$\eta_{q,k} = -\frac{\partial_t Z_{q,k}}{Z_{q,k}}\,. \tag{7.13}$$

Eq. (7.12) is nothing but the flow equation $\partial_t V(\rho)$. The threshold functions $l_0^{B/F,4}$ are defined in App. C.4, and depend on the field-dependent dimensionless renormalized masses

$$\begin{aligned} \bar{m}^2_{\pi,k} &= \frac{\partial_{\bar{\rho}} \bar{V}_k}{k^2} \\ \bar{m}^2_{\sigma,k} &= \frac{\partial_{\bar{\rho}} \bar{V}_k + 2\rho\, \partial^2_{\bar{\rho}} \bar{V}_k}{k^2} \\ \bar{m}^2_{q,k} &= \frac{2\bar{h}_k(\bar{\rho})^2 \bar{\rho}}{k^2}\,. \end{aligned} \tag{7.14}$$

The first and second lines in (7.12) are the pion and the sigma meson contributions respectively. The third line in (7.12) is the quark contribution, where $2N_c N_f$ is the number of internal quark degrees of freedom. The additional factor -2 is generic for fermionic loops.

The flow of the renormalized couplings $\bar{v}_n$ is reads,

$$\partial^n_{\bar{\rho}}\, \partial_t|_\rho\, \bar{V}_k(\bar{\rho})\Big|_{\bar{\rho}=\bar{\kappa}_k} = \left(\partial_t - n\,\eta_{\phi,k}\right) \bar{v}_{n,k}\,. \tag{7.15}$$

We have computed the scale derivative at fixed ρ as we want to connect (7.15) to (7.12): the left hand side of (7.15) is the nth derivative w.r.t. $\bar{\rho}$ of the flow equation (7.12). The equations (7.15) with (7.12) provide a tower of coupled differential equations for higher order mesonic correlators and therefore include meson-meson scattering up to order $2N_V$ into our model.

We close this Section with a discussion of possible order parameters. For a large region of the phase diagram the chiral transition is a cross-over. This only allows for the definition of a pseudo-critical temperature which is not unique. All possible definitions of pseudo order parameters have the property that they provide order parameters in the chiral limit where the cross-over turns into a second order phase transition. Here we discuss several order parameters. The variance of the pseudo-critical temperatures provide a measure for the width of the cross-over.

A simple order parameter of the chiral transition (in the chiral limit) is given by the vacuum expectation value $\bar{\sigma}_{0,k}$ at vanishing cut-off. It also determines the pion decay constant, $f_\pi = \bar{\sigma}_{0,k=0}$. The expectation value $\bar{\sigma}_{0,k}$ is obtained from

$$\partial_{\bar{\rho}} \left[\bar{V}_k(\bar{\rho}) - \bar{c}_k \bar{\sigma}\right]\Big|_{\bar{\rho}=\bar{\rho}_{0,k}} = 0, \tag{7.16}$$

where $\bar{\rho}_{0,k} = \frac{1}{2}\bar{\sigma}^2_{0,k}$ is the quadratic order parameter. Physical observables such as the pion decay constant and the masses are then defined at vanishing cut-off scale $k = 0$ and $\bar{\rho} = \bar{\rho}_{0,\mathrm{IR}}$.

The position of the peak of the chiral susceptibility is an alternative definition of the phase transition temperature. The chiral susceptibility measures the strength of chiral fluctuations. Hence it is, independent of its use for constructing an order parameter, an interesting observable. It is defined as the response of the chiral condensate $\langle \bar{q}q \rangle$ to variations of the current quark mass m_q^c,

$$\chi_{\bar{q}q} = \frac{\partial \langle \bar{q}q \rangle}{\partial \bar{m}_q^c}. \tag{7.17}$$

Within our model the scale dependent chiral condensate is given by [198, 199]

$$\langle \bar{q}q \rangle_k = -\frac{1}{h_\Lambda}\left(v_{1,\Lambda}\sigma_{0,k} - c\right). \tag{7.18}$$

The current quark mass is given by (7.3). Combining (7.18) and (7.3) yields the following relation:

$$\frac{\partial \sigma_{0,\mathrm{IR}}}{\partial c} = -\frac{h_\Lambda^2}{v_{1,\Lambda}^2}\chi_{\bar{q}q} + \frac{1}{v_{1,\Lambda}}. \tag{7.19}$$

Note that for (7.18) to hold with high accuracy, we need to require that the expansion point κ is very close to the physical point $\rho_{0,k}$. This is indeed the case for our choice of the expansion point, see (7.36).

We can rewrite (7.19) by virtue of the implicit function theorem since the relation between $\sigma_{0,k}$ and c is implicitly given by (7.16). This yields:

$$\frac{\partial \sigma_{0,k}}{\partial c} = \left(V_k'(\rho_{0,k}) + 2\rho_{0,k}V_k''(\rho_{0,k})\right)^{-1} = \frac{1}{m_{\sigma,k}^2}. \tag{7.20}$$

Thus, in practice we can compute the sigma meson mass and readily extract the chiral susceptibility for given initial parameters $v_{1,\Lambda}$, h_Λ.

7.2.2. Yukawa Coupling

The scalar part of the Yukawa-term has been introduced in (7.1) as a ϕ-dependent fermionic mass term with mass $h(\rho)\sigma$. This definition also entails that at leading order in ρ the sigma field has been introduced as a field for the composite operator $\bar{q}q$. Accordingly we evaluate the flow of the fermionic two-point function at the minimal fermionic momentum p_{low} and constant mesonic fields, leading to

$$\partial_t h_k(\rho) = -\frac{1}{\sigma}\frac{1}{4N_c N_f}\mathrm{Re}\left[i\lim_{p\to p_{\mathrm{low}}}\mathrm{Tr}\left(\frac{\delta^2\partial_t\Gamma_k}{\delta q(-p)\delta\bar{q}(p)}\right)\Big|_{\rho(x)=\rho}\right], \tag{7.21}$$

where the trace in (7.21) sums over all internal indices. Note that (7.21) is well-defined even in the limit $\sigma \to 0$. The diagrammatic representation of this equation is depicted in Fig. 7.2.

In (7.21) we have set the external spatial momenta to zero and the external Matsubara frequencies to their lowest mode, $p_{\mathrm{low}} = (\pi T, \vec{0})$ for quarks. Implicitly we also use $p_{\mathrm{low}} = (0, \vec{0})$ for mesons as we evaluate the Yukawa coupling for constant mesonic fields. For finite quark chemical potential this procedure yields a manifestly complex valued flow on the right hand side of (7.21). This simply reflects the dependence of the two-point function on $p_0 - i\mu$ and hence the momentum-dependence of the Yukawa coupling h: Evaluated at constant mesonic fields the Yukawa coupling is a function of ρ, $(p_0 - i\mu)^2$, $\vec{p}^2$ and μ with real expansion coefficients: $h(p_0 - i\mu)^* = h(p_0 + i\mu)$. Hence, any projection procedure has to reflect the property that

$$h(p_0 - i\mu) + h(-p_0 - i\mu) \in \mathbb{R}, \tag{7.22}$$

where we have also used that the Yukawa coupling h is a function of $(p_0 - i\mu)^2$. Eq. (7.22) has to hold in any self-consistent approximation scheme. In the present derivative expansion the Yukawa coupling is evaluated at a fixed frequency. This means that the Yukawa coupling in the derivative expansion has to be chosen real, $h(p_0 - i\mu) = h(-p_0 - i\mu)$. Within the flow this can be achieved via an appropriate choice of the expansion point. This singles out vanishing frequency $p_0 = 0$, where (7.22) holds trivially.

More generally one can project the flow of the Yukawa coupling on its real part. The former projection procedure at vanishing frequency has been used in the literature, for a detailed

$$\partial_t h_k = \frac{-i}{4N_c N_f \sigma}$$

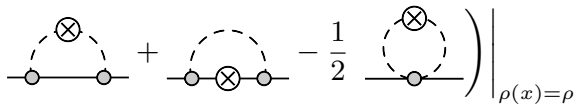

$$\Big|_{\rho(x)=\rho}$$

Figure 7.2.: Diagrammatic representation of the flow of the Yukawa coupling. The grey circles depict the full vertices.

discussion and motivation of this approach see [154]. However, the latter procedure keeps the Matsubara mass-gap of the fermions, which also is potentially relevant for capturing the quantitative physics close to the Fermi surface of the quarks at higher density. Hence, in the present work we project on the real part of the flow in (7.21) for the computation of the Yukawa coupling. We have checked numerically that both procedures agree quantitatively for small chemical potential.

The projection (7.21) using the fermionic two-point function is directly related to the more customary projection where an additional derivative with respect to the pion fields is applied, see (4.46).

With (7.21) we find for the flow of the renormalized Yukawa coupling:

$$\begin{aligned}
\partial_t|_\rho\, \bar{h}_k(\bar{\rho}) = &\Big(\frac{1}{2}\eta_{\phi,k} + \eta_{q,k}\Big)\bar{h}_k(\bar{\rho}) \\
&+ 4v_3\bar{h}_k^3(\bar{\rho})\Big[L^{(4)}_{(1,1)}\Big(\bar{m}^2_{q,k}, \bar{m}^2_{\sigma,k}, \eta_{q,k}, \eta_{\phi,k}; T, \mu\Big) \\
&-(N_f^2-1)\, L^{(4)}_{(1,1)}\Big(\bar{m}^2_{q,k}, \bar{m}^2_{\pi,k}, \eta_{q,k}, \eta_{\phi,k}; T, \mu\Big)\Big] \\
&+ 16v_3\bar{h}_k(\bar{\rho})\bar{h}_k'(\bar{\rho})\bar{\rho}\Big[\bar{h}_k(\bar{\rho}) + \bar{\rho}\bar{h}_k'(\bar{\rho})\Big]L^{(4)}_{(1,1)}\Big(\bar{m}^2_{q,k}, \bar{m}^2_{\sigma,k}, \eta_{q,k}, \eta_{\phi,k}; T, \mu\Big) \\
&- 2v_3k^2\Big[\big(3\bar{h}_k'(\bar{\rho}) + 2\bar{\rho}\bar{h}_k''(\bar{\rho})\big)\, l_1^{(B,4)}(\bar{m}^2_{\sigma,k}, \eta_{\phi,k}; T) + 3\bar{h}_k'(\bar{\rho})\, l_1^{(B,4)}(\bar{m}^2_{\pi,k}, \eta_{\phi,k}; T)\Big].
\end{aligned} \tag{7.23}$$

The function $L^{(4)}_{(1,1)}$ is defined in App. C.4. We note that the terms proportional to $\bar{h}_k^3$ in eq. (7.23) are the triangle-diagram contributions to the flow of a field-independent Yukawa coupling, see e.g. [154]. The flow of the renormalized couplings is

$$\partial^n_{\bar{\rho}}\, \partial_t|_\rho\, \bar{h}_k(\bar{\rho})\Big|_{\bar{\rho}=\bar{\kappa}_k} = (\partial_t - n\,\eta_{\phi,k})\bar{h}_{n,k}\,, \tag{7.24}$$

where $\partial_t \bar{h}_k(\bar{\rho})$ is given by eq. (7.23).

7.2.3. Wave Function Renormalizations

As discussed at the end of Section 7.1.1, at finite temperature the wave function renormalizations perpendicular and parallel to the heat bath differ from each other, $Z_k^\perp \neq Z_k^\parallel$. For scales above the chiral symmetry breaking scale, $k > k_{\chi\mathrm{SB}}$, we have $T/k < 1$ which implies that thermal fluctuations are negligible and thus $Z^\perp_{k>k_{\chi\mathrm{SB}}} \approx Z^\parallel_{k>k_{\chi\mathrm{SB}}}$. In the infrared we have $k \ll T$. In this regime dimensional reduction occurs and we approach the three-dimensional limit. There the finite temperature RG flow is only driven by the lowest Matsubara modes. The lowest Matsubara mode for bosons is zero and therefore $Z^\parallel_{\phi,k\ll T}$ drops out. For fermions the lowest Matsubara mode is proportional to T and thus the fermions with dynamically generated mass effectively decouple from the flow in the infrared. Therefore we choose the approximation

$$\eta_{q,k} = \frac{-1}{8N_f N_c Z_{q,k}} \frac{\partial^2}{\partial |\vec{p}|^2} \mathrm{Tr}\, \vec{\not{p}} \Bigg(\quad + \quad \Bigg) \Bigg|_{\kappa(T,\mu)}$$

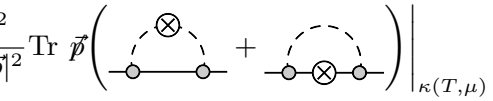

Figure 7.3.: Diagrammatic representation of the quark anomalous dimension.

$$\eta^{\perp}_{\phi,k} = \frac{-1}{2Z_{\phi,k}} \frac{\partial^2}{\partial |\vec{p}|^2} \Bigg(\quad - 2 \quad \Bigg) \Bigg|_{\kappa(T,\mu)}$$

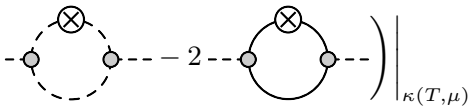

Figure 7.4.: Diagrammatic representation of the meson anomalous dimension.

$Z_k = Z_k^{\perp} = Z_k^{\parallel}$, which is approximately valid for large scales and hardly affects the RG flow in the infrared. Hence it should be a good approximation for calculating the chiral phase boundary.

The flow of (7.6) consistent with the expansion scheme about $\rho = \kappa$ has to involve an evaluation of the two-point function at the expansion point. As the momentum dependence is covered in a coarse-grained form via the k-dependence of the Z_k's, we also use the derivative expansion about the lowest momentum and frequency and arrive at

$$\eta_{q,k} = -\frac{1}{8N_f N_c Z_{q,k}} \mathrm{Re} \left[\lim_{p \to p_{\mathrm{low}}} \frac{\partial^2}{\partial |\vec{p}|^2} \mathrm{Tr} \left(\vec{\gamma}\vec{p}\, \frac{\delta^2 \partial_t \Gamma_k}{\delta q(-p) \delta \bar{q}(p)} \right) \Bigg|_{\rho=\kappa} \right], \tag{7.25}$$

for the quark anomalous dimension. We note that, analogous to the computation of the Yukawa coupling, the projection onto external momentum p_{low} also renders the flow on the right hand side complex valued. Similarly to the Yukawa coupling, the anomalous dimension is a function of the complex variable $(p_0 - i\mu)$, and projecting onto the real part keeps all properties and symmetries intact. This leads to

$$\begin{aligned} \eta_{q,k} = & \frac{2v_3}{3} \left(4 - \eta_{\phi,k}\right) \Big[(N_f^2 - 1)\, \bar{h}_k(\bar{\kappa}_k)^2 \mathscr{F}\mathscr{B}_{(1,2)} \left(\bar{m}^2_{q,k}, \bar{m}^2_{\pi,k}; T, \mu \right) \\ & + \left(\bar{h}_k(\bar{\kappa}_k) + 2\bar{\kappa}_k \bar{h}'_k(\bar{\kappa}_k) \right)^2 \mathscr{F}\mathscr{B}_{(1,2)} \left(\bar{m}^2_{q,k}, \bar{m}^2_{\sigma,k}; T, \mu \right) \Big]. \end{aligned} \tag{7.26}$$

The function $\mathscr{F}\mathscr{B}^{(4)}_{(1,2)}$ is defined in App. C.4. In the case of one quark flavor and for $\bar{h}'_k = 0$ this equation agrees with that found in [200]. The diagrammatic representation of equation (7.26) is shown in Fig. 7.3.

The anomalous dimension of the mesons can be either extracted by taking derivatives w.r.t. σ or π. Here, a similar argument as for the flow of the Yukawa coupling applies and we choose the following projection:

$$\eta_{\phi,k} = -\frac{1}{2Z_{\phi,k}} \lim_{p \to p_{\mathrm{low}}} \frac{\partial^2}{\partial |\vec{p}|^2} \mathrm{Tr} \left(\frac{\delta^2 \partial_t \Gamma_k}{\delta \pi_i(-p) \delta \pi_i(p)} \right) \Bigg|_{\rho=\kappa(T,\mu)}, \tag{7.27}$$

where the choice of $i = 1, 2, 3$ does not matter since the pions always have $O(3)$ symmetry in this representation. This leads to

$$\begin{aligned} \eta_{\phi,k} = & \frac{8v_3}{3} \Big\{ 2k^{-2} \bar{\kappa}_k \left(\bar{V}''_k(\bar{\kappa}_k) \right)^2 \mathscr{B}\mathscr{B}_{(2,2)} \left(\bar{m}^2_{\pi,k}, \bar{m}^2_{\sigma,k}; T, \mu \right) \\ & + N_f N_c \bar{h}_k(\bar{\kappa}_k)^2 \Big[\left(2\eta_{q,k} - 3 \right) \mathscr{F}_{(2)}(\bar{m}^2_{q,k}; T, \mu) - 4 \left(\eta_{q,k} - 2 \right) \mathscr{F}_{(3)}(\bar{m}^2_{q,k}; T, \mu) \Big] \Big\}. \end{aligned} \tag{7.28}$$

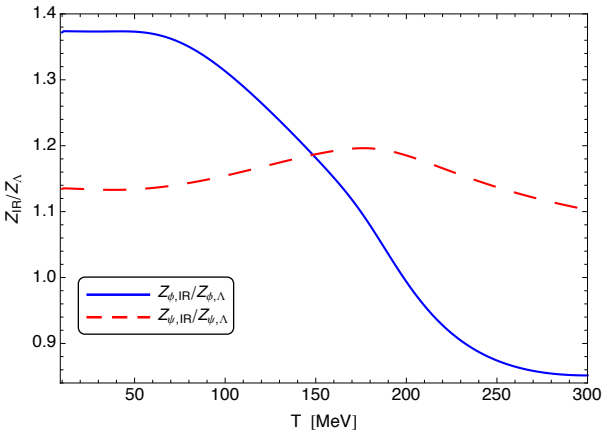

Figure 7.5.: Temperature dependence of the wave function renormalizations in the IR, normalized to their values in the UV.

The functions $\mathscr{B}\mathscr{B}^{(4)}_{(2,2)}$ and $\mathscr{F}^{(4)}_{(n)}$ are defined in App. C.4. This equation also agrees with [200] for one quark flavor. We note that the results shown here are obtained using the optimized regulator shape functions (C.56). The diagrammatic representation of (7.28) is shown in Fig. 7.4.

We want to emphasize again that the wave function renormalizations are defined as the zeroth order of an expansion about $\bar{\kappa}$. From (7.26) and (7.28) it is clear that we can define the wave function renormalizations at any expansion point. Defining them at $\bar{\kappa}_k$ is the consistent way to define the renormalized couplings related to the Yukawa coupling and the effective potential since these couplings are defined at $\bar{\kappa}_k$ as well. For the definition of the physical parameters, e.g. the masses, however, we make use of the option to freely choose the expansion point and evaluate the wave function renormalizations at the minimum $\bar{\rho}_{0,k}$, see Sec.7.3.4.

The wave function renormalizations as a function of temperature are shown in Fig. 7.5. At about the critical temperature $Z_{q,\mathrm{IR}}$ exhibits a peak and $Z_{\phi,\mathrm{IR}}$ shows a tiny kink. This kink gets more pronounced and turns into a dip for smaller pion masses and ends up as a non-analyticity in the chiral limit [199]. An interesting observation is that the meson wave function renormalization falls below its initial value in the UV for temperatures above 200 MeV. This feature is independent of the choice of the UV value and shows that mesonic degrees of freedom become less important for larger temperatures in the crossover region and vanish in the symmetric phase. The inclusion of a dynamical meson wave function renormalization therefore leads to a consistent picture of the QCD matter sector in the sense that mesons are only present in the phase with broken chiral symmetry, while they vanish (or rather turn into auxiliary fields) in the symmetric phase where quarks and gluons are the relevant degrees of freedom. Note that this is analogue to our previous discussions in Sects. 4.4.4 and 5.3.3, but at finite temperature.

7.2.4. Convexity for $\rho < \rho_0$ & Behavior for Large Fields

The flows are initiated at a UV cut-off scale $k = \Lambda$. There, the initial effective action Γ_Λ resembles the classical Yukawa theory with a ϕ^4-potential and a constant Yukawa coupling. This entails

that all flows decay in the limit where $\rho/k^2 \to \infty$, and we conclude

$$\partial_t \bar{h}_k(\bar{\rho}/k^2 \to \infty) = 0 \quad \text{and} \quad \partial_t \bar{V}_k(\bar{\rho}/k^2 \to \infty) = 0\,. \tag{7.29}$$

Hence, neither the Yukawa coupling nor the effective potential are changed during the flow for large enough fields.

For the convexity discussion it is sufficient to restrict ourselves to the chiral limit. As already mentioned before, the explicit symmetry breaking does not influence the dynamics of the fluctuations which are solely responsible for the convexity properties. It is well-known that the effective potential $V_{k=0}$ is convex by construction. It has been shown that the flow equation is indeed convexity-restoring in the limit $k \to 0$ and keeps this property in the local potential approximation, see [201]. This implies in particular, that the the curvature of the effective potential vanishes for field values smaller than their vacuum expectation value, $\partial_\phi^2 V_{k=0}(\rho < \rho_0) = 0$. For non-vanishing cut-off scale, $k > 0$, only the combination $V_k(\rho) + \rho\, R_k^\phi(0)$ is convex. This property follows directly from its definition as the Legendre transformation of the logarithm of the generating functional $\ln Z_k[J]$, evaluated on constant fields and divided by the space-time volume, for a detailed discussion see e.g. [139]. This entails in particular

$$V_k'(\rho) + R_k^\phi(0) \geq 0\,, \quad V_k'(\rho) + 2\rho V''(\rho) + R_k^\phi(0) \geq 0\,, \tag{7.30}$$

for the inverse propagator pion and σ-meson propagator respectively at vanishing momentum. In the chirally broken phase with $\rho < \rho_{0,k}$ we have

$$V_k'(\rho < \rho_{0,k}) < 0 \quad \text{and} \quad V_{k=0}'(\rho < \rho_0) = 0\,, \tag{7.31}$$

with ρ_0 is the vacuum expectation value $\rho_{0,k}$ at vanishing cut-off scale, $k = 0$. Note that (7.31) also implies $V_{k=0}''(\rho < \rho_0) = 0$. Of course, (7.31) entails that the potential V_0 is flat (vanishing curvature) for fields ρ smaller than the vacuum expectation value. Note that for negative V' the inverse pion propagator in (7.30) vanishes for $V' = R_k^\phi(0)$, and the flow potentially diverges for $R_k^\phi(0) \to 0$. However, this divergence is not reached as the increasing flow increases V', see [201] for a discussion of a scalar theory. In Appendix E this discussion is extended to the present Yukawa theory.

The relation between the negative curvature V' and the convexity-restoration in the flow also implies that only the mesonic fluctuations drive the flows for $\rho < \rho_0$ and $k \to 0$, and the two sectors effectively decouple. This facilitates the access to the infrared flow of the fermion propagator in this region studied in detail in Appendix E, which can indeed be derived analytically. We arrive in particular at

$$\bar{m}_q^2(\rho \leq \rho_0) = \sqrt{2\rho_0}\,\bar{h}(\rho_0, 0)\frac{\rho_0}{\rho}\,, \tag{7.32}$$

see (E.19) in Appendix E. In this appendix a momentum-dependent Yukawa coupling $h(\rho, p)$ has been introduced. In (E.18) it is evaluated at vanishing momentum, $h(\rho, 0)$. This leads to the inequality

$$\bar{m}_q^2(\rho) \geq \bar{m}_{q,\mathrm{gap}}^2\,, \quad \text{with} \quad \bar{m}_{q,\mathrm{gap}}^2 = \sqrt{2\rho_0}\,\bar{h}(\rho_0, 0)\,, \tag{7.33}$$

for $k = 0$, see (E.20) in Appendix E, where we have also used the fact that for $\rho > \rho_0$ the mass function grows. As a consequence of (7.33) the fermion propagation is gapped with at least the constitutent quark mass $\bar{m}_{q,\mathrm{gap}}^2$ for all fields. In other words, in the chirally broken phase

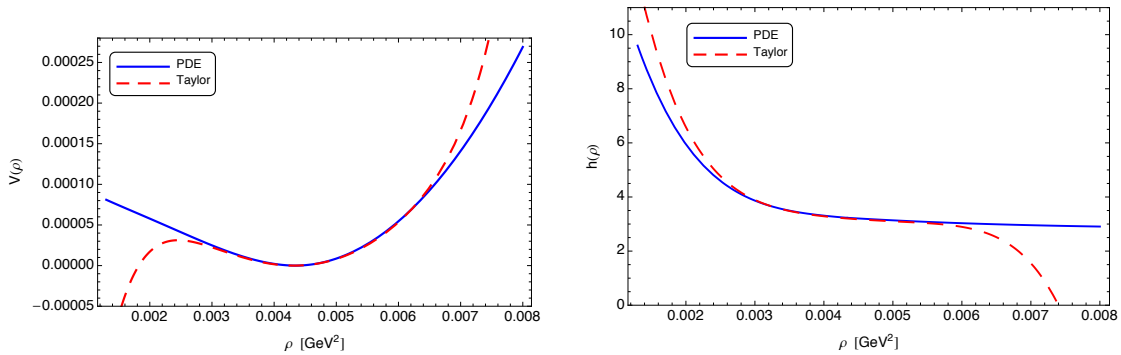

Figure 7.6.: Effective potential (left) and Yukawa coupling (right) at cut-off scale $k=0.1\,\mathrm{MeV}$ within the Taylor expansion and the full solution of the coupled partial differential flow equations for $\eta_{q,k}, \eta_{\phi,k}$, $V_k(\rho)$ and $h_k(\rho)$ at $T=10\,\mathrm{MeV}$ and $\mu=0$. For the Taylor expansion we used $N_V=7$ and $N_h=5$. Note that the results include the explicit $O(4)$ symmetry breaking via $-c\sigma$.

no mesonic background can turn the fermionic dispersion into a massless one. Note however, that $\rho<\rho_0$ is no physical choice in the first place.

We finally remark that the same line of argument can also be applied to full QCD and also holds there. There however, the fermionic mass tends towards the current quark masses for large meson fields ρ and the minimum in (7.33) has to be restricted to $\rho \lesssim \rho_0$. In the present model a linearly rising mass was built-in and strictly speaking one should not evaluate the model for $\rho/\Lambda^2 \gg 1$ in the first place. The full discussion of QCD is postponed to future work.

7.3. Numerical Results

7.3.1. Initial Conditions

It is left to specify the initial conditions for the relevant parameters $\lambda_{1,k}, \lambda_{2,k}, h_{0,k}$ and c_k at the UV-scale Λ for the system of coupled flow equations presented above. As we have mentioned in Sec. 7.1, the effective UV-cutoff scale Λ has a direct physical meaning in our setting. It is the scale where the dominant part of the gluonic degrees of freedom has been integrated out and hadronic degrees of freedom, especially the light mesons, form. There is a certain freedom in the choice of this scale as long as it is well above Λ_{QCD} and not too large so that fluctuations in the gauge sector dominate the dynamics.

As discussed in Section 3.2 we have chosen $\Lambda=700\,\mathrm{MeV}$. The relevant parameters of our model are fixed such that a specific set of vacuum low-energy observables is reproduced in the in the IR. These observables are the pion decay constant f_π, the renormalized sigma and pion masses M_σ, M_π and the constituent quark mass M_q of the degenerate up and down quarks. The explicit symmetry breaking is related to the pion decay constant and the pion mass via $\bar{c}_k = M_\pi^2 f_\pi$ and the relations of our parameters to the quark and mesons masses are shown in

(7.14). At a large scale Λ the model is quasi-classical and hence we choose

$$\begin{aligned} \bar{V}_\Lambda(\bar{\rho}) &= \frac{\bar{\lambda}}{2}(\bar{\rho}-\bar{\nu})^2 \\ \bar{h}_\Lambda(\bar{\rho}) &= \bar{h} = \text{const.} \end{aligned} \tag{7.34}$$

The underlying assumption is that at Λ the dynamics are controlled by the leading order processes, i.e. the four-meson and the quark-antiquark-meson scattering. The higher order couplings are generated at lower scales $k < \Lambda$. We indeed found that the higher order operators, i.e. $\bar{\nu}_{n,k}$ with $n \geq 3$ and $\bar{h}_{m,k}$ with $m \geq 1$ are generated at $k \lesssim 400\,\text{MeV}$, which is well below our choice for the UV-cutoff. Since the higher order operators are not present at our initial scale, the scale where they are generated is a prediction of our model.

In order to reproduce the vacuum IR-observables listed above we used the following initial values: $\bar{\lambda} = 71.6$, $\bar{\nu} = 0$, $\bar{h} = 3.6$, $\bar{c}_\Lambda = 2.1 \cdot 10^{-3}\,\text{GeV}^3$. These initial values result in the following values for the vacuum IR-observables,

$$\begin{aligned} f_\pi &= 93.0\,\text{MeV} \\ M_\pi &= 138.7\,\text{MeV} \\ M_\sigma &= 538.2\,\text{MeV} \\ M_q &= 298.3\,\text{MeV}, \end{aligned} \tag{7.35}$$

which are in good agreement with their values provided by the Particle Data Group [96]. We identify the σ meson with the scalar resonance $f_0(500)$ here. The initial values of the parameters for the present computations are chosen such that they reproduce the vacuum physics displayed in (7.35) for $T, \mu = 0$ and vanishing cut-off for the fully field-dependent effective potential $\bar{V}_k(\bar{\rho})$ and Yukawa coupling $\bar{h}_k(\bar{\rho})$, including running wave function renormalizations $Z_{\phi,k}$ and $Z_{q,k}$. With the convergence pattern discussed in the next section it is sufficient to use $N_V = 7$ and $N_h = 5$ in the expansions (7.7) and (7.8), and fix the initial parameters for these values.

The bare expansion point $\kappa(T,\mu)$ is chosen to be scale-independent. We take it close to the IR-minimum of the effective potential for every temperature and chemical potential:

$$\bar{\kappa}_{\text{IR}}(T,\mu) = (1+\epsilon)\,\bar{\rho}_{0,\text{IR}}(T,\mu), \tag{7.36}$$

where $\epsilon > 0$ gives a small offset that guarantees that $\bar{\kappa}(T,\mu)$ is always slightly larger than the minimum of the effective potential $\bar{\rho}_{0,k}$ and does not lie in the flat region of the convex effective potential $V_{k=0}$. It can be read-off from Fig. 7.11 that a quantitative agreement of the physics results is obtained for expansion points in the range

$$0 \leq \epsilon \lesssim 1\,. \tag{7.37}$$

This self-consistency check within the present expansion scheme is impressively sustained by the comparison with the full solution of the system of partial different equations for $V_k(\rho)$, $h_k(\rho)$, $\eta_{\phi,k}(\bar{\kappa})$ and $\eta_{q,k}(\bar{\kappa})$, see Fig. 7.6. The region where the results from the Taylor expansion and the full solution of the partial differential equation agree give an estimate for the radius of convergence of the Taylor expansion. This is in agreement with the study of the robustness of the expansion in Sec. 7.3.4 and in particular with Fig. 7.11.

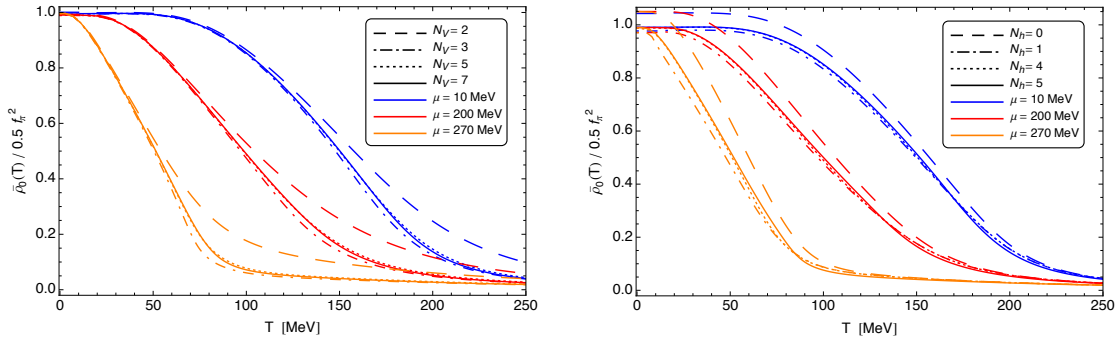

Figure 7.7.: The normalized chiral order parameter as a function of temperature for different orders in the expansion of the effective potential (left) and the Yukawa coupling (right).

7.3.2. The Impact of Higher Order Mesonic Interactions

The effect of higher order mesonic operators is studied within a Taylor expansion of the effective potential and the field dependent Yukawa coupling, see section 7.1.2. This is done by comparing the results of the chiral order parameter for different orders N_V and N_h in the expansions (7.7) and (7.8) of the effective potential and the field dependent Yukawa coupling. In Fig. 7.7 we show the effect of increasing N_V and N_h on the chiral order parameter $\bar{\rho}_{0,\mathrm{IR}}$ as function of temperature for three different chemical potentials.

First of all, we clearly see spontaneous chiral symmetry breaking. Owing to the explicit symmetry breaking, the chiral condensate is very small, but nonzero at large temperatures. By lowering the temperature, the fluctuations of the light current quarks drive the system continuously towards the broken phase. As the value of the chiral condensate increases, the quarks receive more and more constituent mass while the pions get lighter until quarks and mesons decouple at low temperatures where the flow stops and the system ends up in the stable phase with broken chiral symmetry. The quark and meson masses as a function of temperature at $\mu = 0$ are shown in Fig. 7.8. Note that the decreasing slope of the meson masses at temperatures $T \gtrsim 250\,\mathrm{MeV}$ is a result of thermal fluctuations which become of the order of the UV-cutoff Λ in this region. This is discussed in detail in [184].

With increasing quark chemical potential, quark fluctuations are enhanced and the crossover gets steeper while the transition moves towards smaller temperatures as a result of the higher quark density.

Note that since the transition is a cross-over the actual value of the critical temperature T_c depends on the the definition of the crossover. In this case it is only sensible to speak about a transition region. Therefore the full temperature and chemical potential dependence of the observables used to define the critical temperature plays a more important role than the specific critical values.

The left panel in Fig. 7.7 shows the chiral order parameter in the IR normalized to the pion decay constant for different orders $N_V = 2, 3, 5, 7$ of the expansion of the effective potential for $\mu = 10\,\mathrm{MeV}, 200\,\mathrm{MeV}, 270\,\mathrm{MeV}$ and a fixed order $N_h = 2$ in the expansion of the Yukawa coupling. Note that we chose N_h such that $N_h \leq N_V$ for numerical stability. While $\bar{\rho}_0(T)$ is hardly affected by different N_V in the broken phase at small temperatures, we see a large difference between the ϕ^4 and the ϕ^{14} expansion in the lower region of the crossover transition. This effect gets more pronounced for larger chemical potentials. There is a very good agreement

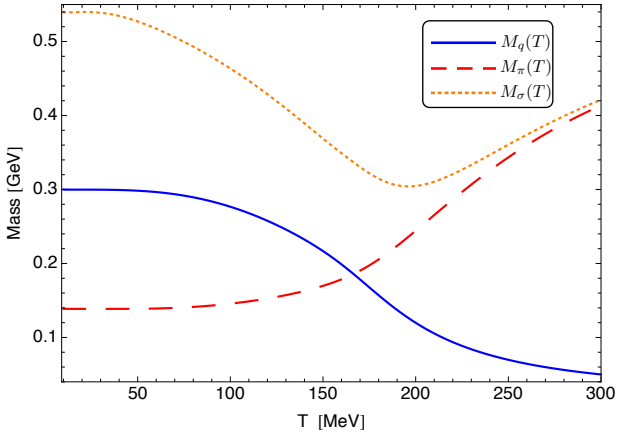

Figure 7.8.: Quark, pion and sigma mass as a function of Temperature for vanishing chemical potential.

between the order parameter for $N_V = 5$ and $N_V = 7$ which implies that the expansion of the effective potential at order $N_V = 5$ has converged to a precision of the critical temperature below 1 MeV. We explicitly checked that larger orders in the expansion do not spoil this observation. Note that the convergence pattern of $\bar{\rho}_0(T)$ is qualitatively the same as $\bar{\rho}_k(0)$ shown in Fig. 3.4.

The effect of the expansion of the field dependent Yukawa coupling on the chiral condensate is shown in the right panel of Fig. 7.7. The difference between the usual running Yukawa coupling $N_h = 0$ and the expansion of order $N_h = 5$ is at about 8% which results in a difference of 8—10 MeV in the critical temperature. The expansion of order $N_h = 4$ seems to be converged to a precision of the critical temperature below 1 MeV. We observed that larger chemical potential slows down the convergence of the Yukawa coupling. This behavior is expected since a larger chemical potential effectively increases quark fluctuations and thus the systems is more sensitive to the details of the quark-meson interactions.

We see that the particular meson-meson and quark-meson interactions we have chosen here have a large quantitative effect on the chiral order parameter. Moreover we nicely see that these higher order operators a become increasingly irrelevant with increasing order of the meson fields and that our expansion converges rapidly, especially for not too large chemical potential. This implies in particular that we have the full effective potential as well as the full field-dependent Yukawa coupling in this region. To demonstrate this, we solved the coupled partial differential flow equations of $V_k(\rho)$, $h_k(\rho)$, $\eta_{\phi,k}(\bar{\kappa}_k)$ and $\eta_{q,k}(\bar{\kappa}_k)$ and compared the result to the one obtained with the expansion employed in this work, see Fig. 7.6.

Note that, as expected, the couplings with negative mass dimension run into a Gaussian fixed point in the IR but certainly play a role at intermediate scales. Furthermore, it is obvious that a low-order expansion is not sufficient in order to obtain a high degree of quantitative precision.

7.3.3. Phase Diagram

Phase Structure

For the computation of the phase diagram, we expand the effective potential up to order $N_V = 7$ and the Yukawa coupling up to $N_h = 5$. According to the previous section, these orders guarantee that both expansions converged to a precision below 1 MeV, at least in the crossover region. The resulting phase diagram in the (T, μ)-plane is shown in Fig. 7.9. The crossover

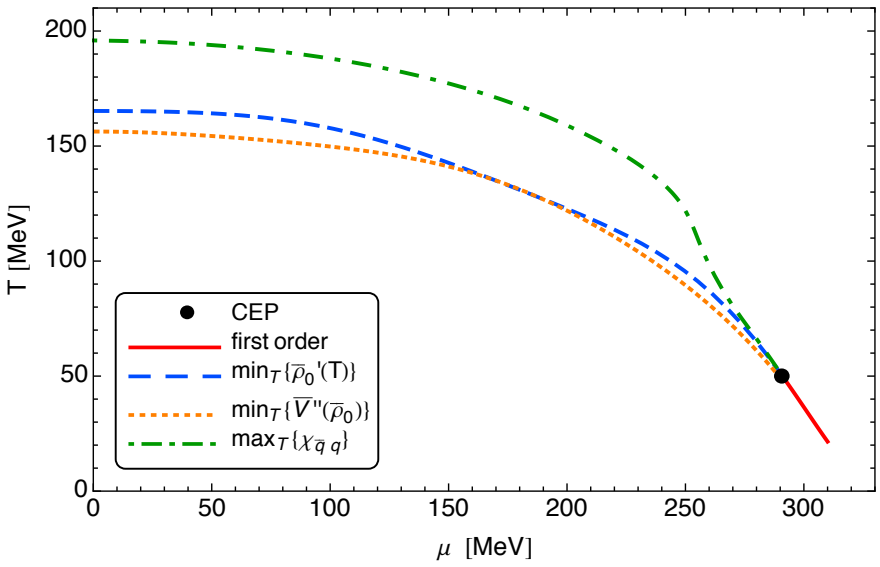

Figure 7.9.: The phase diagram of the chiral transition including the different definitions of the crossover transition line we used. We only show the first order transition up to $\mu = 310\,\mathrm{MeV}$ since our expansion is not fully converged for larger μ.

transition temperature is not uniquely defined and therefore depends on the observable used to define it. Basically any observable that exhibits a non-differentiable behavior at the critical temperature in the chiral limit, where the transition is of second order, can be used to define the crossover transition temperature. Here we use the following three definitions:

(i) The inflection point of the chiral order parameter as a function of temperature,

$$\min_T \left\{ \frac{\partial \bar{\rho}_{0,\mathrm{IR}}}{\partial T} \right\}. \tag{7.38}$$

(ii) The minimum of the quartic meson coupling at the physical point,

$$\min_T \left\{ \frac{\partial^2 \bar{V}_{\mathrm{IR}}(\bar{\rho})}{\partial \bar{\rho}^2}\bigg|_{\bar{\rho}=\bar{\rho}_{0,k}} \right\}. \tag{7.39}$$

(iii) The maximum of the chiral susceptibility (7.17),

$$\max_T \left\{ \chi_{\bar{q}q} \right\}. \tag{7.40}$$

The definition (i) is commonly used in RG-studies of the phase diagram, while susceptibilities as in (iii) are typically used in lattice gauge theory. The exact location and in particular the curvature of the phase boundary obviously depend on the definition of the crossover. Note, however, that all the definitions above exactly agree in the chiral limit.

We observe a large difference of about 40 MeV in the critical temperature at small and intermediate chemical potential between definitions (i) and (iii), while (i) and (ii) give similar phase boundaries. These differences are related to the fact that we have a very broad crossover

in this region and the notion of a phase transition line is certainly not well defined there. At large chemical potential close to the critical point the crossover lines merge and give a uniquely defined phase boundary. This behavior is expected since the crossover gets steeper towards the critical point and the first-order transition is uniquely defined. We find the critical endpoint at $(T_{\mathrm{CEP}}, \mu_{\mathrm{CEP}}) = (50, 291)\,\mathrm{MeV}$. The critical endpoint here is at substantially smaller temperatures as in mean-field studies, see e.g. [119]. This nicely demonstrates the effect of fluctuations on the phase boundary. The critical temperatures at vanishing chemical potential for the different definitions of the crossover transition are show in table 7.1. A further definition of a cross-over

boundary def.	$T_c\,[\mathrm{MeV}]$
(i)	166
(ii)	156
(iii)	196

Table 7.1.: Critical temperatures at vanishing quark chemical potential for the different definitions of the crossover phase boundary we used in this work (see text).

temperature in the literature is given by the temperature where the value of the normalized order parameter is half of that at vanishing temperature, $\rho_{0,\mathrm{IR}}(T,\mu)/\rho_{0,\mathrm{IR}}(0,0) = 0.5$. Here we only note that the critical temperature at $\mu = 0$ is $T_c = 152$ MeV and the transition line is systematically below the lines shown in Fig. 7.9. This behavior is in contrast to studies of the quark-meson model in the local potential approximation, where this phase boundary is always slightly above the boundary defined by (i), see e.g. [196].

The inclusion of running wave function renormalizations decreases the critical temperature. This is a consequence of a growing quark wave function renormalization in the symmetric phase close to the phase boundary. As we see from Fig. 7.5 bot, $Z_\phi(T)$ and $Z_q(T)$ grow in this region. In both cases, this leads to a decrease in the corresponding masses. While lighter mesons imply stronger symmetry-restoring bosonic fluctuations which lead to an increasing T_c, lighter quarks give stronger symmetry-breaking fermionic fluctuations, resulting in a steeper transition and smaller T_c. Since the quarks are the dominant degrees of freedom above T_c, the latter effect prevails and T_c decreases when running wave function renormalizations are taken into account. This is shown in Fig. 7.10.

In turn, the transition temperature is increased if a the running Yukawa coupling is taken into account. The flow of the Yukawa coupling is always positive and thus, h_k decreases towards the IR. This has the effect that the quarks are heavier at larger temperatures as compared to the case with constant Yukawa coupling. Consequently, T_c increases due to suppressed quark fluctuations. This is also shown in figure 7.10. Note that we used the initial conditions specified in 7.3.1. This ensures that for every truncation used in figure 7.10 we start with the same effective action at the initial scale Λ. This approach is motivated by the fact that in principle the initial conditions at Λ are uniquely defined by the solution of full QCD at scales $k \geq \Lambda$.

Curvature

In order to determine the curvature of the chiral phase boundary, we compute $T_c(\mu)/T_c(0)$ in a range $0 \leq \mu/(\pi T_c(0)) \lesssim 0.1$ and extract the curvature of the phase boundary at vanishing chemical potential from these results. At small chemical potential the phase boundary can be

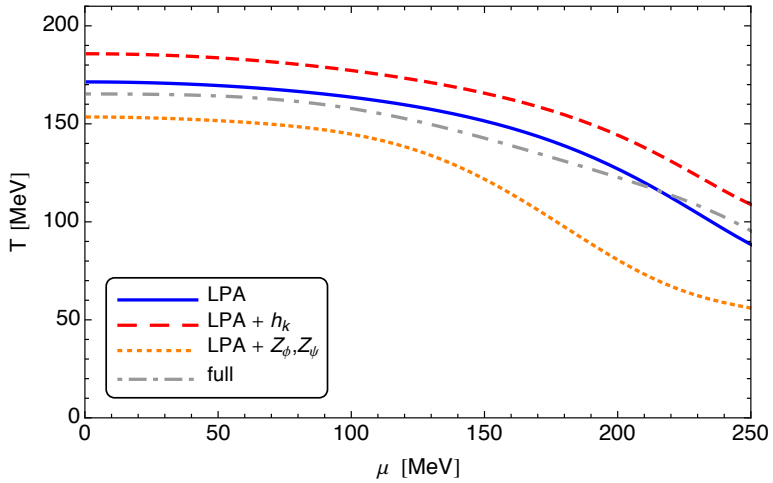

Figure 7.10.: Comparison of the phase boundary for different truncations of the quark-meson model. The solid blue line corresponds to the local potential approximation (LPA), i.e. a truncation with only a running effective potential. For the dashed red curve also a running (field-independent) Yukawa coupling was taken into account and for the dotted orange curve we have running quark and meson wave function renormalizations and the effective potential, but a constant Yukawa coupling. The dot-dashed gray curve shows the full result of our model. Here, we defined the crossover transition via definition (i), see text.

expanded in powers of μ^2 as follows:

$$\frac{T_c(\mu)}{T_c(0)} = 1 - \kappa_\mu \left(\frac{\mu}{\pi T_c(0)} \right)^2 + \mathcal{O}\left(\left(\frac{\mu}{\pi T_c(0)} \right)^4 \right). \tag{7.41}$$

The curvature κ_μ depends on the number of colors N_c, the number of quark flavors N_f and the current quark mass or the pion mass respectively, see e.g. [154]. But since all those parameters are fixed in the present work, we do not study the effect of variations of them. For a crossover transition the curvature depends on the definition of the phase boundary. For our result in comparison with lattice results and other RG calculations see table 7.2.

We extracted the curvature from a fit of the phase boundary according to (7.41) for $\mu \in [0, 20]$ MeV. The errors result from fits with polynomials of the order μ^2, μ^4, μ^6.

Compared to the curvature found in [203], the inclusion of higher order mesonic scattering processes and dressed quark and meson propagators does not change the curvature much. This is related to the observation that running wave function renormalizations and the running Yukawa coupling have opposing effects on the phase boundary, see also Fig. 7.10.

Owing to our findings in the previous section we certainly need to use the same definition of the phase boundary as in [202] in order to do a sensible comparison with the lattice results. But since they used the plaquette susceptibility for the definition of the critical temperature, a direct comparison is difficult since gluonic quantities are not directly accessible in our model. We therefore displayed the results for the curvature for different boundary definitions. We see that while the curvatures extracted from the chiral order parameter and the chiral susceptibility are very similar but much larger than the lattice results, the curvature from the quartic meson coupling is close the lattice result. We see that these results very much depend on the specific definition of the crossover temperature, in line with our findings in the previous section.

Method	Boundary def.	Mass	κ_μ
Lattice: $i\mu$ [202]	plaquette susc.	$am = 0.025$	0.500(54)
FRG: LPA [151]	$\min_T\{\rho_0'(T)\}$	chiral limit	1.135
FRG: LPA [203]	$\min_T\{\rho_0'(T)\}$	$m_\pi = 138$ MeV	1.375(63)
this work: LPA	$\max_T\{\chi_{\bar{q}q}\}$	$m_\pi = 138$ MeV	1.397(1)
this work: full model (7.1)	$\min_T\{\rho_0'(T)\}$	$m_\pi = 138$ MeV	1.397(2)
	$\max_T\{\chi_{\bar{q}q}\}$		1.418(13)
	$\min_T\{\bar{V}''(\bar{\rho}_0)\}$		0.794(1)

Table 7.2.: This table shows the curvature of the chiral phase boundary for $N_f = 2$ quark flavors obtained from various methods. am is the lattice spacing times the degenerate current quark mass. The last three rows correspond to the different boundary definitions we employed in this work.

We note that it was observed for QM-model studies that the curvature increases with increasing pion mass [203], which explains the difference between the curvature found in [151] and in [203], where very similar truncations were used but one in the chiral limit and the other at realistic pion masses. This is in contrast to the general expectation that the system gets less sensitive to the chemical potential for larger current quark mass.

7.3.4. Background Dependence

Here we analyze the stability of the fixed background expansion in the present case. As a byproduct, we can extract informations about the field dependence of the wave function renormalizations.

Instead of doing an expansion about the scale-dependent minimum of the effective potential $\rho_{0,k}$, we expand the non-renormalized theory about a scale-independent field configuration κ. Technically, the advantage is that there is no unnecessary feedback from the expansion point into the flow of higher order operators. In an expansion about the minimum of the effective potential the flow of the minimum feeds back into the flow of every higher order operator, see the discussion below (7.15). This feedback slows down numerical computations and potentially leads to numerical instabilities. But even though the minimum certainly is a distinct point in the effective potential, it is by no means distinct in the flow of the effective potential. The same holds true for the flow of the effective action in general. In principle it is therefore irrelevant whether one solves the flow equations with an expansion about $\bar{\rho}_{0,k}$ or any other point in field space. $\bar{\rho}_{0,k}$ can always be extracted from $\bar{V}_k(\bar{\rho})$ from eq. (7.16) and enters the physical parameters such as the physical masses, $\bar{m}_k^{(\mathrm{phys})} = \bar{m}_k(\bar{\rho}_{0,k})$.

There are two main restrictions we have for the choice of the expansion point κ. The first and most important is that κ always has to be larger or equal to $\rho_{0,k}$ for small k. The reason is that for $k \to 0$ the effective potential becomes a convex function of ρ which is flat for $\rho < \rho_{0,k=0}$ and we can not expect to capture the relevant features of the theory with an expansion in a potentially flat region of the potential, especially since all the physical information is stored in the effective potential and its derivatives at the minimum. However, we can extract all

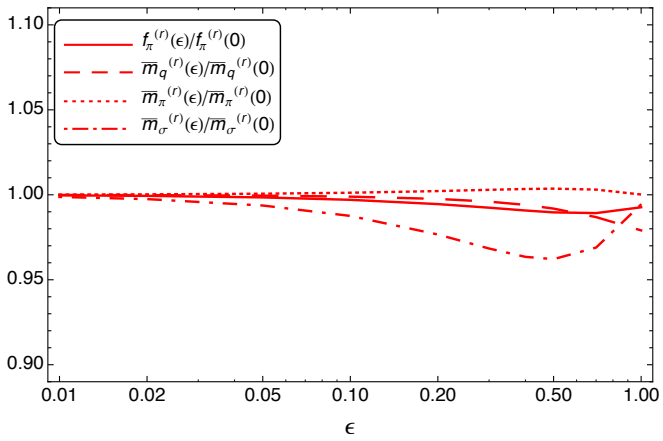

Figure 7.11.: Dependence of the IR-observables on the offset parameter ϵ. Our results for the observables are very robust with respect to variations of the expansion point if we take the corrections (7.43) into account, implying a high degree of convergence of our expansion.

the information we need at much larger scales since the RG-flows of the physical parameters stop at $k \approx m_\pi$. The remaining flow for $k < m_\pi$ flattens the potential but leaves the physical parameters unchanged.

Observables are extracted at the minimum of the potential at $\bar{\rho}_{0,\mathrm{IR}}(T,\mu)$. The present approximation has field-independent wave function renormalizations. This introduces an error which increases with the distance of the expansion point to the minimum. Consequently this leads to a finite radius of convergence in ρ about the minimum, leave aside general convergence issues of the present Taylor expansion. Hence the expansion point should not be too far away from the physically relevant region. This is assured by choosing the expansion point close to the temperature and chemical potential dependent IR-minimum:

$$\bar{\kappa}_{\mathrm{IR}}(T,\mu) = (1+\epsilon)\,\bar{\rho}_{0,\mathrm{IR}}(T,\mu), \tag{7.42}$$

where ϵ is a small offset parameter.

The requirement of small ϵ is at least reduced qualitatively if we would also take field-dependent wave function renormalizations into account. In this work we only have considered wave function renormalization evaluated at the expansion point, see eq. (7.6). Even though this is consistent with our expansion and the proper way to define RG-invariant couplings which are also defined at the expansion point, we expect some residual effects of the constant wave function renormalizations on the physical quantities that are defined at the minimum of the effective potential. In order to partially compensate for this mismatch, we redefine the renormalized IR-observables as follows:

$$\begin{aligned} \bar{f}_\pi^{(r)} &= \sqrt{Z_{\phi,\mathrm{IR}}(\bar{\rho}_{0,\mathrm{IR}})/Z_{\phi,\mathrm{IR}}(\bar{\kappa}_{\mathrm{IR}})}\,\bar{f}_\pi, \\ M_\phi^{(r)} &= \sqrt{Z_{\phi,\mathrm{IR}}(\bar{\kappa}_{\mathrm{IR}})/Z_{\phi,\mathrm{IR}}(\bar{\rho}_{0,\mathrm{IR}})}\,M_\phi, \\ M_q^{(r)} &= \left(Z_{q,\mathrm{IR}}(\bar{\kappa}_{\mathrm{IR}})/Z_{q,\mathrm{IR}}(\bar{\rho}_{0,\mathrm{IR}})\right) M_q. \end{aligned} \tag{7.43}$$

$Z_{\phi/q,\mathrm{IR}}(\bar{\rho}_{0,\mathrm{IR}})$ corresponds to the wave function renormalizations at the IR minimum of the effective potential. It is obtained from integrating the anomalous dimensions (7.26) and

(7.28) at the physical point on the solution of the system at $\bar{\kappa}$. This ensures that the physical quantities are renormalized at the physical point in the IR and furthermore allows us to examine the robustness of our expansion even though we work with field-independent wave function renormalizations. For the sensitivity of our results on ϵ with this correction, see Fig. 7.11. We see that the present expansion is surprisingly robust, even though we dropped the field-dependence of the wave function renormalizations. This observation is also reflected in Fig. 7.6. Furthermore, given the fact that we only made a simple adjustment to the wave function renormalizations in order to define the physical observables, the robustness of our expansion already implies only a mild dependence of the wave function renormalizations on the meson fields. In the expansion (7.4) the zeroth order term certainly depends on the expansion point but already the first order seems to give only a small correction, otherwise we would see a much stronger dependence on the expansion point in Fig. 7.11.

7.4. Conclusions

In this Chapter we have investigated the impact of higher order mesonic scattering processes on the matter sector of two-flavor QCD at finite temperature and quark chemical potential. Quantum, temperature and density fluctuations have been taken into account within a renormalization group analysis of a quark-meson model. In particular, we have introduced for the first time a meson-field dependent Yukawa coupling. The effect of higher order meson-meson and quark-meson operators has been systematically studied by expanding both the Yukawa coupling and the effective potential in orders of the meson fields. These higher order operators play a quantitatively important role for the chiral phase transition. Furthermore, we observed that these operators become increasingly irrelevant with increasing order of the meson fields, see Fig. 7.7. This indicates a rapid convergence of the expansion scheme we used and allows us to have certain control over the quantitative precision of our results.

We have computed the phase diagram of the chiral transition at finite temperature and quark chemical potential, see Fig. 7.9. Owing to the explicit $O(4)$-symmetry breaking which is directly related to finite current quark masses we see a broad crossover phase transition for $\mu < 291$ MeV. Crossover temperatures cannot be defined uniquely. In the present work we have compared standard definitions for the phase boundary and the corresponding temperatures show the expected large deviations. In particular this implies large differences in both the critical temperature at vanishing chemical potential and the curvature. In the chiral limit, all definitions provide the same results.

At large chemical potential close to the critical point the phase boundary is again uniquely defined since the crossover gets steeper in this region. Even though we employed a local expansion of the effective potential in this work, our particular expansion scheme allowed us to resolve some global features of the effective potential. This way we could capture the first order phase transition for not too small temperatures and we found a critical endpoint at $(T_{\mathrm{CEP}}, \mu_{\mathrm{CEP}}) = (50, 291)\,\mathrm{MeV}$.

Note, however, that at large chemical potential and small temperatures quark-meson models in the present approximation are not expected to give an accurate description of the QCD phase structure since diquark and baryonic fluctuations should play an important role in this region. Within the present approximation they are only taken into account implicitly, the improvement of the present work in this direction will be discussed elsewhere.

CHAPTER 8

Summary, Conclusions & Outlook

We have studied various aspects of the chiral phase transition of QCD within a functional renormalization group framework. The possibility to interpolate between the microscopic and the macroscopic regime of the theory in terms of renormalization group flows makes the FRG a well-suited tool to study the complex phenomena involved in the chiral dynamics of QCD. It allows us to describe the dynamical transition from the high-energy phase with quarks and gluons, to the low-energy phase dominated by hadrons. We have argued that the foundation of such an approach is the good understanding of the hadronic and the gauge sector separately, as well as their mutual back reaction. The key ingredient to establish the dynamical connection between these distinct sectors is the dynamical hadronization technique. It is a practical implementation of the intuitive idea that, since hadrons are bound states of quarks and gluons which emerge from the underlying dynamics of the latter, they are in fact RG-scale dependent quantities.

We have extended this technique to the case of fully dynamical two-flavor QCD in Chap. 4. On the basis of the gluon and ghost propagators of the pure gauge theory, we self-consistently incorporated the effects of quark fluctuations to the gauge sector and studied in detail how the hadronic regime emerges during the RG-flow of the system to low energy scales. We computed the unquenched guark and gluon propagators, which nicely reflect the screening effects of dynamical quarks. As we have explained in detail in Sec. 2.4, chiral symmetry breaking can be traced back to the gauge coupling reaching criticality. Owing to the screening due to quark fluctuations, the growing of the gauge couplings gets damped and consequently, chiral symmetry breaking occurs at lower energy scales for smaller quark masses and in particular as compared to quenched QCD. Our result for the unquenched gluon propagator also shows that the gluon mass gap is decreased with increasing quark fluctuations. We have explicitly computed the running quark-gluon, three-gluon and ghost-gluon gauge couplings. Furthermore, we demonstrated that meson fluctuations start to become relevant at momentum scales of about 800 MeV. Their properties are uniquely fixed by the undelying quark-gluon dynamics. The reason is the occurrence of an IR-attractive fixed point in the regime of small gauge coupling, which erases the memory of the system about the initial meson interactions. Thus, the IR-parameters of the mesons, such as their masses, come out as predictions of our computation. We only have to fix microscopic parameters of QCD at large energies, i.e. the strong coupling

and the current quark mass, in order to fix all other parameters of the theory, in particular the rather large number of meson parameters in the IR. We have pointed out that the running wave function renormalizations of the mesons play a crucial role for the fate of the mesons in our setting. With growing energy scale, they fall-off many orders of magnitude as a result of dominant quark fluctuations in the transition region. This triggers a rapid growth of the meson masses at large energy scales which drives their values above the cutoff scale. Thus, the mesons decouple completely and become mere auxiliary fields in the high-energy regime. In fact, we have shown that their RG-flow is exclusively driven by the running of the wave function renormalizations in the quark-gluon regime. This has the consequence that the meson masses can unambiguously be identified from the flow.

The next important step is generalization of this study to finite temperature and density in order to explore the phase structure. The results from low-energy model studies of the phase diagram for the curvature of the phase boundary at vanishing density are much too large as compared to lattice results. Various studies (also Chap. 7 in the present work) indicate that this discrepancy is not rooted in the hadronic sector itself, but in the neglected back reaction of the gauge sector (see e.g. [154] for a first study in this direction). Thus, generalizing our study in Chap. 4 is certainly worthwhile. We also briefly mentioned the connection between the mass gap, which signals confinement, and the fluctuations of the quarks. This, in turn, is another sign for the connection between confinement and chiral symmetry breaking and we can use the framework presented here to gain further insight into this in the future.

These findings were subsequently used as the basis for an investigation of the vacuum structure of vector mesons in QCD in Chap. 5. We pointed out that the light vector mesons, and in particular the ρ meson, play a predominant role in experimental studies aiming at the exploration of phase structure of QCD. The reason is that experimental data, in particular dilepton spectra, show significant in-medium modifications of the ρ meson. A thorough theoretical understanding of the behavior of the rho meson in the vicinity of the chiral phase transition therefore facilitates the identification of chiral symmetry restoration in heavy ion collisions. The framework we put forward in the previous chapter is well-suited to gain insights into the structure of vector mesons, since it uniquely derives from QCD and we do not have to rely on model parameter fine-tuning. We therefore developed a scale-dependent effective action to study the properties of the chiral partners ρ and a_1. We found that the ρ mass first slightly decreases with increasing energy scale towards the chiral transition, before it increases, in particular in the vicinity of the pseudocritical scale. However, the overall scaling of the mass is well approximated as constant for the bigger part of the hadronic regime. This confirms the findings in effective model studies. Furthermore, we have shown that there is an intriguing scale hierarchy in the vacuum: The dynamics of the heavier mesons are completely determined by the dynamics of the lightest meson, the pions and the rho meson at low energies. ρ and a_1 fluctuations are completely decoupled over the full range of scales. Thus, within an Euclidean formulation in the vacuum, it is sufficient to compute the properties of the lightest mesons. The properties of all the other mesons can be inferred from pion and sigma dynamics at low energy scales and quark-gluon dynamics at large energy scales. Since the low-energy parameters are uniquely fixed from quark-gluon fluctuations, we were able to test the assumption of vector meson dominance. Our results show that, even though VMD is a rather drastic simplification of the dynamics of the vector mesons, it can lead to results within about 15% accuracy at low energies. This is in line with phenomenological findings.

We are currently working on the generalization of this study to finite temperature and density. This will allow us to study the in-medium modifications of the vector mesons. Furthermore,

recent developments show that analytic continuation within the FRG, e.g. along the lines of [204], is feasible and, based on our study presented here, the computation of ρ and a_1 spectral functions is within reach. This will then become highly relevant for the interpretation of experimental results.

Since we have access to both, the quark- gluon and the hadronic regime, we were able to analyze the back reaction of the gauge sector on the hadronic sector in Chap. 6. This is particularly relevant for low-energy effective models of QCD, since they neglect fluctuations of the gauge sector and therefore rely on a rapid decoupling of gluons at low energies. We found that the effect of gluon fluctuations extends to rather small energy scales in a quark-meson model, even below the scale of chiral symmetry breaking if one is interested in observables related to the constituent quarks. It is therefore a delicate issue to completely discard the effects of gluon fluctuations in QM-like models. Furthermore, we investigated the relevance of dynamical hadronization for such low-energy models. Our results show that dynamical hadronization does not need to be taken into account at vanishing temperature and density in these models, since they only lead to corrections below the 1% level. We have demonstrated that it is worthwhile gain a better understanding of the region where both, hadron and gluon fluctuations are quantitatively important and the brief analysis presented here should be extended in the near future.

We mentioned above that in order to arrive at a complete picture of the QCD phase structure, it is also important to have a good understanding of the hadron and the guark-gluon sector separately. We therefore studied the hadronic sector of QCD and in particular the phase diagram, at finite temperature and density in terms of a quark-meson model in Chap. 7. We would like to emphasize that the findings of the previous chapter do not render such efforts futile. The purely hadronic sector is always an integral part of the effective action of QCD and relevant parameters in this isolated sector will certainly remain relevant in full QCD, including the back reaction of the gauge sector. We note that we implicitly demonstrated this in Chap. 4, since our truncation of the effective action in the hadronic sector is based on our findings in Chap. 7. We studied the effect of higher order quark-meson scattering processes on the phase diagram of QCD. To be able to do this in a well-controlled way, we had to rely on the fixed background expansion we discussed in Sec. 3.4. There, we pointed out that owing to the resulting structure of the flow equations in this expansion, it shows superior convergence properties of QM-type models. With this, we have shown that higher order quark-meson interactions are quantitatively important for the chiral phase boundary of QCD and it is therefore necessary to take them into account if one is interested in quantitative precision. We then computed the QCD phase diagram in the temperature-density plane. Owing to the wide crossover transition at small and intermediate quark chemical potential, a unique definition of the critical temperature is impossible and we explicitly demonstrated that different order parameters lead to rather different positions of the phase boundary. However, the transition region becomes narrower with increasing chemical potential and we found a critical endpoint at $(T_{\mathrm{CEP}}, \mu_{\mathrm{CEP}}) = (50, 291)\,\mathrm{MeV}$. For chemical potential larger than μ_{CEP}, the transition is of first order. We computed the curvature of the phase boundary at vanishing density for various definitions of the critical temperature. Even though the results strongly depends on the specific definition, we see large a rather large discrepancy with lattice results. However, as our study indicates, this discrepancy can most likely not be explained by missing relevant hadronic degrees of freedom. Its origin presumably lies in the neglected back reaction of the gauge sector, as also mentioned above. Furthermore, we presented a detailed analysis of the effects that the individual parts of our truncation have on the phase boundary. Quark-meson interactions increase the critical temperature, while the

effects of running wave function renormalizations decreases it.

Presently, the studies of the QCD phase structure based on low-energy models with the FRG are lacking one crucial ingredient: diquarks and baryons. They will certainly become relevant at large densities and it is therefore important to include them in the near future.

Appendix

APPENDIX A

Field Space

Here we fix the conventions concerning the field space indices. Since the field space in general contains also Grassmann valued fields, multi-field notation requires a non-trivial metric. For the multi-field $\Phi = (\phi, q, \bar{q}, A, c, \bar{c})^T$ it reads:

$$(\gamma^{\mathbf{ab}}) = \begin{pmatrix} 1 & 0 & 0 & 0 & 0 & 0 \\ 0 & 0 & 1 & 0 & 0 & 0 \\ 0 & -1 & 0 & 0 & 0 & 0 \\ 0 & 0 & 0 & 1 & 0 & 0 \\ 0 & 0 & 0 & 0 & 0 & 1 \\ 0 & 0 & 0 & 0 & -1 & 0 \end{pmatrix}. \tag{A.1}$$

This is a result of the requirement:

$$\Phi^{\mathbf{a}}\Phi_{\mathbf{a}} = \Phi_{\mathbf{b}}\gamma^{\mathbf{ab}}\Phi_{\mathbf{a}} = \int_{\mathbb{R}^d} \left(\phi^2 + 2\bar{q}q + A^2 + 2\bar{c}c\right). \tag{A.2}$$

The delta-distribution in position space is always implicitly contained in γ. Furthermore, integration is implied for contractions. Note that this only applies to the field-space components of the fields. For all other components, the matrix is the identity. This definition entails in particular that

$$\Phi^{\mathbf{a}} = \gamma^{\mathbf{ab}}\Phi_{\mathbf{b}} = (\phi, \bar{q}, -q, A, \bar{c}, -c). \tag{A.3}$$

We use the NW-SE convention, which means that indices are always raised from the left and lowered from the right,

$$\Phi^{\mathbf{a}} = \gamma^{\mathbf{ab}}\Phi_{\mathbf{b}} = \Phi_{\mathbf{b}}\gamma^{\mathbf{ab}}, \qquad \Phi_{\mathbf{a}} = \Phi^{\mathbf{b}}\gamma_{\mathbf{ba}} = \gamma_{\mathbf{ba}}\Phi^{\mathbf{b}}. \tag{A.4}$$

This definition implies

$$\gamma_{\mathbf{a}}{}^{\mathbf{b}} = \gamma^{\mathbf{bc}}\gamma_{\mathbf{ac}} = \gamma^{\mathbf{cb}}\gamma_{\mathbf{ca}} = \delta_{\mathbf{a}}^{\mathbf{b}} \tag{A.5}$$

$$\gamma^{\mathbf{a}}{}_{\mathbf{b}} = \gamma^{\mathbf{ac}}\gamma_{\mathbf{cb}} = \gamma^{\mathbf{ca}}\gamma_{\mathbf{bc}} = (-1)^{\mathbf{ab}}\delta_{\mathbf{b}}^{\mathbf{a}}, \tag{A.6}$$

where

$$(-1)^{\mathbf{ab}} = \begin{cases} -1 & \text{if } \mathbf{a} \text{ and } \mathbf{b} \text{ fermionic} \\ 1 & \text{else} \end{cases}. \tag{A.7}$$

Since we always take derivatives from the left, some caution is necessary concerning the order of the field space element, e.g.

$$\frac{\delta}{\delta\Phi_{\mathbf{b}}} J^{\mathbf{a}}\Phi_{\mathbf{a}} = \frac{\delta}{\delta\Phi_{\mathbf{b}}}\Phi^{\mathbf{a}}J_{\mathbf{a}} = \frac{\delta}{\delta\Phi_{\mathbf{b}}}\Phi_{\mathbf{a}}\gamma^{\mathbf{da}}\gamma_{\mathbf{cd}}J^{\mathbf{c}} = \frac{\delta}{\delta\Phi_{\mathbf{b}}}\Phi_{\mathbf{a}}\gamma^{\mathbf{a}}{}_{\mathbf{c}}J^{\mathbf{c}} = \gamma^{\mathbf{b}}{}_{\mathbf{c}}J^{\mathbf{c}}. \tag{A.8}$$

APPENDIX B

Diagrammatic Derivation of Flow Equations

Here we want to outline the diagrammatic way to derive flow equations. This is the basis for algorithms that automatize their derivation. This is usually a three step process. First, one needs to specify a projection procedure, i.e. a concrete way to extract the scale derivative of a coupling from the scale derivative of the effective action. This the most crucial step, since it actually defines the running coupling. How to extract the running coupling from the effective action is in general not unique. However, even though a simple inspection of the truncation (i.e. the left hand side of the flow equation) seems to indicate that different projections give the exact same result, the right hand side of the flow equation often gives different results. Examples we encounter during this thesis are e.g. the flow of the Yukawa coupling or the meson anomalous dimension. Thus, a running coupling is not defined by specifying the truncation alone, it furthermore needs a projection prescription in order to be uniquely defined. Note that different projection procedures may be related by the symmetries of the system. In this case, they should give the same answer, of course.

The projection usually involves functional derivatives of the Flow. The second step is to derive the diagrams that are generated by the functional derivatives that act on the flow equation. Since the flow itself is one-loop and 1PI by construction, this results in various 1PI one-loop diagrams. The third step is to derive the Feynman rules of the truncation and evaluate the diagrams, i.e. perform the traces and eventually the loop-momentum integration.

This strategy is basically the same as in ordinary perturbation theory. The beautiful thing is that only 1PI one-loop diagrams are involved, so, unlike in perturbation theory, we are always dealing with trivial topologies of the diagrams. The price to pay is of course that usually all parameters in the diagrams are RG-scale dependent, so one always has to solve a tower of coupled differential equations for every scale dependent parameter of the truncation.

In this thesis, we heavily relied on this procedure for the derivation of the flow equations. Our projections are defined either in the main text or in the following appendices. Step three, the evaluation of the diagrams, usually involves algebra and there are many computer algebra systems around to do some of the work. Here, we want to outline the diagrammatics. We note that there is a package based on the computer algebra software *Mathematica* for the derivation of Feynman rules and the diagrams for FRG as well as DSE comutations, called DoFUN, available online [205].

To keep the discussion general, we employ the field-space notation used in Sec. 3.2 and App. A. This allows us to derive a general formula for functional derivatives of any propagator with respect to arbitrary fields. First, we note that

$$\frac{\delta}{\delta \mathbf{x}} G_{\mathbf{ab}} = \left(\frac{\delta}{\delta \mathbf{x}} G_{\mathbf{ab}}\right) + (-1)^{\mathbf{ax}}(-1)^{\mathbf{bx}} G_{\mathbf{ab}} \frac{\delta}{\delta \mathbf{x}}, \tag{B.1}$$

because commuting the functional derivative and the propagator always gives a minus if $\mathbf{x}$ is fermionic and the propagator has exactly one fermionic index. We omit the explcit RG-scale index for the sake of legibility. Second, we know from (3.13)

$$G_{\mathbf{ac}} \left(\Gamma^{(2)} + R\right)^{\mathbf{cb}} = \gamma^{\mathbf{b}}{}_{\mathbf{a}}. \tag{B.2}$$

These are the ingredients for the following derivation:

$$\frac{\delta}{\delta \mathbf{x}} \gamma^{\mathbf{b}}{}_{\mathbf{c}} = 0 = \left(\frac{\delta}{\delta \mathbf{x}} G_{\mathbf{ac}}\right) \left(\Gamma^{(2)} + R\right)^{\mathbf{cb}} + (-1)^{\mathbf{ax}}(-1)^{\mathbf{cx}} G_{\mathbf{ac}} \Gamma^{\mathbf{xcb}}. \tag{B.3}$$

Commuting $\mathbf{x}$ and $\mathbf{c}$ in the vertex cancels $(-1)^{\mathbf{cx}}$. We can further rewrite this as

$$\left(\frac{\delta}{\delta \mathbf{x}} G_{\mathbf{ac}}\right) \delta^{\mathbf{cd}} = -(-1)^{\mathbf{ax}} G_{\mathbf{ac}} \Gamma^{\mathbf{cxb}} \left(\Gamma^{(2)} + R\right)^{-1}_{\mathbf{bd}}. \tag{B.4}$$

If we rewrite the last factor in terms of the propagator, we arrive at our final equation

$$\frac{\delta}{\delta \mathbf{x}} G_{\mathbf{ad}} = -(-1)^{\mathbf{ax}} G_{\mathbf{ac}} \Gamma^{\mathbf{cxb}} G_{\mathbf{ed}} \gamma^{\mathbf{e}}{}_{\mathbf{b}}. \tag{B.5}$$

We can use this to easily derive closed formulas for arbitrary functional derivatives for any kind of propagator. Also here, we see that whenever a derivative hits a propagator, we become two propagator and a three-point function. If it hits a vertex, it simply attaches a new leg to it, e.g. it turns a three- into a four-point function. Thus, a two-point function, i.e. two functional derivatives action on the flow equation, we find:

$$\begin{aligned}
\frac{\delta^2}{\delta \mathbf{y} \delta \mathbf{x}} G_{\mathbf{ab}} \dot{R}^{\mathbf{ab}} &= \frac{\delta}{\delta \mathbf{y}} \left\{ -(-1)^{\mathbf{ax}} G_{\mathbf{ac}} \Gamma^{\mathbf{cxd}} G_{\mathbf{eb}} \gamma^{\mathbf{e}}{}_{\mathbf{d}} \dot{R}^{\mathbf{ab}} \right\} \\
&= +(-1)^{\mathbf{ax}}(-1)^{\mathbf{ay}} G_{\mathbf{af}} \Gamma^{\mathbf{fyg}} G_{\mathbf{hc}} \gamma^{\mathbf{h}}{}_{\mathbf{g}} \Gamma^{\mathbf{cxd}} G_{\mathbf{eb}} \gamma^{\mathbf{e}}{}_{\mathbf{d}} \dot{R}^{\mathbf{ab}} \\
&\quad -(-1)^{\mathbf{ax}}(-1)^{\mathbf{ay}} G_{\mathbf{ac}} \Gamma^{\mathbf{cyxd}} G_{\mathbf{eb}} \gamma^{\mathbf{e}}{}_{\mathbf{d}} \dot{R}^{\mathbf{ab}} \\
&\quad +(-1)^{\mathbf{ax}}(-1)^{\mathbf{ay}}(-1)^{\mathbf{xy}}(-1)^{\mathbf{dy}}(-1)^{\mathbf{ey}} G_{\mathbf{ac}} \Gamma^{\mathbf{cxd}} G_{\mathbf{ef}} \gamma^{\mathbf{e}}{}_{\mathbf{d}} \Gamma^{\mathbf{fyg}} G_{\mathbf{hb}} \gamma^{\mathbf{h}}{}_{\mathbf{g}} \dot{R}^{\mathbf{ab}}.
\end{aligned} \tag{B.6}$$

To illustrate this, let us look at the flow of a scalar field ϕ,

$$\dot{\Gamma}_k[\phi] = \frac{1}{2} \mathrm{Tr}\left(G_k[\phi] \dot{R}_k\right) = \frac{1}{2}$$

(B.7)

The first functional derivative yields according to our findings above

$$\frac{\delta \dot{\Gamma}_k[\phi]}{\delta \phi} = -\frac{1}{2} \mathrm{Tr}\left(G_k[\phi] \Gamma^{(3)}_k[\phi] G_k[\phi] \dot{R}_k\right) = -\frac{1}{2}$$

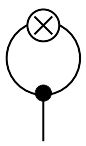

, (B.8)

and the second finally

$$\frac{\delta^2\dot{\Gamma}_k[\phi]}{\delta\phi^2} = \mathrm{Tr}\Big(G_k[\phi]\Gamma_k^{(3)}[\phi]G_k[\phi]\Gamma_k^{(3)}[\phi]G_k[\phi]\dot{R}_k\Big) - \frac{1}{2}\mathrm{Tr}\Big(G_k[\phi]\Gamma_k^{(4)}[\phi]G_k[\phi]\dot{R}_k\Big)$$

$$= \quad - \frac{1}{2} \quad . \tag{B.9}$$

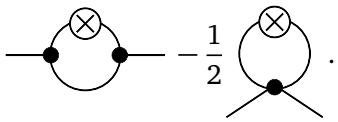

We see that we always get a simple one-loop expression that can easily be evaluated with the Feynman rules of the corresponding truncation, i.e. the algebraic expressions for the propagators and vertices. For more species of fields, including fermions, there may be additional minus signs involved, but the general procedure is always the same. The equations we derived above in the field-space formalism hold for any kind of field.

APPENDIX C

Flow Equations

In this appendix we give some explicit details about the flow equations.

C.1. QCD Flows

Here, we collect the threshold functions which enter the flow equations in Chap. 4 and encode the regulator and momentum dependence of the flows. Note that it is here, where the substitution $\eta_{\phi,k} \to \eta_{\phi,k} - 2\dot{\bar{B}}_k$ has to be made according to (4.61).

Throughout this work, we use $4d$ regulator functions of the form:

$$\begin{aligned} R_k^{\phi}(p^2) &= Z_{\phi,k}\, p^2 r_B(p^2/k^2), \\ R_k^{q}(p^2) &= Z_{q,k}\, \gamma_\mu p_\mu r_F(p^2/k^2), \\ R_k^{A,\mu\nu}(p^2) &= Z_{A,k}\, p^2 r_B(p^2/k^2)\, \Pi^{\perp}_{\mu\nu}(p), \end{aligned} \tag{C.1}$$

with the transverse projector

$$\Pi^{\perp}_{\mu\nu}(p) = \delta_{\mu\nu} - \frac{p_\mu p_\nu}{p^2}. \tag{C.2}$$

Note that in the approximation at hand the ghost regulator does not enter. The optimized regulator shape functions $r_{B/F}(x)$ are given by [149]:

$$\begin{aligned} r_B(x) &= \left(\frac{1}{x} - 1\right)\Theta(1-x), \\ r_F(x) &= \left(\frac{1}{\sqrt{x}} - 1\right)\Theta(1-x). \end{aligned} \tag{C.3}$$

The threshold functions for the effective potential, the Yukawa coupling and the four-quark

coupling are:

$$
\begin{aligned}
l_n^B(\bar{m}_B^2;\eta_B) &= \frac{2(\delta_{n,0}+n)}{d}\Big(1-\frac{\eta_B}{d+2}\Big)(1+\bar{m}_B^2)^{-(n+1)}, \\
l_n^F(\bar{m}_F^2;\eta_F) &= \frac{2(\delta_{n,0}+n)}{d}\Big(1-\frac{\eta_F}{d+1}\Big)(1+\bar{m}_F^2)^{-(n+1)}, \\
L_{1,1}^{(FB)}(\bar{m}_F^2,\bar{m}_B^2;\eta_F,\eta_B) &= \frac{2}{d}(1+\bar{m}_F^2)^{-1}(1+\bar{m}_B^2)^{-1}\Big\{\Big(1-\frac{\eta_F}{d+1}\Big)(1+\bar{m}_F^2)^{-1} \\
&\quad +\Big(1-\frac{\eta_B}{d+2}\Big)(1+\bar{m}_B^2)^{-1}\Big\}, \\
L_{1,2}^{(FB)}(\bar{m}_F^2;\eta_F,\eta_B) &= \frac{2}{d}(1+\bar{m}_F^2)^{-2}\Big\{2\Big(1-\frac{2\eta_B}{d+2}\Big)-\Big(1-\frac{\eta_F}{d+1}\Big) \\
&\quad +2(1+\bar{m}_F^2)^{-1}\Big(1-\frac{\eta_F}{d+1}\Big)\Big\}, \\
L_{1,1,1}^{(FB)}(\bar{m}_F^2,\bar{m}_{B1}^2,\bar{m}_{B2}^2;\eta_F,\eta_B) &= \frac{2}{d}(1+\bar{m}_F^2)^{-2}(1+\bar{m}_{B1}^2)^{-1}(1+\bar{m}_{B2}^2)^{-1}\Big\{\Big[(1+\bar{m}_{B1}^2)^{-1} \\
&\quad +(1+\bar{m}_{B2}^2)^{-1}\Big]\Big(1-\frac{\eta_B}{d+2}\Big)+\Big[2(1+\bar{m}_F^2)^{-1}-1\Big]\Big(1-\frac{\eta_F}{d+1}\Big)\Big\}.
\end{aligned}
\tag{C.4}
$$

For the anomalous dimensions, we have

$$
\begin{aligned}
\mathscr{M}_2(\bar{m}_F^2;\eta_F) &= \big(1+\bar{m}_F^2\big)^{-4}, \\
\mathscr{M}_{2,2}(\bar{m}_{B1}^2,\bar{m}_{B2}^2;\eta_B) &= (1+\bar{m}_{B1}^2)^{-2}(1+\bar{m}_{B2}^2)^{-2} \\
\mathscr{M}_{1,2}(\bar{m}_F^2,\bar{m}_B^2;\eta_F,\eta_B) &= \Big(1-\frac{\eta_B}{d+1}\Big)(1+\bar{m}_F^2)^{-1}(1+\bar{m}_B^2)^{-2} \\
\mathscr{M}_4(\bar{m}_F^2;\eta_F) &= \big(1+\bar{m}_F^2\big)^{-4}+\frac{1-\eta_F}{d-2}\big(1+\bar{m}_F^2\big)^{-3}-\Big(\frac{1}{4}+\frac{1-\eta_F}{2d-4}\Big)\big(1+\bar{m}_F^2\big)^{-2} \\
\tilde{\mathscr{M}}_{1,1}(\bar{m}_F^2,\eta_F,\eta_B) &= \frac{2}{d-1}\big(1+\bar{m}_F^2\big)^{-1}\Big\{\frac{1}{2}\Big(\frac{2\eta_F}{d}-1\Big)+\Big(1-\frac{\eta_B}{d+1}\Big) \\
&\quad +\Big(1-\frac{2\eta_F}{d}\Big)\big(1+\bar{m}_F^2\big)^{-1}\Big\}.
\end{aligned}
\tag{C.5}
$$

Finally, for the flow of $z_{\bar{q}Aq}$ we use

$$
\begin{aligned}
\mathscr{N}_{2,1}^{(m)}(\bar{m}_F^2,\bar{m}_B^2;\eta_F,\eta_B) &= \frac{1}{d}\Big(1-\frac{\eta_F}{d+1}\Big)(1+\bar{m}_B^2)^{-1}\Big\{2\bar{m}_F^2(1+\bar{m}_F^2)^{-3}+(1+\bar{m}_F^2)^{-2}\Big\} \\
&\quad +\frac{1}{d}\Big(1-\frac{\eta_B}{d+2}\Big)(1+\bar{m}_B^2)^{-2}\Big\{\bar{m}_F^2(1+\bar{m}_F^2)^{-2}+(1+\bar{m}_F^2)^{-1}\Big\}, \\
\mathscr{N}_{2,1}^{(g)}(\bar{m}_F^2;\eta_F,\eta_A) &= \frac{1}{d}\Big(1-\frac{\eta_F}{d+1}\Big)\bar{m}_F^2(1+\bar{m}_F^2)^{-3}+\frac{1}{2d}\Big(1-\frac{\eta_A}{d+2}\Big)\bar{m}_F^2(1+\bar{m}_F^2)^{-2}, \\
\mathscr{N}_{1,2}^{(g)}(\bar{m}_F^2;\eta_F,\eta_A) &= \frac{1}{d+1}\Big(1-\frac{\eta_F}{d+2}\Big)\Big\{2\bar{m}_F^2(1+\bar{m}_F^2)^{-2}-(1+\bar{m}_F^2)^{-1}\Big\} \\
&\quad +\frac{4}{d+1}\Big(1-\frac{\eta_A}{d+3}\Big)(1+\bar{m}_F^2)^{-1}.
\end{aligned}
\tag{C.6}
$$

C.2. Vacuum Polarization of the Gluon

Here, we derive the vacuum polarization of the gluon. Is is the direct contribution from quark fluctuations to the gluon two-point function. Therefore it is one of the ingredients we need to compute the unquenched gluon propagator Sec. 4.3

We note that the technical details shown here can be directly applied to the derivation of any flow equation of explicitly momentum dependent couplings with the optimized cutoff at vanishing external momentum.

We need to compute the diagram in the following equation:

$$\Delta\eta_{A,k} = \frac{Z_{A,k}^{-1}}{3(N_c^2-1)} \left(\frac{\partial^2}{\partial p^2} \Pi^{\perp}(p) \cdot \right. \quad \Bigg|_{p=0} \tag{C.7}$$

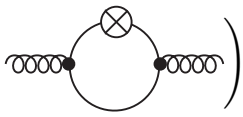

Note that the projection procedure also involves that the external momentum is set to zero after the momentum derivatives. The trace over external indices is implied. We need the quark propagators, the quark regulator and the quark-gluon vertex, including their tensor structure. The quark propagator reads with the optimized cutoff (C.1)

$$G_{q\bar{q},k}(p) = \left(\frac{\gamma_\mu p_\mu}{p} - iM_{q,k} \right) \frac{\Theta(1-p^2)}{1+M_{q,k}^2} + \left(\gamma_\mu p_\mu - iM_{q,k} \right) \frac{\Theta(p^2-1)}{p^2+M_{q,k}^2} \mathbb{1}_c \mathbb{1}_f \,, \tag{C.8}$$

where $\mathbb{1}_c$ and $\mathbb{1}_f$ are the unit matrices of color and flavor. Note that we write everything in terms of dimensionless and renormalized quantities. Thus, also the momenta are rescaled with k, i.e. $p = p/k$. p is the absolute value, $p = |p| = \sqrt{p^2}$. The quark gluon vertex is

$$\Gamma_{k,\mu a}^{(\bar{q}Aq)} = g_{\bar{q}Aq,k} \gamma_\mu t^a \mathbb{1}_c \mathbb{1}_f \,. \tag{C.9}$$

Furthermore, let us assume that the the loop momentum q alone goes through the upper part of the diagram and in particular the regulator. Thus, external plus loop-momentum $p+q$ pass though the lower half of the quark loop. First, we compute the trace of the digram, which we denote by $\Sigma(p)$, including $\Pi^{\perp}$ from the projection

$$\begin{aligned} \mathrm{Tr}\,\Pi^{\perp}(p)\Sigma(p) &= \mathrm{Tr}\left(\Pi_{\mu\nu}^{\perp} G_{q\bar{q},k}(p+q) \Gamma_{k,\nu a}^{(\bar{q}Aq)} G_{q\bar{q},k}(q) \dot{R}_k^A G_{q\bar{q},k}(q) \Gamma_{k,\mu a}^{(\bar{q}Aq)} \right) \\ &= \int_q g_{\bar{q}Aq,k}^2 N_f N_c C_2(N_c) \left[q^{-1} - \eta_{q,k}(q^{-1}-1) \right] (1+M_{q,k}^2)^{-2} \Theta(1-q^2) \\ &\quad \times \left[F(p,q)\Theta(1-(p+q)^2) + H(p,q)\Theta((p+q)^2-1) \right], \end{aligned} \tag{C.10}$$

with the functions

$$\begin{aligned} F(p,q) &= \frac{1}{1+M_{q,k}^2} \frac{4q}{\sqrt{p^2+q^2+2pqx}} \left[(M_{q,k}^2-1)(3px+2qx^2+q) - 6M_{q,k}\sqrt{p^2+q^2+2pqx} \right] \\ H(p,q) &= \frac{4q}{(p+q)^2+M_{q,k}^2} \left[M_{q,k}^2(3px+2qx^2+q-6) - 3px - q(2x^2-1) \right]. \end{aligned} \tag{C.11}$$

We defined x via $p_\mu q_\mu = pqx$, i.e. it is the cosine of the angle between the two 4D-vectors p and q.

The next step is to take the momentum derivatives of (C.10). This yields

$$\frac{\partial^2}{\partial p^2}\mathrm{Tr}\,\Pi^{\perp}(p)\Sigma(p) = \int_q Q(q)\,\Theta(1-q^2) \times \left\{ \frac{\partial^2 F(p,q)}{\partial p^2}\Theta(1-(p+q)^2) - 2(p+qx)\frac{\partial F(p,q)}{\partial p}\delta(1-(p+q)^2) \right. \left. \frac{\partial^2 H(p,q)}{\partial p^2}\Theta((p+q)^2-1) + 2(p+qx)\frac{\partial H(p,q)}{\partial p}\delta(1-(p+q)^2) \right\}, \tag{C.12}$$

with the abbreviation

$$Q(q) = g^2_{\bar{q}Aq,k} N_f N_c C_2(N_c)\left[q^{-1} - \eta_{q,k}(q^{-1}-1)\right](1+M^2_{q,k})^{-2}. \tag{C.13}$$

We have used $\partial_x \Theta(x) = \delta(x)$ and that the terms proportional to the δ distribution from the first derivative vanish.

To proceed, we could now either perform the loop momentum integration in (C.12) and then send the external momentum to zero, or the other way around. The integration at finite p is cumbersome and we would like to avoid it. But taking the $p \to 0$ limit before the integration immediately generates an obvious problem: we would get terms of the form $\Theta(x)\delta(x)$ in (C.12), which are nor well defined, since the delta distribution has it support exactly where the theta function is not defined. To circumvent this problem, we switch to smeared kernels. To this end, we replace the sharp Theta function by a smeared version Θ_ϵ which approaches the sharp function at vanishing ϵ, $\lim_{\epsilon\to 0}\Theta_\epsilon(x) = \Theta(x)$ and define the smeared delta function via the derivative $\delta_\epsilon(x) = \partial_x \Theta_\epsilon(x)$. It is now crucial that we are allowed to exchange the $p \to 0$ limit and the $\epsilon \to 0$ limit if the smeared functions uniformly converge to the sharp limit. Since a representation fulfilling this criterion can always be chosen, we exchange the limits, send p to zero and are left with

$$\lim_{\epsilon\to 0}\frac{\partial^2}{\partial p^2}\mathrm{Tr}\,\Pi^{\perp}(p)\Sigma(p)\Big|_{p=0} = \int_q Q(q)\lim_{\epsilon\to 0}\Theta_\epsilon(1-q^2)\left\{ \frac{\partial^2 F(p,q)}{\partial p^2}\Big|_{p=0} - 2qx\frac{\partial F(p,q)}{\partial p}\Big|_{p=0}\delta_\epsilon(1-q^2) + 2qx\frac{\partial H(p,q)}{\partial p}\Big|_{p=0}\delta_\epsilon(1-q^2)\right\}. \tag{C.14}$$

Note that the first and the third term in (C.12) are well defined term in the $p \to 0$ limit, in which the third vanishes, since $\Theta(x)\Theta(1-x) = 0$. By looking at (C.14) it seems that we have not gaied anything. We simply exchanged an ill-defined limit by another ill-defined limit since the last two terms are still ill-defined, but now in the $\epsilon \to 0$ limit. However, there is an useful identity which is very helpful in this case [132]:

$$\lim_{\epsilon\to 0} f\big(x,\Theta_\epsilon(x)\big)\,\delta_\epsilon(x) = \Theta(x)\int_0^1 du f(0,u), \tag{C.15}$$

for any continuous function f. This identity allows us to send ϵ to zero and we arrive at

$$\frac{\partial^2}{\partial p^2}\mathrm{Tr}\,\Pi^{\perp}(p)\Sigma(p)\Big|_{p=0} = \int_q Q(q)\left\{ \frac{\partial^2 F(p,q)}{\partial p^2}\Big|_{p=0}\Theta(1-q^2) - x\left(\frac{\partial F(p,1)}{\partial p}) - \frac{\partial H(p,1)}{\partial p}\right)\Big|_{p=0}\delta(1-q^2)\right\}. \tag{C.16}$$

Since structurally all flow equations for parameters with explicit momentum dependence, such as the wave function renormalization or the three-gluon vertex, are the same, given we always use the optimized cutoff and the zero external momentum limit, we can use (C.16) with different functions Q, F and H for all these specific class of parameters.

We can now explicitly evaluate the ingredients in (C.16) and arrive at the final integral

$$\begin{aligned}\frac{\partial^2}{\partial p^2}\mathrm{Tr}\,\Pi^{\perp}(p)\Sigma(p)\Big|_{p=0} &= g^2_{\bar{q}Aq,k} N_f N_c C_2(N_c)(1+M^2_{q,k})^{-2}\int_q \left[q^{-1}-\eta_{q,k}(q^{-1}-1)\right] \\ &\times\left\{\frac{4}{q}\frac{M^2_{q,k}-1}{M^2_{q,k}+1}(6x^4-5x^2-1)\Theta(1-q^2)\right. \\ &\left.+\frac{2x^2}{(1+M^2_{q,k})^2}\left[M^4_{q,k}(1+2x^2)+M^2_{q,k}(10-4x^2)+2x^2+1\right]\delta(1-q)\right\}.\end{aligned} \tag{C.17}$$

Note that we have changed the variable in the delta distribution, $\delta(1-q^2)=\delta(1-q)/2$. If we rewrite the integral measure in terms of 4-dimensional spherical coordinates, keeping in mind that our integrand depends only on a single angle, it reads for the simplest choice for the orientation of p

$$\int_q f(q,x) = \int \frac{dq^4}{(2\pi)^4} f(q,x) = \frac{1}{4\pi^3}\int_0^\infty \int_{-1}^1 dq\,dx\,q^3\sqrt{1-x^2}\,f(q,x)\,. \tag{C.18}$$

With this, we find for (C.19)

$$\frac{\partial^2}{\partial p^2}\mathrm{Tr}\,\Pi^{\perp}(p)\Sigma(p)\Big|_{p=0} = \frac{N_f N_c C_2(N_c)}{8\pi^2}\, g^2_{\bar{q}Aq,k}(1+\bar{m}^2_{q,k})^{-4}\left[4-\eta_{q,k}+4\bar{m}^2_{q,k}+(\eta_{q,k}-1)\,\bar{m}^4_{q,k}\right] \tag{C.19}$$

Together with the prefactors of the projection specified in (C.7), this completes the derivation of the vacuum polarization (4.88).

C.3. Vector Meson Flows

Here we provide some details about the RG flow equations of the running couplings of our truncation (5.3) together with the modifications that result from dynamical hadronization (5.26). Due to excessive length of the explicit flow equation, we only present their definitions here. For the derivation of most of the equations we used an extension of DoFun [205] which utilizes Form [206] and FormLink [207]. This extension was developed and first used by the authors of [156]. With the truncation (5.3), the Wetterich equation (5.25) and the definitions given below, the flow equations of the couplings are uniquely specified.

Physical parameters are RG-invariant quantities. To achieve this, all fields are rescaled with their respective wave function renormalizations, $\Phi \to \sqrt{Z_{\Phi,k}}\Phi$, and all couplings are rescaled with appropriate powers of the wave function renormalizations accordingly, see below. This entails in particular, that the wave function renormalizations enter the flow equations only through the corresponding anomalous dimensions,

$$\eta_k = -\frac{\partial_t Z_k}{Z_k}\,. \tag{C.20}$$

The physical, i.e. RG-invariant, parameters of the action are defined as

$$\bar{\xi}_k = \frac{\xi_k}{\left(Z_{A,k}^{n_A} Z_{q,k}^{n_q} Z_{c,k}^{n_c} Z_{\phi,k}^{n_\phi} Z_{V,k}^{n_V}\right)^{1/2}}, \tag{C.21}$$

where

$$\begin{aligned}\xi_k \in \{&g_{\bar{q}Aq,k},\, g_{A^3,k},\, g_{A^4,k},\, g_{\bar{c}Ac,k},\, \lambda_{S,k},\, \lambda_{V,k},\, h_{S,k},\\ &h_{V,k},\, m_{S,k},\, m_{V,k},\, \nu_k,\, c_k,\, g_{1-5,k}\},\end{aligned} \tag{C.22}$$

is one of the running couplings of our truncation (5.3). n_A, n_q, n_c, n_ϕ, n_V are the numbers of gluon, quark, ghost, scalar meson and vector meson fields respectively, that are attached to the coupling ξ_k. The physical masses are given by (5.36). Note that the definition of the gluonic vertices (4.71) implies that the gauge couplings are already RG-invariant. Thus, in that case $\bar{g}_k = g_k$ and we omit the bars.

We use 4d regulator functions of the form

$$\begin{aligned}R_k^A(p^2) &= Z_{A,k}\, p^2 r_B(p^2/k^2)\, \Pi^\perp,\\ R_k^q(p^2) &= Z_{q,k}\, \gamma_\mu p_\mu r_F(p^2/k^2),\\ R_k^c(p^2) &= Z_{c,k}\, p^2 r_B(p^2/k^2),\\ R_k^\phi(p^2) &= Z_{\phi,k}\, p^2 r_B(p^2/k^2),\\ R_k^V(p^2) &= Z_{V,k}\, p^2 r_B(p^2/k^2)\, \Pi^\perp,\end{aligned} \tag{C.23}$$

with the transversal projection operator

$$\Pi^\perp_{\mu\nu} = \delta_{\mu\nu} - \frac{p_\mu p_\nu}{p^2}. \tag{C.24}$$

For the bosonic and fermionic regulator shape functions r_B and r_F we use the optimized shape functions [149]

$$\begin{aligned}r_B(x) &= \left(\frac{1}{x} - 1\right)\Theta(1-x),\\ r_F(x) &= \left(\frac{1}{\sqrt{x}} - 1\right)\Theta(1-x).\end{aligned} \tag{C.25}$$

The flow equations presented in the following are derived using these specific regulators. They have the advantage, that the loop-momentum integration can be performed analytically and, consequently, all beta functions can be given in analytical form. Furthermore, we work in Landau gauge, fix the Euclidean spacetime dimension to $d=4$ and color and flavor are fixed to $N_c=3$ and $N_f=2$.

First, we explain the effective propagators used in Sec. 4.4.4 and 5.3.2 and in particular Fig. 4.10 and 5.5. The propagators in momentum space are of the form

$$\begin{aligned}G_{B,k}(q) &= \frac{1}{Z_{B,k} q^2 \left(1 + r_B(q^2/k^2)\right) + m_{B,k}^2},\\ G_{F,k}(q) &= \frac{1}{Z_{F,k}^2 q^2 \left(1 + r_F(q^2/k^2)\right)^2 + m_{F,k}^2},\end{aligned} \tag{C.26}$$

for bosons and fermions respectively. For the specific choice of regulator shape functions (C.25), they read

$$\begin{aligned} G_{B,k}(q) &= \frac{\Theta(k^2-q^2)}{Z_{B,k}k^2+m_{B,k}^2} + \frac{\Theta(q^2-k^2)}{Z_{B,k}q^2+m_{B,k}^2}\,, \\ G_{F,k}(q) &= \frac{\Theta(k^2-q^2)}{Z_{F,k}^2k^2+m_{F,k}^2} + \frac{\Theta(q^2-k^2)}{Z_{F,k}^2q^2+m_{F,k}^2}\,. \end{aligned} \tag{C.27}$$

To be consistent with the low-momentum expansion our construction of the effective action is based on, we define all running couplings at vanishing external momentum. This entails that all integrands of the loop-momentum integrations are proportional to $\Theta(k^2-q^2)$ which stems from the scale derivative of the regulator $\partial_t R_k^\Phi$ in the flow equation (5.25). Thus, only the first term of the propagators in (C.27) contributes in the final flow equations. We therefore define the effective propagators relevant for the flows of the physical quantities as

$$\bar{G}_{\Phi,k} = \frac{1}{1+(M_{\Phi,k}/k)^2}\,. \tag{C.28}$$

Vanishing $\bar{G}_{\Phi,k}$ implies that the field Φ does not contribute to the dynamics of the system. Note that it is a bounded function, $0 \leq \bar{G}_{\Phi,k} \leq 1$. The larger $\bar{G}_{\Phi,k}$, the more relevant are the fluctuations of the corresponding field.

We proceed with the definition of the flows of the gauge couplings. The explicit form of the flow equations is given in [73]. Here, we only present our definitions for completeness. As we have discussed in Sec. 4.3, we compute all three-point functions of QCD, but restrict them to have only the classical tensor structure. We therefore define the flow of the quark-gluon vertex $g_{\bar{q}Aq}$ as

$$\partial_t g_{\bar{q}Aq,k} = \frac{1}{8N_f(N_c^2-1)} \lim_{p\to 0} \mathrm{Tr}\left(\gamma_\mu t^a \frac{\delta^3 \partial_t \Gamma_k}{\delta q \delta A_\mu^a \delta \bar{q}} \right)\Bigg|_{\Phi=\Phi_0}\,, \tag{C.29}$$

where $\Phi_0 = (0,0,0,0,0,0,\sigma_{0,k},0,0)$ is the vacuum expectation value of the mean field $\Phi = (A,q,\bar{q},c,\bar{c},\pi,\sigma,\rho,a_1)$. The trace runs over all external indices and includes a loop-momentum integration. The limit denotes that all external momenta are set to zero. We define the three-gluon vertex $g_{A^3,k}$ via the projection

$$\partial_t g_{A^3,k} = \frac{i}{12N_c(N_c^2-1)} \lim_{p\to 0} \frac{\partial^2}{\partial p^2} \mathrm{Tr}\left(\delta_{\mu\nu} p_\sigma f^{abc} \frac{\delta^3 \partial_t \Gamma_k}{\delta A(p)_\mu^a \delta A(-p)_\nu^b \delta A_\sigma^c(0)} \right)\Bigg|_{\Phi=\Phi_0}\,. \tag{C.30}$$

Since as an approximation we evaluate all flow equations at vanishing external momentum, the ghost-gluon vertex $g_{\bar{c}Ac,k}$ only has canonical running. The diagrams that contribute to the beta function are proportional to the external momentum and therefore vanish here and we are left with

$$\partial_t g_{\bar{c}Ac} = \frac{1}{2}\left(\eta_{A,k} + 2\eta_{C,k}\right) g_{\bar{c}Ac}. \tag{C.31}$$

Since we approximate the four-gluon vertex with the three-gluon vertex, see (4.105), we do not need a separate equation for this coupling.

Next, we discuss the flow of the four-quark couplings. Here, we consider two channels, the scalar–pseudoscalar channel with coupling $\lambda_{S,k}$ and the iso-vector–iso-axialvector channel with coupling $\lambda_{V,k}$. Some caution is advised when four-fermion interactions are included in the effective action. A specific quark-antiquark interaction channel can always be expressed as an linear combination of different interaction channels with two spinor fields interchanged. This can potentially lead to ambiguities in the corresponding bosonized models since different sets of composite states can be related to one and the same fermionic action (see e.g. [75]). This is known as the Fierz ambiguity. While this ambiguity can lead to large uncertainties in mean-field calculations, appropriate approximations that go beyond mean-field in RG studies can minimize these uncertainties [162].

Indeed, as explicit calculations considering the RG flows of a Fierz-complete basis of four-quark interactions have shown [156], the scalar-pseudoscalar ($S-P$) channel is the dominant channel in vacuum, while all other channels are strongly suppressed compared to this channel. Furthermore, the dynamical hadronization of only the (S–P) is sufficient to render all four-quark interaction channels finite at the chiral phase transition. Thus, the error we make from not using a Fierz-complete basis is expected to be small. We therefore restrict our model to contain only two physically relevant channels. In order to study the properties of the corresponding composite fields, we dynamically hadronize both channels here.

We define the running coupling of the scalar-pseudoscalar channel via the projection

$$\partial_t \lambda_{S,k} = \frac{1}{8N_f N_c(2N_f N_c+1)} \lim_{p\to 0} \mathrm{Tr}\left(\delta_{AB}\delta_{CD}\frac{\delta^4 \partial_t \Gamma_k}{\delta q_A \delta \bar{q}_B \delta q_C \delta \bar{q}_D}\right)\Bigg|_{\Phi=\Phi_0}, \tag{C.32}$$

where A, B, C, D abbreviate the color, flavor and spinor indices of the quarks. For the vector-axialvector channel we choose

$$\partial_t \lambda_{V,k} = -\frac{1}{3}\partial_t \lambda_{S,k} - \lim_{p\to 0} \mathrm{Tr}\left(\mathbb{P}_V^{ABCD}\frac{\delta^4 \partial_t \Gamma_k}{\delta q_A \delta \bar{q}_B \delta q_C \delta \bar{q}_D}\right)\Bigg|_{\Phi=\Phi_0}, \tag{C.33}$$

with the projection operator

$$\mathbb{P}_V^{ABCD} = \frac{1}{192 N_f N_c}\,\delta_{AB}\delta_{CD}\gamma_\mu^{\alpha_A\alpha_B}\gamma_\mu^{\alpha_C\alpha_D}. \tag{C.34}$$

Here, $\alpha_{A,B,C,D}$ is the spinor index of the respective quark field. The Kronecker deltas are summed over the remaining color and flavor indices.

We note that these projections give the flow equations for scale-independent meson fields, i.e. without dynamical hadronization. Dynamical hadronization enforces (5.27). Nevertheless, the flows of the four-quark interactions defined in (C.32) and (C.33) play a major role for the dynamics of the system and enter the hadronized flow equations in the meson sector via the hadronization functions (5.28).

We define the scalar Yukawa coupling $h_{S,k}$ via the quark-antiquark two-point function as:

$$\partial_t h_{S,k} = \frac{-i}{4N_f N_c\,\sigma_0} \lim_{p\to 0} \mathrm{Tr}\left(\delta_{AB}\frac{\delta^2 \partial_t \Gamma_k}{\delta q_A \delta \bar{q}_B}\right)\Bigg|_{\Phi=\Phi_0}. \tag{C.35}$$

Taking dynamical hadronization into account, the total flow of the renormalized scalar Yukawa coupling is

$$\partial_t\big|_\varphi \bar{h}_{S,k} = \partial_t \bar{h}_{S,k} - k^{-2} M_{\pi,k}^2 \dot{A}_k, \tag{C.36}$$

where $\dot{\bar{A}}_k = k^2 Z_{S,k}^{1/2} Z_{q,k}^{-1} \dot{A}_k$ and $\dot{A}_k$ is given by (5.28). According to (5.24), the scalar channel Yukawa coupling defines the quark mass.

We define the vector Yukawa coupling $h_{V,k}$ via the $\rho q\bar{q}$ three-point function as

$$\partial_t h_{V,k} = \frac{1}{16 N_c (N_f^2-1)} \lim_{p\to 0} \mathrm{Tr}\left(\gamma_\mu \vec{\tau} \, \frac{\delta^3 \partial_t \Gamma_k}{\delta \vec{\rho}^{\,\mu} \delta q \delta \bar{q}} \right)\Big|_{\Phi=\Phi_0} , \tag{C.37}$$

where contractions over the remaining indices with Kronecker deltas is implied. Splitting the flow into the contributions with and without dynamical hadronization, we find

$$\partial_t \big|_\varphi \bar{h}_{V,k} = \partial_t \bar{h}_{V,k} - k^{-2} M_{\rho,k}^2 \dot{\bar{B}}_k , \tag{C.38}$$

with $\dot{\bar{B}}_k = k^2 Z_{V,k}^{1/2} Z_{q,k}^{-1} \dot{B}_k$ and $\dot{B}_k$ given by (5.28).

We want to emphasize that the modifications of the Yukawa couplings in (C.36) and (C.36) proportional to $\dot{A}_k$ and $\dot{B}_k$ are crucial for the dynamical hadronization procedure. They guarantee that the ratio $h_{S/V,k}^2/m_{\pi/\rho,k}^2$ replaces the four-quark interactions $\lambda_{S/V,k}$, which vanish due to dynamical hadronization, in the quark-gluon phase. This way, the modified Yukawa couplings capture the relevant quark-gluon dynamics at large energy scales, while they act as the usual Yukawa couplings in the hadronic regime.

Next, we discuss the mesonic couplings of our truncation. They are not modified by dynamical hadronization. We define the running of the chiral order parameter $\sigma_{0,k}$ via the pion two-point function as

$$\partial_t \sigma_{0,k} = -\left(\nu_k \sigma_{0,k} + \frac{c_k}{\sigma_{0,k}^2} \right)^{-1} \frac{1}{N_f^2-1} \lim_{p\to 0} \mathrm{Tr}\left(\delta_{ij} \frac{\delta^2 \partial_t \Gamma_k}{\delta \pi_i \delta \pi_j} \right)\Big|_{\Phi=\Phi_0} , \tag{C.39}$$

with the adjoint flavor indices i, j. The flow of the scalar four-point function ν_k is defined as follows:

$$\partial_t \nu_k = \frac{1}{N_f^4-1} \lim_{p\to 0} \mathrm{Tr}\left(\delta_{ij}\delta_{kl} \frac{\delta^4 \partial_t \Gamma_k}{\delta \pi_i \delta \pi_j \delta \pi_k \delta \pi_l} \right)\Big|_{\Phi=\Phi_0} , \tag{C.40}$$

with the adjoint flavor indices i, j, k, l.

The explicit symmetry breaking term c is a source term and therefore drops out of the flow equation. The RG-invariant coupling $\bar{c}_k$ therefore only runs canonically,

$$\partial_t \bar{c}_k = \frac{1}{2} \eta_{S,k} \, \bar{c}_k . \tag{C.41}$$

The meson masses are defined as the momentum independent part of the corresponding two-point functions. For the scalar mesons, we need the flow of $m_{S,k}$ which is given by

$$\partial_t m_{S,k}^2 = \frac{1}{N_f^2-1} \lim_{p\to 0} \mathrm{Tr}\left(\delta_{ij} \frac{\delta^2 \partial_t \Gamma_k}{\delta \pi_i \delta \pi_j} \right)\Big|_{\Phi=\Phi_0} . \tag{C.42}$$

We cannot define the flow of the vector meson mass parameter $m_{V,k}$ independently of other couplings, since we have to either project on the ρ or the a_1 mass, which gives contributions

from other couplings in the chirally broken phase according to (5.24). We choose to project on the ρ mass and find

$$\partial_t m^2_{V,k} = \frac{1}{4(N_f^2-1)} \lim_{p\to 0} \mathrm{Tr}\left(\delta_{\mu\nu}\delta_{ij}\frac{\delta^2 \partial_t \Gamma_k}{\delta\rho_i^\mu \delta\rho_j^\mu}\right)\Bigg|_{\Phi=\Phi_0} - \sigma^2_{0,k}\partial_t g_{3,k}\,. \tag{C.43}$$

The flow $\partial_t g_{3,k}$ is defined below in (C.45).

For the definition of the three-point function $g_{1,k}$ we choose the $\rho\pi\pi$ vertex and find:

$$\begin{aligned}\partial_t\big|_\varphi g_{1,k} = \frac{-i}{2N_f(N_f^2-1)} \lim_{p\to 0}\frac{\partial^2}{\partial p^2}\mathrm{Tr}\left(p_\mu \epsilon_{ijk}\frac{\delta^3\partial_t\Gamma_k}{\delta\rho_i^\mu(-p)\delta\pi_j(p)\delta\pi_k(0)}\right)\Bigg|_{\Phi=\Phi_0}\\ + \sigma^2_{0,k}\partial_t\left(\frac{g_{1,k}g_{2,k}}{m^2_{a_1,k}}\right) - g_{2,k}\sigma_{0,k}\dot{C}_k\,.\end{aligned} \tag{C.44}$$

As we have discussed in Sec. 5.2.2, the elimination of the π–a_1 mixing leads to two types of modifications of the $\rho\pi\pi$ vertex. The first stems from the modifications of the action due to the replacement (5.30) and leads to a modification of this vertex given by (5.32). The first term in the third line of (C.44) cancels the additional term in the flow to ensure that we compute the flow of $g_{1,k}$ and not of (5.32). The second modification stems from the scale dependence of a_1 that is introduced by (5.30). This leads to the second term in the third line of (C.44) which follows from (5.26).

We define the couplings $g_{2,k}$ and $g_{3,k}$ via the flow

$$\partial_t g_{2/3,k} = \lim_{p\to 0}\mathrm{Tr}\left(\delta_{\mu\nu}\mathbb{P}^{ijkl}_{g_{2/3}}\frac{\delta^4\partial_t\dot{\Gamma}_k}{\delta\pi_i\delta\pi_j\delta\rho_k^\mu\delta\rho_k^\nu}\right)\Bigg|_{\Phi=\Phi_0}, \tag{C.45}$$

with the projection operator for $g_{2,k}$

$$\mathbb{P}^{ijkl}_{g_2} = \frac{1}{4N_f(N_f^2+1)}\left(\frac{1}{N_f^2-1}\delta_{ij}\delta_{kl} - \delta_{ik}\delta_{jl}\right), \tag{C.46}$$

and the projection operator for $g_{3,k}$

$$\mathbb{P}^{ijkl}_{g_3} = \frac{1}{4(N_f^4+1)}\left(\frac{1}{2}\delta_{ij}\delta_{kl} + \delta_{ik}\delta_{jl}\right). \tag{C.47}$$

The vector meson self-interactions $g_{4,k}$ and $g_{5,k}$ are defined as

$$\partial_t g_{4,k} = \frac{-i}{6N_f(N_f^2-1)}\lim_{p\to 0}\frac{\partial^2}{\partial p^2}\mathrm{Tr}\left(p_\alpha\delta_{\beta\gamma}\epsilon_{ijk}\frac{\delta^3\partial_t\dot{\Gamma}_k}{\delta\rho_i^\alpha(p)\delta\rho_j^\beta(-p)\delta\rho_k^\gamma(0)}\right)\Bigg|_{\Phi=\Phi_0}, \tag{C.48}$$

and

$$\partial_t g_{5,k} = \frac{1}{24N_f(N_f^2-1)}\lim_{p\to 0}\mathrm{Tr}\left(\delta_{\alpha\beta}\delta_{\gamma\delta}\delta_{ij}\delta_{kl}\frac{\delta^4\partial_t\dot{\Gamma}_k}{\delta\rho_i^\alpha\delta\rho_j^\beta\delta\rho_k^\gamma\delta\rho_l^\delta}\right)\Bigg|_{\Phi=\Phi_0}. \tag{C.49}$$

Finally, we discuss the wave function renormalizations. As mentioned before, in a RG-invariant formulation they enter the flow equations only via the corresponding anomalous dimensions (C.20). The ghost anomalous dimension and the gauge part of the gluon anomalous dimension are discussed in Sec. 4.3. the quark contribution to the gluon anomalous dimension $\Delta\eta_{A,k}$, i.e. the vacuum polarization, is computed in App. C.2.

The quark anomalous dimension is computed from

$$\eta_{q,k} = \frac{-1}{8N_f N_c Z_{q,k}} \lim_{p\to 0} \frac{\partial^2}{\partial p^2} \mathrm{Tr}\left(\gamma_\mu p_\mu \frac{\delta^2 \partial_t \dot{\Gamma}_k}{\delta \bar{q}(p) \delta q(-p)} \right)\Big|_{\Phi=\Phi_0}, \tag{C.50}$$

where contraction of external color, flavor, and spinor indices is understood.

The scalar meson anomalous dimension $\eta_{S,k}$ has to be defined via the pion-pion two-point function. Using the sigma meson two-point function leads to additional contributions to the flow with couplings that correspond to a higher order derivative expansion. We define the anomalous dimension for scale-independent fields as

$$\eta_{S,k}\big|_\phi = \frac{-1}{2(N_f^2-1) Z_{S,k}} \lim_{p\to 0} \frac{\partial^2}{\partial p^2} \mathrm{Tr}\left(\delta_{ij} \frac{\delta^2 \partial_t \dot{\Gamma}_k}{\delta \pi_i(p) \delta \pi_j(-p)} \right)\Big|_{\Phi=\Phi_0}. \tag{C.51}$$

It receives modifications from the scale dependence of a_1 from the elimination of the $\pi - a_1$ mixing. The full anomalous dimension then is

$$\eta_{S,k} = \eta_{S,k}\big|_\phi - \bar{g}_{2,k} \bar{\sigma}_{0,k} \dot{\bar{C}}_k \tag{C.52}$$

where the second term follows from (5.26). We use the rho meson to define the vector meson anomalous dimension and find

$$\eta_{V,k} = \frac{-1}{6(N_f^2-1) Z_{V,k}} \lim_{p\to 0} \frac{\partial^2}{\partial p^2} \mathrm{Tr}\left(\delta_{ij} \delta^{\mu\nu} \frac{\delta^2 \partial_t \dot{\Gamma}_k}{\delta \rho_i^\mu(p) \delta \rho_j^\nu(-p)} \right)\Big|_{\Phi=\Phi_0}. \tag{C.53}$$

We emphasize that due to chiral symmetry the definition of the mesonic couplings in terms of n-point functions is not unique. We have explicitly checked that different projection procedures give the same results as long as they are equivalent by chiral symmetry. However, some caution is advised since seemingly equivalent definitions may give different results. The reason in those cases is that that inappropriate projections may contaminate the flows with contributions that are not part of the truncation. For example, a definition of ν_k via the sigma meson four-point function instead of (C.40) gives additional contributions from diagrams that are related to the flow of the 6-meson interaction. Another example is $\eta_{S,k}$, which is mentioned above (C.51). To find appropriate projection procedures one therefore has to keep extended truncations, such as general field-dependent couplings, in mind.

C.4. In-Medium Flows of the Matter Sector

In the flow equations in section Chap. 7 we used threshold functions which contain the momentum integration, the summation over the Matsubara modes and the regulator dependence of the propagators of our model.

We use the following definitions for the meson and quark propagators:

$$\begin{aligned} G_\phi(\bar{m}^2_{\phi,k}) &= \frac{1}{z_{\phi,k}\,\omega_n^2/k^2 + x\,(1+r_B(x)) + \bar{m}^2_{\phi,k}}, \\ G_q(\bar{m}^2_{q,k}) &= \frac{1}{z^2_{q,k}(\nu_n + i\mu)^2/k^2 + x\,(1+r_F(x))^2 + \bar{m}^2_{q,k}}, \end{aligned} \tag{C.54}$$

where $x = \vec{q}^{\,2}/k^2$, $\omega_n = 2\pi n T$ is the bosonic Matsubara frequency and $\nu_n = 2\pi\left(n+\frac{1}{2}\right)T$ is the fermionic Matsubara frequency. $z_{\phi,k} = Z^{\parallel}_{\phi,k}/Z^{\perp}_{\phi,k}$ and $z_{q,k} = Z^{\parallel}_{q,k}/Z^{\perp}_{q,k}$ give the ratios of the wave function renormalizations parallel and perpendicular to the heat bath. Within our approximations this ratio is one, $z_{\phi,k} = z_{q,k} = 1$.

We use the following regulators for mesons and quarks:

$$\begin{aligned} R^{\phi}_k &= Z_{\phi,k}\,\vec{q}^{\,2}\,r_B(x), \\ R^{q}_k &= Z_{q,k}\,\vec{\gamma}\vec{q}\,r_F(x). \end{aligned} \tag{C.55}$$

We use optimized regulator shape functions $r_{B/F}(x)$ [149] in this work:

$$\begin{aligned} r_B(x) &= \left(\frac{1}{x}-1\right)\Theta(1-x), \\ r_F(x) &= \left(\frac{1}{\sqrt{x}}-1\right)\Theta(1-x). \end{aligned} \tag{C.56}$$

This choice of regulator shape functions allows us to evaluate momentum integrals and Matsubara summation analytically.

The functions $l_0^{(B/F,d)}$ in d space-time dimensions that appear in equations (7.12) and (7.23) are related to bosonic/fermionic loops and are defined as follows:

$$\begin{aligned} l_0^{(B,d)}(\bar{m}^2_{\phi,k}, \eta_{\phi,k}; T) &= \frac{T}{2k}\sum_{n\in\mathbb{Z}}\int dx\, x^{\frac{d-1}{2}}\left(\partial_t r_B(x) - \eta_{\phi,k} r_B(x)\right) G_\phi(\bar{m}^2_{\phi,k}) \\ &= \frac{2}{d-1}\frac{1}{\sqrt{z_{\phi,k}(1+\bar{m}^2_{\phi,k})}}\left(1-\frac{\eta_{\phi,k}}{d+1}\right)\left(\frac{1}{2}+n_B(T,\bar{m}^2_{\phi,k})\right), \end{aligned} \tag{C.57}$$

and

$$\begin{aligned} l_0^{(F,d)}(\bar{m}^2_{q,k}, \eta_{q,k}; T, \mu) &= \frac{T}{k}\sum_{n\in\mathbb{Z}}\int dx\, x^{\frac{d-1}{2}}\left(\partial_t r_F(x) - \eta_{q,k} r_F(x)\right)(1+r_F(x)) G_q(\bar{m}^2_{q,k}) \\ &= \frac{1}{d-1}\frac{1}{\sqrt{z^2_{q,k}(1+\bar{m}^2_{q,k})}}\left(1-\frac{\eta_{q,k}}{d}\right) \\ &\quad\times\left[1-n_F(T,\mu,\bar{m}^2_{q,k})-n_F(T,-\mu,\bar{m}^2_{q,k})\right], \end{aligned} \tag{C.58}$$

where n_B and n_F are the Bose- and Fermi distribution respectively:

$$\begin{aligned} n_B(T,\bar{m}^2_{\phi,k}) &= \frac{1}{\exp\left(\frac{k}{T}\sqrt{(1+\bar{m}^2_{\phi,k})/z_{\phi,k}}\right)-1} \\ n_F(T,\mu,\bar{m}^2_{q,k}) &= \frac{1}{\exp\left(\frac{k}{T}\left(\sqrt{(1+\bar{m}^2_{q,k})/z^2_{q,k}}-\frac{\mu}{k}\right)\right)+1}. \end{aligned} \tag{C.59}$$

The threshold functions $l_n^{(B/F,d)}$ which represent loops with $(n+1)$ bosons/fermions are defined via:

$$\frac{\partial}{\partial m^2} l_n^{(B/F,d)}(m^2) = -(n+\delta_{n0}) l_{n+1}^{(B/F,d)}(m^2). \tag{C.60}$$

The threshold functions that appear in (7.23) are related to loops with fermion- as well as boson-propagators and are defined as

$$\begin{aligned} L_{(1,1)}^{(d)}\left(\bar{m}_{q,k}^2, \bar{m}_{\phi,k}^2, \eta_{q,k}, \eta_{\phi,k}; T, \mu\right) = \frac{T}{2k} \sum_{n\in\mathbb{Z}} \int dx\, x^{\frac{d-1}{2}} \Big[\left(\partial_t r_B(x) - \eta_{\phi,k} r_B(x)\right) \\ \times G_\phi^2(\bar{m}_{\phi,k}^2) G_q(\bar{m}_{q,k}^2) + 2(1+r_F(x)) \\ \times \left(\partial_t r_F(x) - \eta_{q,k} r_F(x)\right) G_\phi(\bar{m}_{\phi,k}^2) G_q^2(\bar{m}_{q,k}^2) \Big]. \end{aligned} \tag{C.61}$$

By using the optimized regulator shape functions we can perform the integration and summation analytically and find:

$$L_{(1,1)}^{(d)}\left(\bar{m}_{q,k}^2, \bar{m}_{\phi,k}^2, \eta_{q,k}, \eta_{\phi,k}; T, \mu\right) = \frac{2}{d-1}\left[\left(1-\frac{\eta_{\phi,k}}{d+1}\right)\mathscr{FB}_{(1,2)} + \left(1-\frac{\eta_{q,k}}{d}\right)\mathscr{FB}_{(2,1)}\right], \tag{C.62}$$

where we defined the function

$$\mathscr{FB}_{(1,1)}\left(\bar{m}_{q,k}^2, \bar{m}_{\phi,k}^2; T, \mu\right) = \frac{T}{k} \operatorname{Re}\left[\sum_{n\in\mathbb{Z}} G_q(\bar{m}_{q,k}^2) G_\phi(\bar{m}_{\phi,k}^2)\right] \tag{C.63}$$

$$\begin{aligned} &= \operatorname{Re}\Bigg\{ \frac{1}{2\sqrt{1+\bar{m}_{\phi,k}^2}} \left(n_B(T, \bar{m}_{\phi,k}^2) + \frac{1}{2}\right) \Bigg[\frac{1}{\bar{m}_{q,k}^2 + 1 - \left(\mu/k - i\pi T/k - \sqrt{1+\bar{m}_{\phi,k}^2}\right)^2} \\ &\quad + \frac{1}{\bar{m}_{q,k}^2 + 1 - \left(\mu/k - i\pi T/k + \sqrt{1+\bar{m}_{\phi,k}^2}\right)^2} \Bigg] \\ &\quad - \frac{1}{2\sqrt{1+\bar{m}_{q,k}^2}} \left(n_F(T, \mu, \bar{m}_{q,k}^2) - \frac{1}{2}\right) \frac{1}{\bar{m}_{\phi,k}^2 + 1 - \left(\mu/k - i\pi T/k - \sqrt{1+\bar{m}_{q,k}^2}\right)^2} \\ &\quad - \frac{1}{2\sqrt{1+\bar{m}_{q,k}^2}} \left(n_F(T, -\mu, \bar{m}_{q,k}^2) - \frac{1}{2}\right) \times \frac{1}{\bar{m}_{\phi,k}^2 + 1 - \left(\mu/k - i\pi T/k + \sqrt{1+\bar{m}_{q,k}^2}\right)^2} \Bigg\}. \end{aligned}$$

These mixed diagrams are responsible for the complex valued Yukawa coupling and quark anomalous dimension, see section 3.2. It is therefore sufficient to consider only the real part of this contributions in order to render those functions real.

The functions $\mathscr{FB}_{(m,n)}$ which represent the Matsubara summation of loops with m fermion propagators and n boson propagators can be obtained from $\mathscr{FB}_{(1,1)}$ by differentiation with respect to the masses:

$$\begin{aligned} \frac{\partial}{\partial \bar{m}_{q,k}^2} \mathscr{FB}_{(m,n)} &= -m\, \mathscr{FB}_{(m+1,n)} \\ \frac{\partial}{\partial \bar{m}_{\phi,k}^2} \mathscr{FB}_{(m,n)} &= -n\, \mathscr{FB}_{(m,n+1)}. \end{aligned}$$

The function $\mathscr{B}\mathscr{B}$ encodes the Matsubara summation of loops with two different meson propagators are defined as:

$$\begin{aligned}\mathscr{B}\mathscr{B}_{(1,1)}(\bar{m}^2_{\phi_1,k},\bar{m}^2_{\phi_2,k};T,\mu) &= \frac{T}{k}\sum_{n\in\mathbb{Z}} G_\phi(\bar{m}^2_{\phi_1,k})G_\phi(\bar{m}^2_{\phi_2,k}) \\ &= \frac{1}{(\bar{m}^2_{\phi_2,k}-\bar{m}^2_{\phi_1,k})\sqrt{1+\bar{m}^2_{\phi_1,k}}}\left(n_B(\bar{m}^2_{\phi_1,k})+\frac{1}{2}\right) \\ &\quad + \frac{1}{(\bar{m}^2_{\phi_1,k}-\bar{m}^2_{\phi_2,k})\sqrt{1+\bar{m}^2_{\phi_2,k}}}\left(n_B(\bar{m}^2_{\phi_2,k})+\frac{1}{2}\right),\end{aligned} \tag{C.64}$$

and

$$\begin{aligned}\frac{\partial}{\partial\bar{m}^2_{\phi_1,k}}\mathscr{B}\mathscr{B}_{(m,n)} &= -m\,\mathscr{B}\mathscr{B}_{(m+1,n)} \\ \frac{\partial}{\partial\bar{m}^2_{\phi_2,k}}\mathscr{B}\mathscr{B}_{(m,n)} &= -n\,\mathscr{B}\mathscr{B}_{(m,n+1)}.\end{aligned} \tag{C.65}$$

The Matsubara summation of loops with several identical fermions is encoded in:

$$\begin{aligned}\mathscr{F}_{(1)}(\bar{m}^2_{q,k};T,\mu) &= \frac{T}{k}\sum_{n\in\mathbb{Z}} G_q(\bar{m}^2_{q,k}) \\ &= \frac{1}{2\sqrt{1+\bar{m}^2_{q,k}}}\left[1-n_F(T,\mu,\bar{m}^2_{q,k})-n_F(T,-\mu,\bar{m}^2_{q,k})\right]\end{aligned} \tag{C.66}$$

and

$$\frac{\partial}{\partial\bar{m}^2_{q,k}}\mathscr{F}_{(n)} = -n\,\mathscr{F}_{(n+1)}. \tag{C.67}$$

Note that this function is implicitly contained in the threshold function $l_n^{(F,d)}$ that appears in the flow of the effective potential.

APPENDIX D

IR Strength

In our study, we introduced an “infrared-strength" function $\varsigma_{a,b}(k)$ which we define as

$$\varsigma_{a,b}(k) = 1 + a\,\frac{(k/b)^{\delta}}{e^{(k/b)^{\delta}} - 1}\,, \tag{D.1}$$

with $b > 0$ and $\delta > 0$. Note that the specific form of $\varsigma_{a,b}(k)$ is irrelevant for our result as long as it has the properties specified below. It defines a smooth step function centered around b with interpolates smoothly between

$$\varsigma_{a,b}(k \gg b) = 1 \quad \text{and} \quad \varsigma_{a,b}(k \ll b) = 1 + a\,. \tag{D.2}$$

Thus, for $b = \mathcal{O}(1\,\text{GeV})$, $\varsigma_{a,b}(k)$ gives an IR-enhancement, while it leaves the perturbative regime unaffected. We then modify the gauge couplings as

$$g_{s,k} \longrightarrow \varsigma_{a,b}(k)\, g_{s,k}, \tag{D.3}$$

where $g_{s,k} = g_{\bar{q}Aq,k}\,, g_{A^3,k}\,, g_{\bar{c}Ac,k}$. We choose the same parameters a and b for every gauge coupling. Accordingly, the flow equations of the gauge couplings then are

$$\partial_t g_{s,k} \longrightarrow g_{s,k}\,\partial_t \varsigma_{a,b}(k) + \varsigma_{a,b}(k)\,\partial_t g_{s,k}. \tag{D.4}$$

We have found that our results do not depend strongly on the precise value of b as long as it is $\mathcal{O}(1\,\text{GeV})$. For much smaller values, the modification (D.3) has no effect, since the glue sector decouples and for much larger values it spoils the perturbative running of the gauge couplings. To be specific, we choose $b = 1.3\,\text{GeV}$ for $\delta = 3$ in the following.

The parameter a is adjusted such that we get physical constituent quark masses in the infrared, $M_{q,0} = 300\,\text{MeV}$.

Since the results in Ref. [156] demonstrate that the largest source for systematic errors of our truncation is rooted in the approximations that enter the flows of the gauge couplings, a procedure as discussed above is well-justified.

APPENDIX E

Implications of Convexity on the Quark Mass

Here we present the detailed discussion of the results outlined in Section 7.2.4. The following is short of a full proof which is beyond the scope of the present work. Here we are rather interested in an explanation of the properties of the solution found in the present work. Nonetheless the present analysis outlines the complete analysis necessary for the full proof.

For finite k there is a region $\rho < \rho_s \leq \rho_0$ where all the curvature masses $\bar{m}^2$ in (7.14) are negative,

$$-1 < \frac{V_k'(\rho)}{k^2} < 0 \quad \text{and} \quad -1 < \frac{V_k'(\rho) + 2\rho V''(\rho)}{k^2} < 0\,, \tag{E.1}$$

for $\bar{m}^2_{k,\pi}$ and $\bar{m}^2_{k,\sigma}$ respectively. Note that the pion mass, $\bar{m}^2_{k,\pi}$, is already negative for $\rho < \rho_0$. At the lower bound, $\bar{m}^2_{k,\sigma/\pi} = -1$, the flow exhibits a singularity. However, due to the convexity-restoring property of the flow arranges this bound is never saturated and convexity is approached smoothly for $k \to 0$, see [201]. This formal property has the practical consequence that it i.e. implies for the flow of $m^2_{k,\pi}$ derived from (7.12) that

$$\begin{aligned}
&\lim_{k\to 0} \partial_t \bar{m}^2_{\pi,k} = \lim_{k\to 0} \partial_t \frac{V_k'(\rho < \rho_0)}{k^2} \\
&= -\frac{1}{4\pi^2}\Big[3\partial_\rho m^2_{\pi,k}\, l_1^{(B,4)}(\bar{m}^2_{\pi,k}) + \partial_\rho m^2_{\sigma,k}\, l_1^{(B,4)}(\bar{m}^2_{\sigma,k}) \\
&\quad -4N_c N_f\, \partial_\rho m^2_{q,k}\, l_1^{(F,4)}(\bar{m}^2_{q,k}) \Big] - 2\,\bar{m}^2_{\pi,k} = 0\,.
\end{aligned} \tag{E.2}$$

The subscript l_1 in the threshold functions indicates the derivative w.r.t. the respective $\bar{m}^2$, see App. C.4. Here and in the following we omit the dependence on the anomalous dimensions, the temperature and the chemical potential of the threshold functions for the sake of legibility. Note that seemingly also $\lim_{k\to 0} \partial_t \bar{m}^2 < 0$ is allowed but then $\bar{m}^2$ eventually becomes positive which signals the symmetric phase.

First we note that the fermionic contribution in the last line of (E.2) vanishes in the limit $k \to 0$: For finite quark mass function, $m^2_{q,k\to 0} > 0$, the threshold function vanishes, $l_1^{(F,4)} \propto (m_q^2)^{-3/2}$, with cubic powers of k. In turn, for vanishing quark mass function, $m^2_{q,k} \propto k^\gamma \to 0$ for $k \to 0$,

and $\partial_\rho m^2_{q,k\to 0} = 0$ (no oscillation of $m^2_{q,k\to 0}$ with period ρ/k^γ), the threshold function stays finite, $l_1^{(F,4)}(m_q^2) < l_1^{(F,4)}(0) = 1/3$. In either case the fermionic contribution vanishes.

Hence, in the limit $k \to 0$ and for $\rho < \rho_0$ the flow of the mesonic effective potential is dominated by the mesonic fluctuations and reduces to that of an $O(4)$-model. Self-consistency of the constraint (E.2), the similar one for $\bar{m}^2_{k,\sigma}$, and (E.1) leads to

$$\lim_{k\to 0} \frac{1}{1+\bar{m}^2_{\sigma/\pi,k}(\rho<\rho_s)} = \frac{c_{\sigma/\pi}(\rho)}{k^{2+\alpha}} > 0\,, \tag{E.3}$$

with some constant $c_{\sigma/\pi}$ and $\alpha > 0$, and

$$\partial_\rho m^2_{\sigma/\pi}(\rho<\rho_s) \propto k^{4+\alpha}\,, \tag{E.4}$$

where we have assumed that the dominant sub-leading terms in $\bar{m}^2$ carry a ρ-dependence. The threshold function $l_1^{(B,4)}$ scales with $(1+\bar{m}^2)^{-3/2}$ and hence we conclude that

$$\alpha = 2\,, \tag{E.5}$$

in line with the full analytic derivations in [208]. Eq. (E.1) already induces a scaling of $\partial_\rho m^2_{\sigma,\pi}(\rho<\rho_s)$ with at least k^2 in the absence of oscillations in $\bar{m}^2$ with period ρ/k^2. The lack of these oscillations can indeed be proven but the details of this proof are beyond the scope of the present work [1]. The flow contributions in (E.2) have to cancel the order k^0 contributions in $2\bar{m}^2_\pi$. This requires diverging threshold functions leading to (E.4) which implies $\bar{m}^2_{\sigma/\pi} = -1 + O(k^2)$. In turn this leads to the same constant c in (E.3) for σ and $\vec{\pi}$ respectively. Eq. (E.3) reflects the fact that the convexity restoring property of the flow is driven by the denominators of the threshold functions being close to the singularity.

For the behavior of the fermionic two-point function $\Gamma_{q,k}$ in the broken phase for $|\phi| \le |\phi_0|$, we resort to a more general argument. Its flow is dominated by the diagrams with mesonic cutted lines: the lines with regulator insertions are proportional to the mesonic propagators squared, $G_{\phi,k}$, and hence diverge for $k \to 0$. Moreover, the fermionic propagator obeys the flow equation

$$\begin{aligned}\partial_t G_{q,k}[\Phi](p) &= -\frac{1}{2}\mathrm{Tr}\left[G_k\,\partial_t R_k\,G_k\,\frac{\delta^2}{\delta\Phi^2}\right]G_{q,k}[\Phi](p)\\ &\quad -\left(G_{q,k}\,\partial_t R_k^q\,G_{q,k}\right)[\Phi](p)\,,\end{aligned} \tag{E.6}$$

where $\Phi = (q, \bar{q}, \phi)$, see [139]. For momenta $p^2 \gg k^2$, $|\phi| \le |\phi_0|$, and $k \to 0$ this reduces to

$$\partial_t \frac{1}{\Gamma^{(2)}_{q,k}[\phi](p)} = -\frac{1}{2}\mathrm{Tr}\,G_{\phi,k}\,\partial_t R_k^\phi\,G_{\phi,k}\,\frac{\delta^2}{\delta\phi^2}\frac{1}{\Gamma^{(2)}_{q,k}[\phi](p)}\,, \tag{E.7}$$

where we have set $q = \bar{q} = 0$, and $R_k(p^2 \gg k^2) \approx 0$. The full fermionic two-point correlation function in the background of constant mesonic fields ϕ reads

$$\Gamma^{(2)}_{q,k}[\phi](p) = Z_q(\rho,p^2)\left(\not{p} + i\bar{h}(\rho,p^2)[\sigma - i\gamma_5\vec{\tau}\vec{\pi}]\right). \tag{E.8}$$

[1] Such an oscillation may be generated by an inadequate numerical implementation.

at vanishing chemical potential, $\mu = 0$. In (E.8) we have dropped the k-subscripts in Z and $\bar{h}$ for the sake of conciseness. Hence the full propagator in the background of constant mesonic fields ϕ is expanded as

$$\frac{1}{\Gamma^{(2)}_{q,k}[\phi](p)} = A(\rho,p^2)\,\not{p} + B(\rho,p^2)(\sigma\mathbb{1} + i\gamma_5\vec{\tau}\vec{\pi})\,, \tag{E.9}$$

where the coefficient functions A, B depend on both, Z and h,

$$\begin{aligned} A(\rho,p^2) &= \frac{1}{Z_q(\rho,p^2)\left(p^2 + 2\bar{h}(\rho,p^2)^2\rho\right)}, \\ B(\rho,p^2) &= A(\rho,p^2)\bar{h}(\rho,p^2) \end{aligned} \tag{E.10}$$

Finally this leads to the differential equations

$$\begin{aligned} \partial_t A(\rho,p^2) &= -\Big[N_\pi g_{\pi,k}(\rho)\,\partial_\rho \\ &\qquad + g_{\sigma,k}(\rho)\left(\partial_\rho + 2\rho\partial_\rho^2\right)\Big]A(\rho,p^2), \end{aligned} \tag{E.11a}$$

$$\begin{aligned} \partial_t B(\rho,p^2) &= -\Big[N_\pi g_{\pi,k}(\rho)]\,\partial_\rho \\ &\qquad + g_{\sigma,k}(\rho)\left(3\partial_\rho + 2\rho\partial_\rho^2\right)\Big]B(\rho,p^2), \end{aligned} \tag{E.11b}$$

where N_π is the number of pions, in the present $N_f = 2$ case we have $N_\pi = 3$. The $g_{\sigma/\pi,k}$ are the scalar parts of the operator $G_{\phi,k}\,\partial_t R^\phi_k\,G_{\phi,k}$ projected on the σ-meson and pion respectively.

$$g_{\sigma/\pi,k}(\rho) = \frac{1}{2}\left[G_k\,\partial_t R_k\,G_k\right]_{\sigma\sigma/\pi\pi}(\rho) > 0\,, \tag{E.12}$$

For $\rho < \rho_0$ $g_{\pi,k}$ diverges in the limit $k \to 0$, while $g_{\sigma,k}$ diverges for $\rho < \rho_s$,

$$g_{\pi,k}(\rho < \rho_0) \to \infty\,, \qquad g_{\sigma,k}(\rho < \rho_s) \to \infty\,, \tag{E.13}$$

Moreover, in the respective divergence regimes the $g_{\sigma/\pi,k}$ do not depend on the fermionic propagator in leading order. Hence is an external input for the differential equations (E.11). It is here where the decoupling of the (leading part of the) flow equation for the effective potential from the fermionic diagrams comes handy.

For a general class of $g_{\phi,k}$ the differential equations for $A(\rho,p^2)$, $B(\rho,p^2)$ have simple, attractive fixed point solutions for $k \to 0$ and $\rho < \rho_0$,

$$\partial_\rho A_{k=0}(\rho,p^2) = 0\,, \qquad \partial_\rho B_{k=0}(\rho,p^2) = 0\,. \tag{E.14}$$

It is also easily seen that for non-trivial positive boundary conditions the coefficient functions A, B approach constants given by their values at the minimum ϕ_0 in terms of $Z_q(\phi_0,p^2)$ and $\bar{h}(\phi_0,p^2)$. This entails that

$$\bar{h}(\rho \le \rho_0,p^2) = \bar{h}(\rho_0,p^2) \tag{E.15}$$

and hence

$$Z_q(\rho \le \rho_0,p^2) = Z_q(\rho_0,p^2)\frac{p^2 + 2\bar{h}(\rho_0,p^2)^2\rho_0}{p^2 + 2\bar{h}(\rho_0,p^2)^2\rho}\,. \tag{E.16}$$

Note that the prefactor $Z_q(\rho_0, p^2)$, evaluated at $p = 0$, is nothing but the wave function renormalization used in the present work for the deduction of physical quantities. This full solution entails a mass gap for the quark propagator in the broken phase: for non-vanishing momentum $p \neq 0$ the propagator trivially has no pole. For $p = 0$ the wave function renormalization is given by

$$Z_q(\rho \leq \rho_0, 0) = Z_q(\phi_0, 0)\frac{\rho_0}{\rho}\,. \tag{E.17}$$

In (E.17) we have used that both, $\bar{h}(\rho_0, 0)^2 > 0$ and $Z_q(\rho \leq \rho_0, 0) > 0$, which follows from the analysis done here. With (E.8) this leads to

$$\Gamma^{(2)}_{q,k=0}[\phi](p = 0) = i\, Z_q(\rho_0, 0)\bar{h}(\rho_0, 0)\rho_0\frac{\sigma - i\gamma_5\vec{\tau}\vec{\pi}}{\rho}\,. \tag{E.18}$$

The norm of (E.18) is the ρ-dependent mass-gap of the propagator and is read-off from (E.18) as

$$\bar{m}_q^2(\rho \leq \rho_0) = \frac{\|\Gamma^{(2)}_{q,k=0}[\phi](p = 0)\|^2}{Z_q(\rho_0, 0)^2} = \sqrt{2\rho_0}\bar{h}(\rho_0, 0)\frac{\rho_0}{\rho}\,. \tag{E.19}$$

We conlude that the field-dependent mass gap is minimized on the equations of motion, $\rho = \rho_0$ and

$$m_q^2(\rho \leq \rho_0) \geq m^2_{q,\mathrm{gap}} > 0\,. \tag{E.20}$$

Note also that the present scaling analysis is readily extended to finite temperatures and densities. It also entails that the present Taylor expansion in the mesonic field with fixed expansion point and at $p = 0$ is sufficient to extract the physics information. However, it cannot in general reproduce the asymptotic behavior for $k \to 0$ and $\rho < \rho_0$ at one of the necessary condition for the full analysis, $p \gg k$, does not hold.

The above arguments can also be applied to the mesonic propagators for $k^2 \ll p^2 \ll m_\sigma^2$ with the parameterization (at $\vec{\pi} = 0$)

$$\mathscr{P}_{\sigma/\pi}(\rho, p^2) = \frac{1}{Z_\phi(\rho, p^2)\left(p^2 + m^2_{\sigma/\pi}(\rho)\right)}\,, \tag{E.21}$$

where $m^2_{\sigma/\pi,k}(\rho)$ does not depend on momentum. Following the arguments used for deriving the flows (E.11) for the coefficient functions of the fermionic propagator we are led to the flow

$$\begin{aligned}\partial_t\mathscr{P}_{\sigma/\pi}(\rho, p^2) \;&=\\ &-\Big[N_\pi g_{\pi,k}(\rho)\,\partial_\rho + g_{\sigma,k}(\rho)\left(\partial_\rho + 2\rho\,\partial_\rho^2\right)\Big]\mathscr{P}_{\sigma/\pi}(\rho, p^2)\,,\end{aligned} \tag{E.22}$$

For $\rho < \rho_s$ we have $m^2_{\sigma/\pi} < 0$ (but $p^2 + m^2_{\sigma/\pi} > 0$) and both masses vanish in the limit $k \to 0$. We therefore conclude that

$$m^2_{\sigma/\pi}(\rho < \rho_0) = 0\,, \qquad Z_\phi(\rho < \rho_0, p^2) = Z_\phi(0, p^2)\,. \tag{E.23}$$

At $\rho = \rho_0$ there is a discontinuity as m_σ^2 jumps to its physical value.

Danksagung

Mein besonderer Dank gilt meinem Doktorvater Jan Martin Pawlowski. Seine physikalische Einsicht und die Bereitschaft, diese stets großzügig und lebhaft zu teilen, waren eine große Inspiration und haben sowohl zu meiner Entwicklung als auch zur Entwicklung dieser Arbeit während der vergangenen Jahre maßgeblich beigetragen. Er versteht es, ein äußerst angenehmes Arbeitsklima zu erzeugen, wodurch die unendlich vielen Diskussionen privat und innerhalb der Arbeitsgruppe mir immer eine große Freude waren.

Prof. Jürgen Berges danke ich für die freundliche Übernahme der Zweitkorrektur dieser Arbeit.

Für zahlreiche Diskussionen und eine fruchtbare Zusammenarbeit danke ich Jens Braun, Leonard Fister, Lisa Marie Haas, Naseemuddin Khan, Mario Mitter, Michael Scherer und Nils Strodthoff.

Meinen Kollegen am Institut für Theoretische Physik ist es zu verdanken, dass ich eine großartige Zeit während meiner Doktorarbeit hatte. Dabei hat vorallem die Besetzung des Dachzimmers stets zuverlässig für die nötige Zerstreuung gesorgt. Besonders hervorheben möchte ich Igor Böttcher und Nicolai Christiansen, denen ich für die unzähligen Diskussionen und den gemeinsamen Unsinn sehr dankbar bin.

Der Nuclear Theory Group des Brookhaven National Laboratory, wo ich einen produktiven Sommer verbringen durfte, danke ich für ihre Gastfreundschaft. Insbesondere danke ich Rob Pisarski für die angenehme Zusammenarbeit und die inspirierenden Gespräche. Der HGS-Hire, sowie dem ITP Heidelberg danke ich für die Finanzierung dieses Aufenthaltes.

Zuletzt möchte ich meiner Familie – insbesondere Felix, Gisela und Rolf Rennecke – für die bedingungslose Unterstützung in jeglicher Hinsicht danken.

Bibliography

[1] M. Gell-Mann, "Symmetries of baryons and mesons," *Phys.Rev.* **125** (1962) 1067–1084.

[2] M. Gell-Mann, "A Schematic Model of Baryons and Mesons," *Phys.Lett.* **8** (1964) 214–215.

[3] G. Zweig, "An SU(3) model for strong interaction symmetry and its breaking. Version 1," *CERN-TH-401* (1964) .

[4] G. Zweig, "An SU(3) model for strong interaction symmetry and its breaking. Version 2," *CERN-TH-412, NP-14146, PRINT-64-170* (1964) 22–101.

[5] C.-N. Yang and R. L. Mills, "Conservation of Isotopic Spin and Isotopic Gauge Invariance," *Phys.Rev.* **96** (1954) 191–195.

[6] O. Greenberg, "Spin and Unitary Spin Independence in a Paraquark Model of Baryons and Mesons," *Phys.Rev.Lett.* **13** (1964) 598–602.

[7] M. Han and Y. Nambu, "Three Triplet Model with Double SU(3) Symmetry," *Phys.Rev.* **139** (1965) B1006–B1010.

[8] H. Fritzsch, M. Gell-Mann, and H. Leutwyler, "Advantages of the Color Octet Gluon Picture," *Phys.Lett.* **B47** (1973) 365–368.

[9] W. A. Bardeen and R. Pearson, "Local Gauge Invariance and the Bound State Nature of Hadrons," *Phys.Rev.* **D14** (1976) 547.

[10] O. Greenberg and C. Nelson, "Color Models of Hadrons," *Phys.Rept.* **32** (1977) 69–121.

[11] D. J. Gross and F. Wilczek, "Ultraviolet Behavior of Nonabelian Gauge Theories," *Phys.Rev.Lett.* **30** (1973) 1343–1346.

[12] H. D. Politzer, "Reliable Perturbative Results for Strong Interactions?," *Phys.Rev.Lett.* **30** (1973) 1346–1349.

[13] R. Hagedorn, "Statistical thermodynamics of strong interactions at high-energies," *Nuovo Cim.Suppl.* **3** (1965) 147–186.

[14] L. D. McLerran and B. Svetitsky, "Quark Liberation at High Temperature: A Monte Carlo Study of SU(2) Gauge Theory," *Phys.Rev.* **D24** (1981) 450.

[15] J. Engels, F. Karsch, H. Satz, and I. Montvay, "High Temperature SU(2) Gluon Matter on the Lattice," *Phys.Lett.* **B101** (1981) 89.

[16] G. Boyd, J. Engels, F. Karsch, E. Laermann, C. Legeland, *et al.*, "Thermodynamics of SU(3) lattice gauge theory," *Nucl.Phys.* **B469** (1996) 419–444, arXiv:hep-lat/9602007 [hep-lat].

[17] Y. Aoki, G. Endrodi, Z. Fodor, S. Katz, and K. Szabo, "The Order of the quantum chromodynamics transition predicted by the standard model of particle physics," *Nature* **443** (2006) 675–678, arXiv:hep-lat/0611014 [hep-lat].

[18] **Wuppertal-Budapest** Collaboration, S. Borsanyi *et al.*, "Is there still any T_c mystery in lattice QCD? Results with physical masses in the continuum limit III," *JHEP* **1009** (2010) 073, arXiv:1005.3508 [hep-lat].

[19] P. Petreczky, "Lattice QCD at non-zero temperature," *J.Phys.* **G39** (2012) 093002, arXiv:1203.5320 [hep-lat].

[20] T. Matsui and H. Satz, "J/ψ Suppression by Quark-Gluon Plasma Formation," *Phys.Lett.* **B178** (1986) 416.

[21] P. Braun-Munzinger, K. Redlich, and J. Stachel, "Particle production in heavy ion collisions," arXiv:nucl-th/0304013 [nucl-th]. To appear in Quark Gluon Plasma 3, eds. R.C. Hwa and Xin-Nian Wang, World Scientific Publishing.

[22] N. Brambilla, S. Eidelman, B. Heltsley, R. Vogt, G. Bodwin, *et al.*, "Heavy quarkonium: progress, puzzles, and opportunities," *Eur.Phys.J.* **C71** (2011) 1534, arXiv:1010.5827 [hep-ph].

[23] P. Braun-Munzinger, J. Stachel, and C. Wetterich, "Chemical freezeout and the QCD phase transition temperature," *Phys.Lett.* **B596** (2004) 61–69, arXiv:nucl-th/0311005 [nucl-th].

[24] J. Stachel, A. Andronic, P. Braun-Munzinger, and K. Redlich, "Confronting LHC data with the statistical hadronization model," *J.Phys.Conf.Ser.* **509** (2014) 012019, arXiv:1311.4662 [nucl-th].

[25] Y. Aoki, Z. Fodor, S. Katz, and K. Szabo, "The QCD transition temperature: Results with physical masses in the continuum limit," *Phys.Lett.* **B643** (2006) 46–54, arXiv:hep-lat/0609068 [hep-lat].

[26] M. Cheng, N. Christ, S. Datta, J. van der Heide, C. Jung, *et al.*, "The Transition temperature in QCD," *Phys.Rev.* **D74** (2006) 054507, arXiv:hep-lat/0608013 [hep-lat].

[27] P. de Forcrand and O. Philipsen, "The Chiral critical line of N(f) = 2+1 QCD at zero and non-zero baryon density," *JHEP* **0701** (2007) 077, arXiv:hep-lat/0607017 [hep-lat].

[28] **HotQCD** Collaboration, C. E. Detar and R. Gupta, "Toward a precise determination of T(c) with 2+1 flavors of quarks," *PoS* **LAT2007** (2007) 179, arXiv:0710.1655 [hep-lat].

[29] F. Karsch, "Recent lattice results on finite temperature and density QCD. Part II.," *PoS* **LAT2007** (2007) 015, arXiv:0711.0661 [hep-lat].

[30] A. Bazavov, T. Bhattacharya, M. Cheng, N. Christ, C. DeTar, *et al.*, "Equation of state and QCD transition at finite temperature," *Phys.Rev.* **D80** (2009) 014504, arXiv:0903.4379 [hep-lat].

[31] **CERES Collaboration** Collaboration, D. Adamova *et al.*, "Modification of the rho-meson detected by low-mass electron-positron pairs in central Pb-Au collisions at 158-A-GeV/c," *Phys.Lett.* **B666** (2008) 425–429, arXiv:nucl-ex/0611022 [nucl-ex].

[32] **NA60 Collaboration** Collaboration, R. Arnaldi *et al.*, "NA60 results on thermal dimuons," *Eur.Phys.J.* **C61** (2009) 711–720, arXiv:0812.3053 [nucl-ex].

[33] **STAR Collaboration** Collaboration, F. Geurts, "The STAR Dilepton Physics Program," *Nucl.Phys.* **A904-905** (2013) 217c–224c, arXiv:1210.5549 [nucl-ex].

[34] G. Brown and M. Rho, "Scaling effective Lagrangians in a dense medium," *Phys.Rev.Lett.* **66** (1991) 2720–2723.

[35] T. Hatsuda and S. H. Lee, "QCD sum rules for vector mesons in nuclear medium," *Phys.Rev.* **C46** (1992) 34–38.

[36] R. D. Pisarski, "Where does the rho go? Chirally symmetric vector mesons in the quark - gluon plasma," *Phys.Rev.* **D52** (1995) 3773–3776, arXiv:hep-ph/9503328 [hep-ph].

[37] R. Rapp, G. Chanfray, and J. Wambach, "Rho meson propagation and dilepton enhancement in hot hadronic matter," *Nucl.Phys.* **A617** (1997) 472–495, arXiv:hep-ph/9702210 [hep-ph].

[38] P. M. Hohler and R. Rapp, "Is ρ-Meson Melting Compatible with Chiral Restoration?," *Phys.Lett.* **B731** (2014) 103–109, arXiv:1311.2921 [hep-ph].

[39] GSI Darmstadt. https://www.gsi.de/en/start/fair/forschung_an_fair/kernmateriephysik.htm. (accessed April 2, 2015).

[40] M. A. Stephanov, K. Rajagopal, and E. V. Shuryak, "Signatures of the tricritical point in QCD," *Phys.Rev.Lett.* **81** (1998) 4816–4819, arXiv:hep-ph/9806219 [hep-ph].

[41] P. de Forcrand and O. Philipsen, "The curvature of the critical surface (m(u,d),m(s))**crit(mu): A Progress report," *PoS* **LATTICE2008** (2008) 208, arXiv:0811.3858 [hep-lat].

[42] R. Gavai and S. Gupta, "QCD at finite chemical potential with six time slices," *Phys.Rev.* **D78** (2008) 114503, arXiv:0806.2233 [hep-lat].

[43] S. Gupta, "Finding the critical end point of QCD: Lattice and experiment," *PoS* **CPOD2009** (2009) 025, arXiv:0909.4630 [nucl-ex].

[44] T. K. Herbst, J. M. Pawlowski, and B.-J. Schaefer, "The phase structure of the Polyakov–quark-meson model beyond mean field," *Phys.Lett.* **B696** (2011) 58–67, arXiv:1008.0081 [hep-ph].

[45] C. S. Fischer, J. Luecker, and J. A. Mueller, "Chiral and deconfinement phase transitions of two-flavour QCD at finite temperature and chemical potential," *Phys.Lett.* **B702** (2011) 438–441, arXiv:1104.1564 [hep-ph].

[46] T. K. Herbst, M. Mitter, J. M. Pawlowski, B.-J. Schaefer, and R. Stiele, "Exploring the Phase Structure and Thermodynamics of QCD," *PoS* **QCD-TNT-III** (2013) 030, arXiv:1401.1735 [hep-ph].

[47] C. S. Fischer, J. Luecker, and C. A. Welzbacher, "Locating the critical end point of QCD," *Nucl.Phys.* **A931** (2014) 774–779, arXiv:1410.0124 [hep-ph].

[48] K. Fukushima and T. Hatsuda, "The phase diagram of dense QCD," *Rept.Prog.Phys.* **74** (2011) 014001, arXiv:1005.4814 [hep-ph].

[49] B. C. Barrois, "Superconducting Quark Matter," *Nucl.Phys.* **B129** (1977) 390.

[50] D. Bailin and A. Love, "Superfluidity and Superconductivity in Relativistic Fermion Systems," *Phys.Rept.* **107** (1984) 325.

[51] M. G. Alford, K. Rajagopal, and F. Wilczek, "QCD at finite baryon density: Nucleon droplets and color superconductivity," *Phys.Lett.* **B422** (1998) 247–256, arXiv:hep-ph/9711395 [hep-ph].

[52] R. Rapp, T. Schaefer, E. V. Shuryak, and M. Velkovsky, "Diquark Bose condensates in high density matter and instantons," *Phys.Rev.Lett.* **81** (1998) 53–56, arXiv:hep-ph/9711396 [hep-ph].

[53] J. Berges and K. Rajagopal, "Color superconductivity and chiral symmetry restoration at nonzero baryon density and temperature," *Nucl.Phys.* **B538** (1999) 215–232, arXiv:hep-ph/9804233 [hep-ph].

[54] M. G. Alford, J. Berges, and K. Rajagopal, "Unlocking color and flavor in superconducting strange quark matter," *Nucl.Phys.* **B558** (1999) 219–242, arXiv:hep-ph/9903502 [hep-ph].

[55] M. G. Alford, J. A. Bowers, and K. Rajagopal, "Crystalline color superconductivity," *Phys.Rev.* **D63** (2001) 074016, arXiv:hep-ph/0008208 [hep-ph].

[56] R. D. Pisarski and D. H. Rischke, "A First order transition to, and then parity violation in, a color superconductor," *Phys.Rev.Lett.* **83** (1999) 37–40, arXiv:nucl-th/9811104 [nucl-th].

[57] R. D. Pisarski and D. H. Rischke, "Gaps and critical temperature for color superconductivity," *Phys.Rev.* **D61** (2000) 051501, arXiv:nucl-th/9907041 [nucl-th].

[58] D. Deryagin, D. Y. Grigoriev, and V. Rubakov, "Standing wave ground state in high density, zero temperature QCD at large N(c)," *Int.J.Mod.Phys.* **A7** (1992) 659–681.

[59] E. Shuster and D. Son, "On finite density QCD at large N(c)," *Nucl.Phys.* **B573** (2000) 434–446, arXiv:hep-ph/9905448 [hep-ph].

[60] T. Kojo, Y. Hidaka, L. McLerran, and R. D. Pisarski, "Quarkyonic Chiral Spirals," *Nucl.Phys.* **A843** (2010) 37–58, arXiv:0912.3800 [hep-ph].

[61] M. Buballa and S. Carignano, "Inhomogeneous chiral condensates," *Prog.Part.Nucl.Phys.* **81** (2015) 39–96, arXiv:1406.1367 [hep-ph].

[62] P. Chomaz, "The Nuclear liquid gas phase transition and phase coexistence: A Review," arXiv:nucl-ex/0410024 [nucl-ex].

[63] M. Creutz, *Quarks, Gluons and Lattices*. Cambridge University Press, 1984.

[64] I. Montvay and G. Münster, *Quantum fields on a lattice*. Cambridge University Press, Cambridge, 1994. Cambridge, UK: Univ. Pr. (1994) 491 p. (Cambridge monographs on mathematical physics).

[65] T. DeGrand and C. E. Detar, *Lattice methods for quantum chromodynamics*. World Scientific, New Jersey, 2006. New Jersey, USA: World Scientific (2006) 345 p.

[66] C. Gattringer and C. B. Lang, *Quantum chromodynamics on the lattice*. Lect. Notes Phys., 2010.

[67] P. de Forcrand, "Simulating QCD at finite density," *PoS* **LAT2009** (2009) 010, arXiv:1005.0539 [hep-lat].

[68] G. Aarts, "Complex Langevin dynamics and other approaches at finite chemical potential," *PoS* **LATTICE2012** (2012) 017, arXiv:1302.3028 [hep-lat].

[69] H. Gies and C. Wetterich, "Renormalization flow of bound states," *Phys.Rev.* **D65** (2002) 065001, arXiv:hep-th/0107221 [hep-th].

[70] H. Gies and C. Wetterich, "Universality of spontaneous chiral symmetry breaking in gauge theories," *Phys.Rev.* **D69** (2004) 025001, arXiv:hep-th/0209183 [hep-th].

[71] C. S. Fischer, A. Maas, and J. M. Pawlowski, "On the infrared behavior of Landau gauge Yang-Mills theory," *Annals Phys.* **324** (2009) 2408–2437, arXiv:0810.1987 [hep-ph].

[72] J. M. Pawlowski and F. Rennecke, "Higher order quark-mesonic scattering processes and the phase structure of QCD," *Phys.Rev.* **D90** no. 7, (2014) 076002, arXiv:1403.1179 [hep-ph].

[73] J. Braun, L. Fister, J. M. Pawlowski, and F. Rennecke, "From Quarks and Gluons to Hadrons: Chiral Symmetry Breaking in Dynamical QCD," arXiv:1412.1045 [hep-ph].

[74] F. Rennecke, "The Vacuum Structure of Vector Mesons in QCD," arXiv:1504.03585 [hep-ph].

[75] J. Braun, "Fermion Interactions and Universal Behavior in Strongly Interacting Theories," *J.Phys.* **G39** (2012) 033001, arXiv:1108.4449 [hep-ph].

[76] L. Faddeev and V. Popov, "Feynman Diagrams for the Yang-Mills Field," *Phys.Lett.* **B25** (1967) 29–30.

[77] V. N. Gribov, "Quantization of non-Abelian gauge theories," *Nucl. Phys.* **B139** (1978) 1.

[78] D. Zwanziger, "Non-perturbative Faddeev-Popov formula and infrared limit of QCD," *Phys. Rev.* **D69** (2004) 016002, arXiv:hep-ph/0303028.

[79] C. Becchi, A. Rouet, and R. Stora, "Renormalization of the Abelian Higgs-Kibble Model," *Commun.Math.Phys.* **42** (1975) 127–162.

[80] C. Becchi, A. Rouet, and R. Stora, "Renormalization of Gauge Theories," *Annals Phys.* **98** (1976) 287–321.

[81] I. Tyutin, "Gauge Invariance in Field Theory and Statistical Physics in Operator Formalism," arXiv:0812.0580 [hep-th].

[82] J. C. Taylor, "Ward Identities and Charge Renormalization of the Yang- Mills Field," *Nucl. Phys.* **B33** (1971) 436–444.

[83] A. Slavnov, "Ward Identities in Gauge Theories," *Theor.Math.Phys.* **10** (1972) 99–107.

[84] S. Bethke, "The 2009 World Average of alpha(s)," *Eur.Phys.J.* **C64** (2009) 689–703, arXiv:0908.1135 [hep-ph].

[85] M. Le Bellac, *Thermal Field Theory*. Cambridge University Press, 2000.

[86] S. L. Adler, "Axial vector vertex in spinor electrodynamics," *Phys.Rev.* **177** (1969) 2426–2438.

[87] S. L. Adler and W. A. Bardeen, "Absence of higher order corrections in the anomalous axial vector divergence equation," *Phys.Rev.* **182** (1969) 1517–1536.

[88] J. Bell and R. Jackiw, "A PCAC puzzle: pi0 –> gamma gamma in the sigma model," *Nuovo Cim.* **A60** (1969) 47–61.

[89] K. Fujikawa, "Path Integral Measure for Gauge Invariant Fermion Theories," *Phys.Rev.Lett.* **42** (1979) 1195–1198.

[90] G. 't Hooft, "Symmetry Breaking Through Bell-Jackiw Anomalies," *Phys.Rev.Lett.* **37** (1976) 8–11.

[91] E. Witten, "Current Algebra Theorems for the U(1) Goldstone Boson," *Nucl.Phys.* **B156** (1979) 269.

[92] G. Veneziano, "U(1) Without Instantons," *Nucl.Phys.* **B159** (1979) 213–224.

[93] R. Rapp and J. Wambach, "Chiral symmetry restoration and dileptons in relativistic heavy ion collisions," *Adv.Nucl.Phys.* **25** (2000) 1, arXiv:hep-ph/9909229 [hep-ph].

[94] Y. Nambu, "Quasiparticles and Gauge Invariance in the Theory of Superconductivity," *Phys.Rev.* **117** (1960) 648–663.

[95] J. Goldstone, "Field Theories with Superconductor Solutions," *Nuovo Cim.* **19** (1961) 154–164.

[96] **Particle Data Group** Collaboration, K. Olive *et al.*, "Review of Particle Physics," *Chin.Phys.* **C38** (2014) 090001.

[97] D. Griffiths, "Introduction to elementary particles,".

[98] J. Greensite, "The confinement problem in lattice gauge theory," *Prog. Part. Nucl. Phys.* **51** (2003) 1, arXiv:hep-lat/0301023.

[99] R. Alkofer and J. Greensite, "Quark Confinement: The Hard Problem of Hadron Physics," *J. Phys.* **G34** (2007) S3, arXiv:hep-ph/0610365.

[100] A. Di Giacomo, "Mechanisms for color confinement," arXiv:hep-th/9603029 [hep-th].

[101] R. Alkofer and L. von Smekal, "The infrared behavior of QCD Green's functions: Confinement, dynamical symmetry breaking, and hadrons as relativistic bound states," *Phys. Rept.* **353** (2001) 281, arXiv:hep-ph/0007355.

[102] C. S. Fischer, "Infrared properties of QCD from Dyson-Schwinger equations," *J.Phys.G* **G32** (2006) R253–R291, arXiv:hep-ph/0605173 [hep-ph].

[103] D. Diakonov, "Topology and confinement," *Nucl.Phys.Proc.Suppl.* **195** (2009) 5–45, arXiv:0906.2456 [hep-ph].

[104] G. 't Hooft, "Magnetic Monopoles in Unified Gauge Theories," *Nucl.Phys.* **B79** (1974) 276–284.

[105] S. Mandelstam, "Vortices and Quark Confinement in Nonabelian Gauge Theories," *Phys.Rept.* **23** (1976) 245–249.

[106] G. 't Hooft, "On the Phase Transition Towards Permanent Quark Confinement," *Nucl.Phys.* **B138** (1978) 1.

[107] Y. Aharonov, A. Casher, and S. Yankielowicz, "Instantons and Confinement," *Nucl.Phys.* **B146** (1978) 256.

[108] J. M. Cornwall, "Quark Confinement and Vortices in Massive Gauge Invariant QCD," *Nucl.Phys.* **B157** (1979) 392.

[109] T. Kugo and I. Ojima, "Local Covariant Operator Formalism of Nonabelian Gauge Theories and Quark Confinement Problem," *Prog. Theor. Phys. Suppl.* **66** (1979) 1.

[110] D. Zwanziger, "Vanishing of zero momentum lattice gluon propagator and color confinement," *Nucl. Phys.* **B364** (1991) 127–161.

[111] D. Zwanziger, "Fundamental modular region, Boltzmann factor and area law in lattice gauge theory," *Nucl. Phys.* **B412** (1994) 657–730.

[112] D. Zwanziger, "No confinement without Coulomb confinement," *Phys. Rev. Lett.* **90** (2003) 102001, arXiv:hep-lat/0209105.

[113] K. Osterwalder and R. Schrader, "AXIOMS FOR EUCLIDEAN GREEN'S FUNCTIONS," *Commun.Math.Phys.* **31** (1973) 83–112.

[114] K. Osterwalder and R. Schrader, "Axioms for Euclidean Green's Functions. 2.," *Commun.Math.Phys.* **42** (1975) 281.

[115] A. M. Polyakov, "Thermal Properties of Gauge Fields and Quark Liberation," *Phys.Lett.* **B72** (1978) 477–480.

[116] L. McLerran and R. D. Pisarski, "Phases of cold, dense quarks at large N(c)," *Nucl.Phys.* **A796** (2007) 83–100, arXiv:0706.2191 [hep-ph].

[117] C. Gattringer, "Linking confinement to spectral properties of the Dirac operator," *Phys. Rev. Lett.* **97** (2006) 032003, arXiv:hep-lat/0605018.

[118] F. Synatschke, A. Wipf, and K. Langfeld, "Relation between chiral symmetry breaking and confinement in YM-theories," *Phys.Rev.* **D77** (2008) 114018, arXiv:0803.0271 [hep-lat].

[119] B.-J. Schaefer, J. M. Pawlowski, and J. Wambach, "The Phase Structure of the Polyakov–Quark-Meson Model," *Phys.Rev.* **D76** (2007) 074023, arXiv:0704.3234 [hep-ph].

[120] J. Braun and H. Gies, "Running coupling at finite temperature and chiral symmetry restoration in QCD," *Phys.Lett.* **B645** (2007) 53–58, arXiv:hep-ph/0512085 [hep-ph].

[121] J. Braun and H. Gies, "Chiral phase boundary of QCD at finite temperature," *JHEP* **0606** (2006) 024, arXiv:hep-ph/0602226 [hep-ph].

[122] C. D. Roberts and S. M. Schmidt, "Dyson-Schwinger equations: Density, temperature and continuum strong QCD," *Prog. Part. Nucl. Phys.* **45** (2000) S1–S103, arXiv:nucl-th/0005064.

[123] D. Binosi and J. Papavassiliou, "Pinch Technique: Theory and Applications," *Phys.Rept.* **479** (2009) 1–152, arXiv:0909.2536 [hep-ph].

[124] A. Maas, "Describing gauge bosons at zero and finite temperature," *Phys.Rept.* **524** (2013) 203–300, arXiv:1106.3942 [hep-ph].

[125] P. Boucaud, J. Leroy, A. L. Yaouanc, J. Micheli, O. Pene, *et al.*, "The Infrared Behaviour of the Pure Yang-Mills Green Functions," *Few Body Syst.* **53** (2012) 387–436, arXiv:1109.1936 [hep-ph].

[126] S. Scherer, "Introduction to chiral perturbation theory," *Adv.Nucl.Phys.* **27** (2003) 277, arXiv:hep-ph/0210398 [hep-ph].

[127] L. P. Kadanoff, "Scaling laws for ising models near tc," *Physics (Long Island City, N.Y.)* (1966) 263–270.

[128] K. G. Wilson and J. Kogut, "The renormalization group and the ϵ expansion," *Physics Reports* **12** no. 2, (1974) 75 – 199. http://www.sciencedirect.com/science/article/pii/0370157374900234.

[129] K. G. Wilson, "The renormalization group: Critical phenomena and the kondo problem," *Rev. Mod. Phys.* **47** (Oct, 1975) 773–840. http://link.aps.org/doi/10.1103/RevModPhys.47.773.

[130] C. Wetterich, "Exact evolution equation for the effective potential," *Phys.Lett.* **B301** (1993) 90–94.

[131] I. Boettcher, J. M. Pawlowski, and S. Diehl, "Ultracold atoms and the Functional Renormalization Group," arXiv:1204.4394 [cond-mat.quant-gas].

[132] W. Metzner, M. Salmhofer, C. Honerkamp, V. Meden, and K. Schonhammer, "Functional renormalization group approach to correlated fermion systems," arXiv:1105.5289 [cond-mat.str-el].

[133] D. F. Litim and J. M. Pawlowski, "On gauge invariant Wilsonian flows," arXiv:hep-th/9901063 [hep-th].

[134] H. Gies, "Introduction to the functional RG and applications to gauge theories," *Lect.Notes Phys.* **852** (2012) 287–348, arXiv:hep-ph/0611146 [hep-ph].

[135] B.-J. Schaefer and J. Wambach, "Renormalization group approach towards the QCD phase diagram," *Phys.Part.Nucl.* **39** (2008) 1025–1032, arXiv:hep-ph/0611191 [hep-ph].

[136] D. F. Litim, "Fixed Points of Quantum Gravity and the Renormalisation Group," arXiv:0810.3675 [hep-th].

[137] R. Percacci, "Asymptotic Safety," arXiv:0709.3851 [hep-th]. to appear in 'Approaches to Quantum Gravity: Towards a New Understanding of Space, Time and Matter' ed. D. Oriti, Cambridge University Press.

[138] M. Reuter and F. Saueressig, "Quantum Einstein Gravity," arXiv:1202.2274 [hep-th].

[139] J. M. Pawlowski, "Aspects of the functional renormalisation group," *Annals Phys.* **322** (2007) 2831–2915, arXiv:hep-th/0512261 [hep-th].

[140] J. M. Pawlowski, "The QCD phase diagram: Results and challenges," *AIP Conf.Proc.* **1343** (2011) 75–80, arXiv:1012.5075 [hep-ph].

[141] O. J. Rosten, "Fundamentals of the Exact Renormalization Group," *Phys.Rept.* **511** (2012) 177–272, arXiv:1003.1366 [hep-th].

[142] J. Berges, N. Tetradis, and C. Wetterich, "Non-perturbative renormalization flow in quantum field theory and statistical physics," *Phys. Rept.* **363** (2002) 223–386, arXiv:hep-ph/0005122.

[143] L. von Smekal, "Universal Aspects of QCD-like Theories," *Nucl.Phys.Proc.Suppl.* **228** (2012) 179–220, arXiv:1205.4205 [hep-ph].

[144] S. Floerchinger and C. Wetterich, "Exact flow equation for composite operators," *Phys.Lett.* **B680** (2009) 371–376, arXiv:0905.0915 [hep-th].

[145] M. Bonini, M. D'Attanasio, and G. Marchesini, "BRS symmetry for Yang-Mills theory with exact renormalization group," *Nucl.Phys.* **B437** (1995) 163–186, arXiv:hep-th/9410138 [hep-th].

[146] U. Ellwanger, "Flow equations and BRS invariance for Yang-Mills theories," *Phys. Lett.* **B335** (1994) 364–370, arXiv:hep-th/9402077.

[147] U. Ellwanger, M. Hirsch, and A. Weber, "Flow equations for the relevant part of the pure Yang-Mills action," *Z.Phys.* **C69** (1996) 687–698, arXiv:hep-th/9506019 [hep-th].

[148] L. Fister, "On the Phase Diagram of QCD with Dynamical Quarks," *PhD thesis, Heidelberg University,* (2012) , 2012.

[149] D. F. Litim, "Optimization of the exact renormalization group," *Phys.Lett.* **B486** (2000) 92–99, arXiv:hep-th/0005245 [hep-th].

[150] D. F. Litim, "Optimized renormalization group flows," *Phys.Rev.* **D64** (2001) 105007, arXiv:hep-th/0103195 [hep-th].

[151] B.-J. Schaefer and J. Wambach, "The Phase diagram of the quark meson model," *Nucl.Phys.* **A757** (2005) 479–492, arXiv:nucl-th/0403039 [nucl-th].

[152] D. F. Litim, "Critical exponents from optimized renormalization group flows," *Nucl.Phys.* **B631** (2002) 128–158, arXiv:hep-th/0203006 [hep-th].

[153] K.-I. Aoki, K. Morikawa, W. Souma, J.-I. Sumi, and H. Terao, "Rapidly converging truncation scheme of the exact renormalization group," *Prog.Theor.Phys.* **99** (1998) 451–466, arXiv:hep-th/9803056 [hep-th].

[154] J. Braun, "The QCD Phase Boundary from Quark-Gluon Dynamics," *Eur. Phys. J.* **C64** (2009) 459–482, arXiv:0810.1727 [hep-ph].

[155] J. Braun, L. M. Haas, F. Marhauser, and J. M. Pawlowski, "Phase Structure of Two-Flavor QCD at Finite Chemical Potential," *Phys.Rev.Lett.* **106** (2011) 022002, arXiv:0908.0008 [hep-ph].

[156] M. Mitter, J. M. Pawlowski, and N. Strodthoff, "Chiral symmetry breaking in continuum QCD," arXiv:1411.7978 [hep-ph].

[157] J. M. Pawlowski, "Equation of state and phase diagram of strongly interacting matter," *Nucl.Phys.* **A931** (2014) 113–124.

[158] L. Fister and J. M. Pawlowski, "Yang-Mills correlation functions at finite temperature," arXiv:1112.5440 [hep-ph].

[159] L. Fister and J. M. Pawlowski, "," *in preparation* (2014) .

[160] M. Buballa, "NJL model analysis of quark matter at large density," *Phys.Rept.* **407** (2005) 205–376, arXiv:hep-ph/0402234 [hep-ph].

[161] H. Gies, J. Jaeckel, and C. Wetterich, "Towards a renormalizable standard model without fundamental Higgs scalar," *Phys. Rev.* **D69** (2004) 105008, arXiv:hep-ph/0312034.

[162] J. Jaeckel, "Effective actions for strongly interacting fermionic systems," arXiv:hep-ph/0309090 [hep-ph].

[163] J. Hubbard, "Calculation of partition functions," *Phys.Rev.Lett.* **3** (1959) 77–80.

[164] R. L. Stratonovich, "On a Method of Calculating Quantum Distribution Functions," *Soviet Physics Doklady* **2** (July, 1957) 416.

[165] R. D. Pisarski and F. Wilczek, "Remarks on the Chiral Phase Transition in Chromodynamics," *Phys.Rev.* **D29** (1984) 338–341.

[166] A. J. Helmboldt, J. M. Pawlowski, and N. Strodthoff, "Towards quantitative precision in the chiral crossover: masses and fluctuation scales," arXiv:1409.8414 [hep-ph].

[167] J. M. Pawlowski, "," *Nucl.Phys.* **A** (2014) .

[168] C. S. Fischer, A. Maas, and J. M. Pawlowski, "Aspects of confinement from QCD correlation functions," *PoS* **CONFINEMENT8** (2008) 043, arXiv:0812.2745 [hep-ph].

[169] M. D'Attanasio and T. R. Morris, "Gauge invariance, the quantum action principle, and the renormalization group," *Phys.Lett.* **B378** (1996) 213–221, arXiv:hep-th/9602156 [hep-th].

[170] Y. Igarashi, K. Itoh, and H. So, "BRS symmetry, the quantum master equation, and the Wilsonian renormalization group," *Prog.Theor.Phys.* **106** (2001) 149–166, arXiv:hep-th/0101101 [hep-th].

[171] C. S. Fischer and J. Luecker, "Propagators and phase structure of Nf=2 and Nf=2+1 QCD," *Phys.Lett.* **B718** (2013) 1036–1043, arXiv:1206.5191 [hep-ph].

[172] C. S. Fischer, L. Fister, J. Luecker, and J. M. Pawlowski, "Polyakov loop potential at finite density," *Phys.Lett.* **B732** (2014) 273–277, arXiv:1306.6022 [hep-ph].

[173] C. S. Fischer, J. Lücker, and J. M. Pawlowski, "The phase structure of QCD for heavy quarks," arXiv:1409.8462 [hep-ph].

[174] M. Q. Huber and L. von Smekal, "On the influence of three-point functions on the propagators of Landau gauge Yang-Mills theory," *JHEP* **1304** (2013) 149, arXiv:1211.6092 [hep-th].

[175] M. Pelaez, M. Tissier, and N. Wschebor, "Three-point correlation functions in Yang-Mills theory," *Phys.Rev.* **D88** (2013) 125003, arXiv:1310.2594 [hep-th].

[176] G. Eichmann, R. Williams, R. Alkofer, and M. Vujinovic, "The three-gluon vertex in Landau gauge," *Phys.Rev.* **D89** (2014) 105014, arXiv:1402.1365 [hep-ph].

[177] A. Blum, M. Q. Huber, M. Mitter, and L. von Smekal, "Gluonic three-point correlations in pure Landau gauge QCD," *Phys.Rev.* **D89** (2014) 061703, arXiv:1401.0713 [hep-ph].

[178] D. Binosi, D. Ibanez, and J. Papavassiliou, "Nonperturbative study of the four gluon vertex," arXiv:1407.3677 [hep-ph].

[179] J. Gracey, "Off-shell two loop QCD vertices," *Phys.Rev.* **D90** (2014) 025014, arXiv:1406.0649 [hep-ph].

[180] A. K. Cyrol, M. Q. Huber, and L. von Smekal, "A Dyson-Schwinger study of the four-gluon vertex," arXiv:1408.5409 [hep-ph].

[181] M. Hopfer, A. Windisch, and R. Alkofer, "The Quark-Gluon Vertex in Landau gauge QCD," *PoS* **ConfinementX** (2012) 073, arXiv:1301.3672 [hep-ph].

[182] R. Williams, "The quark-gluon vertex in Landau gauge bound-state studies," arXiv:1404.2545 [hep-ph].

[183] A. Aguilar, D. Binosi, D. Ibanez, and J. Papavassiliou, "A new method for determining the quark-gluon vertex," arXiv:1405.3506 [hep-ph].

[184] T. K. Herbst, M. Mitter, J. M. Pawlowski, B.-J. Schaefer, and R. Stiele, "Thermodynamics of QCD at vanishing density," *Phys.Lett.* **B731** (2014) 248–256, arXiv:1308.3621 [hep-ph].

[185] T. Dahms, "Dilepton spectra in p+p and Au+Au collisions at RHIC," arXiv:0810.3040 [nucl-ex].

[186] R. D. Pisarski, "Phenomenology of the Chiral Phase Transition," *Phys.Lett.* **B110** (1982) 155.

[187] J. Sakurai, "Theory of strong interactions," *Annals Phys.* **11** (1960) 1–48.

[188] B. W. Lee and H. Nieh, "Phenomenological Lagrangian for field algebra, hard pions, and radiative corrections," *Phys.Rev.* **166** (1968) 1507–1515.

[189] U. G. Meissner, "Low-Energy Hadron Physics from Effective Chiral Lagrangians with Vector Mesons," *Phys.Rept.* **161** (1988) 213.

[190] M. Urban, M. Buballa, and J. Wambach, "Vector and axial vector correlators in a chirally symmetric model," *Nucl.Phys.* **A697** (2002) 338–371, arXiv:hep-ph/0102260 [hep-ph].

[191] C. Itzykson and J. Zuber, *Quantum Field Theory*. Dover Books on Physics. Dover Publications, 2006.

[192] F. Karsch, "Lattice QCD at high temperature and density," *Lect. Notes Phys.* **583** (2002) 209–249, arXiv:hep-lat/0106019.

[193] O. Philipsen, "Lattice QCD at finite temperature and density," *Eur.Phys.J.ST* **152** (2007) 29–60, arXiv:0708.1293 [hep-lat].

[194] D. Sexty, "Simulating full QCD at nonzero density using the complex Langevin equation," arXiv:1307.7748 [hep-lat].

[195] K.-I. Kondo, "Toward a first-principle derivation of confinement and chiral-symmetry-breaking crossover transitions in QCD," *Phys. Rev.* **D82** (2010) 065024, arXiv:1005.0314 [hep-th].

[196] T. K. Herbst, J. M. Pawlowski, and B.-J. Schaefer, "Phase structure and thermodynamics of QCD," *Phys.Rev.* **D88** no. 1, (2013) 014007, arXiv:1302.1426 [hep-ph].

[197] L. M. Haas, R. Stiele, J. Braun, J. M. Pawlowski, and J. Schaffner-Bielich, "Improved Polyakov-loop potential for effective models from functional calculations," *Phys.Rev.* **D87** (2013) 076004, arXiv:1302.1993 [hep-ph].

[198] U. Ellwanger and C. Wetterich, "Evolution equations for the quark - meson transition," *Nucl.Phys.* **B423** (1994) 137–170, arXiv:hep-ph/9402221 [hep-ph].

[199] J. Berges, D. Jungnickel, and C. Wetterich, "Two flavor chiral phase transition from nonperturbative flow equations," *Phys.Rev.* **D59** (1999) 034010, arXiv:hep-ph/9705474 [hep-ph].

[200] J. Braun, "Thermodynamics of QCD low-energy models and the derivative expansion of the effective action," *Phys.Rev.* **D81** (2010) 016008, arXiv:0908.1543 [hep-ph].

[201] D. F. Litim, J. M. Pawlowski, and L. Vergara, "Convexity of the effective action from functional flows," arXiv:hep-th/0602140 [hep-th].

[202] P. de Forcrand and O. Philipsen, "The QCD phase diagram for small densities from imaginary chemical potential," *Nucl.Phys.* **B642** (2002) 290–306, arXiv:hep-lat/0205016 [hep-lat].

[203] J. Braun, B. Klein, and B.-J. Schaefer, "On the Phase Structure of QCD in a Finite Volume," *Phys.Lett.* **B713** (2012) 216–223, arXiv:1110.0849 [hep-ph].

[204] R.-A. Tripolt, N. Strodthoff, L. von Smekal, and J. Wambach, "Spectral functions from the functional renormalization group at finite temperature and density," arXiv:1407.8387 [hep-ph].

[205] M. Q. Huber and J. Braun, "Algorithmic derivation of functional renormalization group equations and Dyson-Schwinger equations," arXiv:1102.5307 [hep-th]. * Temporary entry *.

[206] J. A. M. Vermaseren, "New features of FORM," *ArXiv Mathematical Physics e-prints* (Oct., 2000) , math-ph/0010025.

[207] F. Feng and R. Mertig, "FormLink/FeynCalcFormLink : Embedding FORM in Mathematica and FeynCalc," *ArXiv e-prints* (Dec., 2012) , arXiv:1212.3522 [hep-ph].

[208] D. F. Litim, J. M. Pawlowski, and L. Vergara, "Convexity from background field flows," *unpublished* (2007) .